Distributed Propulsion for Commercial Transport Aircraft

F.T.H. Wong	4169077	J.I. Nijsse	4218124
V. Margos	4173570	M.J.C. Kolff	4219694
A. Bhowal	4198611	L.E. van den Ende	4227360
J. Peeters Salazar	4208773	R.F.H. van Maris	4229304
T.E.H. Noortman	4211766	M.P. van Hoorn	4232550

Final Report

Design Synthesis Exercise

TU Delft Delft University of Technology

VIMANA

Version	Notes	Date
1.0	Draft Version	23-06-15
2.0	Final Version	30-06-15

This page intentionally left blank.

This page intentionally left blank.

Preface

Delft, June 30, 2015

This report is written by group S17 of the faculty of Aerospace Engineering at Delft University of Technology for the 2015 spring Design Synthesis Exercise (DSE), which forms the closing piece of the bachelor's program. The goal of this project is to design an aircraft that utilises a distributed propulsion system and perform a comparison with an existing reference aircraft to quantify the benefits of the propulsion system.
This report is written in the scope of the project, which is to demonstrate sufficient knowledge to accomplish a successful design of a conceptual aerospace system.
We would like to thank Dr. Ir. Mark Voskuijl, Ir. Daniel Peeters and Ir. Olaf Stroosma for their guidance and dedication during the Design Synthesis Exercise. Furthermore, we thank Dong Liu, MSc. at EWI for his help on superconducting theory and Dr. Erik Kelder of the department of Chemical Engineering for his help on batteries. From the faculty of Aerospace Engineering, we want to thank Peijian Lv, MSc. and Daniele Ragni, Dr. for their help on Boundary Layer Ingestion and propeller design, respectively. Also we thank Ir. Joris Melkert for his help on the overall aircraft configuration.

Group S17

Summary

If air travel ought to continue being the preferred intercontinental transport method for the 21^{st} century, aircraft need to achieve substantial improvements in their environmental footprints. Nowhere is the sustainability challenge more visible than in aerospace propulsion systems, particularly in CO_2, NO_x and noise emissions. The goal of this project entails the development of a distributed propulsion system that would enable a drastic decrease in emissions while also increasing propulsive efficiency and introducing a valuable test-bed for novel hybrid propulsion technologies. DSE group 17 was set the task to design a medium range commercial transport aircraft with a distributed propulsion system and compare its performance to an existing reference aircraft. Top level requirements included a seating capacity of 180 passengers, a range at maximum payload of 6100 km and a cruise Mach number of 0.78. Additional constraints and requirements for this project comprised the use of proven technology for non-propulsion subsystems and being economically competitive with current conventional aircraft.

During the past eleven weeks, group 17 has performed a comprehensive analysis on current developments and research in novel propulsive technologies. Initially, five different aircraft concepts were drafted with different propulsive systems including both conventional geared turbofan engines as well as novel solutions such as hybrid architectures and superconductive technologies. With a final concept selected, software was built or adapted for the propulsion system architecture design. The team focused on developing tools aimed at optimizing the propulsive performance and minimizing the required power of the fundamental design parameters of the propulsion system such as fan and engine numbering, sizing, and propeller airfoil design. Besides, a detailed system architecture as well as a comprehensive economic analysis on the recommended pricing and projected costs of the entire program has been completed, including a roadmap for the proposed future activities.

The airplane design features a revolutionary propulsion architecture: three turboshafts placed at the back of the aircraft provide power to the eight ducted fans located on the top of the wings. An advanced differential thrust yaw control system even allowed the vertical tail plane to be omitted. A large effective by-pass-ratio is obtained due to the significant volume of air being blown by the fans resulting in a high propulsive efficiency. One of the turboshafts is podded in the aft of the fuselage and improves the overall aerodynamic and propulsive efficiency of the aircraft by means of boundary layer ingestion. Superconductivity in both the generators as well as the motors is ensured by a methane heat sink, which, in conjunction with standard jet fuel is used as the energy source. A lower noise level is achieved by means of fan shielding, a reduction in the landing gear size and exhaust jet velocity. Finally, the incorporation of a distributed propulsion system enables reductions in CO_2 and NO_x. Calculations estimate a reduction of more than 20% with respect to conventional modern aircraft.

List of Acronyms and Abbreviations

Acronym / Abbreviation	Description
ac	Aerodynamic centre
AC	Alternating Current
ATC	Air Traffic Control
ATO	Air Transport and Operations
BLI	Boundary Layer Ingestion
BR	Baseline Review
BSCCO	Bismuth Strontium Calcium Copper Oxide
BWB	Blended Wing Body
c.g.	Centre of gravity
DC	Direct Current
DID	Deliverable Item Description
DNo	Deliverable Number
DOC	Direct Operating Cost
DMLS	Direct Metal Laser Sintering
DOT	Design Option Tree
DP	Distributed Propulsion
EASA	European Aviation Safety Agency
ECES	European Committee for Electronical Standardization
EOL	End-of-Life
FAA	Federal Aviation Administration
FBDS	Functional BreakDown Structure
FBW	Fly-By-Wire
FFBD	Functional Flow Block Diagram
FR	Final Review
GSE	Ground Support Equipment
HBD	Hardware Block Diagram
HLD	High Lift Devices
HTS	High Temperature Superconducting
ISA	International Standard Atmosphere
LE	Leading edge of wing
LEMAC	Leading edge of the Mean Aerodynamic Chord
LNG	Liquefied Natural Gas
LP	Low Pressure
MAC	Mean Aerodynamic Chord
MgB_2	Magnesium Diboride
MTOW	Maximum Take-off Weight
MTR	Mid Term Review
MZFW	Maximum Zero Fuel Weight
OBS	Organisational Breakdown Structure
OEI	One Engine Inoperative
OEW	Operational Empty Weight
OMI	One Motor Inoperative
OPR	Overall Pressure Ratio
PS	Periodic Service
RAMS	Reliability, Availability, Maintainability and Safety
RDT	Requirements Discovery Tree
RMF	Revolving Magnetic Field
SFC	Specific Fuel Consumption
TBD	To Be Determined
TE	Trailing edge of the Wing
TIT	Turbine Inlet Temperature
TRL	Technology Readiness Level
VALID	Verifiable, Achievable, Logical, Integral, Definite
WBS	Work Breakdown Structure
WFD	Work Flow Diagram

List of Symbols

Symbol	Description	Unit
A	Aspect Ratio	$[-]$
A_e	Current Density	$[A/m^2]$
b	Wingspan	$[m]$
B	Magnetic flux density	$[T]$
b_f	Fuselage width	$[m]$
c	Chord length	$[m]$
$\bar{c}$	Mean aerodynamic chord	$[m]$
C_D	Drag coefficient	$[-]$
C_{D_0}	Zero-lift drag coefficient	$[-]$
C_L	Lift coefficient	$[-]$
C_{L_h}	Horizontal tail lift coefficient	$[-]$
C_{L_α}	Lift gradient	$[rad^{-1}]$
$C_{L_{\alpha_h}}$	Horizontal tail lift gradient	$[rad^{-1}]$
$C_{L_{A-h}}$	Lift coefficient of tailless plane	$[-]$
C_l	Airfoil lift coefficient	$[-]$
c_j	Specific fuel consumption	$[kg/(N \cdot s)]$
$C_{m_{ac}}$	Moment coefficient around aerodynamic centre	$[-]$
C_{m_α}	Gradient of $Cm - \alpha$ curve	$[-]$
D	Drag	$[N]$
D_m	Diameter	$[m]$
e	Oswald factor	$[-]$
E	Young's modulus	$[Pa]$
F	Force	$[N]$
f	Frequency	$[Hz]$
g	Gravitational acceleration	$[m/s^2]$
h	Height	$[m]$
I	Area moment of Inertia	$[m^4]$
I_e	Current	$[A]$
k	Spring constant	$[N/m]$
L	Lift	$[N]$
l	Length	$[m]$
l_h	Tail arm	$[m]$
M	Mach number	$[-]$
m	Mass	$[kg]$
MTOW	Maximum Take-off Weight	$[N]$
$M_{f_{used}}$	Mass fraction of used fuel	$[-]$
M_{tfo}	Mass fraction of trapped fuel and oil	$[-]$
n	Load factor	$[-]$
n_s	Motor Synchronous speed	$[RPM]$
N_{poles}	Number of magnetic poles	$[-]$
P	Power	$[W]$
P_{alt}	Power at a certain altitude	$[W]$
P_{SL}	Power at sea level	$[W]$
q	Dynamic pressure	$[Pa]$
R	Range	$[km]$
s	Field Length	$[m]$
S	Surface area	$[m^2]$
S_h	Horizontal tail surface area	$[m^2]$
t	Time	$[s]$
T	Thrust	$[N]$
U	Energy density	$[Wh/kg]$
V	Velocity	$[m/s]$
V_e	Exit velocity	$[m/s]$
V_i	Inlet velocity	$[m/s]$
V_h	Velocity at tail	$[m/s]$

W	Weight	$[N]$
x	Location in x-direction	$[m]$
$\bar{x}_{ac}$	Aerodynamic center position normalized with MAC	$[-]$
$\bar{x}_{cg}$	Center of gravity position normalized with MAC	$[-]$
α	Angle of attack	$[deg]$
γ	Climb gradient	$[\%]$
δ_r	Pressure ratio	$[-]$
ϵ	Downwash angle	$[\%]$
η	Efficiency	$[-]$
θ	Pitch angle	$[deg]$
θ_r	Temperature ratio	$[-]$
λ	Taper ratio	$[-]$
Λ	Sweep angle	$[deg]$
ρ	Density	$[kg/m^3]$
σ	Stress	$[Pa]$
ω_m	Angular velocity	$[rad/s]$

Contents

Preface iv

Summary v

List of Acronyms and Abbreviations vii

List of Symbols viii

1 Introduction 1

2 Project Definition 2
2.1 Background . . . 2
2.2 Project Objective . . . 2
2.3 Requirement Analysis . . . 2

3 Concept Trade-off 5
3.1 Design Concepts . . . 5
3.2 Concept Trade-off Criteria and Weights . . . 6
3.3 Sensitivity Analysis . . . 8

4 Design Method 11
4.1 Class I Weight Estimation . . . 11
4.2 Wing and Thrust Sizing . . . 12
4.3 Airfoil Selection and Wing Planform Design . . . 14
4.4 Control Surfaces . . . 16
4.5 Fuselage Design . . . 18
4.6 Propulsion System . . . 18
4.7 Class II Weight Estimation . . . 19
4.8 Empennage Design . . . 19
4.9 Drag Estimation . . . 20
4.10 Iteration Process . . . 21

5 Reference Aircraft 23
5.1 Geometry and Weights . . . 23
5.2 Final Result . . . 24

6 Propulsion System Design 25
6.1 Fan Design . . . 25
6.2 Required Power . . . 29
6.3 Engines . . . 29
6.4 Motors and Generators . . . 38
6.5 Cabling . . . 43
6.6 Controllers . . . 44
6.7 Cooling . . . 45
6.8 Auxilary Power Unit . . . 48
6.9 Final Architecture . . . 49

7 Results 51
7.1 Iteration Results . . . 51
7.2 Mass Budget Breakdown . . . 52
7.3 Aerodynamic Analysis . . . 54
7.4 Structural Analysis . . . 57
7.5 Control and Stability Analysis . . . 61
7.6 Performance Analysis . . . 73
7.7 Verification and Validation . . . 76

8 Aircraft System Characteristics **80**
8.1 Hardware and Software Interaction . . . 80
8.2 Communications and Data Handling . . . 85
8.3 Configuration and Layout . . . 86

9 Sustainability **90**
9.1 Production and Assembly . . . 90
9.2 Operations . . . 90
9.3 Maintainability . . . 91
9.4 Disposal . . . 91
9.5 Sustainability within the Group . . . 92

10 Technical Risk Assessment **93**
10.1 General Risk Assessment . . . 93
10.2 Reflection on Risks . . . 98

11 Economic Analysis **100**
11.1 Market Analysis . . . 100
11.2 Cost Breakdown . . . 102

12 Operational Analysis **114**
12.1 Operations and Logistics . . . 114
12.2 Maintenance . . . 115
12.3 RAMS Analysis . . . 116

13 Compliance with Requirements **118**

14 Future Development Activities **119**
14.1 Project Design and Development Logic . . . 119
14.2 Development of Distributed Propulsion Technologies . . . 121
14.3 Post-DSE Gantt Chart . . . 122
14.4 Recommendations . . . 125

15 Conclusion **126**

Bibliography **127**

A Propulsion System Background **130**
A.1 Detailed Results of Sensitivity Analysis on Number of Engines . . . 130
A.2 Detailed Results of Sensitivity Analysis on Placement of Engines . . . 130
A.3 Coldhead Drawing . . . 131

B Functional Analysis **132**
B.1 Functional Breakdown Structure . . . 132
B.2 Functional Flow Block Diagram . . . 132

C Cost Estimation Factor **137**

D Work Distribution **138**

Chapter 1 | Introduction

Currently, it can be seen that many industries focus on becoming more environmentally friendly. This is due to the depletion of natural resources, but also offers many benefits in terms of marketing, public relations and cost. One of the industries which is inspiring to become "greener" is the aerospace industry. Aircraft have become more and more efficient and less polluting in the past years and this trend will likely continue over the coming years. However, to continue this trend new aircraft concepts which might offer better performance have to be researched and developed, if they show promising advantages.

One of the ways to lower the fuel consumption and reduce the emissions is by making use of distributed propulsion. Distributed propulsion is the discipline of spreading the airflow and propulsive forces across the aircraft, by installing more but less powerful engines. The goal of this technology is to improve the aircraft characteristics, such as the fuel efficiency and the noise emissions. The benefits of distributed propulsion can be obtained by maximizing the effects such as boundary layer ingestion (BLI), reducing the tail size due to the reduced criticality of a one engine inoperative (OEI) scenario and reducing the mass of the landing gear, due to engine clearance.

The goal of this report is to discuss and trade-off the different design options and to document the complete design process taken to arrive at a feasible distributed propulsion aircraft design, that significantly reduces greenhouse gasses, but still fulfills similar requirements as an Airbus A321. Furthermore, the report also provides future planning for after the DSE, to make sure the aircraft is able to enter service in 2035. From now on, the designed distributed propulsion aircraft will be called *Vimana*, being the Hindi term for a mythological flying temple.

The report continues by stating the project definition with a background on the relevant topics, which also includes the top-level requirements and constraints set by the organization. Chapter 3 discusses the concept trade-off initiated in the Mid-Term Report. After that, Chapter 4 gives an overview of the general design method. The reference aircraft, used for quantifying the benefits of distributed propulsion, follows directly after that and is discussed in Chapter 5. The propulsion system design is separately in Chapter 6, whereas the design results are shown in Chapter 7. Chapter 8 discusses the relevant (sub)system analyses, such as communications throughout the aircraft and the electrical system. This is followed by the sustainability analysis, risk and economics chapters. Chapter 12 discusses the operational logistics of the aircraft, such as ground handling. Chapter 13 compares the outcome product with the requirement whereas Chapter 14 provides an overview of the expected activities between the end of this project and its projected entry into service. Finally, the report is concluded in Chapter 15.

Chapter 2 | Project Definition

This chapter gives the outline of the project. First, the background is discussed, followed by the mission objective. Lastly, a requirement analysis will be given.

2.1 Background

The main scope of this DSE project is the design and development of an aircraft which implements a distributed propulsion system. A design solution that features multiple propulsive units spread along the airframe instead of two conventional turbofans can bring several performance benefits. From a first instance analysis, some of these benefits are:

- Reduction in drag and fuel burn by making use of boundary layer ingestion and wake filling [1–3]
- Weight reduction due to better integration of the propulsion system in the airframe [4]
- Weight reduction of the vertical tail due to the one engine inoperative scenario being less critical [4–6]
- Performance increase due to the one engine inoperative scenario being less critical [7]
- Weight reduction in empennage due to novel control methods, such as differential thrust [6]
- Weight reduction in the landing gear because the length can be shorter due to the smaller propulsive devices
- Noise reduction due to the high integration level of the propulsion system [4]

As stated above, one of the main benefits of using distributed propulsion, is that it can efficiently make use of boundary layer ingestion (BLI). Boundary layer ingestion is the ingestion of the flow which, relatively to the aircraft, has been slowed down to speeds lower than the free flow. This boundary layer contributes to the drag of the aircraft. By ingesting this boundary layer and accelerating it again, the wake can be filled and the overall drag of the aircraft can be reduced. This drag reduction will then result in an increase in the aerodynamic efficiency of the aircraft.
Furthermore, several weight reductions are also facilitated by making use of a distributed propulsion system. The most notable are the reduction in empennage weight due to novel control methods such as differential thrust and due to the one engine inoperative scenario being less critical, the reduction in nacelle weight due to the length not being restricted by engine clearance, and the reduction in nacelle weight due to the integration with the airframe.
Finally, the use of a distributed propulsion system opens up possibilities to use different propulsion configurations. Instead of using a conventional configuration using turbofans, other options become more interesting such as multiple fans powered by one turbine. This could be done using mechanical transfer but also using electrical transfer. Especially the electrical transfer is an interesting option since it enables the fans to be scaled down to very small sizes. It also opens up some interesting options regarding superconductivity, because that can decrease efficiency losses caused by separating fans and turbines.

2.2 Project Objective

The objective of this project is to design a commercial transport aircraft with a distributed propulsion system. Significant improved energy efficiency and reduced noise level should be achieved by making use of the distributed propulsion system. The improvements of the designed aircraft will be quantified and compared to a reference aircraft, which in this case will be the Airbus A321. The subsystems other than the propulsion subsystem should be proven technology to the largest extent. In this manner, the reduced emissions and noise level can only be due to the distributed propulsion system [8].

2.3 Requirement Analysis

This section outlines the approach taken to develop a consolidated set of preliminary requirements for the distributed propulsion aircraft. Figure 2.1 shows the Requirements Discovery Tree, which is divided into 2 main categories: functional requirements and constraints.

2.3.1 Requirements

The functional requirements are divided into two further subcategories: top level requirements, which stem from the project guide [8], and the derived parameters. The top level requirements form the baseline from

which a consolidated set of requirements has been during the design process. All these requirements should be met by using a distributed propulsion system. From the project guide [8] the following top level requirements are drawn:

- REQ-TL1: The aircraft shall accommodate 180 passengers in a single class configuration
- REQ-TL2: The aircraft shall be able to transport $18,500kg$ payload
- REQ-TL3: The aircraft shall have a maximum payload range of $6100km$
- REQ-TL4: The aircraft shall have a cruise speed of $M = 0.78$ at $11,000m$
- REQ-TL5: The aircraft shall have a maximum speed of $M = 0.82$ at $11,000m$
- REQ-TL6: The aircraft shall require a take-off field length of no more than $2100m$ at ISA sea level and MTOW condition
- REQ-TL7: The aircraft shall require a landing field length of no more than $1600m$ at ISA sea level and MLW condition
- REQ-TL8: The aircraft shall have a service ceiling of $12,000m$

Many requirements have been derived during the design process. A few examples are presented below:

- REQ-DER1: The aircraft shall have a thrust loading of 0.157
- REQ-DER2: The aircraft shall have a wing loading of $5778N/m^2$
- REQ-DER3: The aircraft shall have a high lift device area of $26.13m^2$
- REQ-DER4: An aircraft motor shall be able to handle at least $4.6175MW$
- REQ-DER5: An aircraft engine shall be able to produce at least $16.16MW$ at sea level

2.3.2 Constraints

The identified constraints were allocated in 5 different categories: airport infrastructure, time, regulations, cost and quality. The inclusion of a distributed propulsion system opens a wide array of new design possibilities. However, the final design must be able to efficiently operate within the actual established air-traffic network. This is particularly applicable for airports: the newly designed aircraft should not require major modifications in their infrastructure. Furthermore it was stated that all subsystems must be designed using technology with a readiness level of 9 (the highest level), with the exception of the propulsion subsystem.
The newly designed aircraft should adhere to international regulations (EASA and FAA standards). Special attention should be paid to the one engine inoperative condition (OEI), as it is assumed that a distributed propulsion system will relieve this otherwise driving requirement. Furthermore, the applicable safety standards defined by the ECES (European Committee for Electrotechnical Standardization) must be investigated and a proposal should be made for possible amendments to the current EASA certification rules. Moreover, the project goals should be attained within the established time frame; this means that deadlines have to be met on time and the whole project must be completed within the established 11 weeks. In order for this project to be successful, quality standards must be met in terms of Reliability, Availability, Maintainability and Safety (RAMS). Finally, the designed aircraft with a distributed propulsion should be able to compete with current standard configuration aircraft such as the Airbus A321 in terms of reduced emissions, direct operating cost and noise.
The target of the design mission is to reduce both CO_2 and NO_x by 25% per passenger kilometre. Furthermore the noise, compared to an A321, should be reduced in the take-off, climb, descent and landing phases.
These top-level requirements and constraints function as a starting point for sizing the aircraft, to perform initial estimates. In Chapter 13 it will be checked whether all these requirements are met. Furthermore, the concept trade-off, which is discussed in Chapter 3, will contain choices based on these requirements. For example, it could be concluded that a propeller aircraft design may not be able to meet the requirements set on the cruise speed.

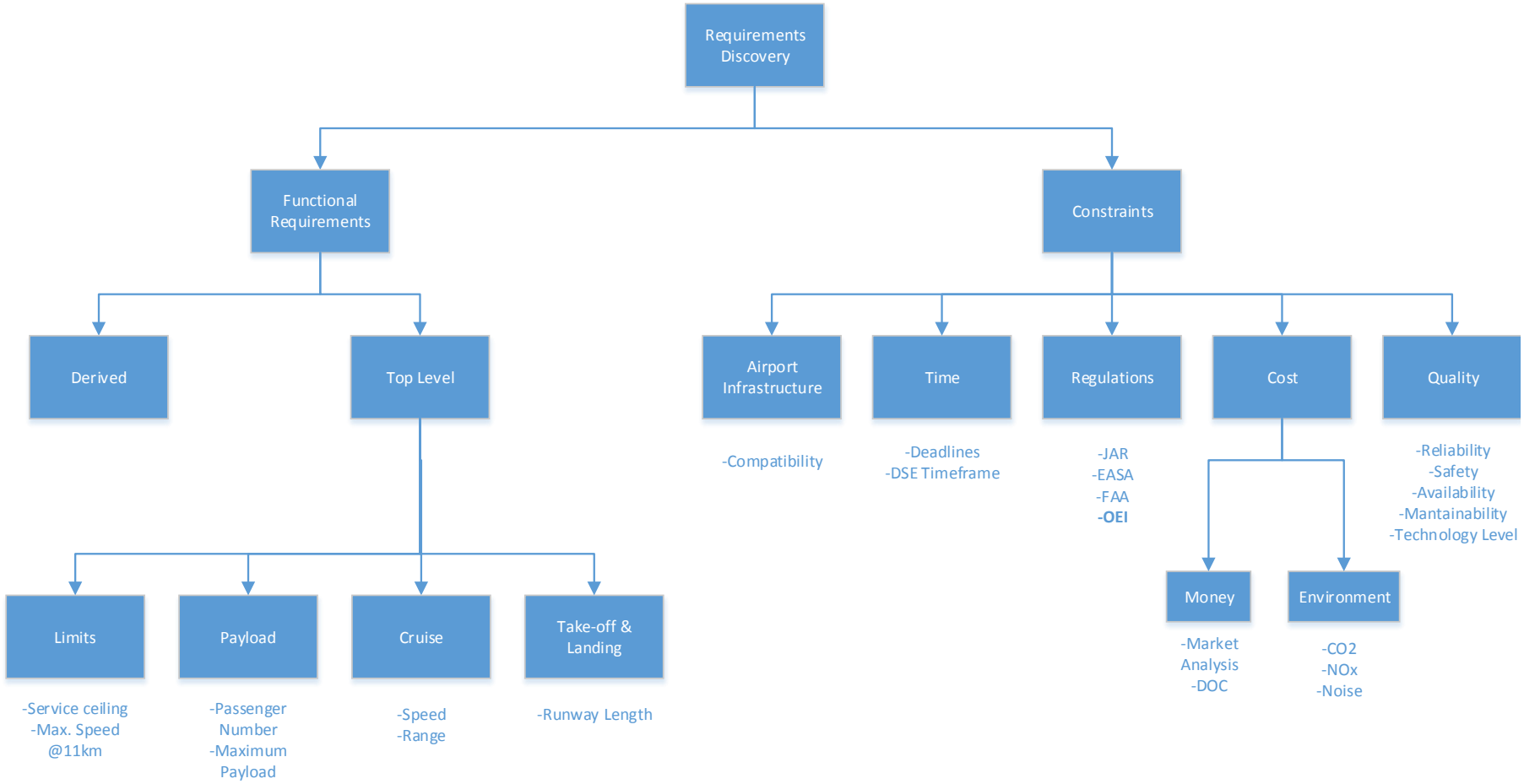

Figure 2.1: Requirements discovery tree

Chapter 3 | Concept Trade-off

In the previous chapter, the key requirements and constraints for the distributed propulsion aircraft Vimana were presented. With this set of requirements and constraints, in conjunction with the knowledge acquired during the literature survey phase, five different concepts were outlined. This chapter will focus on elaborating on these distributed propulsion aircraft concepts and is divided as follows: Section 3.1 outlines the five developed concepts from the MTR and their respective propulsion architectures. Section 3.2 explains the trade-off method and criteria. Furthermore, the actual trade-off is shown here. Finally, Section 3.3 provides insight into the robustness of the chosen trade-off method by performing a sensitivity analysis.

3.1 Design Concepts

This section will present an overview of the five different distributed propulsion concepts explaining their principal characteristics and architectures. Sketches of these concepts can be found in the Mid-Term Report [9].

Concept 1: Geared Turbofan
The first concept deviates the least from existing aircraft. It features a conventional tube-and-wing configuration with 9 geared turbofan engines which are downscaled versions of existing engines featured in state-of-the-art aircraft such as the Airbus A321neo. Taking weight, specific fuel consumption and propulsive efficiency into account, the optimal number of engines was estimated to lie between 9 and 12 elements. The propulsive configuration envisions six engines located below the wings, three on each side. Three additional engines are located at the back of the fuselage; this design choice was made due to the potential benefits of fuselage boundary layer ingestion. Furthermore, a Pi-tail was introduced in order to accommodate the new engine placement.

Concept 2: Geared Transfer
The second concept delves into mechanical systems as the means of energy transfer. This concept separates the power generating turboshaft unit from the thrust producing fans and connects them with a shaft and gear system. From initial power estimates it was determined that 14 fans with a $1.2m$ diameter located spanwise should be sufficient to fulfill the thrust and power requirements. For every fan, two gearboxes are present for power transmission. In terms of redundancy, three engine clutches evenly distribute the power in case of a one engine inoperative condition. From the initial calculations, it became apparent that a small cooling system was required for the gear and shaft system.

Concept 3: Hybrid Non-Superconductive Design Option
The next concept features a hybrid system: it consists of conventional mechanical engine cores with electrically driven fans. The primary architecture of the non-superconductive hybrid design option consists of three gas turbines for turboshaft applications located aft of the fuselage. These are connected to generators which then distribute the power to the individual propulsion units located on the entire wing span. Additionally, a battery is installed on board the aircraft for auxiliary usage during power intensive phases such as take-off and climb.

Concept 4: Hybrid Superconductive Design Option
Using superconducting materials enables weight savings compared to the non-superconductive hybrid system, while delivering the required power. The fourth concept takes the projected improvements in engine technologies as well as in specific superconductive materials into consideration. The introduction of superconductive technologies requires the implementation of a cryocooling system in order to enable the superconductivity of the individual components. Liquid hydrogen and liquid methane can be used as coolants or heat sink respectively which, after cooling, can be mixed with conventional jet fuel in specific fractions to be burnt as propellant. The architecture of the hybrid non-superconductive design features two embedded engine cores also located at the back of the aircraft; 10 fans of $0.78m$ diameters provide the required propulsive power. Finally, the fuel tanks are enlarged to comply with the additional space requirements of the cryocooler system which in this case is liquid methane.

Concept 5: Liquid Natural Gas Blended Wing Body
The final concept aims to include distributed propulsion technologies into an unconventional configuration: the blended wing body. The inherent increase in available volume opened the opportunity to investigate alternative fuel sources: liquid natural gas was chosen as the primary energy source. Adaptations on the propulsion system include the incorporation of heat exchangers and cross-flow valves in order to ensure redundancy. The

final architecture features 10 engines located on top of the center section of the BWB so the system benefits from boundary layer ingestion.

3.2 Concept Trade-off Criteria and Weights

In the previous section, five different concepts were presented. In order to select the design that will meet the objective and requirements the best, a trade-off method must be implemented. This section will elaborate on these chosen criteria and the different weights assigned to each of them. To obtain a good comparison, it is necessary to quantify as many criteria as possible. For some criteria (e.g. noise) estimating a concrete value proved to be difficult at this specific design stage; a qualitative approach was thus deemed to be sufficient, and will be backed up with a sensitivity analysis performed in Section 3.3.

3.2.1 Trade-off Criteria

To compare the concepts, trade-off criteria have to be defined. The selected trade-off criteria and their weights are briefly discussed below. For each criterion the relative weight is presented between brackets.

Technology Readiness Level (20%)

The first trade-off criterion that is being considered, is the technology readiness level of the concepts. An analysis has to be done in order to check if the chosen technology used is actually proven technology, still in development or not feasible at all. This criterion is further categorized into the following sub-criteria with its respective sub-weights presented between brackets:

1. Reliability (25%)
2. Safety (25%)
3. Feasibility (50%)

Operability (15%)

The level of operability is another trade-off criterion for the concepts. It involves the level of difficulty to operate the aircraft, costs associated to operations and maintenance of the aircraft. This criterion has a rather high weight, as there is also a requirement set on operating costs. Additionally, the comfort of the passengers in the particular configuration of the concept has to be considered as well. This criterion is divided into the following sub-criteria:

1. Maintainability/Accessibility (50%)
2. Production costs (15%)
3. Passenger comfort (35%)

Stability (5%)

This trade-off criterion concerns the longitudinal stability of the aircraft. In this criterion, it is assessed how difficult it is to acquire longitudinal stability. Parameters affecting its value are the presence of control surfaces and estimation on the center of gravity position and range during nominal operations.

Sustainability (40%)

Sustainability of the concepts is also a trade-off criterion that is taken into account. It involves the ability to reduce CO_2 and NO_x emissions and overall fuel consumption as these are requirements set by the customer. Using a different fuel, like biofuel or hydrogen might be favourable in terms of emissions. In addition, the production and End-of-Life disposal processes must also be taken into account. This is done by looking at the use of environmental harmful or chemical substances like batteries. The sustainability criterion can therefore be sub-categorized as follows:

1. Efficiency and Emissions Reduction (90%)
2. End-of-life Disposal (5%)
3. Production (5%)

Noise Emissions (20%)

As there is a requirement on noise emissions, this has also been made a trade-off criterion. It takes into account the ability of the concept to reduce noise, especially during low altitude operations such as take-off, approach and landing. This criteria is sub-categorized as follows:

1. Fan: The sound produced by the total number of fans. (25%)
2. Shielding: The ability to shield the noise from the environment. (25%)
3. Jet: The sound produced by the exhaust velocity. (25%)
4. Engines: The mechanical sound produced by the engines. (25%)

3.2.2 Final Rating

Using the weights described above and a qualitative and quantitative analysis as presented in the Mid-Term Report [9], the final result is presented below in Table 3.1 and Table 3.2. The Airbus A321 is used as a benchmark and an improvement of a criterion is graded with $+1$, $+2$ or $+3$ depending on how large the improvement is. The same logic holds if something is worse than the A321, hence negative grades are given. As can be seen, the superconductive hybrid is the concept which is selected from the trade-off. The main trade-off criteria which resulted in the hybrid superconductive aircraft, are the sustainability and noise emissions. This was expected, as the main focus of the distributed propulsion aircraft is reducing its harmful emissions and noise.
Although it seems from this trade-off that all concepts are worse than the A321 as they have all negative scores, this is not the case. The technological readiness level is obviously not as good as the A321 and therefore reduces the final score. Also, the operability criterion for every concept is negative because innovation comes at a price.

Table 3.1: Final results of the trade-off procedure

		Rating				
Trade-off Criteria	**Weight**	**Concept 1**	**Concept 2**	**Concept 3**	**Concept 4**	**Concept 5**
1. Technology Readiness Level	**20**	**-0.25**	**-1.00**	**-0.75**	**-1.50**	**-2.50**
1.1 Reliability	25	-2.00	-2.00	0.00	-1.00	-2.00
1.2 Safety	25	1.00	0.00	-1.00	-1.00	-2.00
1.3 Feasibility	50	0.00	-1.00	-1.00	-2.00	-3.00
2. Operability	**15**	**-1.35**	**-2.35**	**-0.30**	**-1.10**	**-1.30**
2.1 Maintainability and Accessibility	50	-2.00	-3.00	-1.00	-2.00	-1.00
2.2 Production Cost	15	0.00	-1.00	-1.00	-3.00	-3.00
2.3 Passenger Comfort	35	-1.00	-2.00	1.00	1.00	-1.00
3. Stability	**5**	**-1.00**	**0.00**	**1.00**	**1.00**	**-3.00**
3.1 Longitudinal	100	-1.00	0.00	1.00	1.00	-3.00
4. Sustainability	**40**	**0.34**	**0.13**	**-1.47**	**0.23**	**-0.02**
4.1 Efficiency and Emissions Reduction	90	0.38	0.14	-1.47	0.54	0.26
4.2 End-of-life Disposals	5	0.00	0.00	-2.00	-3.00	-2.00
4.3 Production	5	0.00	0.00	-1.00	-2.00	-3.00
5. Noise Emissions	**20**	**-0.25**	**0.25**	**0.75**	**0.75**	**0.00**
5.1 Fan noise	25	-2.00	-2.00	-3.00	-2.00	-2.00
5.2 Shielding	25	1.00	2.00	1.00	1.00	2.00
5.3 Jet	25	0.00	3.00	3.00	2.00	0.00
5.4 Engines	25	0.00	-2.00	2.00	2.00	0.00
	Final	**-0.2157**	**-0.4521**	**-0.5824**	**-0.1724**	**-0.8532**

Table 3.2: The breakdown of the efficiency/emissions sub-criteria

				Rating				
			Weight	C.1	C.2	C.3	C.4	C.5
4.1	**Efficiency and Emissions Reduction**			**0.38**	**0.14**	**-1.465**	**0.535**	**0.255**
	4.2.1	**MTOW**	**25**	**0.52**	**-0.44**	**-0.86**	**-0.86**	**0.02**
		4.2.1 Vertical Tail	8	1	2	3	3	3
		4.2.2 Horizontal Tail	8	3	0	0	0	-1
		4.2.3 Landing Gear	10	1	3	1	1	-1
		4.2.4 High Lift Devices	10	0	0	0	0	-1
		4.2.5 Ailerons	4	0	0	0	0	-1
		4.2.6 APU	10	1	1	3	3	1
		4.2.7 Propulsion system	50	0	-2	-3	-3	0
	4.2.2	**SFC**	**50**	**0**	**0**	**-3**	**1**	**-1**
	4.2.3	**Lift/Drag**	**25**	**1**	**1**	**1**	**1**	**3**

3.3 Sensitivity Analysis

This section will cover the sensitivity analysis for the different design options that are currently being considered. This analysis will allow the assessment of the robustness of design options, when there are changes in system input parameters. It can also give an overview of the allowed extent to which these parameters can change. For consistency, all important input parameters will be increased or decreased by 5%, and the relative increase or decrease to related parameters are stated. The increase or decrease of input parameters will be based on the most detrimental consequences to performance and weight.

3.3.1 Performance Sensitivity Analysis

A sensitivity analysis related to different performance topics has been presented in the Mid-Term Report [9]. All five concepts have been analyzed in terms of range, aerodynamic efficiency and specific fuel consumption. Next to that, cruise speed and altitude, payload and field length were included.

3.3.2 Trade-off Sensitivity Analysis

As part of the sensitivity analysis, a closer look was also taken at the actual trade-off. For each rated criterion, an estimate was made in what amount it was expected to vary. A worst case and a best case scenario was evaluated for each concept. Some criteria are not expected to vary at all, because they are fairly certain and other are relatively more uncertain. Therefore, in Table 3.4 it can be seen that some ratings do not vary at all, whilst others vary substantially.
The worst case and the best case scenario for the different concepts are summarized in Table 3.3. The extensive analysis and the results obtained using the different ratings can be seen in Table 3.4. These results are also plotted in Figure 3.1.

The other concepts, except for the GTF, deviate enough from the hybrid concept to be discarded. The sensitivity analysis for the GTF comes relatively close to the superconducting hybrid. When assigning the worst possible grades, the superconducting hybrid still has the best rating. For the best case scenario, the superconducting hybrid also has the best rating. It can thus be concluded from the sensitivity analysis that the superconducting hybrid consistently comes out as the best possible concept.

Table 3.3: Sensitivity analysis values

Concept	Final Grade	Worst Case	Best Case
GTF	-0,216	-0,224	-0,202
Geared Transfer	-0,452	-0,492	-0,416
Hybrid	-0,582	-0,623	-0,533
SC Hybrid	-0,172	-0,182	-0,148
BWB Gas	-0,853	-0,932	-0,787

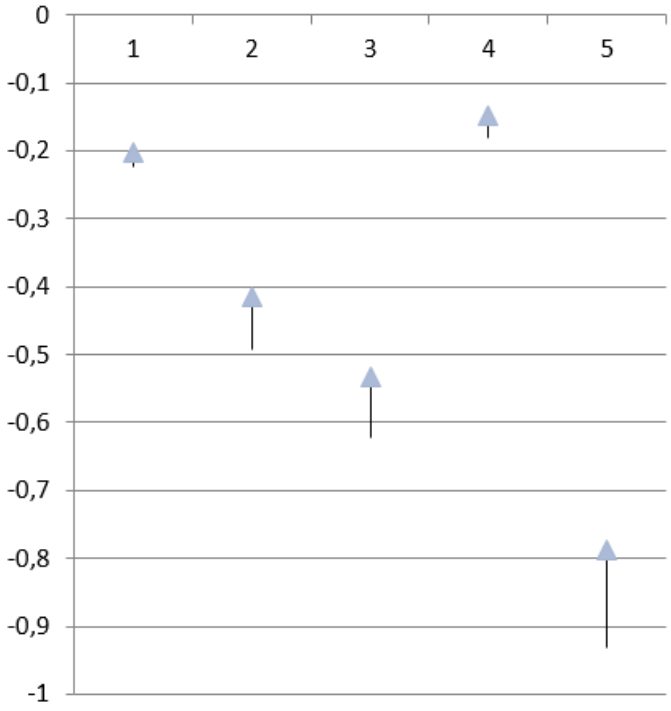

Figure 3.1: Plotted values for the sensitivity analysis. From left to right: GTF, Geared transfer, Hybrid, SC Hybrid and BWB Gas

Table 3.4: Trade-off criteria ratings and uncertainties

	Weight	C.1			C.2			C.3			C.4			C.5		
Trade-off Criteria	**Sub**	**Rating**	**Worst**	**Best**	**Rating**	**Worst**	**Best**	**Rating**	**Worst**	**Best**	**Rating**	**Worst**	**Best**	**Rating**	**Worst**	**Best**
1. Technology Readiness	20	-0.25	-0.25	-0.25	-1.00	-1.00	-0.90	-0.75	-0.75	-0.68	-1.50	-1.50	-1.26	-2.50	-2.65	-2.30
1.1 Reliability	25	-2.00	-2.00	-2.00	-2.00	-2.00	-1.80	0.00	0.00	0.00	-1.00	-1.00	-0.90	-2.00	-2.00	-1.80
1.2 Safety	25	1.00	1.00	1.00	0.00	0.00	0.00	-1.00	-1.00	-0.90	-1.00	-1.00	-0.95	-2.00	-2.00	-2.00
1.3 Feasibility	50	0.00	0.00	0.00	-1.00	-1.00	-0.90	-1.00	-1.00	-0.90	-2.00	-2.00	-1.60	-3.00	-3.30	-2.70
2. Operability	15	-1.35	-1.40	-1.27	-2.35	-2.52	-2.31	-0.30	-0.34	-0.27	-1.10	-1.23	-1.03	-1.30	-1.45	-1.27
2.1 Maintainability and Accesibility	50	-2.00	-2.10	-1.90	-3.00	-3.30	-3.00	-1.00	-1.10	-0.95	-2.00	-2.20	-1.90	-1.00	-1.10	-1.00
2.2 Production Cost	15	0.00	0.00	0.00	-1.00	-1.10	-0.95	-1.00	-1.05	-0.95	-3.00	-3.30	-2.85	-3.00	-3.45	-3.00
2.3 Passenger Comfort	35	-1.00	-1.00	-0.90	-2.00	-2.00	-1.90	1.00	1.05	1.00	1.00	1.05	1.00	-1.00	-1.10	-0.90
3. Stability	5	-1.00	-1.05	-0.95	0.00	0.00	0.00	1.00	1.00	0.90	1.00	1.00	0.90	-3.00	-3.45	-2.85
3.1 Longitudinal	100	-1.00	-1.05	-0.95	0.00	0.00	0.00	1.00	1.00	0.90	1.00	1.00	0.90	-3.00	-3.45	-2.85
4. Sustainability	40	0.34	0.36	0.32	0.13	0.14	0.13	-1.47	-1.54	-1.40	0.23	0.27	0.15	-0.02	-0.02	0.00
4.1 Efficiency and Emissions Reduction	90	0.38	0.40	0.36	0.14	0.15	0.14	-1.47	-1.54	-1.39	0.54	0.59	0.43	0.26	0.28	0.26
4.2 End-of-life Disposals	5	0.00	0.00	0.00	0.00	0.00	0.00	-2.00	-2.00	-2.00	-3.00	-3.15	-2.85	-2.00	-2.10	-1.90
4.3 Production	5	0.00	0.00	0.00	0.00	0.00	0.00	-1.00	-1.05	-0.95	-2.00	-2.10	-1.90	-3.00	-3.30	-2.70
5 Noise Emissions	20	-0.25	-0.28	-0.23	0.25	0.15	0.30	0.75	0.71	0.79	0.75	0.73	0.78	0.00	-0.03	0.03
5.1 Fan noise	25	-2.00	-2.10	-1.90	-2.00	-2.10	-1.90	-3.00	-3.15	-2.85	-2.00	-2.10	-1.90	-2.00	-2.10	-1.90
5.2 Shielding	25	1.00	1.00	1.00	2.00	2.00	2.00	1.00	1.00	1.00	1.00	1.00	1.00	2.00	2.00	2.00
5.3 Jet	25	0.00	0.00	0.00	3.00	3.00	3.00	3.00	3.00	3.00	2.00	2.00	2.00	0.00	0.00	0.00
5.4 Engines	25	0.00	0.00	0.00	-2.00	-2.30	-1.90	2.00	2.00	2.00	2.00	2.00	2.00	0.00	0.00	0.00

Chapter 4 | Design Method

In order to properly quantify the potential benefits of a distributed propulsion system with respect to a conventional configuration aircraft, a common design method needs to be created. This chapter discusses the approach that was taken to design the two different aircraft: it describes all the steps to design the aircraft, the procedures and methods used.
To design the aircraft, Roskams method is chosen. In the case this method is not available for a certain system, a different method has been chosen, which will be indicated in its respective section. This chapter closely follows Roskams methodology and is divided as follows: Section 4.1 and 4.2 present the Class I weight estimation and the wing loading diagram, respectively. Sections 4.3 and 4.5 delve more deeply into the design process by treating the initial planform and fuselage design, whereas Section 4.4 discusses the control surfaces design. The propulsion system is briefly treated in Section 4.6. The Class II weight estimation follows in Section 4.7, whereas the empennage sizing method is treated in Section 4.8. This chapter is concluded with a drag estimation in Section 4.9 and the explanation of the iteration process in Section 4.10.

4.1 Class I Weight Estimation

To make a first estimate of the operational empty weight (OEW) and maximum take-off weight (MTOW), a Class I weight estimation is performed. This was based on reference aircraft of similar roles, shown in Table 4.1. This table also includes the amount of passengers for each aircraft, as this serves as a top-level requirement and can thus be used to size for the MTOW. Furthermore, an estimation of the OEW can be made.
The aircraft shown in the table have comparable roles in terms of the aircrafts passenger capacity and range. It is expected that the MTOW and OEW will also lie in those regions.

Table 4.1: Operational empty weight and take-off weight for reference aircraft in comparable roles [10]

Aircraft	Passengers	OEW [kg]	MTOW [kg]
Airbus A319-100	156	40160	64000
Airbus A320-200	180	42200	73500
Airbus A321-200	220	48500	89000
Boeing 717-200	117	31674	49900
Boeing 727-200	189	46700	95000
Boeing 737-700	126	38147	70080
Boeing 737-800	162	41145	70535
Boeing 737-900	177	42493	74390
Boeing 757-200	239	59295	115665
Bombardier CS100	125	33340	53060
Comac C919	168	42100	74300
Douglas DC-8-32	176	60781	140614
Embraer ERJ-195	118	28550	48790
Ilyushin Il-62	174	71600	165000
Irkut MS-21	162	35000	67600
McDonnell Douglas MD-87	139	33200	63500
McDonnell Douglas MD-90-30	172	39916	70760
Sukhoi SSJ100	98	25100	49450
Tupolev Tu-154M	160	55300	104000
Tupolev Tu-204-300	164	58300	107500

To make an estimation of the aforementioned weights, linear regression is performed. The data points of the aircraft and the regression can be seen in Figure 4.1. This gives the relation that can be used to calculate the OEW and MTOW.
Now that the relation between OEW and MTOW has been found, the design MTOW can be calculated. The equation used can be found in Equation (4.1).

$$\begin{aligned} W_{TO} &= W_E + W_F + W_{PL} + W_{tfo} \\ &= (0.383 \cdot W_{TO} + 11640.2) + M_{f_{used}} W_{TO} + W_{PL} + M_{tfo} W_{TO} \end{aligned} \tag{4.1}$$

The payload weight, W_{PL}, has been defined in the requirements as $18500kg$. The mass fraction of trapped fuel and oil, M_{tfo}, is approximately 0.002 [11]. The fuel weight, W_F, can be calculated using the fuel weight

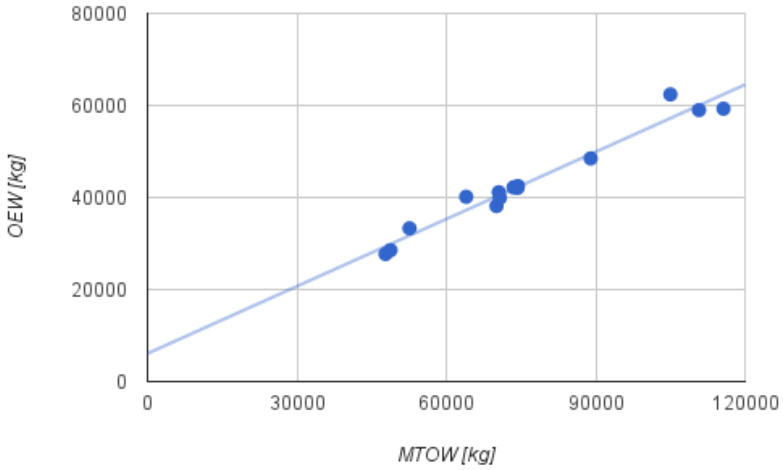

Figure 4.1: Linear regression of the OEW versus the MTOW

ratios for each flight phase. The mission profile can be found in Figure 4.2. For the cruise flight phase, the fuel fractions have been calculated using the Breguet range and endurance equations shown in Equations (4.2) and (4.3). The other flight phase fractions were estimated using Roskam [12].

$$R = \left(\frac{V}{g \cdot c_j}\right)_{cruise} \cdot \left(\frac{L}{D}\right)_{cruise} \cdot \ln\left(\frac{W_{start}}{W_{end}}\right) \tag{4.2}$$

$$E = \left(\frac{1}{g \cdot c_j}\right)_{loiter} \cdot \left(\frac{L}{D}\right)_{loiter} \cdot \ln\left(\frac{W_{start}}{W_{end}}\right) \tag{4.3}$$

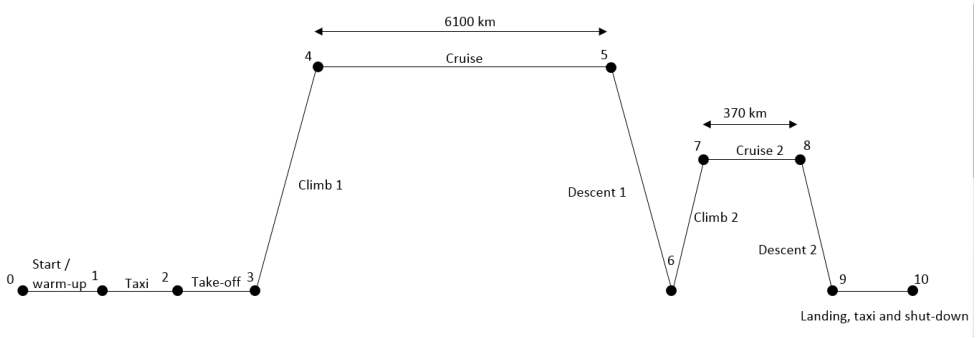

Figure 4.2: Mission profile for Vimana and the reference aircraft

4.2 Wing and Thrust Sizing

With an estimate of the MTOW present, an analytical approach to the wing sizing is taken. For the aircraft a T/W-W/S range can be made to show the possible design points, mostly determined by the aircraft limits in-flight. For this, estimations have to be made, together with the estimation of values. These estimations are mostly based on typical values and will be discussed individually. Having these parameters available, together with the aircraft weight, it is possible to compute the required thrust and wing area.

For an optimal design, the T/W value should be as low as possible, because a decrease in thrust implies a further decrease in engine weight as well. Furthermore, the value for W/S should be as high as possible, to have the lowest possible wing area, which lowers drag. Both characteristics imply snowball effects, reducing the overall aircraft weight.

4.2.1 Sizing for Stall Speed

The first limit is defined by the stall speed. With this stall speed the wing loading can be found by equalling thrust and weight. By dividing the lift equation (Equation (4.4)) by the surface area, an equation for W/S is formed, as shown in Equation (4.5). This equation depends on the lift coefficient, which is maximal prior to stall, the velocity, which is minimal before stall, and the density, which is given at a certain height. This defines the wing loading for the stall speed.

$$L = W = \frac{1}{2} C_L \rho S V^2 \tag{4.4}$$

$$\left(\frac{W}{S}\right)_{stall} = \frac{1}{2} C_{L_{max}} \rho V_{stall}^2 \tag{4.5}$$

For the lift coefficient it is initially assumed that it is similar to comparable aircraft, which is approximately $C_{L_{max}} = 3$. Equation (4.5) does not depend on T/W, therefore the resultant W/S will be constant. This equation results in a vertical line in the T/W-W/S diagram.

4.2.2 Sizing for Take-off

Take-off is a crucial flight phase for each aircraft, as it accounts for over 20% of all fatal accidents[1]. Therefore it is crucial to have a good understanding of the limits during this flight phase, which are largely defined by the take-off field length. This phase also includes an airborne segment of $35ft$ or $10.7m$ as a clearance height, after which the climb will be performed. The field length has a statistical relationship with the Take-Off Parameter, as shown in Figure 4.3. The TOP itself is defined as:

$$TOP = \left(\frac{W}{S}\right)_{TO} \left(\frac{W}{T}\right)_{TO} \frac{1}{C_{L_{TO}}} \frac{\rho_0}{\rho} \tag{4.6}$$

The $\frac{W}{S}$ and $\frac{W}{T}$ fractions are to be determined, and at sea level conditions $\frac{\rho_0}{\rho}$ will be 1. The empirical value of the TOP can be determined using Figure 4.3, as a function of the field length. In this way, the value for the thrust loading T/W can be found.

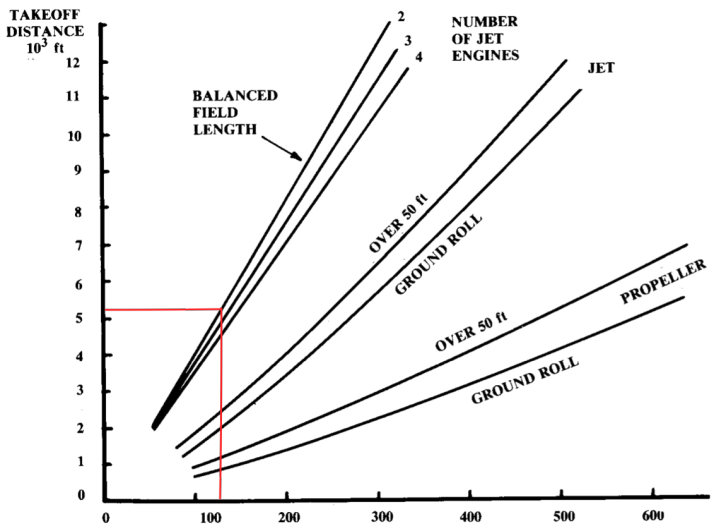

Figure 4.3: Field length as a function of the Take-Off Parameter

4.2.3 Sizing for Landing

When the aircraft is coming in for landing, it will be subjected to stall speed limits, but also to the runway length. During the actual landing phase this is the critical parameter that determines the wing loading limit. For the stall speed requirement, Equation (4.7) holds.

[1] URL "http://www.planecrashinfo.com/cause.htm", [cited 16 June 2015]

$$L = W = \frac{1}{2}\rho C_L S V^2 \tag{4.7}$$

During the landing phase, the weight will be significantly lower compared to the take-off weight. This reduction is accounted for by applying a factor f. A relation for the landing velocity is used that is based on the landing distance, which is an empirical method given by Melkert [11]:

$$V_L = \sqrt{\frac{s_{land}}{0.5847}} \tag{4.8}$$

Combining Equations (4.7) and (4.8), an approximation of the wing loading limit is made:

$$\left(\frac{W}{S}\right)_{land} = \frac{1}{2}\ \rho\ C_{L_{max}} \frac{s_{land}}{0.5847 f} \tag{4.9}$$

Again, the relation is independent of the T/W parameter, thus resulting in a vertical line which defines the limit.

4.2.4 Sizing for Climb Rate

The climb rate performance of an aircraft determines how fast it can traverse vertically, i.e. its vertical velocity. The importance of this parameter is that it allows the aircraft to reach its cruise altitude fast in order to reduce fuel burns. By the definition of the climb rate:

$$c = \frac{P_a}{W} - \frac{P_r}{W} = \frac{TV}{W} - \frac{DV}{W} \tag{4.10}$$

The assumption that lift equals weight results in Equation (4.11) and rewriting results in Equation (4.11).

$$\frac{TV}{W} - \frac{C_D V}{C_L} = \frac{TV}{W} - \frac{C_D}{C_L^{\frac{3}{2}}}\sqrt{\frac{W}{S}\frac{2}{\rho}\frac{1}{C_L}} \tag{4.11}$$

$$\left(\frac{T}{W}\right)_{rate} = \frac{c}{\sqrt{\frac{W}{S}\frac{2}{\rho}\frac{1}{C_L}}} + \frac{C_D}{C_L} \tag{4.12}$$

4.2.5 Sizing for Climb Gradient

The climb gradient is the ratio between the climb rate and the airspeed. A high climb gradient mainly reduces the horizontal traversed distance, thus making it an important characteristic for aircraft in the vicinity of high obstacles. The gradient is defined in Equation (4.13) and rewriting results in Equation (4.14). There is no dependency on $\frac{W}{S}$, meaning that the value for $\frac{T}{W}$ is constant. On the diagram this results in a horizontal line.

$$\gamma = \frac{c}{V} = \frac{T}{W} - \frac{D}{W} = \frac{T}{W} - \frac{C_D}{C_L} \tag{4.13}$$

$$\left(\frac{T}{W}\right)_{grad} = \frac{c}{V} + \frac{C_D}{C_L} \tag{4.14}$$

4.3 Airfoil Selection and Wing Planform Design

After determining the wing loading, the wing area can be determined using the weight estimated in Section 4.1. This is done using Equation (4.15). The design lift coefficient can be determined using Equation (4.16).

$$S = \frac{W_{start_{cruise}} + W_{end_{cruise}}}{2}\left(\frac{W}{S}\right)^{-1} \tag{4.15}$$

$$C_{ldes} = 1.1\frac{1}{q_s}\frac{1}{cos^2\Lambda}\left(\frac{1}{2}\left[\left(\frac{W}{S}\right)_{start_{cruise}} + \left(\frac{W}{S}\right)_{end_{cruise}}\right]\right) \tag{4.16}$$

Now that the wing surface area and the design C_l are determined, a database of relevant airfoils is constructed. These airfoils are the NACA 5 and 6 series as well as supercritical airfoils. Using the Korn equation[2] as given by Equation (4.17), the drag divergence mach number was calculated. Using this drag divergence number, the leading edge sweep can be calculated for each airfoil using Equation (4.18) [13] where $M_{cr_{swept}}$ is 0.82.

$$M_{dd} = k - \frac{C_l}{10} - \frac{t}{c} \tag{4.17}$$

$$\Lambda_{LE} = cos^{-1} \frac{M_{dd}}{M_{cr_{swept}}} \tag{4.18}$$

Using the data obtained from these calculations, the airfoils were compared in terms of sweep angle required, at what lift coefficient they would be flying (the closer to the design lift coefficient, the better), the drag at cruise conditions and on their thickness to chord ratio. From this comparison, a final airfoil is chosen. In Table 4.2, the considered airfoils can be found with their design lift coefficient, thickness over chord ratio, and drag divergence mach number. The airfoil choice will also determine the sweep angle and wing incidence angle.

Table 4.2: Airfoils considered for the design

Airfoils	**Design C_l**	**t/c**	**M_{dd}**
NACA 63-415	0.4	0.15	0.68
NACA 63-412	0.4	0.12	0.71
NACA 23012	0.3	0.12	0.72
NACA 23015	0.3	0.15	0.69
NACA 23018	0.3	0.18	0.66
SC(2)-0714 Supercritical airfoil	0.7	0.139	0.74
Whitcomb Integral Supercritical Airfoil	0.4	0.11	0.741
CAST 7	0.76	0.118	0.756
CESSNA EJ Red. Airfoil	0.508	0.115	0.7842
NLR 7301	0.45	0.163	0.742
SC(2)-0710 Supercritical airfoil	0.7	0.1	0.78
SKF 1.1	0.532	0.1207	0.7761
NPL 9510	0.6	0.11	0.78
SC(3)-0712(B)	0.7	0.12	0.76

Taper Ratio

After the primary wing planform parameters are chosen, the taper ratio has to be defined. A wing with taper ratio of 1 would be the easiest to manufacture and would have the largest fuel storage volume, but would also have a much larger weight than necessary. Because the lift will decrease to zero at the wing tip it is useful to decrease the tip chord length. This will also reduce the induced drag, because it makes the lift distribution get closer to an elliptical lift distribution, which has the best drag characteristics. A downside to a low taper ratio is an increased risk for tip stall. Because the wing tip will have a lower Reynolds number, the maximum lift coefficient will be lower too. Therefore the taper ratio must not be lower than 0.2 [13].

Wing Twist Angle

In order to decrease wing tip stall, a wing twist angle may be desired. This will decrease the angle of attack of the wing tip, and thus delay the tip stall. In general, twist angles of only a few degrees are used.

Dihedral Angle

The dihedral angle is used to guarantee ground clearance and ensure extra stability. For low-wing aircraft with wing-mounted engines this angle is approximately 5 degrees. Without wing-mounted engines, it can be lower.

[2] URL "http://www.dept.aoe.vt.edu/~mason/Mason_f/ConfigAeroTransonics.pdf", [cited 20 May 2015]

4.4 Control Surfaces

To adequately steer the aircraft in-air control surfaces are used, which can be divided in primary and secondary control surfaces. The primary controls are vital for the controllability of the aircraft, whereas the latter only enhance the performance characteristics.

4.4.1 Primary Control Surfaces

The aircraft's attitude should be controllable in all directions, thus imposing the need of ailerons, rudder and elevator. An explanation of the used method is presented below.

Ailerons

Ailerons are the aircraft's main mechanism for lateral control. In a similar way as high lift devices, ailerons increase or decrease the effective chord at that particular wing span and hence a difference in lift arises between both wings resulting in a rolling moment about the longitudinal axis. Two main parameters are of vital importance during the aileron sizing: the force exerted and the moment arm. Both parameters are thus coupled to the aileron area and their wing span position.
When considering a design featuring only outboard ailerons two paramount safety issues arise: tip stall and reversal phenomena. The first one concerns the spanwise order on which stall occurs on a wing; if it starts on the trailing edge of the most outboard span position, the ailerons may become ineffective, seriously endangering the controllability of the aircraft. Hence, if such a design choice is made, utmost care should be taken in developing a control and monitor system that prevents this effect from happening. Reversal phenomena, on the other hand occur when the entire wing is twisted due to the high aileron forces, resulting in the opposite desired attitude of the aircraft.

Rudder

Located at the back of the vertical tail surface, the rudder provides yaw control to the aircraft, which is mainly relevant during the landing phase. In general, the rudder is located along the complete chord of the vertical tail. The difference in design of the distributed propulsion aircraft is that the tail will be significantly smaller or even non present due to the possibility of sizing it on the stability and controllability characteristics, rather than the one motor inoperative (OMI) condition. This requires some additional attention as it is likely to have a smaller chord and thus a smaller possible rudder. This can be solved by adapting a differential thrust strategy, in which yaw control is performed by varying the thrust in an asymmetric manner. This brings up the additional problem that traditional turbines cannot be used, as these suffer from lag effects, delaying the yaw control.

Elevator

The elevator is located at the back of the horizontal tail surface and provides pitch control. It cannot benefit from any specific distributed propulsion characteristics and will therefore be very similar to a conventional elevator. For the horizontal tail surface, the complete trailing edge can be used for the elevator, meaning that sizing the horizontal tail surface will lead to sizing the elevator as well.

4.4.2 Secondary Control Surfaces

The increment of lift coefficient should be obtained by a combination of trailing edge and leading edge high lift devices (HLD). In general, leading edge HLD do not provide a significant increase in lift coefficient, but merely delay the flow separation on the wing [11].

Trailing Edge HLDs

To increase the lift during landing and take-off, and thus lowering the minimal speed at these phases, the aircraft can be equipped with flaps. In reality all modern commercial and military aircraft use flaps, as an increase of lift is not necessary during cruise and would only further increase the drag and thus the fuel consumption.
As the aircraft maximum lift coefficient and maximum landing coefficient can be assumed to be 1.4 and 3 respectively, based on the A321, an increase in C_L of 1.6 can be expected to be needed by the high lift devices. This increase will mainly be created by the flaps at the trailing edge.

In an ideal case, the flaps should be placed along the complete trailing edge of the wing, to maximize the lift increase during flap-down situation. However, some place has to be reserved for ailerons. Furthermore a part of the wing area is inside the fuselage, and it is assumed that placing flaps near the tip is not possible due to the small local thickness. An example of the flapped wing area is shown in Figure 4.4, which is the area of the wing which has a flap at its trailing edge. For the A321, the fraction of area with flaps over the total area $\frac{S_{wf}}{S}$ is in the range of 0.75-0.85. This value is estimated with a schematic drawing, as no sources are available for this parameter.

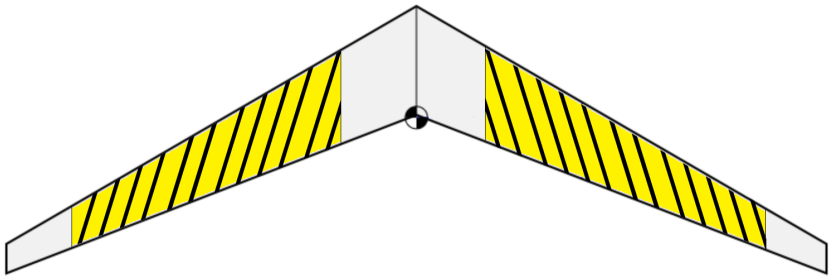

Figure 4.4: Visual representation of the flapped wing area (striped) and the total wing area (striped and grey)

To size for the high lift devices, Roskams method [14] is used. The increment in landing lift coefficient is given by Equation (4.19).

$$\Delta C_{L_{max_L}} = 1.05(C_{L_{max_L}} - C_{L_{max}}) \tag{4.19}$$

This means that the sizing should at least accommodate for this increase. The factor of 1.05 accounts for additional trim penalties because of the use of flaps. The flap type should be optimal such that it provides a sufficient increase in lift, but at the same time be easy to maintain and be unlikely to fail. The different flap type configurations are shown in Table 4.3. Here it can be seen that the triple slotted Fowler flaps are very effective, which comes at the cost of a high complexity. As a comparison, the Airbus A321 uses double slotted Fowler flaps.
For the distributed propulsion aircraft it is also possible to make use of blown flaps, which uses the exhaust stream of the engines to make the flaps more effective. This is specifically interesting for distributed propulsion, as it can be applied over a larger section of the extended flaps compared to conventional aircraft. However, the most critical phase in terms of flap devices is during landing. In this situation the fans are almost idle. Therefore, this effect has been neglected for this point in time. More research has to be done as will be presented in Chapter 14.

Table 4.3: Different TE HLD configurations with their increase in lift and configuration complexity. [13]

Flap Type	$\Delta C_{L_{max}}$	Complexity
Plain	0.9	Low
Split	0.9	Low
Slotted	1.3	Average
Fowler Single Slotted	1.3 c'/c	Average
Fowler Double Slotted	1.6 c'/c	High
Fowler Triple Slotted	1.9 c'/c	High

Leading Edge HLDs

Leading edge HLDs have a limited effect on the lift coefficient due to their marginal increase in chord length, but have a beneficial effect on the flow separation near the leading edge. Table 4.4 shows the different slat options available. For the leading edge, a similar parameter as S_{wf}/S exists, which is close to one, as these HLDs are usually located along the whole leading edge. Only near the wingtips and the root, the leading edge HLDs are not present.

Table 4.4: Different LE HLD configurations with their increase in lift and configuration complexity. [13]

Slat Type	$\Delta C_{L_{max}}$	Complexity
Fixed Slot	0.2	Low
Leading Edge Flap	0.3	Average
Kruger Flap	0.3	High
Slat	0.4 c'/c	High

4.5 Fuselage Design

From requirements given by the Joint Aviation Regulations (JAR) [15], several requirements are identified for the fuselage design. For 180 passengers it is required to have 2 type I and 2 type III exits on each side of the fuselage. A type I exit is a floor level exit of at least $0.61m$ wide and $1.22m$ high. A type III exit is a rectangular opening of no less than $0.51m$ wide by $0.91m$ high with corner radii not larger than $0{,}18m$ and with a step up of no more than 20 inches. It is also required that no more than 3 seats are on either side of the aisle and the aisle is at least $0.51m$ wide. If these exits are over $1.83m$ of the ground, a means of descent should be provided, e.g. a ladder or a slide.
For the fuselage, a seat pitch of $0.79m$ is used and a seat width of $0.56m$. A lavatory length and width of 1.02 by $1.02m$ is used and a galley length of $1.52m$ is used. The galleys will take up the entire width of the fuselage. It is assumed that one galley and four toilets are sufficient for the amount of passengers [16].
For the nose and tail of the fuselage, a fineness ratio is selected using Roskam [16] optimized for the cruise speed of mach 0.78. Fineness is the ratio between the length of a part and its diameter. For the tail the fineness ratio is selected to be 2.25 and for the nose the fineness ratio is selected to be 1.14.
Adding the length of 30 rows of seats, 4 aisles for the (emergency) exits, two rows of lavatories, the tail and the nose, the total length of the fuselage is computed. It is assumed the galley is inside the root of the tail. A total fuselage length is computed of $40.14m$. Using the seat width, the aisle width and a clearance of $0.13m$ next to the outside seats, an inner cabin width of $3.50m$ is computed. It is assumed the fuselage is $15cm$ thick, thus the outside diameter will be $3.80m$.
The cargo bay width is set to be $1.14m$ to fit the standard A321 LD-3-45W containers[3]. If the entire length of the seating area is used to store cargo, 15 of these containers can be carried. This is however not expected since some of the potential cargo area will be occupied by the center wing box.
To offer sufficient passenger comfort, every row of seats will have at least one window on each side. Therefore it is chosen to use a window pitch of $0.66m$ and a total of 36 windows will be installed on each side of the fuselage. An overview of the dimensions mentioned in this section is given in Table 4.5.

Table 4.5: Fuselage dimensions and configuration parameters

Parameter	Value	Unit
Fuselage outer diameter	3.8	$[m]$
Seat pitch	0.79	$[m]$
Seat width	0.46	$[m]$
Window pitch	0.66	$[m]$
Lavatory dimensions (L x W)	1.01 x 1.01	$[m]$
Galley length	1.52	$[m]$
Tail fineness ratio	2.25	$[-]$
Nose fineness ratio	1.14	$[-]$

4.6 Propulsion System

Since the main feature of the Distributed Propulsion aircraft is the propulsion system, it is described in a separate chapter, Chapter 6.
The main difference with the distributed propulsion aircraft is that the reference aircraft features a conventional propulsion system, comparable to the current generation of commercial aircraft. This significantly reduces the

[3]URL "http://www.anacargo.jp/en/int/service/aircraft/a320_1.html", [cited 5 June 2015]

complexity of the system, and thus increases the technology readiness level to 9. An empirical approach towards designing the propulsion system using scaling is therefore not necessary and existing turbofan engines can be used.
Table 4.6 contains thrust levels and weights for different engine options, which also includes an SFC for each engine. These engines have been chosen due to their recent use in comparable commercial aircraft, as well as the thrust range. The PW1135G and LEAP 1A are both options on the Airbus A321neo and because these do not have a weight specified by the manufacturer yet, a linear regression has been performed to make an estimate, which is shown in Figure 4.5. The regression is based on comparable engines in terms of expected size and role, yielding Equation (4.20).

$$W = 0.0159 \cdot T + 276.247 \tag{4.20}$$

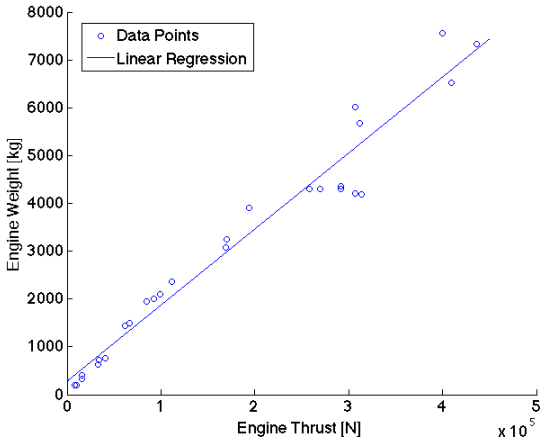

Figure 4.5: Linear regression of the engine weight versus the engine thrust.

Table 4.6: Performance parameters for different engine options on the reference aircraft.

Manufacturer	Model	Thrust [kN]	Weight [kg]	SFC [mg/Ns]
CFM International	CFM56-5C2	151	2587	9.05
Pratt & Whitney	PW2037	170	3314	9.06
Pratt & Whitney	PW1135G	160	3028	7.66
General Electric	LEAP 1A	146	2781	7.81
International Aero Engines	V2533-A5	147	2359	15.36

4.7 Class II Weight Estimation

Using the designed subsystems of the aircraft, the overall dimensions of the aircraft are known and a Class II weight estimation is performed using methods from Roskam [17]. From this, a weight is determined for each components such as the wing, the fuselage and the vertical tail. Using this, the center of gravity of the airplane can be determined for different wing positions and loading diagrams can be generated. This will be used to determine the empennage size and the wing position.
The Operational Empty Weight (OEW) from this method will be used to compare to the Class I weight estimation and if necessary the design process will be iterated.

4.8 Empennage Design

In terms of stability, the empennage is a vital part of the aircraft. The horizontal tail surface must counteract the moment on the wing against pitch movement, whereas the vertical tail surface prohibits yaw- and roll moment. Furthermore, it holds the rudder and elevator, which are both vital for the aircraft's controllability.

The driving parameters for the tail sizing are the tail arm, which is the distance between the aerodynamic centers of the wing and the tailplane, and the tail volume. The tail volume is estimated from reference aircraft, while the surface ratio can be obtained from the stability and controllability diagrams. These should be created first, after a first weight estimation is made for the Class II weight estimation described before.
Because the Class II weight estimation results in weights for each component and an estimated c.g. position of each component, the combined c.g. of the empty aircraft can be calculated. When this is divided into a 'wing group' and a 'fuselage group', the longitudinal wing position can be changed for stability and controllability reasons.
For a number of longitudinal wing positions, passengers, cargo and fuel is loaded to assess the maximum c.g. range the aircraft experiences, thus a loading diagram can be made. From multiple loading diagrams, a c.g. range diagram can be created. This shows the front and rear c.g. positions with respect to the LEMAC position for every wing position. This diagram will be used in combination with the stability and controllability curves, which results in an optimal ratio for S_h/S.
The stick-fixed static stability curve can be calculated using Equation (4.21).

$$\bar{x}_{cg} = \bar{x}_{ac} + \frac{C_{L\alpha_h}}{C_{L\alpha}}\left(1 - \frac{d\epsilon}{d\alpha}\right)\frac{S_h l_h}{S\bar{c}}\left(\frac{V_h}{V}\right)^2 - S.M. \tag{4.21}$$

In this equation, $\bar{x}_{cg}$ is the c.g. position, $\bar{x}_{ac}$ is the aerodynamic center of the aircraft without the tail, $C_{L\alpha_h}$ is the lift rate coefficient of the horizontal tail, $C_{L\alpha}$ is the lift rate coefficient of the aircraft without the tail, $\frac{d\epsilon}{d\alpha}$ is the downwash effect of the wing on the tail, l_h is the tail arm, $\left(\frac{V_h}{V}\right)^2$ is the tail/wing speed ratio due to the perturbing presence of the fuselage, and $S.M.$ is the stability margin, which is not a requirement, but allows for other constraints besides stability. Generally, this is approximately 0.05 [18].
Now also the controllability curve has to be created, using Equation (4.22).

$$\bar{x}_{cg} = \bar{x}_{ac} - \frac{C_{m_{ac}}}{C_{L_{A-h}}} + \frac{C_{L_h}}{C_{L_{A-h}}}\frac{S_h l_h}{S\bar{c}}\left(\frac{V_h}{V}\right)^2 \tag{4.22}$$

In this equation, $C_{m_{ac}}$ is the zero lift pitching moment coefficient of the aircraft without tail, $C_{L_{A-h}}$ is the lift coefficient of the aircraft without tail and C_{L_h} is the lift coefficient of the tail.
With these four curves, a so called X-plot can be assembled using the dimensionless c.g. position on the x-axis and the dimensionless LEMAC position and S_h/S on the y-axes. These plots should then be matched by making sure the intersection between the minimum c.g. position and the controllability curve, and the intersection between the maximum c.g. position and the stability curve are at the same LEMAC position and Sh/S ratio. This should be done by scaling the y-axes. This results in an optimal value for wing position and Sh/S. Using this Sh/S value, the tail length and the entire horizontal tail can be sized. The leading edge sweep angle of the horizontal tail generally is 10% higher than the leading edge sweep angle of the wing. The airfoil should be a symmetric airfoil, because the horizontal tail should be able to generate lift upward or downward when it is trimmed. The vertical tail will mainly be sized for stability and controllability. Its tail volume will be sized using statistics from similar aircraft.

4.9 Drag Estimation

To estimate the lift over drag ratio of the aircraft, the method described in Roskam is used [19]. This method is based on the fact that drag has two sources, zero-lift drag and drag due to lift. These drag sources are then evaluated for different parts of the aircraft, such as the fuselage, the wing, the empennage and nacelles. These different drag terms are then added up to find the total drag of the aircraft. In Figure 4.6 a typical drag breakdown is presented.

4.9.1 Method Adaptation for Distributed Propulsion

The method supplied by Roskam is modified to be used for the distributed propulsion aircraft. This is done to incorporate the drag reduction effects of boundary layer ingestion and wake filling. The drag estimation method is adapted at two different points. First the zero-lift drag of the wing is reduced by 5%. Secondly, the zero-lift drag of the fuselage is decreased by 10%. These drag reductions are assumed to be obtained due to the use of boundary layer ingestion and wake filling by the propulsion system [2], [21] [4].

[4] URL "http://2014.oversetgridsymposium.org/assets/presentations/2_5/Pandya_ogs_2014.pdf", [cited 17 June 2015]

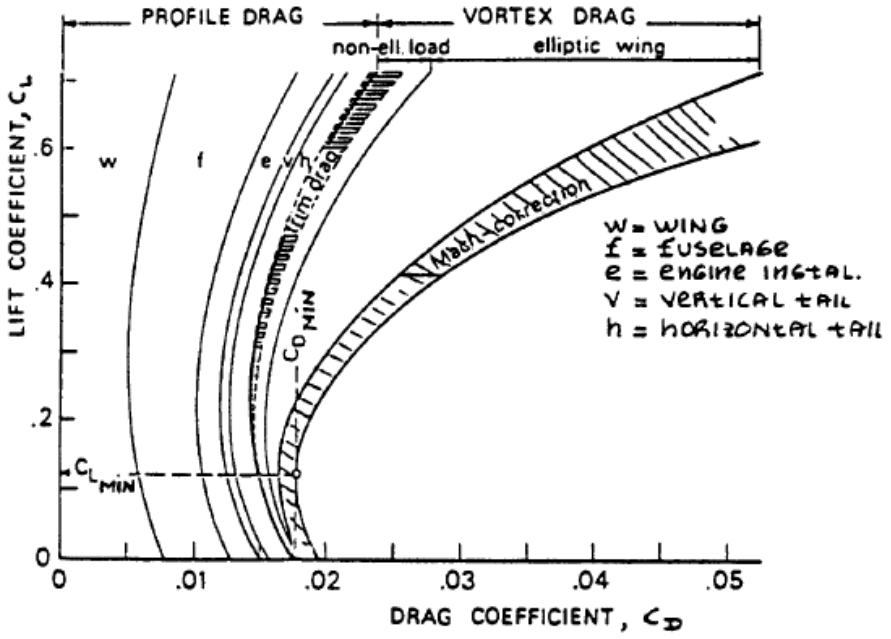

Figure 4.6: Typical drag breakdown for an aircraft [20]

4.10 Iteration Process

Now that all parts are designed, an iteration will be started to add all parts together, and check whether they are still feasible and can be added together.
In Figure 4.7 the iteration procedure is visualized. At least one full iteration will be done to guarantee a convergent design. The iteration starts with a number of initial, estimated inputs, these are the lift over drag ratio, the specific fuel consumption, the payload mass, the cruise conditions, the range, and a number of statistics of existing aircraft. Using these values, a Class I weight estimation is done as described in Section 4.1. From the Class I, a maximum takeoff weight (MTOW), a fuel weight, and an operational empty weight (OEW) are obtained.
The next steps in the iteration are the planform design, the fuselage design, and the propulsion system design which are described in Section 4.3, 4.5, and 4.6 respectively. From these, the geometry and performance follow. The geometry defines the lift and drag performance, which is estimated using Roskam [17]. Also, the specific fuel consumption follows from the propulsion system design. These are then compared to the initial values used as input for the Class I weight estimation. If the specific fuel consumption or the lift over drag are off by a margin greater than 1%, all the procedures up to this point are repeated using the new inputs.
If the initial inputs match the calculated values after the planform, fuselage, and propulsion system design, the design is continued. First, a few relevant systems are designed such as the landing gear. After this, initial tail volumes are chosen. Using these tail volumes, the tail is designed using methods from Roskam Part 3 [16] as described in Section 4.8. After this, a Class II weight estimation is performed using methods from Roskam Part 5 [17] as described in Section 4.7. Using the Class II, the center of gravity is found for the wing and fuselage group and the loading diagrams are generated.
Using the design parameters generated up to this point, an X-plot is generated giving the most forward and afterward center of gravity positions for which the aircraft is stable and controllable. This plot is matched with the most afterwards and forwards center of gravity positions for different wing positions [18]. From this, a wing position and a new tail volume is found. If this tail volume differs more than 10% from the initial tail volume, the procedure is started from the Class II on again.
Finally, when the empennage is designed and the Class II estimation is complete, the OEW obtained from the Class II is compared with that of the Class I. If these match within a margin of 2%, a final design is obtained. If these weights do not match within a margin of 2%, the process is started from the Class I again. This iteration then uses the operational empty weight obtained from the Class II to estimate the maximum takeoff weight. This is done using statistical relations.

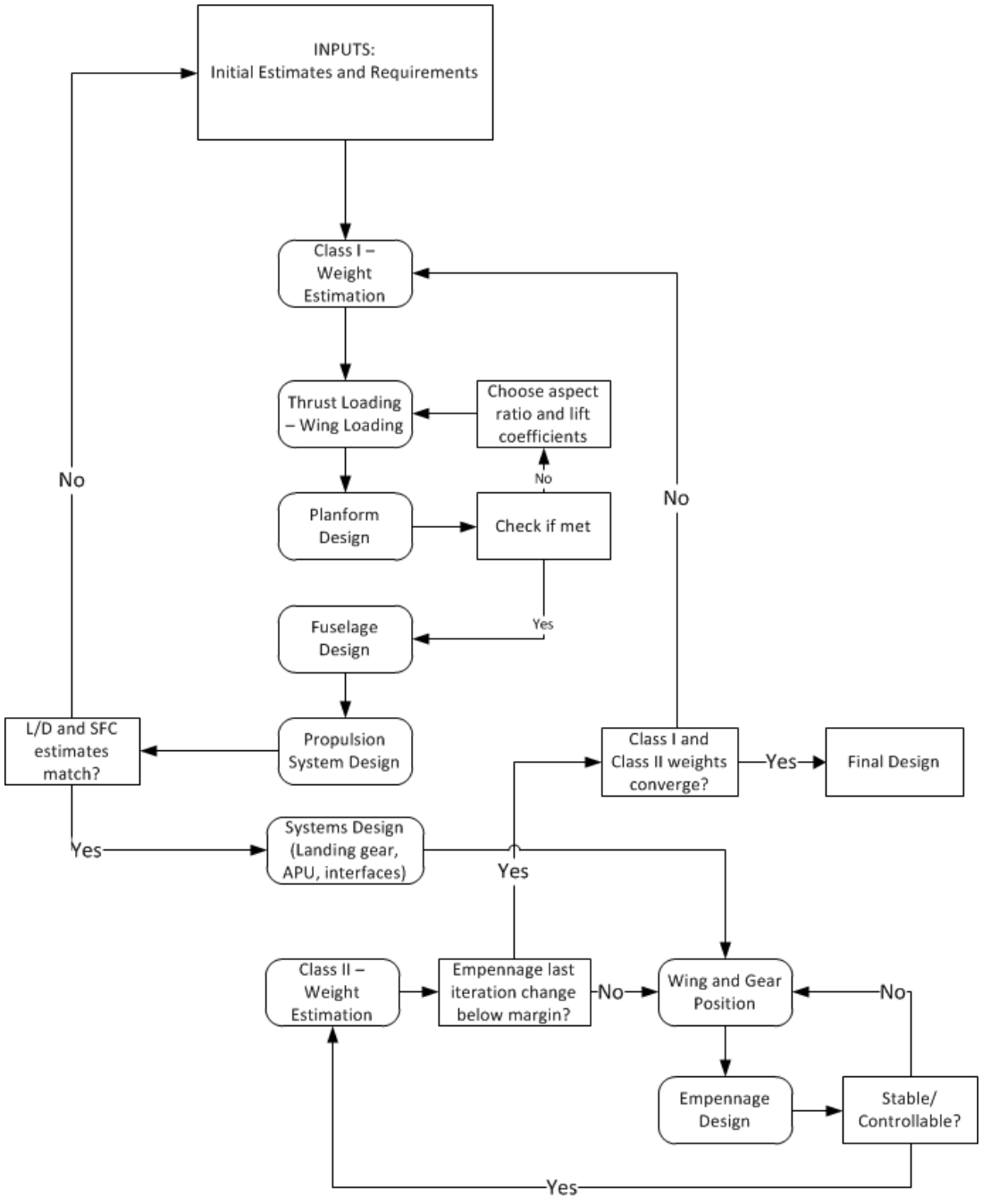

Figure 4.7: Iteration process for the aircraft design

Chapter 5 | Reference Aircraft

In this chapter the reference aircraft will be presented which was designed to quantify the potential benefits of the distributed propulsion aircraft and to verify the design methods. This aircraft has been designed to meet the requirements given in Section 2.3 using the methods as described in Chapter 4.

5.1 Geometry and Weights

The reference aircraft has been designed using the methods as described in Chapter 4. In Figure 5.1 the convergence of the iteration procedure is displayed and in Table 5.1 the main design parameters are given. As can be seen, a final operational empty weight of 42891kg is obtained. Using this value, a maximum takeoff weight of 85494kg and a fuel weight of 23932 kg are calculated. The aircraft will have a length of 40.14m and a span of 37.62m.

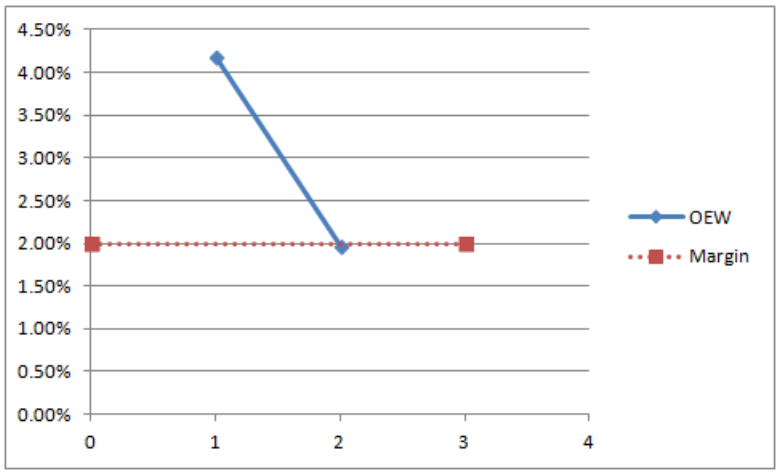

Figure 5.1: The error between the Class I and Class II iterations displayed per iteration

Table 5.1: Design parameters for the reference aircraft

	Value	**Unit**
Weights		
MTOW	85494	$[kg]$
OEW	42891	$[kg]$
Fuel Weight	23932	$[kg]$
Performance		
SFC	1.347E-05	$[kg/(N \cdot s)]$
L/D	16.86	$[-]$
Wing		
Wing area	128.65	$[m^2]$
Span	37.62	$[m]$
M.A.C.	3.80	$[m]$
Aspect ratio	11.00	$[-]$
Taper	0.27	$[-]$
Quarter chord sweep	22.49	$[deg]$
Fuselage		
Length	40.14	$[m]$
Diameter (outer)	3.81	$[m]$
Horizontal Tail		
Sh/S	0.29	$[-]$
Tail area	37.31	$[m^2]$

5.2 Final Result

Using the parameters presented in Section 5.1, the aircraft is modelled in CATIA. In Figure 5.2 this model can be seen. A three-view drawing of the reference aircraft can be found in Figure 5.3.

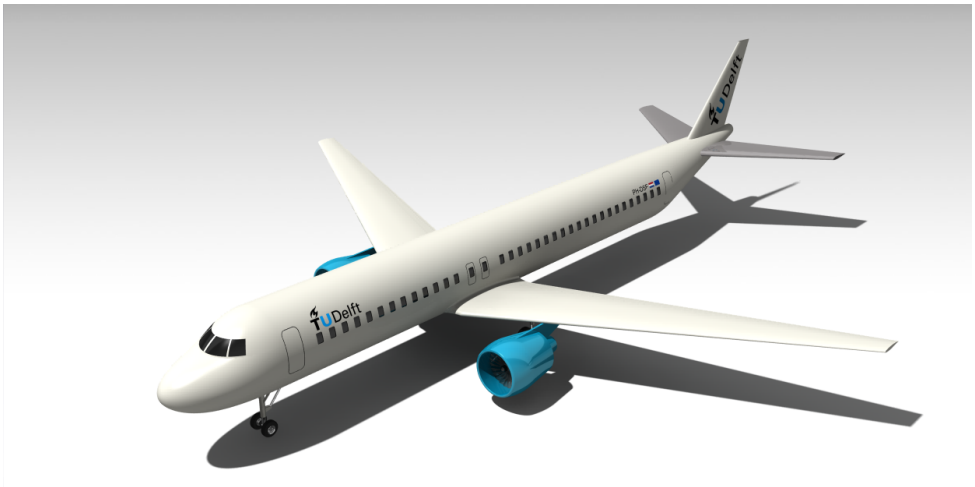

Figure 5.2: Visual representation of the reference aircraft

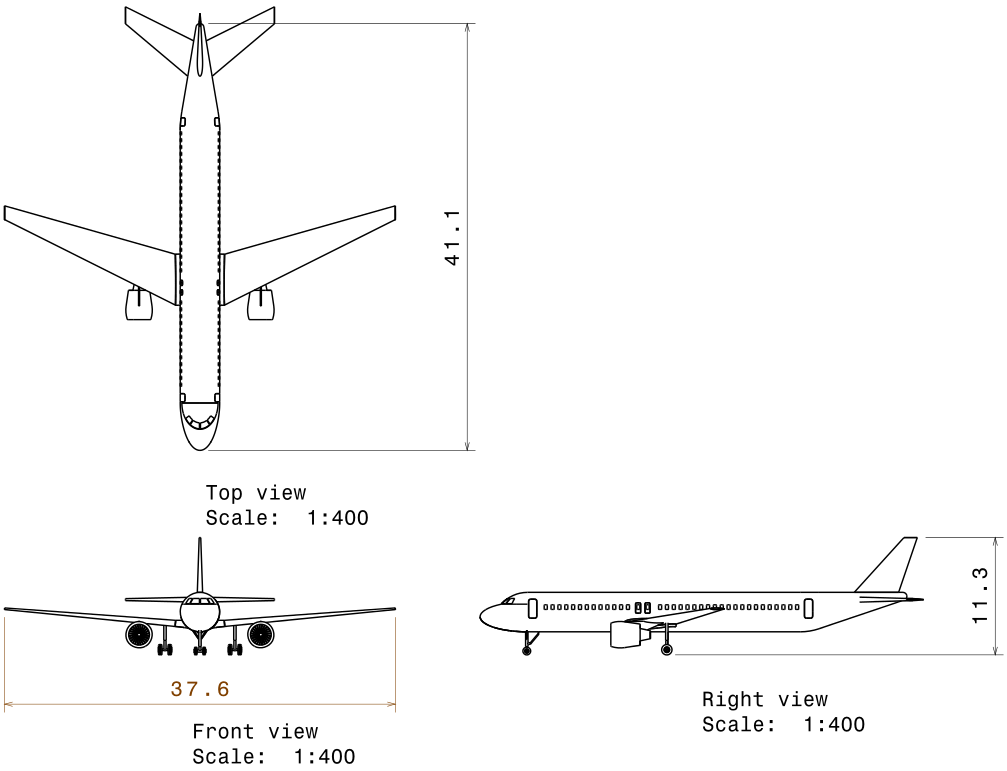

Figure 5.3: Technical drawing of the reference design

Chapter 6 | Propulsion System Design

From the trade-off between the different concepts presented in Chapter 3, the High Temperature Superconducting (HTS) hybrid propulsion system came out as the most suitable propulsion system for Vimana. This chapter goes into more depth regarding the design method and choices for the propulsion system. This architecture consists of a turboshaft engine behind which a high-speed generator is placed to convert the mechanical power into electric power. This is then transferred by cables and several controllers to multiple high speed motors which in turn drive the fans [22].
The HTS term means that several components such as the motors, generators and cabling can be made superconducting by use of special materials which need to be kept at cryogenic temperatures $(20 - 65K)$. This is taken care of by a cryocooler which uses neon as a cryogen. To keep the weight of the cryocoolers as low as possible, methane is used as a heat sink. After the methane has fulfilled its function as heat sink, it can be mixed with the jet fuel and burnt in the turboshaft engine [23].
This chapter is divided as follows: First, Section 6.1 will determine the size of the fans. This results in the power requirement for the motors, which will be explained in Section 6.2. After this, the engines will be sized and positioned in Section 6.3. Other propulsion components, such as motors and generators, cabling, controllers, cooling and Auxiliary Power Unit will be treated in Sections 6.4 through 6.8. This chapter is concluded with the presentation of the propulsion system architecture in Section 6.9.

6.1 Fan Design

In this section the method and results are presented for the design of the ducted fans. For this analysis use has been made of JavaProp, a tool similar to JavaFoil that generates a fan design and analyses it simultaneously.

6.1.1 Fan Placement

The fans will be placed on top of the wing on the aft part of the chord; this placement has been chosen for several reasons. Firstly, this position hardly influences the lift negatively since the biggest part of the lift is generated near the leading edge. This has been ascertained in XFLR5 resulting in the pressure distribution along the top side of the wing, as can be seen in Figure 6.1. Secondly, the exhaust flow can be used for wake filling of the wing and possibly fan blowing. However, more aerodynamic analysis is needed at this point. Finally, it facilitates a shorter landing gear length, since the gear can be designed to provide ample clearance for the tail and wing instead of the engines. This will result in a lower landing gear weight thus lower operational empty weight.

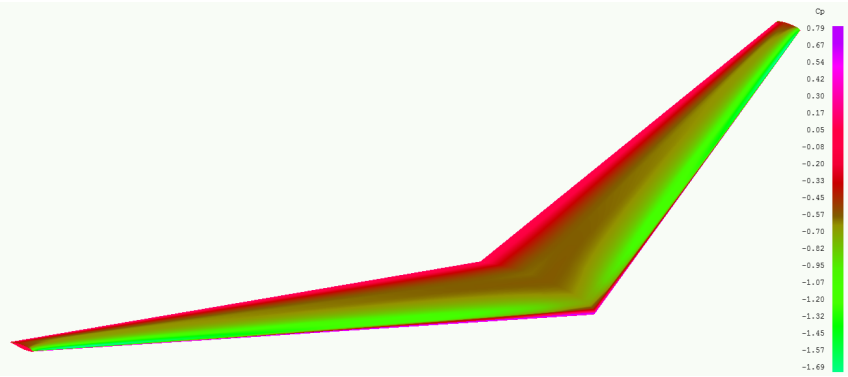

Figure 6.1: Pressure distribution along the top side of the wing

6.1.2 The Tool

JavaProp makes use of blade-element-theory which comes with some limitations. The most important limitation for this design is the fact that it is not capable of fully analyzing compressible effects. However, it is chosen to still make use of this tool since it is easy in use and offers all the capabilities needed. Moreover, according to Dr. D. Ragni, tip speeds of above Mach 1 are allowable if the operating regime of the blades are more or less constant, which is the case. Apart from the applet in Java, JavaProp is also available as Matlab code which is very beneficial to limit the amount of work needed during the optimization process. Moreover, JavaProp is a widely used tool and is therefore thoroughly verified.

6.1.3 The Procedure

Several optimization tools have been created in Matlab. These tools have to be executed sequentially in order to come up with the optimal design. Besides, as for other aspects of the design, the process has been repeated to converge and to incorporate newly generated values. The fan has been designed and therefore optimized for cruise conditions (M=0.78, h=11000m). Afterwards, an analysis has been performed to check the fan performance during take-off and climb.

Input

In order to run the tool some parameters are required. Since at this point a lot is still unknown, some estimations have been made. The angular velocity is set at 3500rpm, the number of blades at 7 and the airfoil at Clark Y. For the spinner, the fairing over the central hub of a propeller, a diameter of 10% of the fan diameter is assumed.

Number and Size Optimization 1

To start off, the number of fans and the size of the fans have been determined. For that purpose, tables have been generated with the columns representing different fan diameters ranging from 0.2 to 3 meters with steps of 0.2 meter. Every row represents a number of fans, ranging from 2 to 30 with steps of 2 to keep the aircraft symmetrical. The part of the span of an A321 usable to position the fans on is used as input to eliminate combinations of fan number and size impossible to fit on the aircraft. In further phases the actual span of Vimana is used.
Per combination of fan diameter and number of fans, an optimal propeller is designed and the propulsive efficiency and required power are generated. This made it possible to have a first selection of fan number and size. To this extent the first choice was to have 10 fans of 2 meter in diameter with an efficiency of 81.3% and a required power of $14.2MW$.

RPM Optimization

After the first selection of fan size and number, the optimal angular velocity of the fans during cruise was selected using a different optimization tool. This tool generates a table with required power and propulsive efficiency as function of revolutions per minute. The result can be seen in Figure 6.2 and the optimum is found to be 5600rpm.

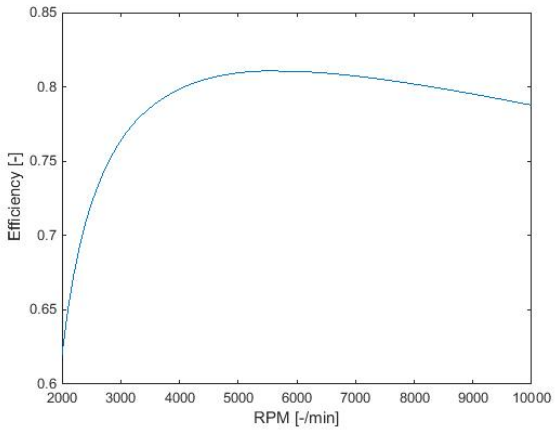

Figure 6.2: Propulsive efficiency as function of angular velocity of the fan

Blade Number Optimization

The number of blades is optimized in the same manner as the angular velocity. Plotting the propulsive efficiency against the number of blades results in Figure 6.3.
It is chosen to implement five blades per fan since this results in the best combination of efficiency and mass.

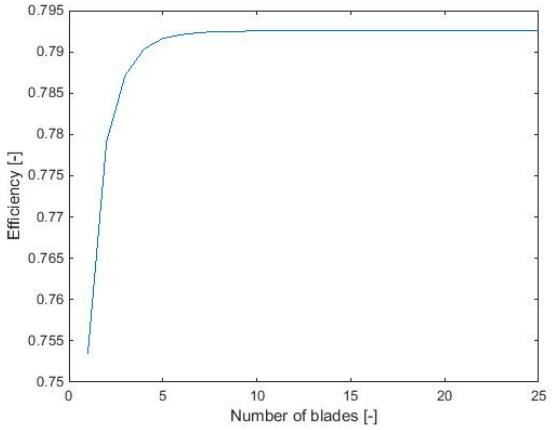

Figure 6.3: Propulsive efficiency as function of number of blades of a fan

Airfoil Optimization

Up to this point the standard selected airfoil Clark Y is used at an angle of attack of three degrees. In order to significantly improve the performance of the fan, an optimization on this point is required. JavaProp comes with 14 predefined airfoils, which can be defined at four distinct points along the span of the blade. Interpolation will take place between these points as is for the angle of attack which is defined at five points. Analyzing the performance for all possible combinations will result in an enormous amount of data points and therefore requires too much computing time.
The technique implemented is to optimize the airfoil first at the first point along the span, then at the next point and so on. Afterwards this loop is run repeatedly until the solution converges to the optimum. The same is done with the angle of attack after which the airfoil optimization loop is run again. In the end the solution is found to be optimum since it does not change anymore while running any of the two loops.
The optimum airfoil is found to be MH 116 with 9.8% thickness and a Reynolds number of 500,000 along the entire span with an angle of attack of 6 degrees. This leads to a blade angle of 55.7^o at the root and 31.2^o at the tip. A visualization of the airfoil can be found in Figure 6.4. The propulsive efficiency increased from 80.0% up to 87.5% due to the implementation of this airfoil which resulted in significantly lower power requirements.

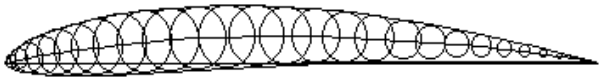

Figure 6.4: MH 116 airfoil

Number and Size Optimization 2

Now that a more suitable airfoil has been selected, the angle of attack, angular velocity and blade number and size optimization is performed a second time. However, before that is done some additional factors are implemented: First of all the nacelle drag is included and added to the total drag required after subtracting the nacelle drag of the A321 engines. Based on literature[1] it was found that a NACA4312 airfoil would be most beneficial to create a duct. Since the duct will be closed, a 2-D airfoil analysis has been performed, resulting in a drag coefficient value of 0.008. The optimization tool calculated the length of the duct to be 25.4% of the diameter [24], and a maximum thickness of the chord was set to 12.5% of the duct length [25]. Therefore, the diameter found in the optimization tool has been used to find the drag of a single nacelle by using the above mentioned drag coefficient and corresponding drag formula. This drag has been added to the value of the thrust that the ducted fan has to deliver.
Secondly the mass of the fans and duct are added. The mass of the duct has been found by using the above mentioned airfoil and the duct dimensions for a certain iteration. Carbon fiber with a density of $2500 kg/m^3$

[1] URL "http://4hv.org/e107_files/public/1386100085_2431_FT0_1353043533_2431_ft145838_duct_pdf.pdf", [cited 14 June 2015]

has been used. Furthermore, the mass of the fan has been based on the blades of the General Electric GE90 engines of the Boeing 777. For that specific case, an engine blade has a mass of 50 pounds [2], which corresponds to a length of $1.702m$. This mass has been scaled with the factor of duct radius over GE90 engine radius to the power of 2.
Running the optimization tool this time, it is chosen to select the optimum fan number and size on the basis of the total required power since this has a direct impact on the fuel consumption. The propulsive efficiency does not exactly correlate with the required power anymore due to the added mass and drag contributions.
Moreover, it is chosen to have at least eight fans to support the distributed propulsion concept. In that region, eight fans of 2 meter in diameter has the lowest required power. Although the added drag due to the added mass of the fans, as said, is incorporated, the increase in for example take-off performance due to lower weight is not. Therefore it is chosen to have eight fans of 1.8 meter because the required power difference is minimal (increase of 0.011%) and this option is significantly lighter. This results in a total required power of $10.7MW$ and a propulsive efficiency of 88.4%.
For a lot of combinations of fan size and number, no required power value is obtained. This is either due to the fact that it is impossible or inefficient to propel the aircraft with for example six fans of $40cm$ or because it is impossible to fit 30 fans of two meters on the span of an A321-sized aircraft.
Because of the multiple optimizations, $3.5MW$ is saved and the propulsive efficiency is increased from 81.3% to 88.4%. Afterwards it was checked if the other parameters need to be updated. However, after running the optimizations again it became clear that no updates were necessary for the RPM, blade number and airfoil.

6.1.4 Iteration

In the iteration phase of the entire design, some parameters such as cruise drag and lift-to-drag ratio were altered resulting in changes in the fan performance.
Also the spinner diameter was adjusted to an initial value of $0.7m$ for the motor to fit behind the spinner. After some iterations this diameter converged to $0.76m$.
The final fan design is concluded in Table 6.1 and visualized in Figure 6.5. For take-off, the maximum attained values for a constant thrust are taken. The propulsive efficiency is not displayed for take-off since it has no real meaning for low velocities, as can be seen by equation (6.1):

$$\eta_{prop} = \frac{T \cdot V}{W_{req}} \tag{6.1}$$

Table 6.1: Final design parameters of the fans

Number of fans	8
Fan diameter $[m]$	1.8
Spin diameter $[m]$	0.76
Airfoil	MH 116 9.8%, Re = 500'000, alpha=6°
Cruise (M=0.78, h=11000m)	
Total required power $[MW]$	10.7
Propulsive efficiency [%]	88.4
RPM $[-/min]$	5600
Thrust per fan $[N]$	5135
Torque $[Nm]$	2279
Take-off (maximum values, h=0m)	
Total required power $[MW]$	34.4
Propulsive efficiency [%]	-
RPM $[-/min]$	5365
Thrust per fan $[N]$	16787.5
Torque $[Nm]$	7661

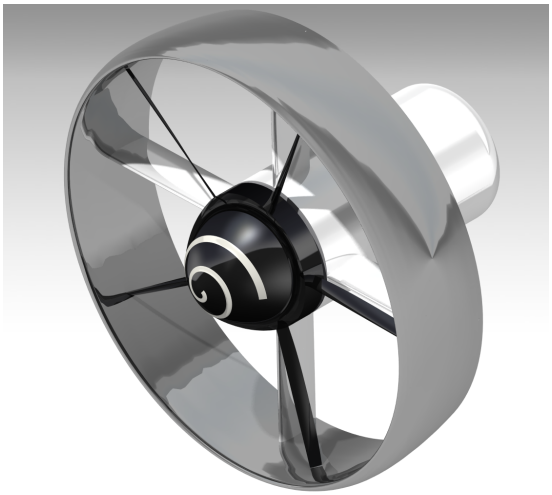

Figure 6.5: Render of the fan

[2] URL "http://www.geaviation.com/commercial/engines/ge90/", [cited 14 June 2015]

6.2 Required Power

In order to accurately size the engines and batteries, the required power during different flight phases should be known. A One Engine Inoperative (OEI) scenario is taken into account for every phase except for start of take-off until V1 [3] since the aircraft can still abort take-off in this phase [26]. In the case of OEI, the aircraft should still be able to attain a minimum climb gradient which is set by regulations. These climb gradients are shown in Table 6.2 for three-engined aircraft, where the aircraft belongs to due to the three power generating turboshafts.

Table 6.2: Minimum climb gradients set by regulations [15, 26]

Segment	Altitude range	Climb gradient
1st	$0m$ - $11m$	0.3 %
2nd	$11m$ - $122m$	2.7 %
Final	$122m$ - cruise	1.5 %

During the entire climb, points have been selected at which the required power requirement will be evaluated, as presented in Figure 6.6. These points correspond to the points between different climb phases used by Eurocontrol[4]. To calculate the required power, the following steps have to be taken for each point: first of all, the required thrust loading is calculated using the wing and thrust loading diagrams with either the take-off or climb performance as constraint together with the landing performance constraint. With the thrust loading determined, the thrust is calculated by multiplying by the MTOW, which is a conservative approach since the weight slightly decreases during climb. JavaProp is then used as analysis tool with the design as will be presented in Section 6.1 as input. Using the 'Multi-Analysis Card' and filling in the corresponding thrust and aerodynamic properties, the required power for different airspeeds can be determined.

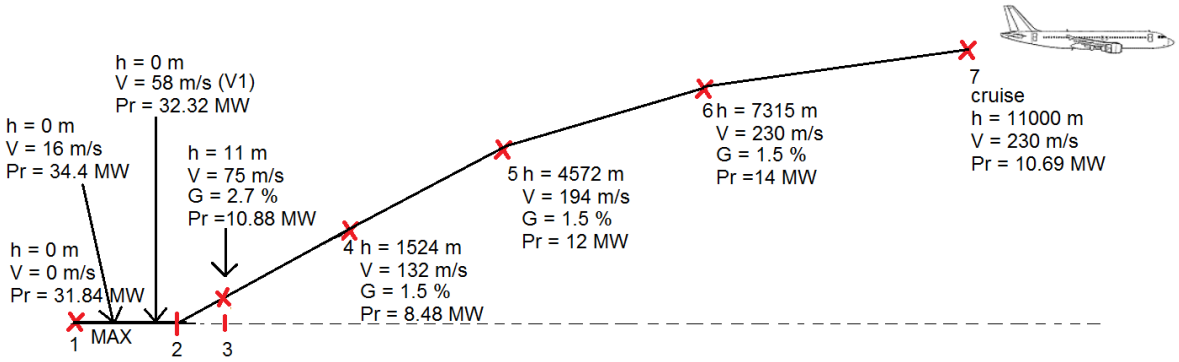

Figure 6.6: Climb flight profile with required powers per point for required performances

The results can be found in Figure 6.6: it is assumed that the required power for the entire phase remains as the highest power required during that phase. The point from V1 to lift-off is not presented since the required power is lower for this phase than at V1. Also, the phase from lift off to point 3 is left out due to the low climb gradient requirement of 0.3%. This phase also has lower power requirements than from point 3 onwards. Between points 1 and 2, an additional point has been added, labeled 'MAX', because this is the maximum required power during the entire ground run and therefore contains valuable information.
The highest power of $34.4MW$ is required at point 'MAX' but at this point all engines are operative. The highest power required with one engine inoperative is at V1 which is $32.32MW$. These values for required power will be used when sizing the engines and batteries in Section 6.3.

6.3 Engines

As proposed in the Mid-Term Report [9], the engines are placed in the back of the fuselage. This was done for the possibility of boundary layer ingestion (BLI) and noise reduction for passengers, due to their relative

[3] URL "http://www.satavirtual.org/fleet/A320PERFORMANCE.PDF", [cited 23 June 2015]
[4] URL "https://contentzone.eurocontrol.int/aircraftperformance/details.aspx?ICAO=A320&", [cited 4 June 2015]

distance from the passenger cabin, when compared to a conventional under-wing podded design. First, a trade-off has been performed to determine the number of turboshaft engines, based on criteria such as weight and reliability. After this, a mass estimation procedure is presented, detailing aspects such as battery use and flight phase based power requirements. A few procedures on volume estimation are then briefly presented, including a discussion on the accuracy and validity of these estimation methods. Another trade-off on engine placement is executed afterwards. This refers to the circumferential placement of the engines, since it has already been decided to place them at the aft of the fuselage.

6.3.1 Trade-off 1: Number of Engines

Based on comparable aircraft with similar range, such as the Airbus A321, and on the expected level of technology readiness of proposed turboshaft engines, four concepts on the amount of engines were presented. A trade-off was performed to determine the most suitable configuration. These concepts included 2, 4, 3 and 12 engine layouts. The first two follow from conventional designs, while the third and fourth options may suffer from asymmetry if not designed appropriately. The last, 12 engined concept is rather unusual, but does lend itself to the distributed propulsion concept quite nicely. The number 12 was chosen based on engine and generator mass estimations. The specific formulas used for these estimations are presented in Subsection 6.3.2 and Section 6.4 respectively. The outcome can be seen in Figure 6.7, where the total engine and generator mass has been plotted against the number of engines. Here it can be seen that the 12 engined option has the lowest total weight ($1367kg$). Now that the different concepts are defined, the next step to take is introducing the trade-off criteria.

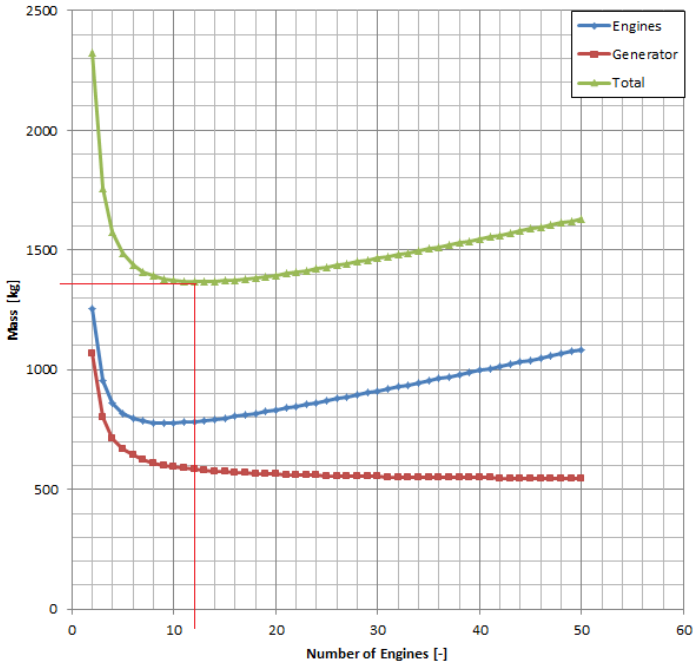

Figure 6.7: Engine and generator mass estimations, including total weight

1. **Weight:** Since the engines are designed for an OEI condition, they will be overdesigned if there are only two of them. On the other hand, if more engines are installed, more generators are also required, although the weight per generator may be smaller due to a smaller load. After an estimate on the weight of the engines including generators, 2 engines seemed to be the heaviest while 12 engines and generators seemed to be the lightest.
2. **Reliability:** Having a bigger number of thrust producing units increases the overall probability of having an engine failure. Hence, the configuration with the lowest amount of engines was awarded the highest rating on this category.
3. **Maintenance:** Having fewer engines will be favourable in terms of maintenance simply because fewer elements need to be inspected. This will save time and operating costs. However, the complexity of maintenance of each unit may be higher if only 2 engine units are present. Furthermore, it is perhaps

more critical and time consuming to repair one big engine (which will be the case if only 2 engines are used), as opposed to one small one (in case more engines are present).

4. **Installation space:** When having more engines, they will be smaller as they will together still produce the same power. However, they cannot be easily stacked because they have a cylindrical shape. In addition more generators will be present thus requiring more space. Therefore, fewer engines will be favourable for this criteria.
5. **Specific Fuel Consumption (SFC):** From a large database of civil turboshaft engines[5], it was observed that bigger engines will have a lower SFC which is both favourable in terms of emissions and fuel weight.

Now that every aspect has been discussed, the trade-off table is shown below in Table 6.3 with the weights next to the criteria. The different points assigned to each concept are done qualitatively and can be reasoned by the explanation given above. Only for the weight criterion, the points are given based on a linear scale where the weight of concept 1 is the left boundary and the weight of concept 12 is the right boundary. This interval is then divided by 4 to get the range of point 1, 2, 3 and 4. After this division of the scale into equal sections, the weights of the remaining concepts were then placed into the corresponding category. This allowed for a clearer and more logical division of the rankings. As is highlighted in Table 6.3, the design option with 3 engines will be implemented into Vimana.

Table 6.3: Engine trade-off table

Number of Engines	**2**	**4**	**3**	**12**
Weight (30%)	1	4	3	4
Reliability (10%)	4	2	3	1
Maintenance (15%)	4	3	3	1
Installation space (15%)	4	3	4	1
SFC (30%)	4	3	4	1
Total	3.1	2.6	**3.15**	1.9

Sensitivity Analysis

The weights given to the criteria in Table 6.3 were based on group discussions and agreements upon the relative importance of each aspect. These mostly followed from the high level requirements placed on Vimana. However, these weights are on a base level very subjective, of course. Therefore, a sensitivity analysis is performed on the weighting given to the criteria, in order to identify any highly variable criteria which may significantly affect the final result. Normally, a sensitivity analysis is also done for the rating given to a certain concept. As the mass of the engine is already estimated quite accurately, any inaccuracies in the calculations will be small and therefore will not have a significant impact in the criterion weighting. The other criteria are not defined quantitatively and therefore is it quite arbitrary to change values which are already determined qualitatively.
For the sensitivity on the weights, it was chosen to vary the weights of the two most important factors (the weight and SFC) as they have the largest influence on the result. The order of magnitude in comparison to the other criteria are larger, thus the result will not change a lot. This was done for every configuration and the variance can be seen on the diagonal highlighted in bold. The other values are irrelevant as weights do not add up to 100% anymore. The result can be seen in Appendix A.1 in Tables A.1 until A.4. The important values to compare are shown below in Table 6.4.
As can be seen from the table, the option using three engines will is in all five cases the best option. From this, one can deduce that three engines will be the most suitable for Vimana's design.

6.3.2 Mass Estimate

The approach taken to size the engines is largely based on the identified flight phases (Section 6.2) and on a study done by NASA on hybrid distributed propulsion engines, where a trend has been provided on projected weights of turbine engine cores [27]. This trend can be seen in Figure 6.8, it is worth noting that the figure does not use SI units. From this figure, Equation (6.2) is deduced, where the power is inserted in MW and the mass is obtained in kg.

[5]URL "http://www.jet-engine.net/civtsspec.html", [cited 29 May 2015]

Table 6.4: Results of the sensitivity analysis on 'Number of engines' trade-off criteria

Number of engines		2	4	3	12
Weight	0.2	3.1	2.8	**3.25**	1.9
SFC	0.4				
Weight	0.25	2.95	2.75	**3.15**	2.05
SFC	0.35				
Weight	0.3	2.8	2.7	**3.05**	2.2
SFC	0.3				
Weight	0.35	2.65	2.65	**2.95**	2.35
SFC	0.25				
Weight	0.4	2.5	2.6	**2.85**	2.5
SFC	0.2				

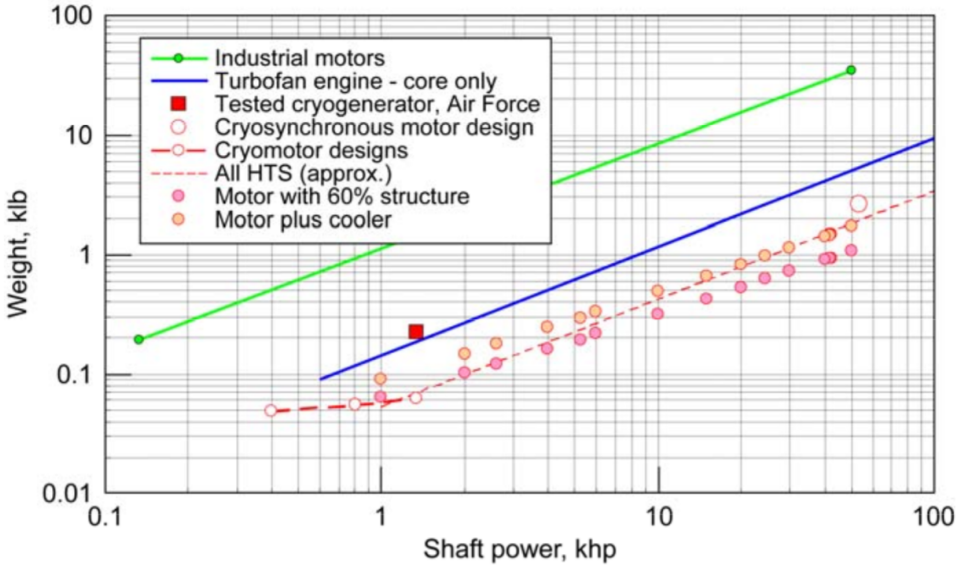

Figure 6.8: Relation between mass and power of turboshaft engines [27]

$$m = 57.79 \cdot P + 9.07 \tag{6.2}$$

Since a battery is considered for power intensive phases as well, Equation (6.3) allows for an estimation of the battery mass. Here, m is the battery mass, P is the power of the battery and U is the energy density. With batteries that are currently available, their mass and volume will be too large for this concept to be viable. Lithium-ion batteries only have an energy density of $250Wh/kg$, while the being developed Lithium-air batteries will have an energy density of $1500Wh/kg$ [28]. In terms of volume, a study performed in Germany expects that these lithium-air batteries will attain a volumetric energy density of $1500kWh/m^3$ [28]. However, for these batteries there is one big disadvantage. According to Dr. Erik Kelder, an expert on battery technology, the Li-air battery will double its weight when discharged. Therefore they will need to be recharged with excess power of the turbines when they are not used.

$$m_{batt} = \frac{P_{batt} \cdot t}{U} \tag{6.3}$$

To find a balanced distribution between engines and batteries in terms of mass, the power setting of the engine is varied from $1MW$ to the maximum power $32.32MW$ for one engine inoperative, (thus $16.16 \cdot 3 = 48.48MW$ in total), observed in the flight profile (Figure 6.6). In order to be able to see a trend, steps of $0.5MW$ to the contribution of the engine to the total power was added. This can be seen in Figure 6.9.
As can be seen from this figure, the minimum point is the point where the engines deliver all the power. This is because the expected trend for the development for engines is better than the ones for batteries. Thus, one engine delivers $16.16MW$ and weights $760.5kg$. Although it may not be favourable in terms of weight, the usage of a battery can still be considered. As can be seen from Figure 6.10, there is a reasonable amount

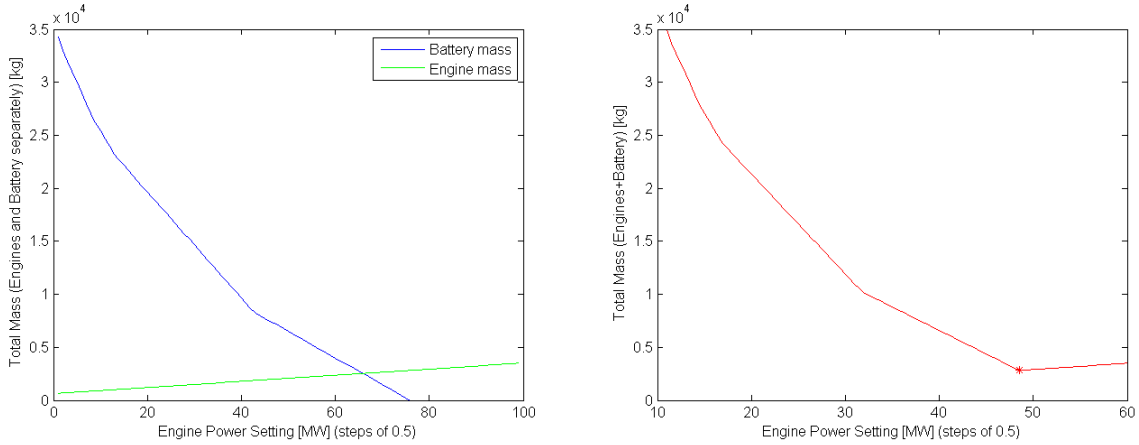

Figure 6.9: Battery and engines mass for different power settings (left); minimum mass (right)

of excess power during the different climb phases which are defined in Figure 6.6. This excess power can be used to charge the battery or increase the climb gradient. This latter will be decided by air traffic control on a case-by-case basis.

Two things can be noted from Figure 6.10. The first one is that the power available (i.e. delivered by the turboshaft) decreases when the aircraft is at a higher altitude. This decrease in available power is due to lower massflow through the core at higher altitudes and is given by Equation (6.4) which is valid for turboshafts [29]. δ_r is the pressure ratio and θ_r the temperature ratio in this equation. The second thing is that if one engine becomes inoperative during cruise (phase 7), there is a power deficit. This means that the aircraft needs to go to a lower altitude such that the available power increases and closes the gap to the power required. It is favourable to descend even a bit more such that the excess power of the two other engines can be used for attempting a re-start of the inoperative engine. If the engine cannot be restarted, regulations stipulate that the aircraft needs to land at a nearby airport.

$$P_{alt} = P_{SL} \cdot \frac{\delta_r}{\theta_r} \tag{6.4}$$

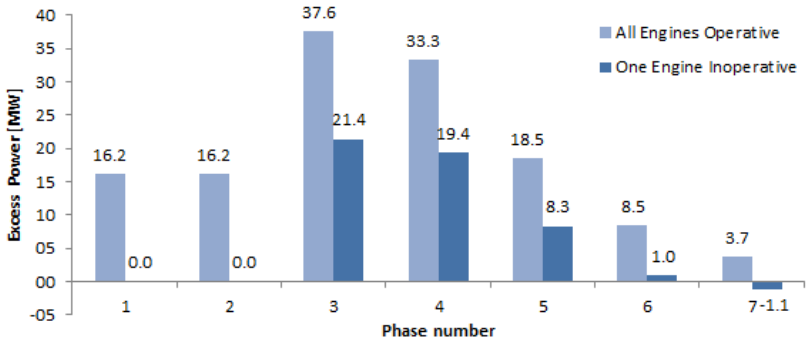

Figure 6.10: Excess power per flight phase

Despite the inconvenient weight doubling, the use of batteries seems very promising. That is why the battery was included in the conceptual design for this concept to begin with. The use of batteries during power intensive phases near the ground, i.e. take-off, is to reduce noise. However, when looking into more depth when sizing the batteries, it was found that the power density is far too low for the application in mind. As can be seen in Figure 6.11, the power density lies around $1000W/kg$. This means that at least $1000kg$ will be needed because the order of magnitude in terms of power is in MW.

[6]URL "http://www.extremetech.com/extreme/198462-new-aluminum-air-battery-could-blow-past-lithium-ion-be-refilled-with-water", [cited 17 June 2015]

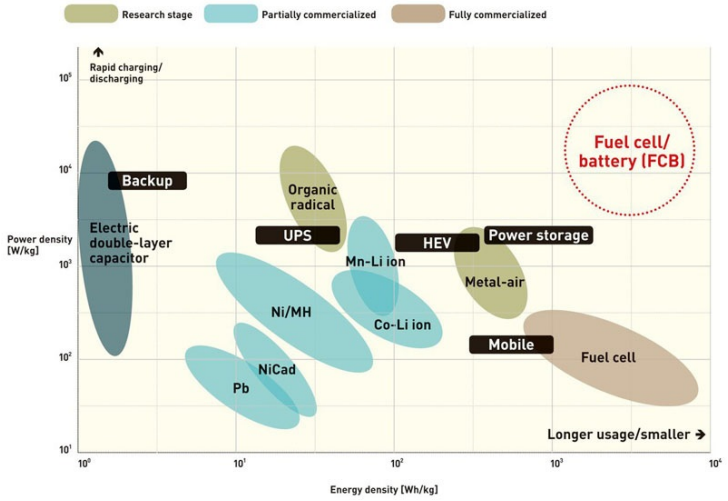

Figure 6.11: Energy and power densities of batteries, capacitors and fuel cells[6]

For this increase in mass, it is better to design the engines such that they can provide the power themselves during power intensive phases. There is still a battery present which replaces the APU to start the engines, as will be discussed in Section 8.1. Since Li-air battery is seen as the future in terms of energy storage and because they do not fulfill the power requirements set, it is chosen to go for a design without batteries and provide all the power by the engines. This will result in a power of $16.16MW$ and a mass of $760.5kg$ per engine.

6.3.3 Engine Volume Estimation

In this subsection, the volume of the engines is estimated. In the current design stage, no numerical estimation methods are available to make an accurate estimation on the engine volume. The volume is therefore estimated with data of current aircraft engines in the same power specifications range. Vimana's engines require a power of 16.32 MW each. The turboshaft engine which is the bases for the volume estimation is the Lycoming T53-L-13, because this engine's specifications are comparable to Vimana[7]. The power to volume value of this engine is used to determine the volume and the turboshaft engines of Vimana.
For the diameter and length of the turboshaft, the same diameter/length ratio of the Lycoming T53-L-13 is used. All the relevant parameters are given in Table 6.5.

Table 6.5: Engine initial dimension estimates

Parameter	Value	Unit
Volume	4.19	$[m^3]$
Diameter	1.35	$[m]$
Length	2.92	$[m]$

6.3.4 Trade-off 2: Engine Placement

Now that the mass and volume of the engines are known, a trade-off can be made on how they should be placed. The trade-off is based on 5 different criteria: safety, noise, aerodynamics, maintainability and structures, as outlined in Table 6.6. Aerodynamics implies making more efficient use of phenomena such as boundary layer ingestion and wake filling. After the trade-off is done, a sensitivity analysis on certain criteria is presented in order to justify the validity of the trade-off results in light of possible variances in weighting and ranking. Also, as mentioned in the previous section, this analysis helps to identify any highly variable criteria which may significantly affect the final result.

[7]URL "http://airandspace.si.edu/collections/artifact.cfm?object=nasm_A19730230000", [cited 17 June 2015]

The highest weight in the trade-off is given to safety, since Vimana is a passenger aircraft and above all, it is imperative that the passengers are not subjected to any possible physical harm due to design flaws. Noise and aerodynamics are given the second and third highest weights. This is done as another notable goal of Vimana is to reduce noise emissions, and have lower harmful gas emissions, in accordance with its sustainable image. Maintainability is given a higher weight than structures. This is because structural complexity is experienced during the design phase of the aircraft, while maintainability is performed during its whole lifetime and will lead to recurring costs. A weight between 1 and 4 is given to each concept, corresponding to the presented criteria; 4 being the highest, thus the most beneficial for the configuration. Earlier in the report it was determined that the number of engines should be 3. In the Mid-term report, it was reasoned that the engines should be placed in the back [9]. Four different configurations regarding the engine placement in the back are considered. The different configurations are given in Figure 6.12. Table 6.6 presents the trade-off result with the assigned weights. For each configuration, an explanation is given as to why those specific weights were assigned.

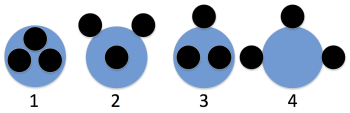

Figure 6.12: Four different engine placements

Table 6.6: Engine placement trade-off

Configuration	**1**	**2**	**3**	**4**
Trade-off criteria				
Safety (30%)	1	3	2	3
Noise (20%)	4	2	3	1
Aerodynamics (25%)	4	2	3	1
Maintainability (15%)	1	3	2	4
Structures (10%)	1	3	2	4
Final result	2.35	**2.55**	2.45	2.35

Configuration 1 has the lowest grading for maintainability and structures. This is because all the engines are integrated into the fuselage, increasing the complexity in both criteria. Safety is also given the lowest grading, because an engine blowout inside the fuselage is more critical than it being outside since it may be more difficult to contain and the heat and debris being transmitted more directly to the passenger cabin. Noise is given the highest grading, because of noise shielding. Since the engines are not outside the aircraft, there is less noise being transmitted directly to the ground. Aerodynamics is also given the highest grading because of the increased use of boundary layer ingestion, wake-filling and low drag.

Configuration 4 has the lowest grading for noise and aerodynamics. All the engines are placed on the outside of the fuselage and this is expected to be very noisy for a person on the ground. Furthermore, by placing the engines outside, the design disturbs the aerodynamic shape of the fuselage, thereby increasing the drag penalty of the design. Safety was given an intermediate rating of 3 because it cannot be said that, by virtue of all engines being outside the fuselage shell, it is the safest option. An engine blowout could still negatively affect the structural integrity of the aft of the fuselage, and with all the engines being positioned there, this might not be very safe in the worst case scenario either. Finally, maintainability and structures is where this configuration scores the highest rating of 4. Since all the engines are mounted on the outside, it is expected that the engines will be easier to dismount, dismantle and maintain. Structures is a difficult criterion to define but for the purposes of this trade-off, it was defined that the complexity of having to implement fairings and extra structural elements for external engine mounting would offer a smaller degree of complexity than, for example, having to build support structures inside the confined space of the fuselage, as is expected for Concept 1.

Configurations 2 and 3 were chosen as the logical compromise alternatives after the previous two configurations. They differ in safety, noise and aerodynamics. Concept 3 was deemed to be better in terms of noise and aerodynamics following a similar reasoning as was done for the other twp configurations. Having two engines in the flow introduces more drag. Furthermore, having less engines outside the fuselage is better since there is less emitted noise that is not shielded by the fuselage shell. However, for safety, Concept 2 was rated

higher than Concept 3; the reasoning being that the less engines present inside the fuselage, the smaller is the chance of uncontained engine failure following a blowout.

Sensitivity Analysis

The sensitivity analysis presented here takes a similar approach to the first one that was presented on the engine number trade-off; albeit pertaining to engine placement this time. The weights given to the criteria in Table 6.6 were based on the high level requirements placed on passenger carriers of this size, such as safety and also on more specific requirements for Vimana, such as noise. These criteria were mostly qualitatively analyzed and the assigned weights follow from group discussions and logical reasoning. Therefore, it is essential to perform such a sensitivity analysis, in order to identify any highly variable criteria which may significantly affect the final result.
For this second sensitivity analysis, it was chosen to vary the weights of the three most important factors, where two different combinations between them were made. First of all, an combined analysis was done on safety and aerodynamics, followed by an analysis on safety and noise. Safety was chosen twice, as it is the criterion with the highest original weighting, and thus will have the largest influence on the results. This was done for every configuration and the results can be seen in the tables below. Table 6.7 shows the results of the sensitivity analysis for each of the four configurations while varying the weights of the safety and aerodynamics criteria while Table 6.8 does the same for the safety and noise criteria.

Table 6.7: Results of the sensitivity analysis on placements of engines; trade-off criteria: safety and aerodynamics

Configuration		**1**	**2**	**3**	**4**
Safety	0.2	**2.65**	2.45	2.55	2.15
Aerodynamics	0.35				
Safety	0.25	2.5	**2.5**	2.5	2.25
Aerodynamics	0.3				
Safety	0.3	2.35	**2.55**	2.45	2.35
Aerodynamics	0.25				
Safety	0.35	2.2	**2.6**	2.4	2.45
Aerodynamics	0.2				
Safety	0.4	2.05	**2.65**	2.35	2.55
Aerodynamics	0.15				

Table 6.8: Results of the sensitivity analysis on placements of engines; trade-off criteria: safety and noise

Configuration		**1**	**2**	**3**	**4**
Safety	0.2	**2.65**	2.45	2.55	2.15
Noise	0.3				
Safety	0.25	2.5	**2.5**	2.5	2.25
Noise	0.25				
Safety	0.3	2.35	**2.55**	2.45	2.35
Noise	0.2				
Safety	0.35	2.2	**2.6**	2.4	2.45
Noise	0.15				
Safety	0.4	2.05	**2.65**	2.35	2.55
Noise	0.1				

It is immediately observed that despite the various weights given to these criteria, the outcome per configuration is exactly the same. This is because noise and aerodynamics have the same ranking order per configuration, as can be seen in Table 6.6. This is not a coincidence since external noise and the definition of aerodynamics used in this trade-off are inter-related. The numbers in bold in Tables 6.7 and 6.8 show the 'winning' configuration for each weighting, and it can be seen that Configuration 2, which was the selected concept after the trade-off, is rather insensitive to changes in the magnitude of the weighting, and is therefore quite a safe choice. Configuration 1, that is with all engines housed inside the fuselage, seems to be the better option when safety

has a relatively low weight, while aerodynamics and noise are given higher weights. However, this is just one scenario out of a possible five; and furthermore, it is a highly unusual one. Vimana, being a passenger transport aircraft, places a high importance on passenger safety, and it should therefore always be highly weighted in comparison to the other criteria.
In Appendix A.2 a more detailed table with all the possible combinations obtained in the sensitivity can be found. Only the ones highlighted were applicable, of course, since the other combinations would result in a weighting total that would not be equal to 100%. It is also worth mentioning here that the appendix only includes the tables referring to the 'Safety' and 'Aerodynamics' sensitivity, since these was deemed to be the most important.

6.3.5 Specific Fuel Consumption

Next, the thrust specific fuel consumption of the turbines is obtained. This is done by using a base value of an existing conceptual aircraft developed by NASA. The reference aircraft has a thrust specific fuel consumption of $0.57 N/N \cdot hr$ [27]. This base value is then multiplied by 3 different factors which apply to this specific case. The rest of this subsection will elaborate on each of these factors individually.
First of all, since the Vimana mixes methane with the kerosene for the turbines, the specific fuel consumption decreases because methane has a higher specific energy. This factor is calculated using the mass fraction of methane, which is 17.9%, and the specific energy of both kerosene and methane, which are $46 MJ/kg$ and $55.5 MJ/kg$ respectively [8]. A factor of 0.9647 is finally obtained.
The second factor applied is due to the increased propulsive efficiency of Vimana. During cruise the fans attain a propulsive efficiency of 88.42% according to JavaProp. This is substantially higher than the 78% for conventional high bypass turbofans, see Figure 6.13. Since the specific fuel consumption stipulated in the NASA article [27] is for this conventional type of turbofan, a factor including the higher propulsive efficiency of Vimana is valid. Including the efficiencies of the motors and generators of 99.5% this results in the following factor:

$$f_{\eta_{prop}} = \frac{\eta_{prop,conventional}}{\eta_{prop,Vimana}} = \frac{0.78}{0.8842 \cdot 0.995 \cdot 0.995} = 0.891 \tag{6.5}$$

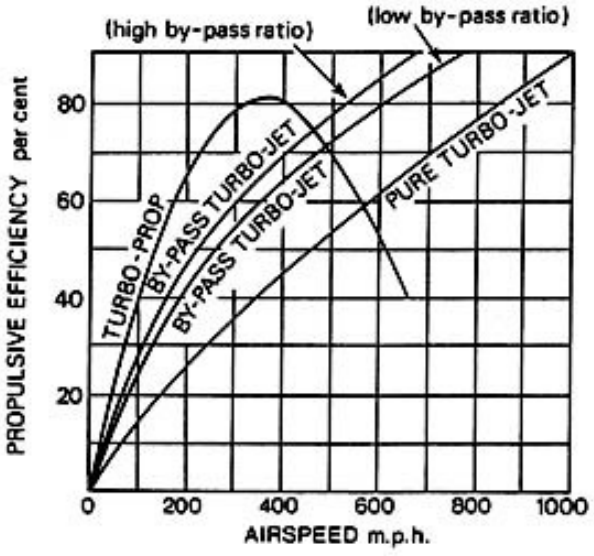

Figure 6.13: Propulsive efficiency for different gas turbine engines[9]

The third and final factor which is applied, is a factor of 0.85 to account for developments of turbine technologies over the coming 20 years. This factor is obtained by extrapolating past developments in turbine efficiency. The past trend can be seen in Figure 6.14. Using this trend, it is expected the efficiency increases 12 percentage points over 20 years. This results in an increase from 66% turbine efficiency in 2015 to a turbine efficiency of 78% in 2035. This is equivalent to a factor of approximately 0.85.

[8] URL "http://www.people.hofstra.edu/geotrans/eng/ch8en/conc8en/energycontent.html", [cited 22 June 2015]
[9] URL "http://web.mit.edu/16.unified/www/FALL/thermodynamics/notes/node82.html", [cited 22 June 2015]

Finally, multiplying the base specific fuel consumption with the 3 factors mentioned above results in an specific fuel consumption of $0.421 N/N \cdot hr$ which is equivalent to $1.1675 \cdot 10^{-5} kg/N \cdot s$.

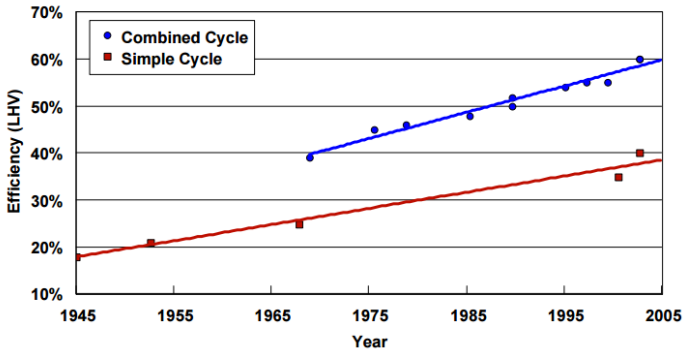

Figure 6.14: Turbine development in the past [30]

6.4 Motors and Generators

The fans that are used in the propulsion system of this concept will be driven by electric motors, which in turn receive their power from the generators driven by turboshafts placed at the back of the fuselage.
An electric motor is an electro-mechanical device that converts electrical energy to mechanical energy (the opposite is achieved by electrical generators), accomplished by the interaction of magnetic fields and winding currents, generating forces within the motor. Furthermore, the rotating machines (motors and generators) will be HTS machines, as was proposed in the concept description. Even though benefits of HTS machines were mentioned before, some more details will be given on why HTS-machines are preferred over conventional ones, since this is the detailed design phase.

6.4.1 Features of HTS Machines

One of the most important advantage of a HTS system (motors and generators) is that it shows compactness in both weight and volume, compared to conventional machines. This is due to the fact that superconducting windings have higher current densities compared to conventional copper windings, which allow for a higher supply of magnetic fields to the stator windings. This in turn results in an increased power density of HTS machine [31]. Therefore, for a given amount of power, the HTS machines can have a smaller volume and weight. Another feature of HTS-machines is that they offer the capability to conduct direct current practically without Ohmic losses at very high current densities, compared to the conventional machines. This results in a higher overall efficiency, even when additional refrigerating powers are included. Efficiencies of 99.5% can be achieved through HTS utilization [28]. A last notable advantage is that HTS machines show a reduction in both noise and vibration levels. This is mainly due to the fact that the magnetic iron teeth can be removed, allowing for reduced harmonics in the airgap field [32].
These features are the main reasons of why HTS machines were considered for this particular concept. However, these advantages of course come with a price, which can be expressed in terms of high technological input requirements and high costs. Technological solutions however, are already proven with success and are also available [32]. There is still room for improvement however, and it is assumed that the performance of these machines will indeed improve.

6.4.2 Machine Type

From Subsection 6.3.2, it has been determined that the most critical power requirement is $48.48MW$. The motors will of course be sized for this phase, where maximum power is required, and the total required power will be equally distributed over the eight motors. This is also the case for the generators. It was determined in Section 6.2, that one of the climb phases was the most critical in terms of power. A required power of $36.94MW$ for the motors was needed and $48.48MW$ for the generators (since there are eight motors and three generators). The power output and size of the rotating machines are the main considerations taken into account when a suitable one is chosen. The main requirements for the machines are given in Table 6.9.

Table 6.9: Motor and generator power requirements

Component	Power per unit	Total Power	Unit
Motor	4.62	36.94	$[MW]$
Generator	16.16	48.48	$[MW]$

Based on these requirements on power output, suitable machines will have to be chosen. For convenience, the analysis done on motors will be assumed to be applicable to the generators as well, as their main difference is only the order of conversion. Therefore, only motors will be mentioned in the coming sections.
Two popular types of electric motors which are currently widely used for this power output range were considered to be used for this propulsion system: the synchronous motor and induction motor. Their working principle is the same. The main difference between these two types of machines is that induction motors, experience AC currents over their windings on both the rotor and the stator. Superconductive losses are only negligible in a DC environment, hence the induction motor is not suitable for an HTS environment, where losses are hard to overcome [33, 34].
It was chosen to use a three-phase, synchronous machine for both the generator and motor. This decision was based on the considerations of superconducting elements, machine efficiency, possible power output and size. The most important consideration is the fact that a synchronous motor has a DC supply. For the selection of an appropriate type of machinery, no trade-off process was conducted as was done for the engines. The reason for this is that there is in effect only one suitable type of machine, when the aforementioned required aspects are considered.

6.4.3 Working Principle

A synchronous motor can be distinguished by two main parts: a rotor and a stator. The rotor produces a constant magnetic field, whereas the stator produces a rotating magnetic field. The rotor in the machine consists of rotating active parts and is excited by a DC power supply, which acts like a permanent magnet, and can therefore also be replaced by one. The stator in its turn, is excited by a three-phase AC supply, producing a revolving magnetic field (RMF), rotating at a speed which is called the synchronous speed. It consists of stationary magnetic parts, including the core and windings.
The magnet of the rotor will be locked with the rotating magnetic field allowing them to rotate at the same speed, hence the name of this particular motor. If now a DC current is applied to the rotor pole windings, the rotor can supply the necessary ampere turns to generate the flux which produces the internal motor voltage. The rotating magnetic field is typically twice as large in magnitude when HTS armature is being used, as opposed to the conventional motor.
Under steady-state operation, this synchronous speed between the rotating magnetic field and the rotor as mentioned before, can be achieved. The super-conducting field winding will then only experience DC magnetic fields, which is desirable for HTS applications as mentioned before [35]. Operations under non steady-state however, will cause the rotor to rotate at a different speed with respect to the rotating magnetic field. This implies that an AC magnetic field will be induced, which is undesirable. Therefore, an electromagnetic shield located between the HTS coils and the stator windings will shield the HTS field windings from these induced AC fields [36].

6.4.4 Material Selection

As mentioned before in Subsection 6.4.3, the machines (motor and generator) will be superconducting, which in effect means that the windings on the machines are made of a HTS material. These windings will be present on both the rotor and stator. There are various materials that are used for the superconducting windings, and an appropriate selection will have to be done. A material selection is done based on several aspects of the electric machines, when certain types of materials are used.
Based on a number of plots generated by Brown [22], weights and efficiencies of generators and motors, including their associated coolers, are compared when two different materials are used. Each point in the Figures 6.15 and 6.16 is optimized for minimum weight while taking some base values into consideration. As mentioned before in Subsection 6.7.1, the Carnot efficiency of the cryocooler is taken to be 30% and its weight per input power is $5lb/hp$ [22]. Two superconductor materials will be considered here, namely Bismuth strontium calcium copper oxide (BSCCO) and Magnesium diboride (MgB_2).
Based on the same paper, using BSCCO-like superconducting materials, a slight efficiency improvement for very little change in the mass can be observed. For a system based on MgB_2 superconductor, however, the

total mass of the electrical system increases by about 25% and the efficiency is effectively unchanged. Despite this, the weight estimations in the sections to follow will consider both options in order to do a more detailed trade-off.

Generator and Cooler Weights Associated to Material Type

It is mentioned that the best existing cryocoolers weigh $30lb/hp$ input [37]. Decreasing this value leads to significant weight benefits, as can be seen in Figure 6.15. Taking a $5lb/hp$ value for the weight per input power of the cryocooler, this leads to a generator+cooler weight of $2500lb$, or $1134kg$. This value is for BSCCO, which is significantly smaller than that for MgB_2 (Figure 6.16), which gives a generator (incl. cooler) weight of $3500lb$ or $1588kg$.
It can clearly be seen then that in terms of generator (incl. cooler) weight, BSCCO is the better option. It must be noted that these weights are by no means the weights that are associated to the machines used in the propulsion system of Vimana. These weights are only associated to the electric machines used for the analysis done by Brown [22].

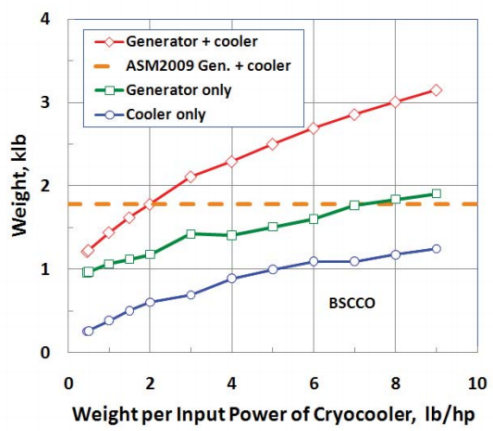

Figure 6.15: Generator weight, cryocooler weight, and combined weight as functions of the weight per unit input power of the cryocooler for BSCCO [22]

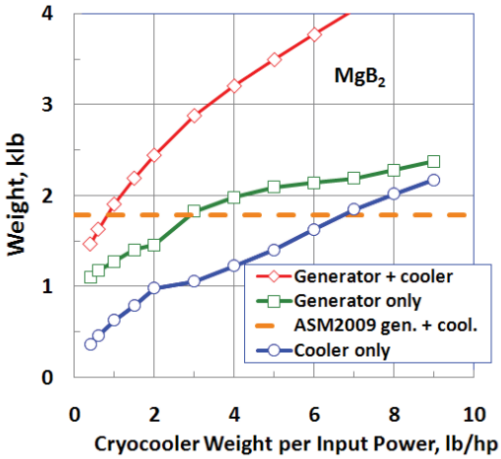

Figure 6.16: Generator, cooler, and combined weight as functions of cooler weight per input power for MgB_2 [22]

6.4.5 Motor and Cooler Weight

For the motor weight estimation, Figures 6.17 and 6.18 indicate that, with a weight per cryocooler input power of $5lb/hp$, the weight would be $600lb$ or $273kg$ for BSCCO and $800lb$ or $363kg$ for MgB_2 respectively. Just as with the generators, it is better in terms of weight savings, to use BSCCO. The figures also include an estimation with inverters and associated coolers. This is not being considered because it is perhaps not necessary to use one inverter for each motor pack (incl. cooler). Again, these weights are not the weights associated with Vimana.

6.4.6 Filament Winding Diameter

The size the filaments on the electric machines, in terms of their diameter, will of course have an effect on both weight and performance of the machines. A relatively small diameter for instance, will have a positive effect on the reduction of ac losses in the stator [38]. Generally, it is beneficial to reduce the filament diameter. The weights of the generators and motors with their associated coolers were determined in the previous subsections. These weights have an optimal filament diameter associated to them, and these can be determined with generated graphs similar to the one from Figure 6.17.
Based on the analysis done by Brown [22], an optimal filament diameter of $10\mu m$ was determined to be optimal, for both BSCCO and MgB_2. Therefore, when looking only at the generators, it makes no difference if MgB_2 is used or BSCCO. For the motors using MgB_2, a filament diameter of $2\mu m$ was optimal, whereas a diameter of $6\mu m$ was optimal for BSCCO. Therefore, for the motors, it is beneficial to use MgB_2.

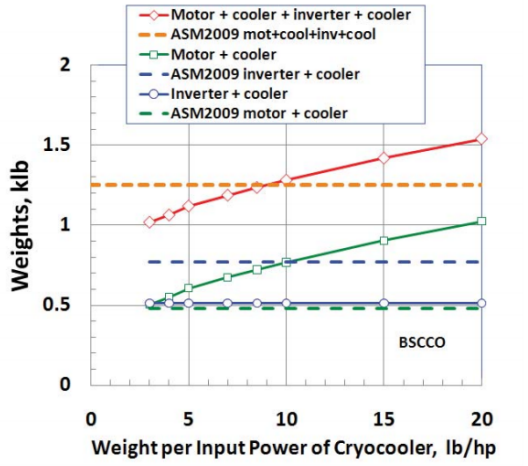

Figure 6.17: Weights of motor (with cooler), inverter (with cooler), and total as functions of the weight per input power of the cryocooler for BSCCO [22]

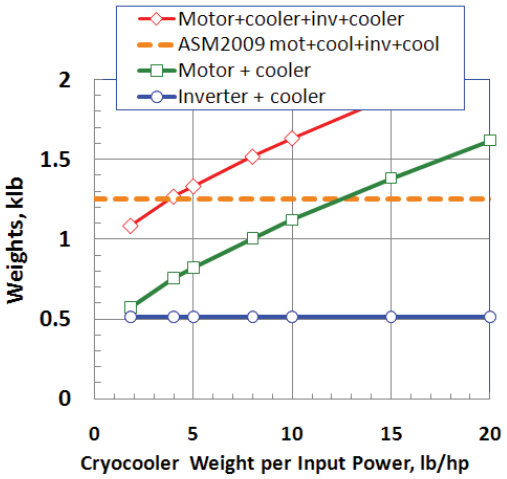

Figure 6.18: Motor (with cooler) and inverter (with cooler), and total weights as functions of cooler weight per input power for MgB_2 [22]

6.4.7 Efficiency

In an analogous fashion, analyses have been conducted to relate the filament winding diameter with a maximum allowable efficiency. For the generators, it was determined that an efficiency of 99.55% can be achieved with a filament diameter of $10\mu m$, for BSCCO, and an efficiency of 99.4% for MgB_2. Therefore, BSCCO shows a slightly better performance in terms of machine efficiency.
An overview of all the aspects that were considered to make a filament material selection, along with their associated 'results', are given in Table 6.10.

Table 6.10: Design parameters related to the usage of MgB_2 and BSCCO

Parameter	MgB_2	BSCCO	Unit
Generator + cooler weight	1588	1134	$[kg]$
Motor + cooler weight	362.87	273	$[kg]$
Filament winding diameter (generator)	10	10	$[\mu m]$
Filament winding diameter (motor)	2	5	$[\mu m]$
Efficiency	99.4	99.55	[%]

From this analysis, it can be seen that BSCCO performs better than MgB_2, except for the filament winding diameter in the motors. As mentioned before, a smaller diameter is beneficial in terms of reducing AC losses. The benefit of a $3\mu m$ reduction in filament diameter however, is considered to be negligible compared to the significant weight reductions and a slightly higher efficiency for both the generators and motors, when BSCCO is used. Therefore, it is decided to use BSCCO as the superconductive material.

6.4.8 Mass and Volume Estimation

After selecting the appropriate machine and material type to provide power, mass and volume estimations have to be conducted. Sizes of electrical machines are predominantly determined by their torque capability. Another performance parameter related to the size is the rated speed of the machines [39].
For convenience, the mass and volume estimations are done for the motor only. It is assumed that this analysis is also valid for the generators, as the only difference between these two machines is the direction of energy conversion [40]. Therefore, only motors will be mentioned in this part.
The first thing that has to be determined is the synchronous speed mentioned in Subsection 6.4.3. The synchronous speed is a function of the supply frequency and the number of poles. Assuming direct drive, this will also be the rotational speed at which the fans will be rotating. As will follow from Section 6.1, an optimal speed for the fans is $5600 RPM$. This will also be the desired synchronous speed of the motor. One thing that

has to be noted, is that this speed of revolution is relatively high, when compared to the output revolution speed of other electric motors. Therefore, adequate measures might have to be taken regarding the structural aspects, by for instance having a stronger bearing.
The determined optimal RPM corresponds to a required supply frequency to the synchronous motor. The relation given by Equation (6.6) holds for a synchronous motor, which relates the synchronous speed to the supply frequency.

$$n_s = \frac{120 \cdot f}{N_{poles}} \tag{6.6}$$

Therefore, to achieve this desired revolution speed, a supply frequency of $93.33Hz$ is needed. A two-pole, three phase synchronous motor with a supply frequency of $93.33Hz$ was chosen as it allows for the desired synchronous speed.
The aforementioned torque capability, is caused by the force that is acting on a wire carrying a current in a uniform magnetic field. Their relation is given by Equation (6.7).

$$F = I_e B l \tag{6.7}$$

This force is actually applied to the conductors, and an associated shear stress will then be associated to this force. If n is defined as the number of conductors per meter on a rotor, and the product of n and the current I_e defined as the linear current density A_e, the shear stress can be defined as given by Equation (6.8).

$$\sigma = \frac{F}{A} = BnI_e = BA_e \tag{6.8}$$

However, if the magnetic flux density B and current density A_e are amplitudes instead of the root mean square value, Equation (6.8) becomes Equation (6.9).

$$\sigma = \frac{1}{2}\hat{B}\hat{A} \tag{6.9}$$

This shear stress will then produce a torque, which is the driving parameter of the machine size. Their relationship is given by Equation (6.10), where D_m is the diameter of the rotor on which the torque is applied.

$$T = F\frac{D_m}{2} = \sigma A\frac{D_m}{2} = \sigma\pi D_m l\frac{D_m}{2} = \frac{\pi}{2}D_m^2 l\sigma \tag{6.10}$$

As can be seen from Equation (6.10), the torque is related to the volume of the machine, with $T \propto D_m^2 l$.
The torque can also be determined through a relation between the power output of the motor and the angular velocity of the machine. This is given by Equation (6.11).

$$T = \frac{P}{\omega_m} = \frac{P}{2\pi \cdot \frac{n_s}{60}} \tag{6.11}$$

For conventional machines, the magnetic flux density has a typical value of $1T$. However, for HTS machines, this value is generally two times higher and can even increase to $3T$ [41]. To stay at the conservative side however, it is decided to assume a value of $2T$, which is already achieved by existing HTS motors.
The linear current density can be assumed to be $100kA/m$, which is also the same as for conventional machines. According to [41], it is valid to assume that this value also holds for HTS machines.
With the torque known, the motor volume expressed as $D_m^2 \cdot l$ can then be solved for using Equation (6.10).
The input and output parameters used for Equations (6.6) through Equation (6.11) are listed in Table 6.11. The power requirements for the motors and generators are changed with respect to the listed ones in Table 6.9, since efficiencies are now taken into account.
The volume of one motor has been determined, however the exact dimensions in terms of the motor length and diameter still have to be determined. As will be explained in Subsection 6.7.1, the cryocoolers needed to cool the motors will have a certain length. Since these cryocoolers will be 'attached' along the circumference of the motors, the minimum length of the motors will be determined by the length of the cryocoolers.
To account for the cryocooler length and to have an extra offset for 'open' space left directly behind the fans, it is decided to have a motor length of $1m$. This results in a motor diameter of $0.28m$.
The volumes and dimensions of the generators are determined in an analogous way. Furthermore, with the volumes of the machines known, a mass estimation can now be conducted. For HTS machines, it can be assumed that these are completely made of a composite, except for the conducting windings. In particular, G10 Glass fiber is a suitable material type for this application. These type of machines are currently being developed, and show a significant weight reduction, at the cost of an increased price. The mass density of

Table 6.11: In- and output parameters for machine volume estimation

Input parameters	**Motor**	**Generator**	**Unit**
Power required (per unit, 99.5 % efficiency)	37.13	16.24	$[MW]$
Supply frequency f	93.33	93.33	$[Hz]$
Number of poles p	2	2	$[-]$
Magnetic flux density (amplitude) $\hat{B}$	2	2	$[T]$
Linear current density (amplitude) $\hat{A}$	100	100	$[kA/m]$
Power P (per unit)	4617.5	16,160	$[kW]$
Synchronous speed n_s	5600	5600	$[RPM]$
Output parameters			
Torque	12.31	129.24	$[kNm]$
Volume $(L \cdot D^2)$	0.062	0.822	$[m^3]$

G10 Glass fiber is $1800kg/m^3$ [41], and this value is used to come up with a mass estimation of the electric machines. Furthermore, it is assumed that the mass of the filament windings is negligible. The final weights and dimensions of the electric machines are listed in Table 6.12.

Table 6.12: Electric machines weight and volumes

Input parameters	**Motor**	**Generator**	**Unit**
Weight excluding cooler (per unit)	110.79	812.06	[kg]
Length	1	1	[m]
Diameter	0.279	0.907	[m]
Filament material	BSCCO	BSCCO	

6.5 Cabling

For the hybrid propulsion design, there is an option to use High Temperature Superconducting (HTS) cabling. The motivation for using such cabling as opposed to regular electricity conducting copper wiring is that HTS cables have an efficiency of 100%, which means that they have almost no electrical resistance. This will have an effect on the engine and generator sizing as well, since no losses are present in the cables. Besides this, there are many other different advantages such as life extension as there is no thermal overload [42].
However, in order to retain the superconducting property of the cabling, it must be kept at cryogenic temperatures. According to PhD-candidate Dong Liu at the EWI faculty of TU Delft who is a specialist in superconducting materials, this needs a special way of cooling. The cables are immersed in a fluid with a low boiling point, such that the fluid is in the liquid state ensuring superconductivity. Commonly used fluids for this purpose are liquid hydrogen and neon, with boiling points of $20.1K$ and $26.9K$ respectively. Taking into account the critical temperature for HTS cabling ($77K$ [42]), it would be better to use neon as it can absorb more heat before evaporating. This is confirmed by the HTS cable designs that are currently available. The neon flow system is already incorporated is this design and taken into account for the weight calculations.
Upon evaporation, the gas would either need to be ejected or re-liquefied. The latter option would require the use of a separate compressor which would liquefy and cool the gaseous neon. It was also considered to use methane as a coolant for cabling immersion since liquid methane is already being used as a cryocooler (used for cooling generators and motors) heat sink and (mixed with jet fuel) energy source. However, the melting point of methane is $90.7K$, which is a temperature regime where HTS does not provide good performance, since the allowed current is too low.

6.5.1 Mass Estimate

Now that the placement of all components of the propulsion system is known, the length of the cables can be estimated. This approach is visualized in Figure 6.19. It is important that redundancy is taken into account. Especially for the connection between the controllers next to the generators and the controllers between the motors. Also, if one controller fails, there is a crossflow in order that not a single components can get isolated. A more detailed figure on how the architecture looks like can be found in Figure 6.22. Once the total length has been determined, the mass is determined since HTS cables have a mass density of $9.2kg/m$ [28].

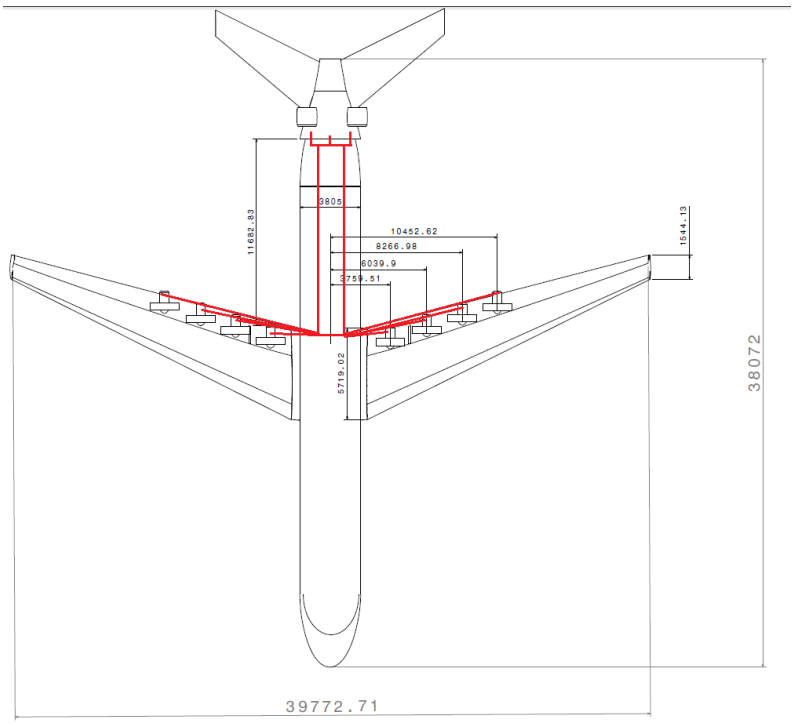

Figure 6.19: Projected cabling pathways based on the aircraft planform

Figure 6.19 shows the cabling layout. Based on this, the total length is estimated and has a value of $80.4m$. Multiplying this with the density, the cabling has a mass of $740kg$. Since an electric circuit needs to be closed, cables also need to go back to make a loop. Assuming that the cabling can be put into the same cooling system together with the other cable, it is multiplied by a factor of 1.5 instead of 2. Resulting in a total mass of the cabling of $1110kg$. This is however only the mass of the cabling, not including additional weight of the cryocoolers. This will be addressed in Section 6.7.

6.6 Controllers

As can be seen in the architecture of the propulsion system (Figure 6.22) several controllers are present. These are the Battery Control Unit (BCU), Motor Controller (MC) and the Solid State Power Controller (SSPC). The weights of the BCU, MC and SSPC's are insignificant when compared to the total weight of the aircraft[10]. They are therefore not taken into account for the propulsion system weight. A more elaborate explanation about the SSPC is given in Subsection 6.6.1 [28]. The motor is controlled by the motor controller, which delivers and regulates the electric energy to the electric motor.

6.6.1 Solid State Power Controller (SSPC)

SSPCs are superconductive devices that regulate the current supplied to the components. In the propulsion system architecture, they are placed between the generator and controller, and between the controller and motor[11]. They also perform several other functions, as they have diagnostic functions which identify overload conditions and prevent short circuits. There are different kinds of controllers. These are the DC, AC and AC/DC controllers. Each is designed to switch a specific voltage, and the AC/DC controllers are designed to switch both AC and DC voltage. Between the generators and controllers, AC SSPCs are placed, as generators output AC current. The input for the motors driving the fans also use AC current. Thus the SSPC's connecting them switch AC voltage.

[10]URL "http://www.globalspec.com/search/products?page=mi#comp=4721&vid=90828&sqid=12784541", [cited 2 June 2015]

[11]URL "http://www.globalspec.com/learnmore/semiconductors/power_power_management_ic/solid_state_power_controllers_sspc", [cited 2 June 2015]

6.7 Cooling

In order to efficiently make use of the superconductive properties, the temperature has to be below the critical temperature of HTS material, which is $30K$ [43]. The HTS superconductors used inside the generators and motors are explained and determined in this section. The HTS superconductors operate at cryogenic temperatures. Cryocoolers need to be used to ensure this temperature. Liquid methane is present as a heat sink. A more elaborate discussion on sizing and placement is done in the following subsections.The fluid that is used to cool the superconducting materials is called the cryogen. There are several fluids that can be used for this, for example H_2. It has a boiling temperature of $22.39K$, making it a suitable option, as it is in the superconductive range. However, because of the enormous volume needed for this option, it is discarded. Another option is liquid helium, but this is mostly reserved for low temperature superconductivity (LTS). The most suitable option for high-field applications, for HTS, is neon (Ne) [41], which has a boiling temperature of $27.09K$.

6.7.1 Cryocoolers

One of the main drawbacks of HTS hybrid propelled aircraft is the weight of the cryocoolers [44]. In order for this concept to be viable, they need to have a power density of $3kg/kW$ or lower and a high Carnot efficiency [44]. At the moment there is one preliminary design that can achieve this goal, i.e. it has a power density of $3kg/kW$ and a Carnot efficiency of 30%. This still has to be validated by actual fabrication and testing, but it seems promising as this goal has to be achieved in 20 years [22].
To keep the generators and motors at a cryogenic temperature, it is required for the cryocoolers to have a separate cryostat and cryocooler arrangement for each of the 3 generators and 8 motors. Optimization could lead to a configuration where less crycoolers are required as one cooler could be split between multiple components. In order to cryogenically cool the neon to suitable temperatures, a compressor is used. Once the neon passes the component which has to be cryocooled, it is pumped to a compressor. This compressor compresses the fluid and reroutes it to the cryocooler.

6.7.2 Cryostat

The cryostat is the system that maintains the superconductor magnet coils in an environment suitable for operation. These magnet coils are located inside the generators and motors. According to PhD-candidate Dong Liu, the superconducting magnets are bathed in a pool of neon, which has a boiling temperature of $27K$. Any heat that is generated by the magnets is transferred to the cryogen (i.e. the neon). Due to the added heat to the cryogen, some of it vaporizes. This vaporized neon is directed to the compressor, which compresses the neon back into a liquid form, suitable again for cryogenically cooling the superconductor. The cryostat is regulated by coldheads located on the outer circumference. Multiple coldheads might be required to effectively cool the motor or generator to cryogenic temperatures.

6.7.3 Methane Tanks

Using liquefied methane along with jet fuel allows for many potential benefits while retaining the advantage of the high inherent energy density of jet fuel. Liquid methane acts as a heat sink for the cryocoolers since it is stored at around $111K$[12]. Due to the low temperature it provides a comparatively favourable temperature jump, in relation to a hot day ambient temperature of $325K$. The liquid methane is also cool enough to cool the power inverters. As a primary estimate, this means that the cryocoolers would have to remove heat due to losses in the superconducting components, which are expected to be at $40K$. Therefore, an increase of only $71K$ $(= 111 - 40)$ would be required instead of $285K$ $(= 325 - 40)$.
Some rudimentary approximations done by Felder et al. [45] suggest that the total power loss of a system partially fuelled by liquid methane (which is also used for cooling), would be 0.4%. It then follows that, in comparison to a fully methane powered aircraft, the required methane flow rate (for cooling) of such a methane jet fuel combination is approximately 17%. Therefore, it is possible to carry enough methane to provide cooling and also 17% of the energy required by the turboshaft engines. Liquid methane also has a density of $421kg/m^3$, which is about half that of jet fuel ($810kg/m^3$). The result is that, compared to a fully jet fuelled aircraft, the proposed concept would have 17% of the jet fuel replaced by methane and this

[12] URL "http://science.nasa.gov/science-news/science-at-nasa/2007/04may_methaneblast/", [cited 1 June 2015]

would result in a net increase in total fuel tank volume of about 17%. Thus, the volume fraction of the liquid methane in the enlarged tanks is 29% while the mass fraction is 17%.

Sizing and Placing Methane Tank

The total amount of jet fuel needed for flight is $23735kg$. As mentioned above, the methane is also used as fuel, 17% of the mass of jet fuel is replaced by methane and 17% volume is added. This gives a total volume of $8.6m^3$ of liquid methane that needs to be stored in special tanks. To liquefy methane it must be stored at $111K$. To get the methane to this temperature, it needs to be cooled on the ground during turn-around time. The tank in the aircraft needs to be insulated to limit temperature change. A process called auto-refrigeration can be used to keep the methane cool. For this to happen the tank needs to be kept at a pressure of 1 atmosphere [46] and a small amount of gas needs to be able to leave the tank due to temperature changes. The gas is then cooled and liquefied again.
AIR-LNG, a company which focuses on using liquid methane (LNG) as an alternative fuel for mobility, conducted a study on using LNG in existing commercial transport aircraft. From this study [47] ideas are taken to integrate LNG into aircraft without making major changes. The tanks, with their own pumps are placed in cargo containers. For the required volume, three cargo containers (LD3-45 containers) are needed as they each have a volume of $3.68m^3$. They are loaded near the center of gravity for decreasing the centre of gravity shift. The tank mass is estimated to be $620kg$. This value is a scaled down one from an aircraft design which runs on 70% LNG. The benefits of having the tanks placed in the cargo container, as shown in Figure 6.20, is that they are interchangeable. This provides easier maintenance and decreasing turn around time as they can already be filled and stored at the airport. One is located just in front of the central wing box and two right behind it. This still leaves eight places for cargo containers to carry the required 18500kg of payload.

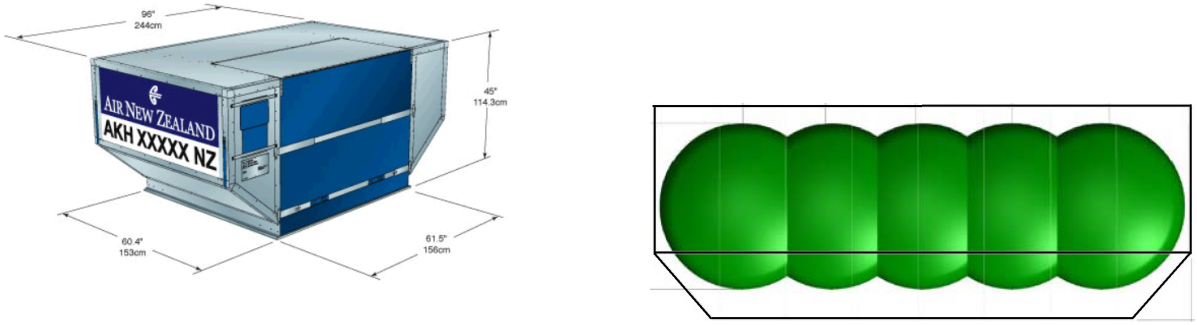

Figure 6.20: Integration of methane tanks in cargo containers[13] [47]

6.7.4 Cryocooler Weight and Volume Sizing

According to PhD-candidate Dong Liu, the typical required cryocooler power needed to cool at $20K$ is 0.01% of the total power of the component. To cool one motor of $4.62MW$ to a cryogenic temperature of $27K$, the refrigeration power of $462W$ is thus sufficient. Cryocoolers have to be sized to comply with these power requirements.

There are several types of cryocoolers that could be utilized. The two most optimal ones are the Gifford McMohan (G-M) cryocoolers or Stirling cryocoolers. In terms of weight and cost, the G-M cryocoolers are preferred [41]. A downside of this system is the high vibrations from the moving displacers. A way to mitigate this problem is by locating the cryocooler at a sufficient distance from the component which is cooled. A single-stage cooler will be used in the design of Vimana, as this is sufficient for cooling at $20K$ and above.

Volume and Weight Estimation

The volume required for the compressors and coldheads are calculated in this subsection. The compressors are located in the fuselage, while the coldheads are located around the circumference of the generators and motors. Thus, the coldheads add to the overall diameter of these electrical machines. The volume of the

[13] URL "http://www.airnewzealand.co.nz/assets/Images-AirNewZealand/container-akh-ld3-45-538x315.gif", [cited 22 June 2015]

cryocoolers is estimated by looking at existing ones. The reason for this approach is that currently no suitable volume estimation methods are available for cryocoolers that will be used in 20 years to get an adequate approximation. For the coming 20 years, it is not expected that cryocoolers will increase in size. On the contrary, a decrease in size is possible with more advanced technologies that might be developed. However, the worst case scenario has to be taken into account. Hence, dimensions of currently existing cryocoolers are used.
The weights are estimated with the assumption that in the near future, by 2025, the cryocooler weight for the same power input, has reduced by a factor of 6 [22]. This is, as mentioned in the source, a very aggressive assumption. For the design of Vimana, a factor of 3 is taken. This is done to decrease the risk of not having the technology ready in the future. With a factor of 3, the cryocooler weights are still suitable for use in the aircraft. Once again, the current weight is estimated based on currently available cryocoolers. The cryocoolers that are needed to cool the HTS cabling, can be neglected, as these weights are insignificant compared to the total cryocooler weight [48].
As was mentioned before, one of the main components of a cryocooler is the coldhead. A suitable coldhead for the application in mind is the AL325[14], which has a cooling capacity of $100W$ at $25K$. This means that each motor, which has a power of $4.62MW$, needs 5 coldheads to provide the required cooling power of $462W$. One coldhead is added to this number for redundancy, making it a total of 6 coldheads.
As mentioned above, the cryocoolers increase the diameter of the electrical machines. The diameter of the motors and generators will therefore be increased by $0.49m$[15]. This is when the coldheads are evenly distributed over the motor. An engineering drawing of the AL325 coldhead can be viewed in Appendix A.1. The total diameter of each motor will therefore be $0.77m$.
The coldheads do not only increase the volume of the motors, but consequently also increases the mass of it. One coldhead has a mass of $22kg$, but it is expected that the mass of one coldhead, when the aircraft will be build thus taking into account the factor of 3, has a weight of $7.33kg$. The total mass of the coldheads per motor is therefore $6 \cdot 7.33 = 43.98kg$. The mass of all the coldheads for all the motors is $351.84kg$

The approach that has been taken to get estimates for the motors can be used for the generator as well. The results for both the generators and motors can be found in Table 6.13. Once the power requirements for the coldhead are known, the compressors can be sized. The power consumption for the compressor is equal to the the total refrigeration power needed, which is $8.5kW$. A suitable compressor for this operation is the CP1110[14]. This compressor has a power consumption of $11.2kW$. Again, redundancy is taken into account thus two compressors are installed. The volume of one compressor is $0.61m$ x $0.61m$ x $0.79m$ (L x W x H), giving a volume of $0.29m^3$. This gives a total volume taken up by the compressors for the motors of $0.58m^3$. The compressors themselves can get very hot and this might cause efficiency losses. Therefore current compressors make use of water-cooling system. Vimana makes use of methane for this, as it can be used as fuel later. Modifications have to be performed to accommodate the methane cooling instead of water cooling. The weight of the CP1110 is $190.5kg$. The expected weight is therefore $63.5kg$, taking the factor of 3 again into account. Two compressors therefore have a total weight of $127kg$. An overview for the cryocooler weights is given in Table 6.13. The total weight of the cryocooler is $834.23kg$.

Table 6.13: Overview of the cryocooler weights

Parameter	Single component weight [kg]	Total weight [kg]
Coldhead for motor	41.21	329.71
Coldhead for generators	125.84	377.52
Compressor	63.5	127

In Section 6.4 the dimensions of the motors and generators were calculated. These dimensions however, did not take into account the extra space that would be taken up by the cryocoolers. The dimensions and weights of the coldheads were calculated in this section and have to be added to the motors and generators. In Table 6.14 the final machine dimensions and weights, including the coldheads, are given.

[14]URL "http://www.cryomech.com/specificationsheet/AL325_ss.pdf", [cited 2 June 2015]
[15]URL "http://www.cryomech.com/coldhead/AL325_ch.pdf", [cited 19 June 2015]

Table 6.14: Final motor and generator weights and dimensions

Component	Single weight [kg]	Total weight [kg]	Dimensions (length x diameter) [m]
Motor	152.00	1216.03	1.0 x 0.77
Generator	937.84	2813.52	1.0 x 1.40

6.8 Auxilary Power Unit

Vimana is a commercial transport aircraft for 180 passengers and therefore, it is of paramount importance that redundancies are built into every key system. In order to avoid overloading the propulsion powerplants in terms of providing energy to elements in the aircraft not directly related to propulsion, and to add to redundancy, a feature that is present on conventional aircraft is an Auxiliary Power Unit (APU). This section will elaborate on three important aspects: the Vimana auxiliary power system description, the battery mass estimation and the power fluctuation control method.

6.8.1 Auxiliary Power System

Current APUs such as the Honeywell 131-9 series[16], used by Boeing in its 737 model, are downsized gas turbines designed to provide electrical and pneumatic assistance to the aircraft, during flight and ground phases. It allows the aircraft to be self sufficient on the ground, so that it does not need power from ground stations.

One of the key roles of the gas turbine APU in aircraft operations is to start up the engines. High pressure bleed air from the APU is used for a pneumatic start-up procedure. One of the main components is the starter generator, which supplies the initial rotation of the APU during its start cycle and provides a source of electrical power for aircraft systems once the APU is running.

However, it was decided to use a battery based APU system in the design for Vimana. This will be less noisy than a conventional gas turbine APU. Furthermore, twin engined aircraft have to adhere to ETOPS restrictions [49], which state that there is a strict requirement to include a gas turbine APU in the aircraft design. However, this does not apply to Vimana since it has three turboshaft engines. Similar to the current Boeing 787 Dreamliner design[17], the battery pack will essentially consist of two separate sections, the APU battery section and the main battery section, located independently in the aircraft for safety reasons. The main battery will be placed near the forward cockpit electronics equipment bay, in the lower fuselage near the front of the aircraft while the APU battery is placed in the aft electronics equipment bay in the lower fuselage near the back. The main battery provides power to systems such as lighting, displays and instruments before the turbines are started. Once the engines are up to power, the associated generators take over the role of providing the electrical energy. The main battery is also used in situations where the engines are not able to provide the adequate power, mostly in ground operations such as refueling and powering the braking system while the aircraft is being towed[17].

In the Boeing 787, the APU battery supplies power to start the gas turbine APU, which in turn can start the aircraft engines. However, the concept being proposed here is to eliminate the APU gas turbine entirely and to size the APU battery to only power the auxiliary systems. The battery will provide power to an electric starter motor, which will, in turn assist in engine start. The bleed air required during start, however, will be provided by an external gas turbine; a so-called "huffer cart". Thereafter, the battery pack provides power to the auxiliary units as mentioned above and is eventually re-charged with any excess power that may be available during the flight. The huffer cart, which is an external source, will be utilized to start up the three turboshaft engines at the back of the aircraft. A huffer is an external engine which creates large volumes of pressurized air. This compressed air will be blown to the aircraft's bleed system, and subsequently to the engine's starter generator.

It is also imperative to consider the case of engine failure or stoppage during flight and the associated re-start procedure. In standard aircraft, if one engine stops and a re-start is necessary, an electric starter motor starts

[16] URL "http://www.deltatechops.com/mro-capabilities/view/category/apu", [cited 22 May 2015]
[17] URL "http://787updates.newairplane.com/787-Electrical-Systems/Batteries-and-Advanced-Airplanes", [cited 22 June 2015]

the APU (if it is not running already), which then provides bleed air to attempt an engine re-start. However, for Vimana, alternate strategies have to be considered since there is no gas-turbine APU present. One option is to use the excess power supplied by the other operational engines in order to attempt a cross-bleed start. Alternatively, a windmill restart may be attempted. The latter option requires the aircraft to be at an altitude and descent rate that allows sufficient massflow into the turbines. Since this is a strategy with more stringent requirements, it should be kept as the secondary strategy, only to be used if a cross-flow start is not possible.

6.8.2 Battery Mass Estimate

An estimate of the battery mass is difficult to obtain since it would require a detailed analysis of all the expected power usage components and their associated power requirements. However, for the purposes of this report, a preliminary estimate was obtained based on the power density of Lithium-Air batteries (Figure 6.11) and an approximation of the standard auxiliary power fractions expected for an aircraft of this size. The latter was established based on an information brochure detailing the power output of the APU used on the Airbus A321, the Honeywell APU 131-9[A]. This states that the APU unit is capable of providing 'full electrical power of $90kW$ up to 35,000ft for the aircraft'[18]. Using a power density from the aforementioned figure of $1000W/kg$, an estimated battery mass of $90kg$ is obtained. The Honeywell APU providing this power weighs $164kg$. In order to account for safety factors and to ensure that the battery can provide the required power while also contributing to engine start-ups, the battery mass is taken to be $150kg$. Based on the power density, this leads to a power output at peak of $150kW$. Finally, although the battery is rechargeable (refer to Subsection 6.8.3) and excess power will be used to keep the battery topped up and charged, any mass estimate should take a value of two times the charged battery mass value, that is, $300kg$. This is due to the chemical property of Lithium Ion battery cells, which double in weight on discharge. This information is taken from a discussion with an expert on battery technology, Dr. E.M. Kelder of the Faculty of Chemical Engineering.

6.8.3 Power Fluctuation Control

If there are discrepancies between required power by the motors and produced power by the generators, this excess power should be drained somewhere. The first power sink and source are the batteries, see previous Subsection 6.8.2. When the motors require more power than the generators and batteries generate at that very instant, the fan will slow down. The electricity production will then be increased which leads to the desirable condition after a short delay. This aircraft will thus slow down slightly in this situation. When the generators produce more power than the motors require and can be used to charge the batteries at that very instant, there is a power excess. This may lead to the fans and thus the aircraft speeding up. Again, the desirable condition can be restored after a short delay by throttling down the turboshafts.
There might be a possibility to dump excess power. This can be done by integrating a long thin cable, working as a resistor, in the horizontal tail. When electricity flows through this resistor, this resistor works as a power dump. As a consequence, the resistor will heat up. This heat can however very effectively be transferred to the airflow since the resistor is in direct contact with the flow. The resistor can therefore also be considered as a radiator, transferring electricity to heat and dumping that thermal energy to the air. This is however a novel idea, needing further research on the concept itself as well as on the need for this system.

6.9 Final Architecture

After conducting analyses on all components and aspects related to the propulsion system of Vimana, an overview of the final calculated parameters is presented in this section. The weights and volumes of the components related to the HTS propulsion system are listed in Table 6.15.
It must be noted that the volume of the battery is not determined. This analysis will have to be conducted in future phases, as it depends on many factors, like battery cell packing density, which is still unknown. However, it is expected that there is enough space in the fuselage for a relatively small battery of 150kg (300kg when discharged). In addition to these values, a visual representation of the engines is given in Figure 6.21.

[18] URL "http://www.comlaw.gov.au/Details/F2007L00101", [cited 22 May 2015]

Table 6.15: Mass and volume budgets for the different component in the HTS hybrid propulsion system

Component	Weight [kg]	Volume [m^3]
Engine	942.9 (x3)	4.19 (x3)
Generator (incl. refrigeration)	937.84 (x3)	1.337 (x3)
Motors (incl. refrigeration)	152.00 (x8)	0.357 (x8)
Battery	300	[-]
Cabling	1110	[-]
Fan Blades	32 (x8)	[-]
Fan Duct	253 (x8)	[-]
Fan Structure	60 (x8)	[-]

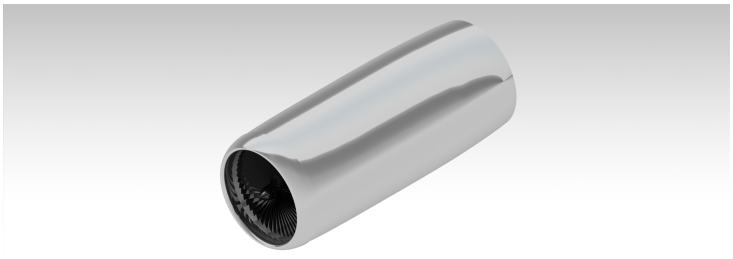

Figure 6.21: Visual representation of the turbine

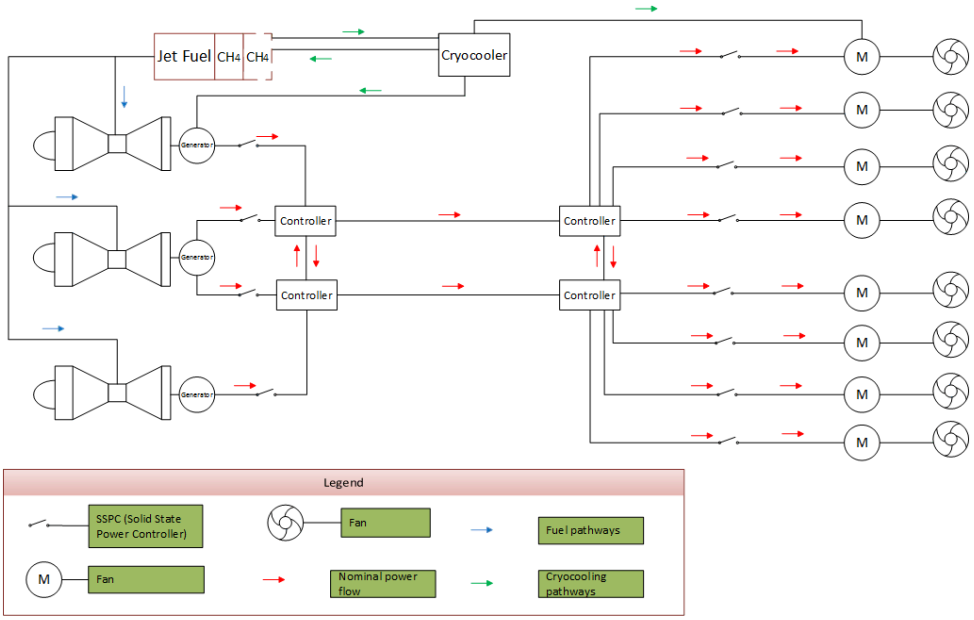

Figure 6.22: Propulsion system architecture

Chapter 7 | Results

This chapter presents the results of the distributed propulsion aircraft, Vimana, that has been designed. In Section 7.1, the values for different iteration steps are stated, followed by a mass budget breakdown in Section 7.2. Analyses regarding aerodynamics and structures are shown in Sections 7.3 and 7.4 respectively. The controllability and stability of the aircraft has been investigated in Section 7.5, after which the performance analysis is done in Section 7.6. Section 7.7 completes the chapter by stating the verification and validation results.

7.1 Iteration Results

In this section, the results of the design iterations as described in Chapter 4 are presented for Vimana. From the iteration procedure described in Chapter 4, several important design parameters are found. First, in Figure 7.1 the convergence of the method is displayed and in Table 7.1 the most important parameters of the design are given.

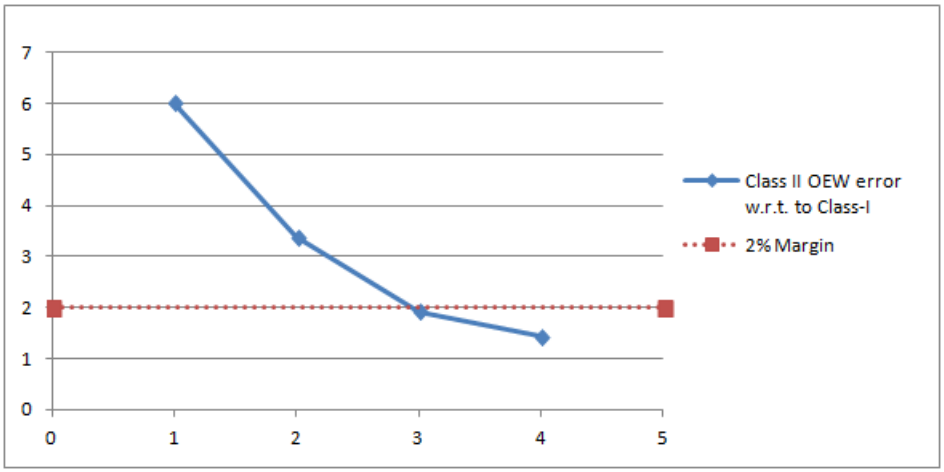

Figure 7.1: The error between the Class I and Class II iterations displayed per iteration

Table 7.1: Design parameters of Vimana

	Value	**Unit**
Weights		
MTOW	86302	$[kg]$
OEW	46524	$[kg]$
Fuel Weight	21105	$[kg]$
Performance		
SFC	1.166E-05	$[kg/Ns]$
Lift/Drag	18.19	$[-]$
Wing		
Wing area	148.04	$[m^2]$
Span	39.27	$[m]$
M.A.C.	4.33	$[m]$
Aspect ratio	12.50	$[-]$
Taper	0.20	$[-]$
Quarter chord sweep	23.92	$[deg]$
Fuselage		
Length	42.14	$[m]$
Diameter (outer)	3.81	$[m]$
Horizontal Tail		
Sh/S	0.285	-
Tail area	38.8	$[m^2]$

7.2 Mass Budget Breakdown

In this section the mass budget breakdown will be presented. These mass budgets are obtained from the Class II weight estimation and the contingency allowance for this specific design phase.

7.2.1 Class II

As described in Section 4.7, a Class II weight estimation was performed for Vimana. In Table 7.2, the results of this Class II weight estimation are presented. In Table 7.3 a more detailed breakdown of the preliminary propulsion system weight breakdown is given. In Chapter 6 it has been explained how these values are obtained. Some notable exclusions in Table 7.2 are the vertical tail, the APU, the nacelles and the engine starters. As will be described in Subsection 7.5.4, it was chosen to use differential thrust for yaw control instead of a vertical tail. Also, the APU's functions are performed by the batteries combined with the turbine which makes the APU obsolete. The nacelle weight is incorporated in the propulsion system weight as can be seen in the more detailed propulsion system mass breakdown in Table 7.3. Lastly, the engine starters functions are performed by the generators which can be used as electric motors to start the turbines.
In Table 7.3, the mass estimates can be seen for the preliminary and detailed design of the propulsion system.

Table 7.2: Class - II weight estimation for the Vimana

Group	Component	Weight [lb]	Weight [kg]
Airframe Structure	Wing	17175.0	7790.5
	Horizontal Tail	1717.2	778.9
	Fuselage	33290.3	15100.4
	Main Landing Gear	1829.3	829.8
	Nose Landing Gear	212.0	96.2
Propulsion group	Engine Controls	58.9	26.7
	Propulsion (Tail)	12062.8	5471.6
	Fuel System	863.9	391.9
	Propulsion (Wing)	11509.2	5220.5
Airframe Systems	Flight Controls	3964.8	1798.4
	Instruments	2200.0	997.9
	Electrical	4343.5	1970.2
	Air Conditioning	4376.7	1985.3
Airframe Services	Furnishing	8962.784	4065.492
Total		**102566.3**	**46523.78**

7.2.2 Comparison with Reference Aircraft

The obtained masses for the different are compared to those of the reference aircraft. In Table 7.4 the mass of each of the components can be found for both the reference aircraft and for Vimana. In the last column the offset of the Vimana aircraft with respect to the reference aircraft can be found. As can be seen, there are a few notable differences.
First of all, it can be seen that the horizontal tail of Vimana is 21.68% heavier. $\frac{Sh}{S}$ is almost identical for the two aircraft, but since the wing surface area of Vimana is larger the tail is larger. Secondly, the landing gear system is less heavy for the Vimana aircraft due to the gear being shorter. No nacelle weight is given for the Vimana since these are included in the propulsion system. As can be seen, this propulsion system is also substantially heavier than that of the reference aircraft. This can be contributed to the fact that a more complicated propulsion system is used and that nacelle weight, battery weight and the methane systems weight are included in the propulsion system. Lastly, it is noted no starter weight and APU weight is present for the Vimana. This due to the fact that the starters functions are performed by the generators and the APU is replaced by a battery which is included in the propulsion system.

Table 7.3: Propulsion system mass breakdown

Component	Included in	Unit	Weight preliminary design	Weight detailed design
Turbines	Propulsion (Tail)	$[kg]$	5471.64	5642.40
HTS Cabling	Electrical	$[kg]$	800.00	1110.00
Total Airframe		$[kg]$	6271.64	6752.40
Ducted Fans	Propulsion (Wing)	$[kg]$	4489.52	3976.00
Motors (x8)		$[kg]$	216.19	152.00
Ducts & Fans (x8)		$[kg]$	285.00	285.00
Structure & Stators (x8)		$[kg]$	60.00	60.00
Batteries	Propulsion (Wing)	$[kg]$	5.00	300.00
Cryocoolers	Propulsion (Wing)	$[kg]$	126.00	127.00
Methane tank	Propulsion (Wing)	$[kg]$	600.00	620.00
Total Wing		$[kg]$	5540.52	5023.00
	Total		11492.16	11775.40

This finally result in a operational empty weight of the Vimana which is 8.47% higher than that of the reference aircraft. But even with this weight increase, the Vimana has a 11.81% smaller fuel weight. A maximum takeoff weight of Vimana 0.94% higher than that of the reference aircraft is obtained.

7.2.3 Mass Contingency

For each of the different subsystems, a contingency allowance is set. These contingencies are displayed below in Table 7.5. The items in this table are explained below.

- **Fuselage & Empennage:** The numbers for fuselage and empennage are the same because of a heavy expected inter-dependency.
- **Wing:** Since distributed propulsion as an idea is still very much in a conceptual stage, its integration in/on the wing will have to be more thoroughly examined. Therefore, a higher margin was used.
- **Nacelle:** The nacelle values were assigned by using a similar reasoning as for the wing. However, as the design matures into the preliminary design and detailed design phases, a smaller contingency than the wing has been assigned since it is expected that the variance in mass of the nacelle will be smaller than that of the wing, which has higher inter-dependencies with other components.
- **Propulsion:** A high initial value here due to lack of propulsion system maturity, as mentioned before. As the project progresses towards detailed design, contingency values become smaller, but the smallest value is still higher than for other elements, again due to the modernity of distributed propulsion concepts.
- **Fuel:** The values in the beginning are similar to propulsion but towards detailed design, it is expected that there is less variance in the amount of fuel to be used (as compared to the propulsion system type).
- **Subsystems:** These contingency values are comparatively smaller. This is because most subsystem values will be sized based on existing aircraft since this is not the focus of the project. Therefore, the values are not expected to have a high variance.

These values were chosen with the DSE timetable in mind. Because of this, for this mass budget analysis, the detailed design phase contingency allowance is the applicable contingency allowance.

7.2.4 Mass Budgets

Using the mass contingency allowance defined in Subsection 7.2.3 and the mass of different subsystems obtained in Section 7.2.1, the mass budgets are obtained. In Table 7.6 these mass budgets are presented.

Table 7.4: Comparison of component weight of the Vimana aircraft with the reference aircraft

	Reference Aircraft	**Vimana**	
Component	Weight $[kg]$	Weight $[kg]$	Offset $[\%]$
Wing	7786.10	7790.52	0.06%
Horizontal Tail	640.15	778.92	21.68%
Vertical Tail	668.99	0.00	-100.00%
Fuselage	14268.87	15100.38	5.83%
Main Landing Gear	1750.96	829.78	-52.61%
Nose Landing Gear	583.65	96.17	-83.52%
Nacelle Group	551.67	0.00	-100.00%
Engine Controls	25.71	26.72	3.93%
Propulsion System	6054.80	10692.16	76.59%
Fuel System	384.91	391.87	1.81%
Starter	190.59	0.00	-100.00%
Flight Controls	1774.46	1798.42	1.35%
APU installed	100.00	0.00	-100.00%
Instruments	997.91	997.91	0.00%
Electrical	1072.37	1970.18	83.72%
Air Conditioning	1985.26	1985.26	0.00%
Furnishing	4054.88	4065.49	0.26%
OEW	42891.28	46523.78	8.47%
Fuel Weight	23932.00	21105.00	-11.81%
MTOW	85494.27	86301.39	0.94%

Table 7.5: Contingency allowances on the mass

A/C Mass contingency allowance	**Contingency (%)**						
Design Maturity	Structure				Propulsion System	Fuel	Sub-systems
	Fuselage	Wing	Empennage	Nacelle			
Initiation Phase	30	35	30	35	40	40	25
Conceptual Design Phase	30	30	30	30	30	30	20
Preliminary Design Phase	20	25	20	20	25	20	10
Detailed Design Phase	10	15	10	10	20	10	10

7.3 Aerodynamic Analysis

This section will cover the aerodynamic analysis of Vimana. The chosen airfoil is presented in Subsection 7.3.1. the wing planform of the aircraft is shown in Subsection 7.3.2, followed by a sizing of the high lift devices in Subsection 7.3.3. Subsection 7.3.4 and 7.3.5 will treat the drag analysis and lift drag polar respectively.

7.3.1 Airfoil Selection

It was stated in Section 7.1 that a wing area of 148.04m^2 had to be delivered by a wingspan of 39.27m. This is all related to a design lift coefficient C_L of 0.536. With all the aforementioned parameters defined, a set of requirements and desired performance characteristics can be established for the aircraft's airfoil. For this exercise, five different performance criteria were evaluated, each with a respective weight between 1 and 5.

- **Critical Mach Number:** Due to the inherent free-stream flow accelerations occurring on the wing surface, each airfoil possesses a critical Mach number. This number represents the freestream Mach number at which the flow will become sonic on the lowest pressure point on the airfoil. Due to the considerable drag increases inherent of sonic flow, it must be assured that the Mach number perpendic-

Table 7.6: Mass budget for the different subsystems

Group	Component	Contingency Allowance [%]	Lower limit weight [kg]	Weight [kg]	Upper limit weight [kg]
Airframe Structure	Wing	15	6621.9	7790.5	8959.1
	Horizontal Tail	10	701.0	778.9	856.8
	Fuselage	10	13590.3	15100.4	16610.4
	Main Landing Gear	10	746.8	829.8	912.8
	Nose Landing Gear	10	86.5	96.2	105.8
Propulsion group	Engine Controls	10	24.0	26.7	29.4
	Propulsion (Tail)	20	4377.3	5471.6	6566.0
	Fuel System	10	352.7	391.9	431.1
	Propulsion (Wing)	20	4176.4	5220.5	6264.6
Airframe Systems	Flight Controls	10	1618.6	1798.4	1978.3
	Instruments	10	898.1	997.9	1097.7
	Electrical	10	1773.2	1970.2	2167.2
	Air Conditioning	10	1786.7	1985.3	2183.8
Airframe Services	Furnishing	10	3658.9	4065.5	4472.0
Total			**40412.7**	**46523.8**	**52634.9**

ular to the airfoil remains below the airfoil's critical Mach number. However, higher freestream Mach numbers can be achieved by means of a wing sweep angle. The use of sweep, nonetheless, introduces several negative consequences such as increased structural and geometrical complexity (high lift devices placement becomes more difficult) and more stall tendencies. This parameter was considered to be of utmost importance and was given the weight of 5.

- **Airfoil thickness:** The use of a hybrid superconductive distributed propulsion system introduces several new components to the propulsion system such as generators, batteries, cooling equipment and motors. It has to be validated whether the cabling systems and landing gear will also fit within the available wing volume. Due to the fact that the vast majority of the wing volume is used by the jet fuel, available space might become an issue. Using airfoils with high thicknesses allows an increase in the available volume for additional aircraft systems and components. This parameter was given a value of 4.

- **Aerodynamic Efficiency (L/D):** In order to reduce the required thrust and hence the fuel consumption, drag should always be kept at the lowest possible level. Using simple open-source software such as Javafoil, the aerodynamic efficiency of each airfoil can be determined at the specified cruise conditions. Together with the critical Mach number, aerodynamic efficiency is an essential performance requirement an was also awarded a weight of 5.

- $\mathbf{C_{l,max}}$: As mentioned above, in the Mid-Term Report a design point was chosen based on several assumed parameters including lift coefficient values for take-off and landing. In most cases, the airfoil by itself is not able to provide the increase in lift required and thus high lift devices are employed. However, the smaller the $\Delta C_{l,max}$ required, the less complex (and thus lighter) HLDs will be needed. This parameter was considered to be of lower importance and thus a weight of 3 was deemed appropriate.

- $\alpha_{\mathbf{stall}}$: Good stall characteristics are always preferred for any kind of airfoil. A quantifiable parameter for the trade-off table is that of the stall angle of attack α_{stall}. The higher this angle is, the further stall will be delayed. Out of the 5 parameters identified, this one carries the least importance and thus a weight of 2 was established.

With the five trade-off criteria clearly defined, six airfoils were primarily selected: CAST 7, CESSNA EJ Red. Airfoil, SC(2)-0714, SKF 1.1, NPL 9510 and SC(3)-0712(B). The results of the trade-off exercise are portrayed in Table 7.7. From the selected methodology, it becomes apparent that the SKF 1.1 airfoil is best suited for the distributed propulsion aircraft concept.

Table 7.7: Defined design choices from the Mid-Term Review

	Cast 7	Cessna	SC2	SKF	NPL	SC3
Sweep (5)	1	3	2	2	2	1
t/c (4)	2	2	1	3	2	3
L/D (5)	3	2	2	3	2	1
$C_{l_{max}}$ (3)	3	2	2	3	1	3
α_{stall} (2)	2	3	1	3	1	2
	41	45	32	52	33	35

7.3.2 Wing Planform

From a trapezoidal point of view, a root chord of 6.28m and tip chord of 1.26m is needed as presented in the iteration results in Section 7.1. However, it was chosen by the team that two conditions have been implied. For the determination of the taper ratio, it was taken into account that one of the main advantages of a distributed propulsion system is the possibility to implement boundary layer ingestion technologies. BLI is particularly efficient at the sections close to the root, as they are barely affected by the 3D characteristics of the wing. For this aircraft it was thus agreed upon that a design with a significantly low taper ratio was the most beneficent, as a large root chord was desired. Raymer deems a taper value between 0.2 and 0.3 appropriate for high subsonic swept wings [50] and hence the lower bound of 0.2 was chosen. Besides that, a 5m wing section has been set with zero trailing edge sweep, such that highly effective high lift devices (flaps) can be put there. This value is based on 2 fans of 1.8m excluding duct dimensions, a spacing of 0.5m in between, and additional margin. These conditions result in the dimensions as presented in Table 7.8. The planform can be seen in Figure 7.2.

Table 7.8: Vimana wing parameters

Parameter	Value	Unit
Taper Ratio (λ)	0.2	[–]
Root chord (c_{root})	6.58	[m]
Kink chord	4.09	[m]
Tip chord (c_{tip})	1.32	[m]

7.3.3 High lift devices

As presented in Subsection 7.3.2, the SKF 1.1 airfoil has been selected. This airfoil has a maximum lift coefficient of 1.4, while from the thrust and wing loading diagram it was concluded that a landing lift coefficient of 2.9 was needed. This results in a delta lift coefficient of at least 1.50 that has to be delivered by the high lift devices. From Section 7.1 it was found that a high lift device area of 26.13m^2 had to be positioned on the Vimana aircraft to obtain the required ΔC_L. This value has been obtained from the design method as presented in Chapter 4. A tool has been used to optimize the flap and slat area sizing to obtain the required increase in lift coefficient. This subsection will present the sizing of the high lift devices. First the flaps dimensions will be shown, after which the slat area will be given.

Flaps

As presented in Subsection 7.3.2, the rear spar will be located at 65% of the chord. It has been decided that the flaps, slats and ailerons will be placed from 75% till the trailing edge of the chord. This leaves a 10% chord length for the deploy / control systems. An iterative process resulted in a value of 17.62m^2 for the required flap based on verified methods in Roskam [14]. This area has been divided over two separate sections. The first section is located at the straight part, next to the fuselage. Out of the available spanwise length of 5m, the team has decided to put a flap of 4.8m such that a 10cm space was left at both sides of the flap. The flap extension was set to 25% of the chord length of the kink, resulting in 1.02m. The obtained flap area for this first section is 4.92m^2 per wing. The remaining 7.78m^2 is placed at the second section, which is at the kink part of the wing. This value is obtained by having a 5.1m long flap, with an offset of 0.5m from the first flap. This is designed in such a way that the two flaps will not interfere with each other. The flaps are indicated with number 1 in Figure 7.2. The flap area is significantly lower than the one of the Airbus A321, which has

an area of 21.1m^2 [1]. This is due to the fact that the required delta lift coefficient is lower: Vimana's airfoil has a higher maximum lift coefficient and needs a lower landing lift coefficient.

Slats

A required slat area of 8.51m^2 was the output of the delta lift coefficient tool. It was assumed that the slats will be located on 95% of the wingspan. This value is possible due to the fact that the fans are located at the back of the wing instead of the conventional engine configuration. This results in the fact that at both sides of the slats a flap spacing of 2.5% is present. At the tip location, the slats will have a length of 6% of the wing chord, while at the root it is only 5.9%. These values result in the required 8.24m^2 slat area. The slats are indicated with number 3 in Figure 7.2.

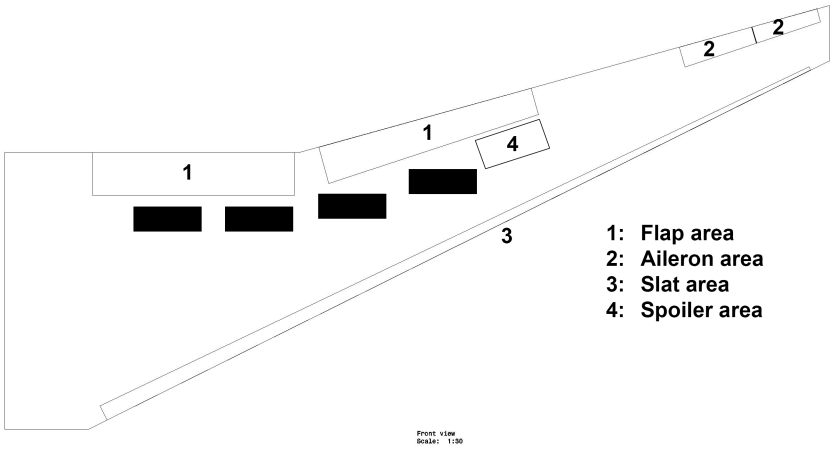

Figure 7.2: Wing planform with fan positioning indicated in black

7.3.4 Drag Analysis

A drag estimation as explained in Section 4.9 has been performed. This method as provided by Roskam takes two drag sources into account. The first is related to the zero-lift drag, while the second looks at the drag created by lift. Most of the parameters have been derived from the reference aircraft. The largest changes relate to drag of the fan ducts and possible boundary layer ingestion. For the former effect, a 2D drag analysis has been performed for the selected NACA 4312 airfoil[2]. Based on this value and the skin surface of the duct, an estimation for this value has been made. The latter effect has already been presented in Subsection 4.9.1. The lift has been set equal to the weight halfway the cruise phase, resulting in a lift over drag ratio of 18.23 as presented in Section 7.1.

7.3.5 Lift Drag Polar

Using the drag analysis tool created in Section 4.9, a lift-drag polar was created for both Vimana and the reference aircraft. As can be seen in Figure 7.3, the Vimana has lower drag than the reference aircraft.

7.4 Structural Analysis

This section will present the results related to the structure of the propulsion system. Focus has been laid upon the structural elements that will be affected by the propulsion system. First, the structural design of the fans will be discussed, after which the changes in the wing box will be presented.

[1] URL "http://booksite.elsevier.com/9780340741528/appendices/data-a/table-1/table.htm", [cited 29 June 2015]
[2] URL "http://4hv.org/e107_files/public/1386100085_2431_FT0_1353043533_2431_ft145838_duct_pdf.pdf", [cited 14 June 2015]

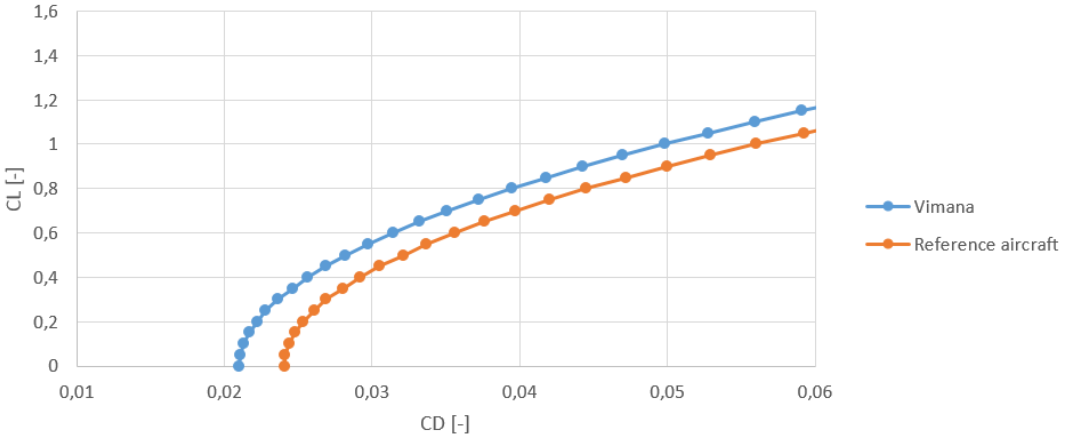

Figure 7.3: Drag polar of Vimana and the reference aircraft

7.4.1 Structural Design of the Fans

It is chosen to have four stators, attached as structural elements, sustaining the motor and fan. The loads will be directed by these four stators towards the duct which will be connected to the rear spar of the wing box with another structure, as will be clarified afterwards. The duct will not be designed in detail, but its size and its mass are estimated in Subsection 6.1.3.

Structural Design of the Stators

Based on discussions with assistant professor Daniele Ragni of the Wind Energy section of the Faculty of Aerospace Engineering, it was determined to use less stators than fan blades for optimal performance. In Subsection 6.1.3, the decision of using five fan blades is explained. The choice to have four instead of three stators has been made to increase the positive effect the stators have on decreasing the swirl behind the fan. Stators deflect the circumferential flow towards the direction of thrust, therefore increasing the thrust.
To minimize stator drag, an airfoil of the symmetric NACA 4-digit airfoil series has been implemented. The chord has been set to $0.2m$ since the fan will be halfway along a duct of $0.5m$ length. Therefore, there is $5cm$ left for half of the chord of the fan blade plus a small tolerance space between fan and stator. Aluminium has been chosen as the material since the stator is partly loaded in compression and composites tend to delaminate in compressive loading.
Afterwards, a tool to calculate the moments of inertia of the solid airfoil was produced. Using the moments of inertia obtained, plus the loads at the critical phase during take-off, stresses have been calculated. Using a safety factor of 1.5, the yield stress of aluminium 2024-T4 of $324MPa$[3], and making sure the highest Von Mises stress stays under the yield stress divided by the safety factor, the t/c ratio of the airfoil has been calculated to be 0.154.
These calculations have been verified by performing hand calculations with simple input values. Besides, validation is not required since the methods used are standard methods which are widely used.

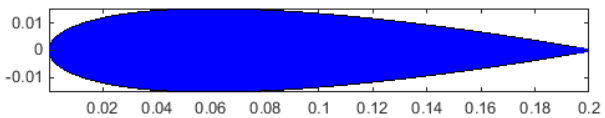

Figure 7.4: NACA 4-digit airfoil with chord of $20cm$ and thickness of $3.08cm$ used as cross section of the stators

Structural Design of the Connecting Structure

The duct is connected to the rear spar with a triangular construction which gradually transfers the loads to the spar. The cross section of this construction at the point where it connects to the duct is designed in

[3]URL "http://www.crpmeccanica.eu/PDF/aluminium-2024-t4-2024-t351.pdf", [cited 29 June 2015]

detail. The design procedure is the same as for the stators, except for the fact that this structure carries all the loads. Therefore it is chosen to use a safety factor of 2 in this case. The material to be used is aluminium. The loads due to the mass of the motor and fan, the thrust, the torque of the fan and also a crosswind of a $100m/s$ are taken into account.
Three possible cross sections are considered: a NACA 4-digit airfoil, as is used in the stators, a square cross section and a triangular cross section. A fairing will be placed around the square and triangular cross section for aerodynamic reasons. This is not the case for the NACA airfoil which is already streamlined. The width of all cross sections is set at $20cm$, corresponding to the chord of the stators. The minimum required thicknesses were calculated and can be seen in Table 7.9 accompanied by the cross sectional area. A visualization can be found in Figure 7.5.

Table 7.9: Parameters for three different cross sections of the connecting structure

	Width $[\mathrm{cm}]$	**Thickness** $[\mathrm{cm}]$	**Area** $[\mathrm{cm}^2]$
NACA airfoil	20	8.1	111
Square	20	4.9	98
Triangle	20	9.7	97

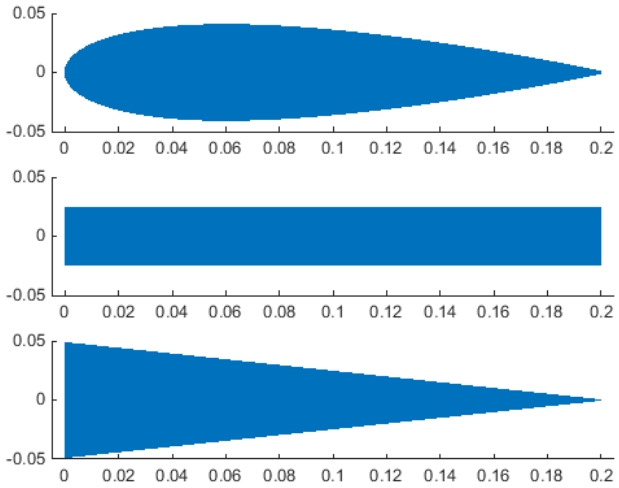

Figure 7.5: Cross sections of the connecting structure visualized on the same scale

It is chosen to use the triangular cross section for multiple reasons. First of all, it is lighter than the NACA airfoil, but it is also better for maintainability. The structure can be bolted to the duct since the fairing surrounding the structure shields the bolts from the airflow. The fairing carries no loads and can therefore be designed in such a way that it can be easily removed. Using bolts with the NACA airfoil is difficult since the bolts will be in the airflow which is detrimental for the aerodynamic drag.
Secondly, the triangular cross section is preferred over the square because the sharp corner of the triangle will be at the trailing edge such that the fairing can be fitted closely around it needing less wetted area. The fairing can thus be smaller for the triangular cross section.
Finally, the triangle has a high thickness at the leading point where it connects to the rear spar. This is beneficial since this point carries the most loads. Figure 7.6 shows in detail how the fan structure will be attached to the back spar.
The connecting structure is visualized in Figure 7.6, where the fairing is omitted to increase the visibility of the structure itself. The skin of the wing and additional components such as the flaps are not presented.

7.4.2 Wing Box

For the design of the wing box, the structural analysis tool used in AE3212-II Simulation, Verification & Validation has been altered to be used for this purpose. The planform of both Vimana and reference aircraft with the engine position, thrust and weight have been implemented. The benefit of this tool is that it has already been extensively verified and validated, on which only changing the input values will have no impact.

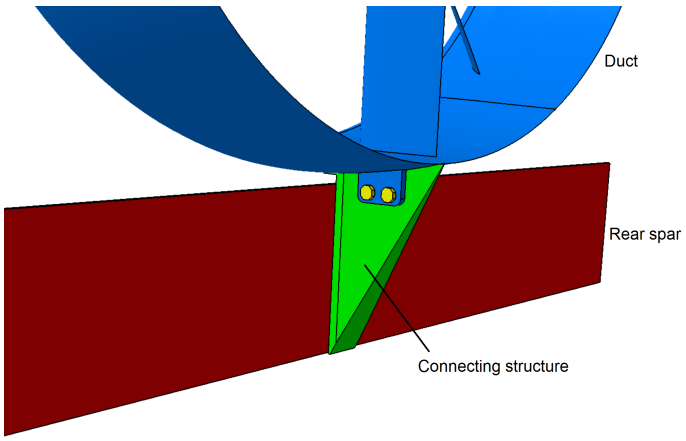

Figure 7.6: Visualization of the connecting structure

A maximum load factor of 2.80 for Vimana and 2.63 for the reference aircraft have been calculated as can be seen in Figures 7.7 and 7.8. The higher load factor for Vimana is due to the higher MTOW of Vimana. The ultimate load can therefore be calculated by the maximum load factor times the MTOW. This ultimate load factor is once again multiplied by a safety factor of 1.5.

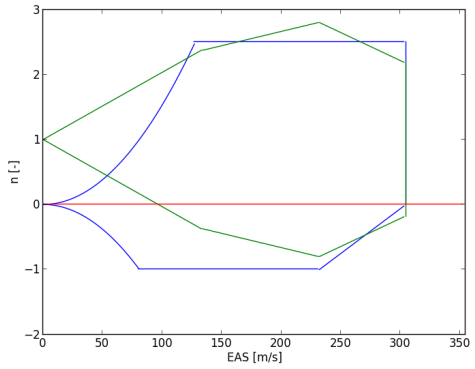

Figure 7.7: Load diagram of Vimana

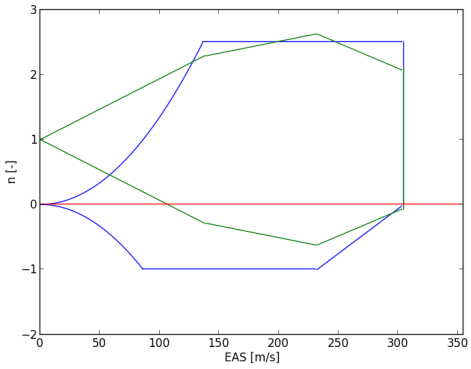

Figure 7.8: Load diagram of reference aircraft

Since the used tool is mainly developed for analysis rather than design, the skin thicknesses have been set a fixed value of 0.1 equivalent thickness for both aircraft. Afterwards, the maximum attained Von Mises stress at each cross section of the wing box is calculated. Then, these stresses were plotted as a function of spanwise location, see Figures 7.9 and 7.10. The Von Mises stresses are also visualized in Figure 7.11.

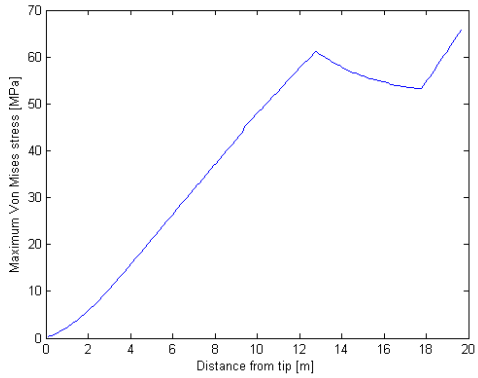

Figure 7.9: Maximum Von Mises stress along the span for Vimana

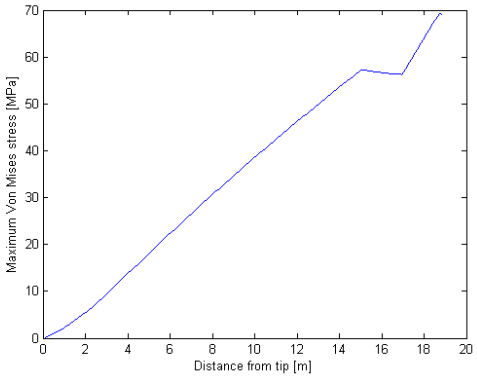

Figure 7.10: Maximum Von Mises stress along the span for the reference aircraft

When summing these maximum Von Mises stresses, one for every element along the span, a measure is obtained for the required wing box weight. The required thickness at every spanwise location is related to the maximum Von Mises stress at that location since a higher Von Mises stress requires a higher thickness. Therefore summing these maximum Von Mises stresses is equivalent to summing the thicknesses of all the cross sections along the span, which is a measure for the total wing box weight.
This measure is 11.8% bigger for Vimana than for the reference aircraft. It can be therefore concluded from this that the weight of the wing box for Vimana has to be 11.8% greater than for the reference aircraft.
Several reasons for this can be stated. First of all, Vimana has a slightly higher MTOW and maximum load factor. Moreover, the motors are lighter which decreases the bending relief due to engine weight. Also the fuel weight is lower due to the use of methane which is stored inside the fuselage.
However, there are some arguments against this higher required wing box thickness for Vimana. The motors are on average placed more towards the tip which increases the bending relief. Also the total maximum thrust generated by four fans is significantly lower than the maximum thrust generated by one engine of the reference aircraft.
Finally, there is another benefit of the fans and motors being placed more outward. As can be seen in Figure 7.9, the maximum Von Mises stress and therefore the thickness is fairly constant from $12m$ to $18m$ from the tip. This leads to easier manufacturing since the thickness can stay constant here. This is not the case for the reference aircraft, as can be seen in Figure 7.10.

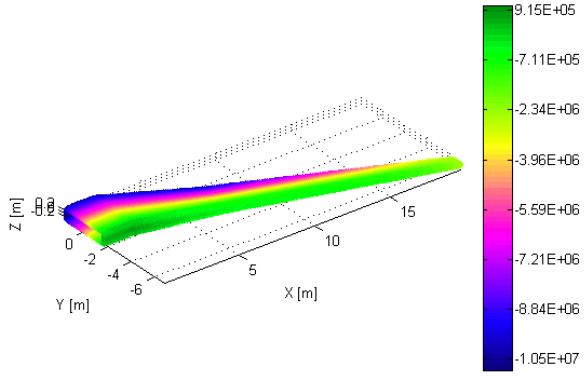

Figure 7.11: 3D plot of the stresses for Vimana

7.5 Control and Stability Analysis

This section will cover the stability and controllability characteristics of Vimana. First of all, center of gravity analyses are conducted. A center of gravity loading diagram is generated, which shows the variation in the position of the center of gravity due to passenger loading, for instance. Furthermore, a 'scissor plot' is generated, which shows the maximum allowable front and aft position of the center of gravity for a stable and controllable aircraft. An optimal horizontal tail size will also follow from these analyses. After these center of gravity analyses, the longitudinal stability of Vimana is analyzed, where eigenmodes and trim conditions are analyzed. Finally, the control aspects regarding the use of a distributed propulsion system, like differential thrust, are discussed.

7.5.1 Loading Diagram

In this subsection, the loading diagram will be generated. As mentioned before, this diagram shows the variation in the center of gravity position, when the aircraft is being loaded with cargo, passengers and fuel.
After a few iterations, the final weights, center of gravity positions of the components and wing parameters were defined. These will all be used for the generation of the loading diagrams. The loading diagram shows the variation in center of gravity position, for two cases: when the aircraft is being loaded from the front to the back and the other way round. It is assumed that the cargo is being loaded first, after which the passengers are loaded, and finally the fuel.

First of all, the center of gravity position of the aircraft at OEW is determined. The total moment with respect to the aircraft nose, caused by the individual components, are summed. This moment is then divided over the weight of all the components, after which the center of gravity can be determined.After the determination of this initial c.g. position, the c.g. variations caused by non fixed items, such as payload and fuel are added.
The cargo holds are divided into a forward and an aft compartment. There will be a total of five and six cargo containers located at the front and aft cargo compartments respectively. Three of these containers will be used to store the methane, as was described in Subsection 5.7.3. A more detailed layout will be discussed and given in Section 8.2.
Furthermore, the fuel weight is divided into two sections as well. For Vimana, there there is a tank in each wing, and a tank located at the center of the fuselage.
It must be noted that, for the generation of the loading diagram, the center of gravity position is calculated with respect to the mean aerodynamic chord leading edge position, X_{LEMAC}, and is then normalized with the MAC length (i.e. $X_{cg,LEMAC} = (X_{cg} - X_{LEMAC})/MAC$). This is due to the fact that the center of gravity is always located close to the wing aerodynamic center, to obtain small tail loads. It is therefore convenient to express the c.g. position as a percentage of MAC. All relevant parameters used to generate the loading diagram are listed in Table 7.10.

Table 7.10: Relevant weights, lengths and center of gravity positions used to generate the loading diagram

Parameters	**Value** $[\mathbf{kg}]$	$\mathbf{X_{cg}[m]}$ (w.r.t. aircraft nose)
OEW	46524	16.99
MZFW	64978.33	17.51
Fuel Weight (Center Tank)	7333.65	12.71
Fuel Weight (Wing Tank x2)	13990.35	17.95
MTOW	86302.34	16.82
Passenger Weight	80	[-]
(+5 kg hand carry baggage)		
Front cargo compartment (including methane containers)	1406.67	4.49 (Most front container of the FWD hold)
Aft Cargo Weight	2647.66	20.24 (Most front container of the AFT hold)
(including methane containers)		
Lengths	**Value** $[\mathbf{m}]$	
MAC	3.95	15.8 (LEMAC position)
Seat Pitch	0.79	

The final generated loading diagram can be seen in Figure 7.12.
From Figure 7.12, it can be seen that the overall center of gravity position of the aircraft shifts towards the back, when the aircraft is being loaded with cargo, passengers and fuel. Furthermore, the most forward and aft positions of the center of gravity can be determined from this diagram.
A last thing that is determined from this diagram is the required longitudinal position of the main landing gear, to avoid tip-over situations during loading of the aircraft. From the diagram, it was determined that the most aft center of gravity position, when the aircraft is being loaded, is $X_{cg,LEMAC}/MAC = 0.688$. Taking a 10% variation into account, the required longitudinal position of the main landing gear is determined. This corresponds to a position of $0.757 \cdot MAC + X_{LEMAC} = 19.07m$ with respect to the aircraft nose.
In addition to these center of gravity positions, a 2% variation is added to the most aft and forward center of gravity positions, to account for in-flight variations, due to for instance movement of flight attendants and passengers. The most forward and aft position of the center of gravity position are listed in Table 7.11.

Table 7.11: Most forward and aft center of gravity position, including a 2% in-flight variation

Parameters	**Value** $[\mathbf{X_{cg,LEMAC}/MAC}]$	$\pm$ **2% In-flight variation**
Most forward c.g. position	0.406	0.398
Most aft c.g. position	0.664	0.667

An additional plot can be generated, which shows the variation in most forward and aft position of the c.g., when the longitudinal wing position of the aircraft is varied. This plot can be combined with the scissor plot, which will be generated in Subsection 7.5.2, to come up with the optimal horizontal tail area. Once again, the center of gravity position is normalized with MAC, whereas the y-axis shows the variation of the leading edge position of the MAC, varied with respect to the length of the fuselage. This plot can be seen in Figure 7.13.

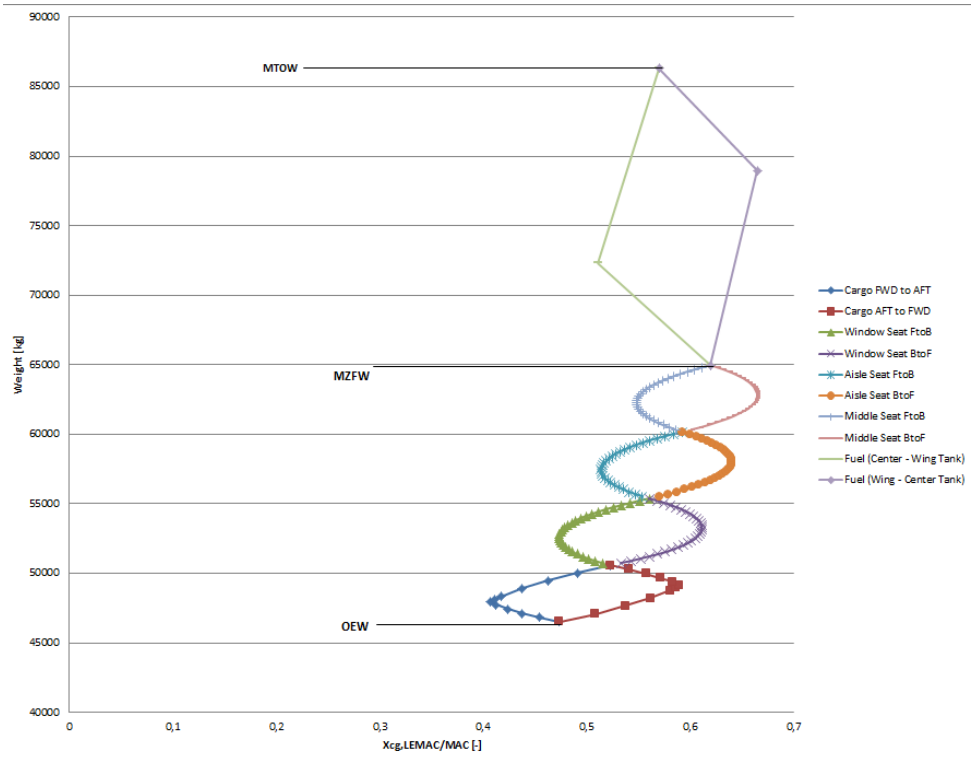

Figure 7.12: Loading diagram of Vimana

7.5.2 Center of Gravity Limits and Stability

The final aircraft design should be able to react to any variation of its position (eg. an external force induced pitching moment) with an opposite moment, so by definition, it should be statically stable. In order to assure longitudinal static stability of the aircraft, the allowed center of gravity travel has to be analyzed. This travel is limited by the controllability and stability characteristics of the aircraft. The c.g. location and allowed travel will therefore also have to be studied. This can be done by generating the controllability and stability curves, which are related to the horizontal tail size. These curves can then be plotted to create a so-called 'scissor plot', which shows the allowed c.g. position travel for a certain horizontal tail size. This scissor plot or X-plot was already mentioned before in Section 4.8 and was used to obtain an initial horizontal tail size. A more elaborate description of the generation is discussed in this subsection.

Stability Curve Parameter Determination

First of all, the maximum allowable aft c.g. position is analyzed. This position is limited by the static stability of the aircraft, and can be determined by the relation between the horizontal tail size and this maximum aft position. It is given by Equation (7.1).

$$\bar{x}_{cg} = \bar{x}_{ac} + \frac{C_{L_{\alpha_h}}}{C_{L_\alpha}}(1 - \frac{d\epsilon}{d\alpha})\frac{S_h l_h}{S\bar{c}}(\frac{V_h}{V})^2 \tag{7.1}$$

The parameters from Equation (7.1) will have to be determined in order to generate the stability curve. The first parameter that is determined is the horizontal tail lift rate coefficient, $C_{L\alpha_h}$. This is done by using the DATCOM method [18], and this is presented in Equation (7.2).

$$C_{L\alpha_h} = \frac{2\pi A_h}{2 + \sqrt{4 + (\frac{A_h \beta}{\eta})^2 (1 + \frac{tan^2(\Lambda_{0.5C_h})}{\beta^2})}} \tag{7.2}$$

The next parameter which is determined is the lift rate coefficient of the aircraft without the tail, C_{L_α}, given by Equation (7.3).

$$C_{L_\alpha} = C_{L_{\alpha_w}}(1 + 2.15\frac{b_f}{b})\frac{S_{net}}{S} + \frac{\pi}{2}\frac{b_f^2}{S} \tag{7.3}$$

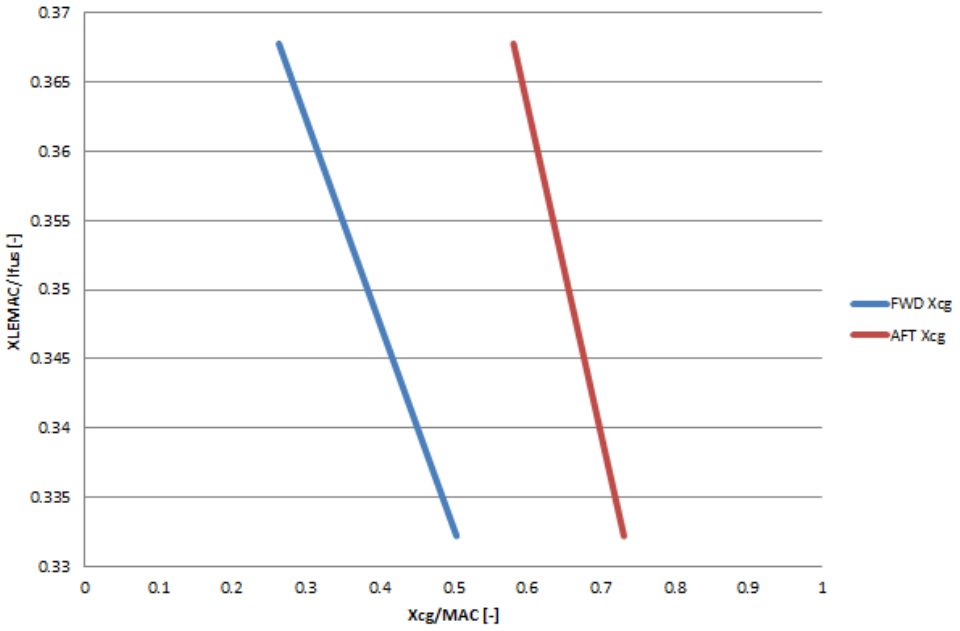

Figure 7.13: Most forward and aft c.g. position with varying longitudinal wing position

In Equation (7.3), $C_{L_{\alpha_w}}$ is the wing lift rate coefficient, which can be determined with the same DATCOM method as proposed by Equation (7.2).
The general equation to determine the wing downwash gradient effect is dependant on two terms accounting for the wing sweep angle and parameters related to the tail length and horizontal tail height with respect to the vortex shed plane. It is given by Equation (7.4).

$$\frac{d\epsilon}{d\alpha} = \frac{K_{\epsilon_\Lambda}}{K_{\epsilon_{\Lambda-0}}}\left(\frac{r}{r^2+m_{tv}^2}\frac{0.4876}{\sqrt{r^2+0.6319+m_{tv}^2}} + \left[1+\left(\frac{r^2}{r^2+0.7915+5.0734m_{tv}^2}\right)^{0.3113}\right]1-\sqrt{\frac{m_{tv}^2}{1+m_{tv}^2}}\right)\frac{C_{L_{\alpha_w}}}{\pi A} \tag{7.4}$$

Similar equations are present for the determination of the parameters related to the geometry of the aircraft, m_{tv} and r. They are however not stated but can be found in Reference [18].
The final parameter that has to be determined to generate the curves is the position of the aerodynamic center of the aircraft minus the tail, it is determined by summing the contributions of the wing-fuselage system, nacelles and the jet stream, given by Equations (7.5) to (7.7).

$$\left(\frac{x_{ac}}{\bar{c}}\right)_{wf} = \left(\frac{x_{ac}}{\bar{c}}\right)_w - \frac{1.8}{C_{L_{\alpha_{wf}}}}\frac{b_f h_f l_{fn}}{S\bar{c}} + \frac{0.273}{1+\lambda}\frac{b_f c_g (b-b_f)}{\bar{c}^2(b+2.15b_f)tan(\Lambda_{1/4})} \tag{7.5}$$

$$(\bar{x}_{ac})_n = \sum k_n \frac{b_n^2 l_n}{S\bar{c}(C_{L_\alpha})_{wf}} \tag{7.6}$$

$$\left(\frac{x_{ac}}{\bar{c}}\right)_T = -\sum_1^N \frac{T}{W}\frac{Z_T}{\bar{c}} \tag{7.7}$$

The final aerodynamic center position will then be the sum of these contributions:

$$\bar{x}_{ac} = (\bar{x}_{ac})_{wf} + (\bar{x}_n) + (\bar{x}_{ac})_T \tag{7.8}$$

All relevant parameters for the stability curve are listed in Table 7.12.

Controllability Curve Parameter Determination

The maximum allowable forward center of gravity position is limited by the controllability characteristics of the aircraft. This again can be described by an equation relating this position and horizontal tail size, and is given by Equation (7.9).

Table 7.12: Parameters for the stability curve

Planform Parameters	Value	Unit
A_h	5	$[-]$
$d\epsilon/d\alpha$	0.332	$[-]$
$\bar{x}_{ac}$	0.223	$[m]$
$(\frac{V_h}{V})^2$	0.85 [18]	$[-]$
l_h	20.71	$[m]$
MAC	4.33	$[m]$
r	0.945	$[-]$
$m_t v$	0.178	$[-]$
Coefficients	**Value**	
$C_{L_{\alpha_w}}$	6.788	rad^{-1}
$C_{L_{\alpha_h}}$	4.409	rad^{-1}
C_{L_α}	6.962	rad^{-1}

$$\bar{x}_{cg} = \bar{x}_{ac} - \frac{C_{m_{ac}}}{C_{L_{A-h}}} + \frac{C_{L_h}}{C_{L_{A-h}}} \frac{S_h l_h}{S\bar{c}} (\frac{V_h}{V})^2 - S.M. \tag{7.9}$$

These parameters will have to be determined again, as was done for the generation of the stability curve. In Equation (7.9), S.M. is the stability margin, defined as $\bar{x}_{np} - \bar{x}_{cg}$. A value of 5% is taken, to account for variations.

The first parameter that is determined is the zero lift pitching moment coefficient of the aircraft without the tail, $C_{m_{ac}}$. It is determined by the individual contributions of the wing, flaps, fuselage and nacelles to the pitching moment. Therefore, these contributions will have to be determined first and is done with Equations (7.10) and (7.11).

$$C_{m_{ac_w}} = Cm_{0,airfoil} \cdot \frac{Acos^2\Lambda}{A + 2cos\Lambda} \tag{7.10}$$

$$\Delta_{fus} C_{m_{ac}} = -1.8(1 - \frac{2.5 b_f}{l_f}) \frac{\pi b_f h_f l_f}{4S\bar{c}} \frac{C_{L_0}}{C_{L_{\alpha_{wf}}}} \tag{7.11}$$

As can be seen from Equation (7.11), the contribution of the fuselage depends on fuselage geometry and additional lift coefficient.

$C_{L_{\alpha_{wf}}}$ represents the same thing as C_{L_α} used earlier for the stability curve, which is the lift rate coefficient of the aircraft without the tail. However, their values are not the same. This is because controllability is more critical at low speeds. Therefore, $C_{L_{\alpha_{wf}}}$ is assessed for low speeds, and the approach speed $(140kts)$ is taken. Equation (7.3) is used again to determine this parameter.

C_{L_0} is the lift coefficient of the flapped wing at zero angle of attack, and is determined by an earlier aerodynamic analysis.

The contributions of the nacelles and the flaps have a predetermined value based on aircraft configuration [18] and are determined with similar relations as for the other contributions The total zero lift pitching moment is then the sum of these contributions. It is given by Equation (7.12).

$$C_{m_{ac}} = C_{m_{ac_w}} + \Delta_{flaps} C_{m_{ac}} + \Delta_{fus} C_{m_{ac}} + \Delta_{nac} C_{m_{ac}} \tag{7.12}$$

With all the parameters known, the scissor plot can now be generated. The stability curve with the stability margin is the neutral stability, whereas the curve without this margin is the 'normal' stability curve, and is the actual curve that limits the aft position of the center of gravity. As mentioned in Subsection 7.5.1, this plot can be combined with the plot seen in Figure 7.13. The intersection of these graphs, will then yield the optimal horizontal tail size.

The combination of these plots is generated and can be seen in Figure 7.14. Once again, the center of gravity position on the x-axis, is normalized with MAC, for the same reason that was mentioned for the c.g. loading diagram.

The optimal horizontal tail size is the point where the 'center of gravity variation curves' cross the stability and controllability curves. From Figure 7.14, it can be seen that a horizontal tail to wing ratio of $\frac{S_h}{S} = 0.29$ is the most optimal.

Table 7.13: Parameters for the controllability curve

Planform Parameters	Value	Unit
l_h	20.71	$[m]$
MAC	4.33	$[m]$
$(\frac{V_h}{V})^2$	0.85 [18]	$[-]$
Λ	0.345	$[rad]$
$\bar{x}_{ac}$	0.195	$[-]$
A	12.5	$[-]$
Coefficients	**Value**	
$Cm_{0,airfoil}$	-0.07	
C_{L_0}	2.346	
$C_{m_{ac_w}}$	-0.054	
$\Delta_{fus}C_{m_{ac}}$	-0.517	
$\Delta_{flaps}C_{m_{ac}}$	-0.6	
$\Delta_{nac}C_{m_{ac}}$	-0.05 [18]	
$C_{m_{ac}}$	-1.221	
$C_{L_{A-h}}$	1.33	
C_{L_h}	-0.8 [18]	
S.M.	5	[%]

7.5.3 Longitudinal Stability and Controllability

In this subsection, the longitudinal stability of Vimana will be analyzed in more detail. First of all, the trim condition of Vimana is assessed, after which the longitudinal eigenmodes are analyzed. Furthermore, the longitudinal controllability of the Vimana is discussed.

Aircraft Trim

Beside the fact that longitudinal static stability of Vimana should be assured, the ability to trim it should also be assured. A combination of wing-fuselage and tail lift coefficients should exist such that the total aircraft moment coefficient, C_m, is zero. The aircraft is then said to be in trim condition, in which Equation (7.13) holds [18].

$$C_{m_{ac}} + C_{L_{A-h}}(\frac{x_{cg} - x_{ac}}{\bar{c}}) = \frac{C_{L_h} S_h l_h}{S\bar{c}}(\frac{V_h}{V})^2 \tag{7.13}$$

Using an analysis tool for airfoil, wings and planes (XFLR5), which was also used for the analyses conducted in Section 7.3, a $C_m - \alpha$ curve was generated. Two different curves were generated, one for the aircraft without the tail, and one for the complete aircraft. These curves are presented in Figure 7.15.
From Figure 7.15, it can be seen that, as expected, the tailless aircraft is unstable ($C_{m_\alpha} > 0$), and is untrimmable, as it does not reach the $C_m = 0$ condition. Furthermore it can be seen that the complete aircraft does show stability, where $C_{m_\alpha} < 0$ and a trim condition is present. For Vimana, the trim condition is at an angle of attack of $\alpha = 3\,\mathrm{deg}$.
The lift distribution over the wing and horizontal tail of the Vimana, in trim condition, can be seen in Figure 7.16. This figure is generated in the analysis tool mentioned earlier. As expected, it can be seen that the horizontal tail is generating negative lift (distributions perpendicular to wing and horizontal tail), when the aircraft is trimmed.

Longitudinal Eigenmodes

Next to the trim condition analysis, two longitudinal eigenmodes are analyzed: the phugoid and the short period. The responses of these two eigenmodes can be seen in Figures 7.17 and 7.18 respectively. The same analysis tool has been used for the generation of these two plots.
From these two graphs, it can be seen that both the phugoid and short period converge to a stable condition. It can therefore be said that Vimana is inherently (longitudinally) stable.

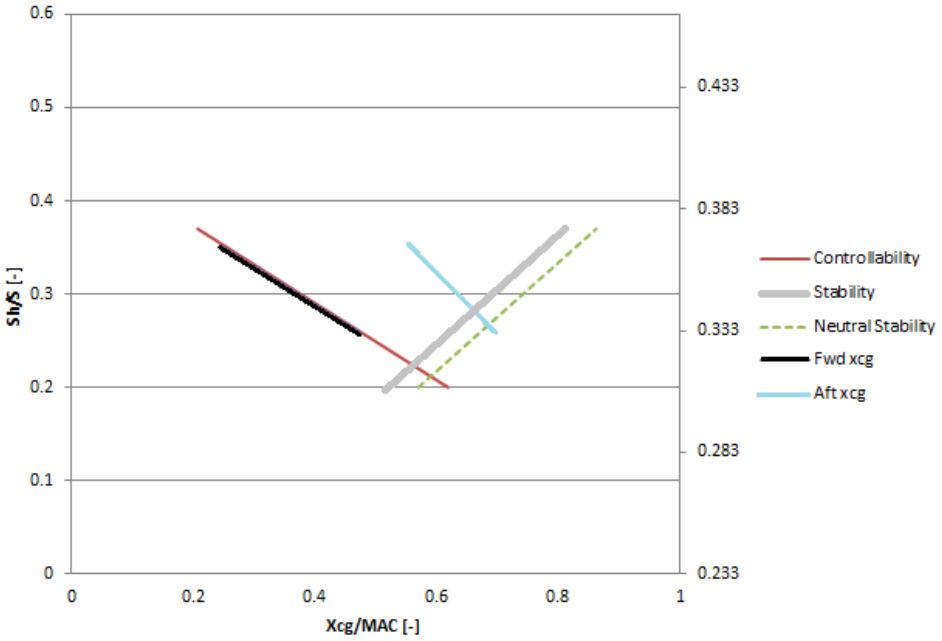

Figure 7.14: Scissor plot and center of gravity variation

Longitudinal Controllability

For longitudinal controllability of Vimana, 'conventional' measures will be taken. This particular controllability will be achieved by the use of the elevators located at the horizontal tail.

7.5.4 Lateral Stability and Controllability

Since it is chosen to have no vertical tail, lateral stability and controllability are of extra importance. First, the choice to omit the vertical tail is explained, after which the solutions to provide lateral stability and controllability are presented.

Vertical Tail

Due to the distributed propulsion properties of Vimana, the One Motor Inoperative (OMI) scenario is no longer the critical case for the sizing of the vertical tail. Moreover, the OMI scenario is of no importance considering the sizing of the vertical tail. Furthermore, directional controllability and stability is provided by the differential thrust system as will be described in Subsection 7.5.4. These two are the main reasons for the omission of the vertical tail, which enables a weight saving of approximately $668kg$.
In case of a fan/motor failure, the rpm of the operative fans on the side with the fan failure can be temporarily raised from 5600 to $6130rpm$, leading to enough thrust to compensate for the failure, by means of a corrective yawing moment. This action requires $0.3MW$ more from the generators than in normal cruise (values obtained from JavaProp).
The moment created by the failure can be counteracted by decreasing the thrust of the fans on the all-fans-operative side. If the outermost fan fails (considering the most critical scenario), the two inner fans on the side should create more thrust, whereas the outer two fans on the opposite side should create less, in order to achieve the corrective yawing moment.
One thing that has to be noted is that the overload case of the motors cannot be sustained for longer than approximately five minutes [51]. Therefore, the aircraft has to descend to lower altitudes where the required rpm is lower for the same thrust. Analyses in JavaProp show that an altitude of $9,000m$ would already be enough to lower the angular velocity of the fans to $5600rpm$. On this lower altitude, the aircraft can safely fly to a nearby airfield. When excess power is available, the motors of course do not have to be overloaded.

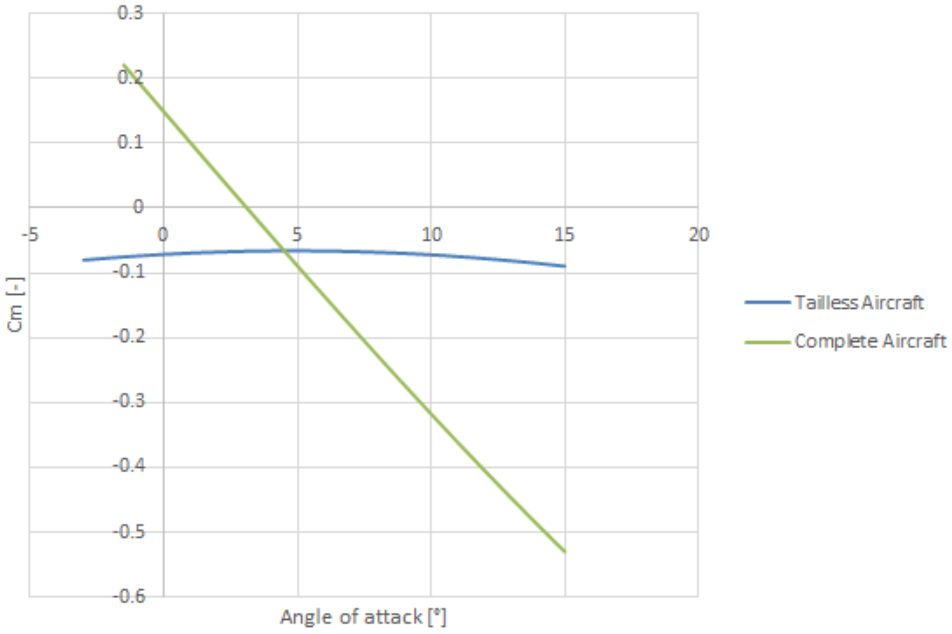

Figure 7.15: $C_m - \alpha$ curve of the Vimana

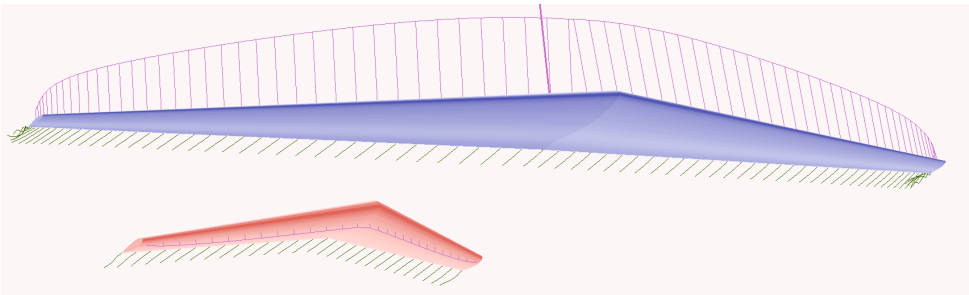

Figure 7.16: Lift distribution of Vimana in trim condition

Lateral Stability

Omitting a vertical tail does require different means of lateral stability. A positive C_{n_β} is required for stability along the Z-axis pointing downwards. Without a vertical tail and body, analysis in XFLR5 resulted in a C_{n_β}-value of -0.0064. Vimana is therefore laterally unstable. This value including a body would be even more negative, due to the unstable nature of the body. It is therefore obvious that measures have to be taken to provide lateral stability.
A considered solution is a variable blade pitch actively controlling stability around the Z-axis. This solution is however rejected since an angle increase of 10 degrees leads to approximately $1460N$ thrust decrease per fan (JavaProp). Applying this to four fans on one side leads to a total moment of $40kNm$. With a moment of inertia I_{zz} of $3.9 \cdot 10^6 kgm^2$ [52] this comes down to an angular acceleration of $0.588 \frac{deg}{s^2}$. This is considered too low, especially since analysis in XFLR5 with a vertical tail with an area 4 times lower than the A321 resulted in a moment of $200kNm$. Moreover, using a blade pitch system as active stability system is extremely complex. If the fans are rotating at $5600rpm$ while constantly needing very fast adjustments of pitch angle, it would require difficult designs and reliability would be hard to assure. Therefore this method for lateral stability is considered to have too high risks and is therefore rejected. The fan blades are still adjustable in pitch, needed during landing but also in case of an inoperative fan such that the blades can be feathered. However, fast response is not needed in these cases, which simplifies the system drastically.
The chosen solution is a so called split aileron system, see Figure 7.19. In this system, the ailerons are in fact two flaps positioned on top of each other. While moving them at the same time results in a rolling moment as would be caused by ordinary ailerons, moving them opposed to each other results in increased drag. When increasing the drag on one wing tip results in a yawing moment. Coupling this system to an active stability system such as is used on fighter aircraft results in an artificial stable system which is inherent unstable. For

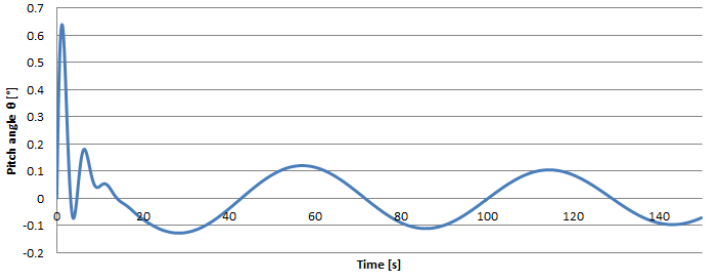

Figure 7.17: $\theta - t$ curve of the Vimana during the phugoid

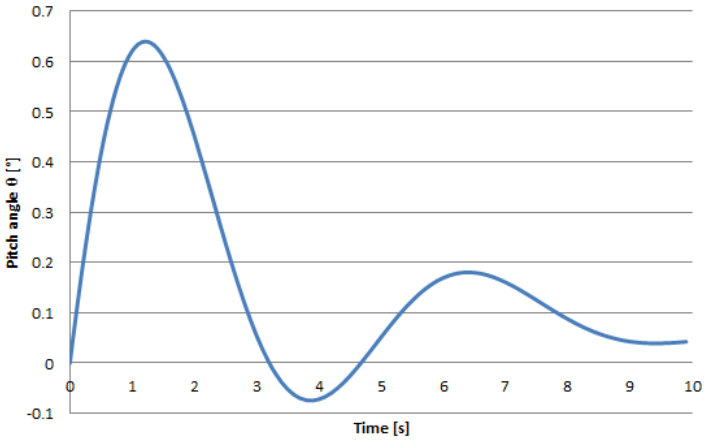

Figure 7.18: $\theta - t$ curve of the Vimana during the short period

redundancy, two split ailerons are placed on each wing tip, see Figure 7.2.

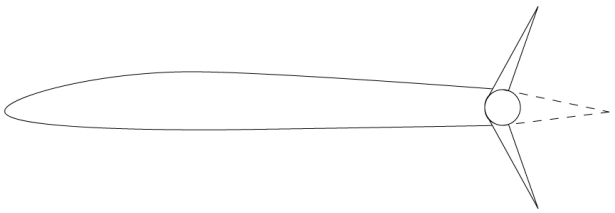

Figure 7.19: The split aileron concept[4]

The split aileron system however, causes some performance disadvantages. Having drag increasing control surfaces as stability measures, would mean that the overall produced drag during flight is increased, assuming that lateral stability is assured constantly. One way to cope with this issue is to use the differential thrust or a combination of differential thrust and split ailerons that will be used for the lateral controllability, as will be described in the following section.
However, it is chosen to not rely on this differential thrust system for stability, as there is still uncertainty of the fact that immediate adjustments to power settings can be achieved when perturbations are present. To account for the worst case scenario, it is assumed that the differential thrust alone cannot provide adequate measures to immediately cope with perturbing forces. It is therefore decided to keep it at the use of the split aileron system only. Future research could show that a lateral stability system using only differential thrust or a combination of differential thrust and split ailerons is feasible.

[4]URL "http://www.desktop.aero/library/whitepaper/Figures/Trim_Figure_Pg9_Split_Ailer.png", [cited 22 June 2015]

Lateral Controllabilty

For lateral controllability, the split ailerons will be utilized as well, where the effect is strengthened by the propulsion system. As mentioned before, the speed of revolution of the fans can be temporarily raised, by overloading the motors. This can be used in combination with the ailerons to make turns by overloading the motors on one side of the aircraft.
This differential thrust is more efficient than an ordinary rudder since there is no drag increase but instead, an overall increase in thrust which overcomes the increased drag in turns. This leads to no velocity loss during turns.
Differential thrust is a feature of Vimana which is new compared to conventional aircraft, which was also one of the features that allowed for the omission of the vertical tail, as mentioned before. By altering the power distribution over the fans, yawing moments can be created in order to give Vimana the desired and required directional control. The power on one side of the aircraft will be increased, whereas the motors positioned at the side of the desired direction are decreased in power.
The way this is integrated into the aircraft in terms of controllability and aircraft system is shown in Figure 7.20. How the differential thrust is actually incorporated in the cockpit regarding the control instruments can be found in Section 8.3.
As is shown in Figure 7.20, instruments measure the current position and attitude of the aircraft. The pilot gives an input to the pedals, where in normal aircraft this gives an input to the rudder.

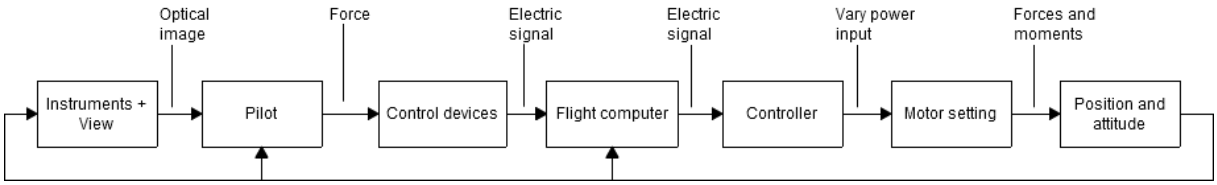

Figure 7.20: Differential thrust flow diagram

For Vimana, this input gives an electric signal to the flight computer. The flight computer in turn, sends a signal to the motor controller, which determines how much power every motor should deliver to the fan. Having different power inputs to the motors, forces and therefore moments change which will cause the aircraft to change its heading.
Figure 7.21 shows a bit more depth into the data handling system. This can be applied to the differential thrust characteristic of Vimana, but also handling data in general. Inputs are received by various sensors and processed by an input processor. These sensors include pitot tubes, angles of attack meters, multi-function probes and slide slip angle probes. From this input processor a one way data cable goes to the central processing unit (CPU). After analyzing the data and also receiving inputs from the pilot, the CPU gives a one way output signal to the output processor.
For Vimana, these output processors are associated to the motor controllers or hydraulics to operate the high lift devices. In aircraft where fly-by-wire systems are used, as is the case for Vimana, real-time computing is used for this type of data handling.

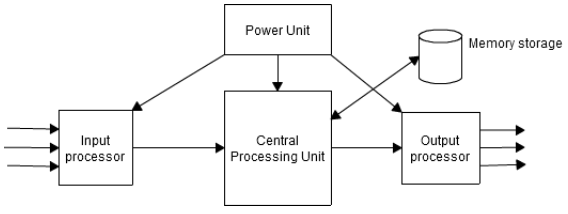

Figure 7.21: Data handling system

Following the historical guidelines of Raymer [50] and historical data as presented in Subsection 4.4.1, it was found that an aileron surface of $2.74m^2$ has to be present on the aircraft. By placing the ailerons most outwards of the span, it will create the largest moment for the given aileron area. The first decision made by the team is that the most outward location will be $30cm$ away from the wingtip, and will span the last 25% of the wing chord. The result is to place two ailerons totalling $3.37m$ in span on each side of the wing. The result is displayed as number 2 in Figure 7.2. As stated, the aileron will be part of a split aileron / deceleron system, which will be developed in the upcoming years in more detail. This research includes a better defined location for the decelerons in order to provide full control of the aircraft in case tip stall occurs.

One final thing that has to be noted about the analyses conducted for the stability and controllability aspects of Vimana, is that it is assumed that the aerodynamic tools XFLR5 and Javaprop, the latter tool also used for fan design in Section 6.1, are verified and validated tools. XFLR5 is an integration of XFOIL, which is developed by Professor Mark Drela at the Massachusetts Institute of Technology for the MIT Daedalus Project[5].

7.5.5 Fly-by-Wire System

As mentioned in Subsection 7.5.4, Vimana will be using a Fly-by-wire system (FBW system), which replaces the conventional manual flight controls of an aircraft with an electronic interface. This implies that a purely electrically-signalled control system is present.
When a pilot moves the control column, a signal will be sent to a controller or computer, and is sent through multiple cables to account for redundancy. So, a manual input is modified in accordance with control parameters. When these signals are received, calculations will be performed (voltage calculations) which are sent to a control surface actuator as another signal. This actuator then enables the control surface to move. These actuators will then send a signal back to the computer, by means of a potentiometer (three-terminal resistor). When the desired position is reached by the actuator, the incoming and outgoing signals will cancel each other out, enabling the actuator to stop. This then completes a feedback loop.
This FBW system, also requires a certain level of redundancy and safety. Vimana will have a quadruplexed FBW system, which in effect means that there are four independent channels present to prevent signal losses in the event of a channel loss. Furthermore, pre-flight safety checks will have to be conducted, in order to ensure proper function of the FBW system. This can be done by means of built-in test equipment, which is a passive fault management and diagnosis equipment.
In addition to accounting for redundancy with respect to signal losses, the aforementioned controllers will also require a level of redundancy. Vimana will have additional computers,so that in a case of failure of a computer, the others will overrule the faulty one. The faulty computer can either be rebooted or turned off completely.
Finally, the flight-envelope control system of the Vimana, a subsystem of the FBW system, will always retain ultimate flight control, when flying under normal law. This is also the case for the Airbus A321[6]. Normal law is a specific computer controlled flight control mode, that is capable of determining the operational mode of the aircraft and it implies the control mode over the following stages of flight:

1. Stationary at the gate
2. Taxiing from the gate to a runway or the other way round
3. Beginning the take-off roll
4. Initial climb
5. Cruise climb and cruise flight at altitude
6. Final descent, flare and landing

7.5.6 Reverse Thrust

During landing, more benefits of the propulsion system design of Vimana become apparent. The reverse thrust capabilities of the combination of fans with electrical superconducting motors are very high. As mentioned before, the pitch of the fan blades can be adjusted. After touchdown the pitch of the blades can be reversed such that the pitch angle of the blades is negative. This has to be done gradually to ensure that the torque does not cross the structural limits of the motors and the sustaining structure of the fans. During but primarily after the adjustment, the motors can apply full power which results in high engine braking and a short landing distance.
It should be noted that the pitch angle of the blade tips cannot be adjusted. Since they are curved and carefully shaped to fit the duct as closely as allowable, it is no option to turn them. Therefore they are stationary, fitted to a shaft running through the rest of the blade. The rest of the blade uses this shaft as an axis of rotation. The stationary tip is kept as small as possible since it increases drag when the fans are feathered during a malfunction.
Reverse thrusting not only works as a way of engine braking but also as a spoiler because of the selected fan location. While applying reverse thrust the airflow on top of the wing is distorted in a way similar to the working principle of spoilers. Therefore, it has been decided that only a small spoiler area will be placed on the wing planform. This area is indicated as number 4 in Figure 7.2.

[5]URL "http://web.mit.edu/aeroastro/news/magazine/aeroastro-no3/2006drela.html", [cited 22 June 2015]
[6]URL "http://www.skybrary.aero/index.php/Flight_Control_Laws#Airbus_Flight_Control_Systems", [cited 29 June 2015]

7.5.7 Critical Flight Conditions

During critical flight conditions, Vimana still has to be controllable. These conditions will be discussed, along with the means to control Vimana during these conditions.

One Motor Inoperative Scenario

The first critical condition is the motor-out scenario. Since Vimana does not have a vertical tail, no rudder deflection can compensate for the constant yawing moment that is produced during an OMI situation.
The FBW system and controller will have to redistribute the power over the motors, such that a symmetrical power setting is acquired again. This can be achieved by either increasing the power of the motors on the side of the inoperative fan/motor, or by decreasing the power of the motors on the opposite side, as was discussed earlier in Subsection 7.5.4. This is in effect the same as controlling the differential thrust, which is achieved by the flight computer as was described in Subsection 7.5.4.
Furthermore, the split ailerons can be used to further increase the drag that is required for the yawing moment that needs to be counteracted.

OEI Scenario

An OEI scenario implies that the total power provided by the turboshafts decrease. Since the required power values for the engines already take this scenario into account, it should not lead to critical conditions. However, the aircraft would have to descend to a lower altitude, depending on what flight phase it is in, and execute a reroute to the closest airfield.

All Engine Out Scenario

It is evident that an all engine out scenario is way more critical than an OEI scenario. Even during this scenario, Vimana will still have to be controllable. Once again, the split ailerons can be used to achieve yaw control, whereas other directional control can be achieved by the 'conventional' control surfaces.

Crosswind Landing

Special attention is needed to ensure safe landing during heavy crosswind conditions due to the lack of a vertical tail surface. Since the moment that can be created by powering the outer two fans on one side is very high, no problem is envisioned here. This effect can be even intensified by applying engine braking on the other side, as was mentioned in Subsection 7.5.6. Small perturbations caused by gusts can be counteracted by the split ailerons.
Furthermore, the engines will be kept spooled-up in this scenario, such that additional required power can be provided directly to the motors/fans.
In case of very large crosswind speeds, the fans can even be speed up to take-off speed of revolution (5000 RPM), providing an amount of thrust equivalent to take-off thrust. If this is applied to one side of the aircraft, it is considered to be sufficient to have adequate control for a de-crab.

Minimum Control Speed

At low speeds, the active yaw control due to differential thrust is even more effective. Whereas the performance of control surfaces based on dynamic pressure decreases at low airspeeds, the performance of the differential thrust control increases since the difference in thrust can be increased. At low speeds the total required thrust is lower and therefore one side can, for example provide all the thrust keeping the other side idle, which leads to a significant yawing moment.

Electrical System Failure

A failure in the electrical system of the Vimana is already accounted for, by means of added redundancy into this system. That is why there is also redundancy in the cabling system.

Cooling System Failure

The final critical condition which is considered, is the failure of the cooling system. The cooling system is of paramount importance, as it enables one of the main features of the Vimana, namely the HTS characteristics of the propulsion system.

However, redundancy is also added to this particular system. As mentioned before in Section 5.7, additional cryocoolers and compressors are added to account for cooling system failure.

7.6 Performance Analysis

In this section the different performance aspects of the distributed propulsion aircraft will be discussed. The payload-range diagram will be presented, the flight profile and climb performance are discussed and the emissions in terms of green house gasses and noise are analyzed.

7.6.1 Payload-Range

An important performance characteristic of an aircraft is the amount of payload it can transport over different ranges. In Figure 7.22 the payload range diagram of the distributed propulsion aircraft can be seen. On the horizontal axis the range is given and on the vertical axis the payload mass is given. The aircraft has a range at maximum payload of 6100km, a range at maximum fuel of 8798km, and a ferry range of 9507km.
In order to calculate the ranges corresponding to different payloads, use have been made of weight fraction. Using standardized weight fractions for phases such as taxi, take-off and climb, a weight fraction for the cruise phase can be calculated. The take-off weight is either limited by MTOW or by the fact that the payload or fuel bay is filled. At landing, it is assumed that all the fuel is burned, taking into account a $370km$ diverging range. With the Breguet range formula, the range can be calculated as function of the weight fraction during cruise. These calculations are performed four times to get four points in the diagram. The first one is full payload and no fuel, the second one is full payload with maximum range for that payload mass (design range), the third one is full fuel and maximum payload for that fuel mass and the final one is the ferry range with only maximum fuel on board.

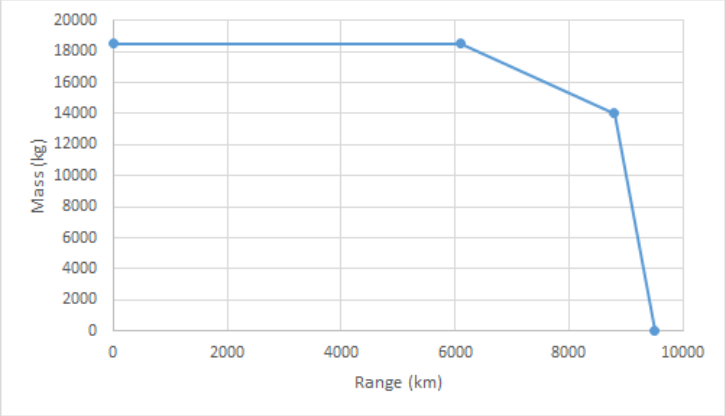

Figure 7.22: Payload range diagram for Vimana

7.6.2 Flight Profile and Climb Performance

For the distributed propulsion aircraft, the mission consists of several different phases such as climb, cruise and descent. In Figure 4.2 each of these phases is depicted. The cruise phase is the most fuel and time intensive phase. Cruising 6100km would use 13.2$tons$ of fuel and would take approximately 7$hours$.
In Figure 7.23 the phases from taxi to cruise are presented in more detail. As can be seen, the maximum rate of climb of the aircraft can attain is 9.5m/s. The time it takes to get to cruise is around 33min.

7.6.3 Performance Diagrams

At this point, it is possible to plot performance diagrams with available and required power as function of airspeed. The required power is calculated by multiplying the drag with velocity. The method for the drag calculation can be found in Subsection 7.3.4. The available power comes from multiplying the thrust with the velocity. The thrust is calculated with JavaProp with as input the power generated by the turbines. As discussed in Subsection 6.3.2 this power alters with altitude.

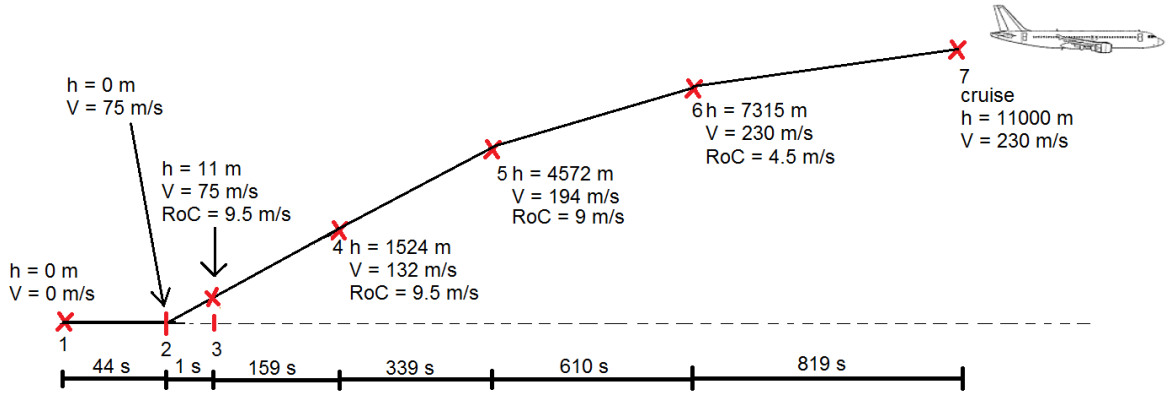

Figure 7.23: Climb performance for Vimana

The performance diagrams for cruise and take-off can be found in Figures 7.24 and 7.25. Also the minimum stall speed, including flaps for take-off, and the maximum velocity, corresponding to a Mach number of 0.82 are represented.

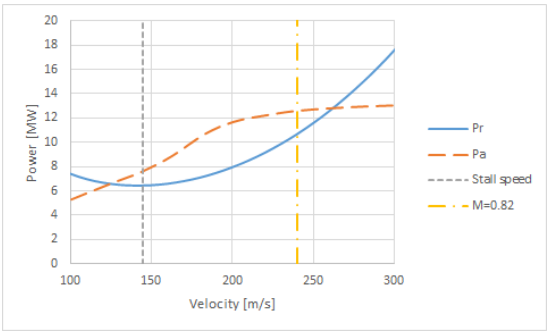

Figure 7.24: Performance diagram of Vimana at cruise altitude $(11,000m)$

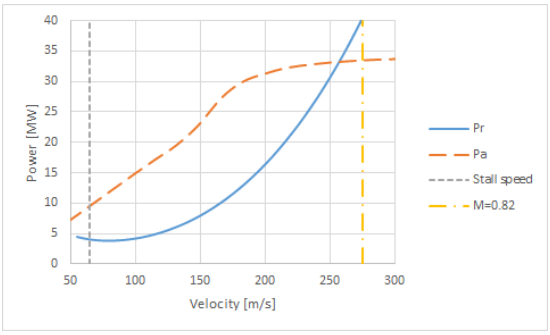

Figure 7.25: Performance diagram of Vimana at sea level

Service Ceiling

As required by REQ-TL8, the service ceiling shall be $12,000m$ (2.3.1). Analysis at this altitude has been performed to confirm that Vimana meets this requirement. If the available power for a certain airspeed is higher than the required power at $12,000m$, REQ-TL8 is met. As can be seen in Figure 7.26, the available power is indeed higher than the required power.

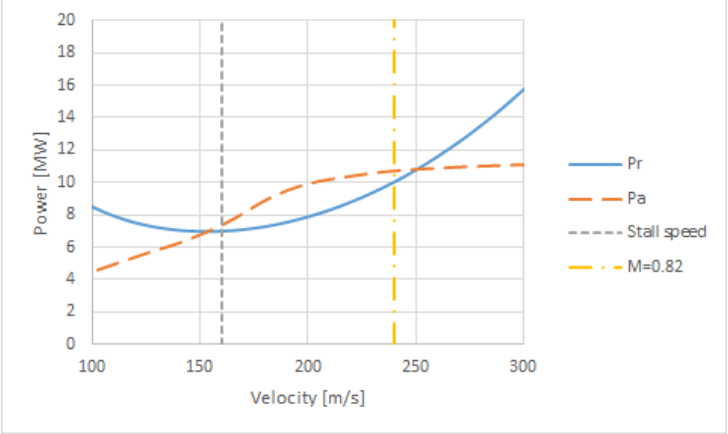

Figure 7.26: Performance diagram of Vimana at $12,000m$

In order to determine the actual service ceiling of Vimana, the performance diagrams have also been produced for $13,000m$ and $14,000m$, see Figures 7.27 and 7.28. Since the available power at $13,000m$ is higher than the required power at a velocity of $200m/s$, this altitude can be reached. At $14,000m$ there is no velocity anymore where the available power is bigger than the required power and therefore this altitude cannot be reached. The service ceiling is thus slightly above $13,000m$.

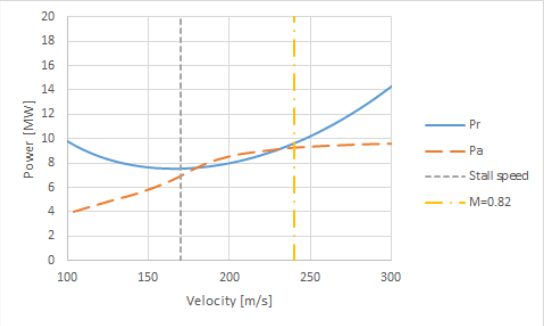

Figure 7.27: Performance diagram of Vimana at $13,000m$

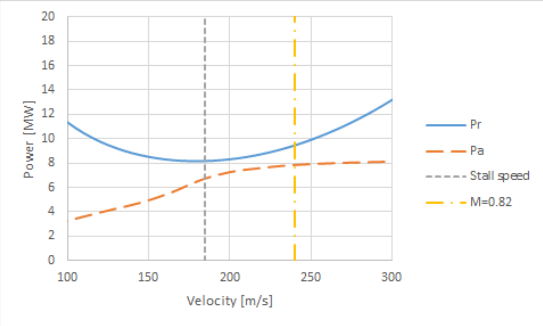

Figure 7.28: Performance diagram of Vimana at $14,000m$

7.6.4 Emissions

To analyze the emissions of carbon-dioxide and nitrogen oxides (CO_2 and NO_x) which are produced by the distributed propulsion aircraft, the emissions of the reference aircraft are used as a benchmark. The total fuel burned during cruise is obtained using the Breguet range equation used for the fuel fraction as described in Section 4.1. Using the total amount of fuel burned, the CO_2 and NO_x emissions are calculated. This is done by using the amount of CO_2 and NO_x emitted per kilogram kerosene burned and the amount of CO_2 and NO_x emitted per kilogram methane burned. These are presented below in Table 7.14.
Also, for the distributed propulsion aircraft, a fraction of the fuel burned is methane which, when burned, is less polluting in terms of CO_2 and NO_x as can be seen in Table 7.14 Using these values, together with a cruise range of 6100 km and a passenger payload of 180 passengers, the emission per kilometer per passenger is calculated.
These results are presented in Table 7.15 for the reference aircraft and the distributed propulsion aircraft. As can be seen, the emissions are reduced by over 20% in terms of carbon-dioxide and nitrogen oxides. These benefits are mainly achieved due to a decrease in specific fuel consumption and an increase in aerodynamic efficiency. Two percent of the emission reduction is achieved due to the novel fuel mixture used. Because methane produces less emissions when combusted and has a higher specific energy, the emissions are reduced by using a mixture of methane and kerosene for fuel.

Table 7.14: CO_2 and NO_x emitted per kilogram kerosene and methane burned[7]

	kg CO_2/kg	kg NO_x/kg
Kerosene	3.17984878	0.012359
Methane	2.79859229	0.010377

7.6.5 Noise Characteristics

Since the aircraft is quite conventional in terms of fuselage and planform design, this chapter will mainly focus on the changes in noise characteristics due to the different propulsion system and other configuration changes made.
The biggest change of configuration is of course the propulsion system. Two main benefits in terms of noise reduction are identified due to this configuration change. The first is the system used, which is a hybrid system. Because of this, part of the system is electric and a high bypass ratio is achieved. This is expected to result in a reduction in noise produced by the propulsion system. Also, since the turbines are mounted not

[7]URL "http://www.epa.gov/climateleadership/documents/emission-factors.pdf", [cited 16 June 2015] and URL "http://www.epa.gov/ttnchie1/conference/ei12/area/haneke.pdf", [cited 16 June 2015]

Table 7.15: Emissions for the reference aircraft and the distributed propulsion aircraft in terms of CO_2 and NO_x

Reference Aircraft			Distributed Propulsion Aircraft		
	Unit	Value		Unit	Value
Cruise fuel	kg	16199	Cruise fuel	kg	13232.3
Methane fraction	-	0	Methane fraction	-	0.179
CO_2 emission cruise	kg	51510.37	CO_2 emission cruise	kg	41173.68
CO_2 emission/pax/km	kg/pax/km	0.046913	CO_2 emission/pax/km	kg/pax/km	0.037499
			Difference w.r.t. reference aircraft	**%**	**-20.0672**
NO_x emission cruise	kg	200.2072	NO_x emission cruise	kg	158.8455
NO_x emission/pax/km	kg/pax/km	0.000182	NO_x emission/pax/km	kg/pax/km	0.000145
			Difference w.r.t. reference aircraft	**%**	**-20.6594**

under the wing but in and on top of the fuselage, the noise pollution on the ground is expected to be reduced due to noise shielding.
Another major source of noise is the landing gear, due to the friction with the surrounding air, noise is generated [53]. In normal flight the gear is retracted, but during the most critical phases of the flight in terms of noise pollution, the gear is extended. Mainly during approach, the gear is extended for a longer period of time.

7.6.6 Results

In Table 7.16 the performance characteristics of both the reference aircraft and Vimana are summarized. It can be seen Vimana performs better in terms of lift over drag, specific fuel consumption and emissions. The reference aircraft however performs better in terms of climb rate due to a higher thrust loading.
In Figure 7.29 a model of Vimana can be seen. A three-view drawing of the aircraft can be found in Figure 7.30.

Table 7.16: Performance characteristics of the reference aircraft and Vimana

	Unit	**Reference Aircraft**	**Vimana**
Maximum L/D	$[-]$	18	20.3
Cruise L/D (begin - end)	$[-]$	17.5 - 15.92	19.06 - 17.29
Specifici fuel consumption	$[kg/Ns]$	1.34708E-05	1.1675E-05
Climb rate at sea level	$[m/s]$	25	9
Take-off field length	$[m]$	2100	2100
Landing field length	$[m]$	1600	1600
Surface ceiling	$[km]$	12.5	12
Cruise mach	$[-]$	0.78	0.78
Maximum cruise mach	$[-]$	0.82	0.82
Range at maximum payload	$[km]$	6100	6100
CO_2 **emissions**	$[kg/km/pax]$	4.691E-02	3.750E-02
NO_x **emissions**	$[kg/km/pax]$	1.823E-04	1.447E-04

7.7 Verification and Validation

In Chapter 4 the chosen design method was described. In order to check whether these methods are implemented correctly, they have to be verified. Verification is the process to check whether this model is built correctly, whereas validation is the process to check whether built model accurately represents reality. Sub-

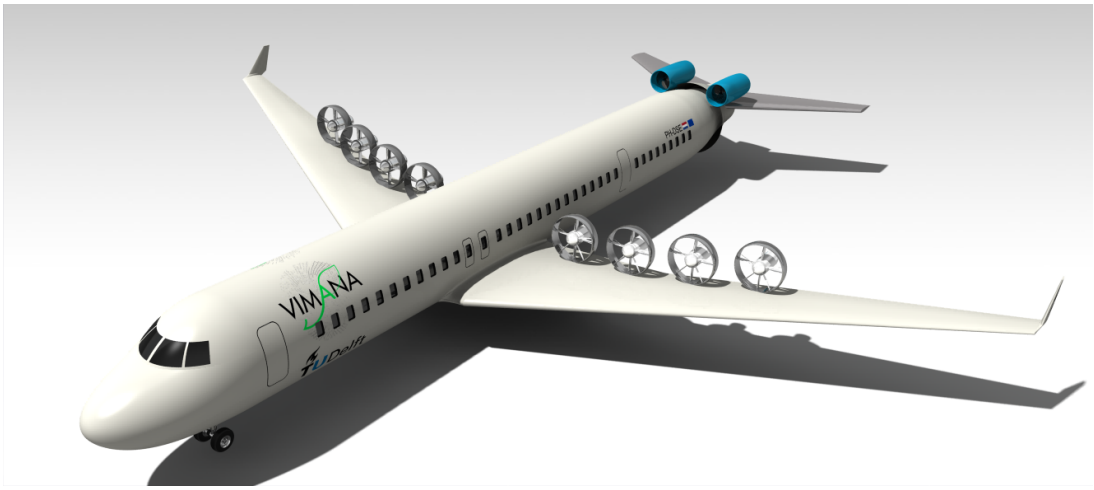

Figure 7.29: Visual representation of Vimana

section 7.7.1 will explain the verification procedure and results, and the validation procedure is explained in Subsection 7.7.2.

7.7.1 Verification

To verify the design calculations, several models need to be checked for errors. This is done by using Airbus A321 data as input for each model and comparing the output with the actual A321 specifications. A321 data has been chosen, because this aircraft matches the requirements the best. The different models that have been verified are the following:

- **Class I weight estimation:** In this model, the found relations between MTOW, OEW and fuel weight are applied to the Airbus A321.
- **Wing planform design:** Here, the calculations for the planform parameters are applied to the T/W and W/S values for the A321, and applied to one of the airfoils the A321 uses, which approximates the specifications of the entire wing.
- **High-lift devices design:** The method to size the high-lift devices is used with the $C_{L_{max}}$ values of the A321. After this, it is checked whether these values are approximately the same as the ones on the A321.
- **Engine sizing:** The required thrust per engine is compared to the engines used on the A321.
- **Empennage sizing:** The tail volume and tail lengths are put in the model to calculate the wing surface areas.

The results of this verification process can be found in Table 7.17.

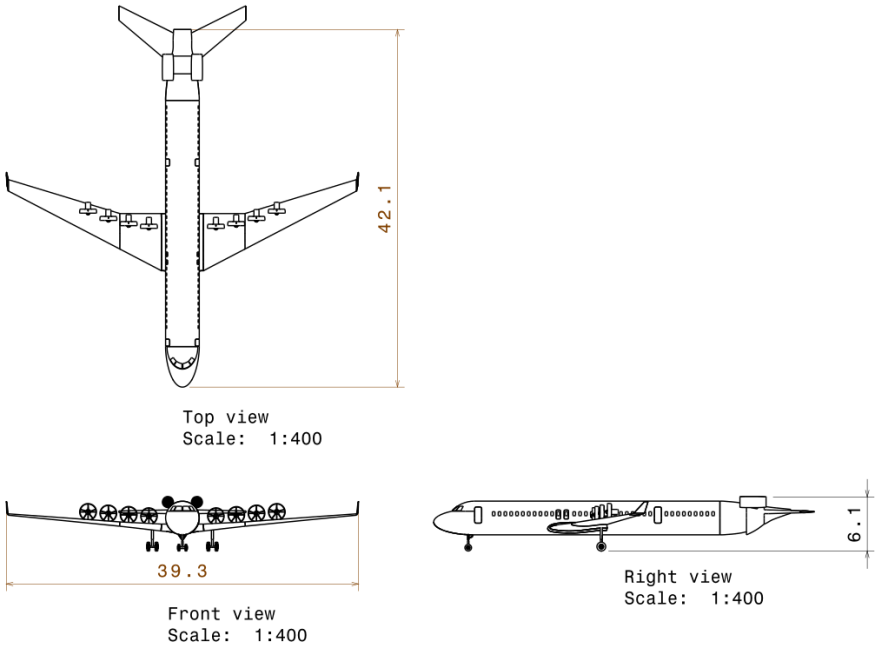

Figure 7.30: Technical drawing of Vimana

Table 7.17: Comparison between the A321 modelled version and actual values of the A321

	Reference model	A321	Difference [%]
Class I			
MTOW $[kg]$	87568	89000	-1.6
OEW $[kg]$	45179	48000	-5.9
Fuel weight $[kg]$	23714	22322	6.2
Wing Design			
S $[m^2]$	125.8	122.4	2.8
b $[m]$	34.4	33.9	1.5
c_r $[m]$	5.77	6.07	-4.9
c_t $[m]$	1.56	1.5	4.0
$\Lambda_{0.25c}$ $[deg]$	25	25	0.0
Mean geometric chord $[m]$	3.66	3.61	1.4
MAC $[m]$	4.06	4.29	-5.4
MAC spanwise position $[m]$	6.95	5.7	21.9
HLD Design			
S_{flaps} $[m^2]$	20.29	21.1	-3.8
S_{slats} $[m^2]$	11.19	12.64	-11.5
Engines			
Thrust required per engine $[kN]$	135	141	-4.3
Empennage			
Horizontal tail area $[m^2]$	30.2	31	-2.6
Vertical tail area $[m^2]$	22.5	21.5	4.7

From the table above one can see that there are a few parameters that have a large percentage difference with respect to the A321. Some of these differences can be explained by the fact that several parameters are obtained using empirical relations. Of course, the A321 does not follow these relations exactly. However, this can only explain the percentage differences to about 4%. As can be seen there is one value that really jumps out, being a 21.9% difference in the MAC spanwise position. This is caused by the different design of the wing. The A321 has a kink in the trailing edge of the wing which influences both the length and the position

of the mean aerodynamic chord, as well as the root and tip chord lengths of the wing.
Two values that are also slightly off, are the empty weight and fuel weight. The fuel weight can of course not be a 100% fit since the specific fuel consumption of the A321 is unknown. Furthermore, if an A321 is configured with the maximum number of fuel tanks, the fuel weight already is more than 24000kg. [10] The difference in empty weight is caused by the usage of a statistical relation to obtain the OEW in the model, which does not represent the A321 correctly.
The difference in the flap and slat area is mainly caused by the airfoil choice in the model. Because the A321 airfoil data is kept confidential by Airbus, only an estimate could be made for the airfoil profile. Furthermore, a real wing consists of multiple airfoils with a decreasing t/c ratio towards the span, while the model only has one airfoil. Therefore, the values for $C_{L_{max}}$ may not accurately represent the A321 wing, so that a larger slat area is needed in the model.

7.7.2 Validation

The same parameters are checked for the validation process, only this time the values from the designed reference aircraft (Chapter 5) are compared to the ones from the Airbus A321. The results can be seen in Table 7.18.

Table 7.18: Comparison between the reference aircraft and the values of the Airbus A321

	Reference aircraft	**A321**	**Difference [%]**
Class I			
MTOW [kg]	86359	89000	-3.0
OEW [kg]	43754	48000	-8.8
Fuel weight [kg]	23932	22322	7.2
Wing Design			
S [m^2]	128.7	122.4	5.1
b [m]	37.62	33.9	11.0
c_r [m]	5.38	6.07	-11.4
c_t [m]	1.45	1.5	-3.3
$\Lambda_{0.25c}$ [deg]	22.49	25.00	-10.0
Mean geometric chord [m]	3.42	3.61	-5.3
MAC [m]	3.8	4.29	-11.4
MAC spanwise position [m]	7.6	5.7	33.3
HLD Design			
S_{flaps} [m^2]	21.72	21.1	2.9
S_{slats} [m^2]	13.03	12.64	3.1
Engines			
Thrust required per engine [kN]	152.5	141	8.2
Empennage			
Horizontal tail area [m^2]	37.31	31	20.4
Vertical tail area [m^2]	26.78	21.5	24.6

Validation is all about determining if the right tool has been built. As can be seen from the results in the table some results are slightly off. The wing characteristics depend on the design of the wing and the chosen airfoil. These designs are different for the A321 and the reference aircraft, which explains the differences in wing characteristics. The empennage is based on statistical data, but it seems the A321 differs a lot from that trend.
Finally, it is also unknown what the exact requirements were for the design of the A321, which explains the offset in values. From this table there can be seen that all the outcomes are in a realistic range, and while there are large differences between the reference aircraft and the A321 due to different mission requirements, there are no indications that the model is built incorrectly.

Chapter 8 | Aircraft System Characteristics

In this chapter the aircraft system characteristics are covered. First, the hardware and software interaction is discussed. Second, the communication and data handing of the aircraft to its environment are covered. Lastly, the cabin layout is shown, together with the cockpit.

8.1 Hardware and Software Interaction

In this section, the hardware and software interactions are covered. It covers the environmental control, the hydraulic system, the fuel system, the auxiliary power system, and the electrical system.
A hardware block diagram visualizes all the physical resource flows in the aircraft. For the Vimana aircraft, the hardware flow block diagram can be seen in Figure 8.1. In this figure, the different systems are represented in different colors. Also, the different resource flows are given. There has to be noted that the neon system is slightly different as in the picture. In real, it is a redundant system connecting each cryocooler to every motor and every generator.

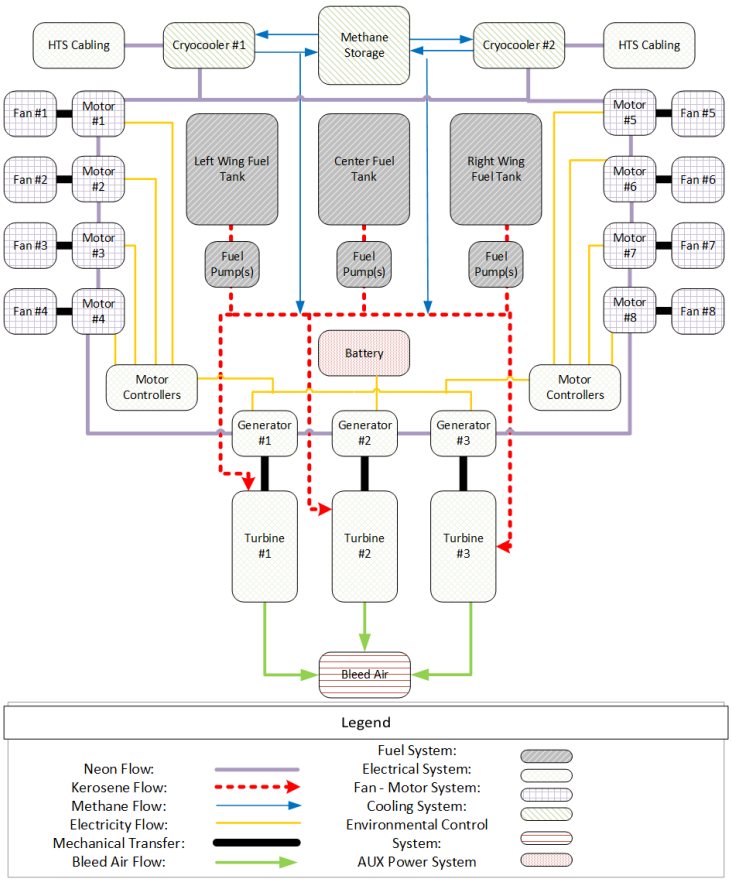

Figure 8.1: Hardware Block Diagram

The systems need to interact and be controlled. These processes are visualized in the software block diagram presented in Figure 8.2. Some key functions which have to be performed are the regulation of the temperature of the different superconductive components and the power regulation. The temperature control is performed by measuring the temperature of the different components and consequently adapting the rate of flow of neon to these components. The power is controlled by regulating the RPM of the turbine. Increasing the RPM will generate more power which can be sent to the fans or the auxiliary power system.
Figures 8.1 and 8.2 are meant to give a general overview of the systems interactions. The systems represented in these figure are covered in more detailed in Subsections 8.1.1 - 8.1.4. for the environmental control system, the hydraulic system, the fuel systems and the electric system respectively. The cooling, propulsion and auxiliary power system were covered more in depth in Chapter 6.

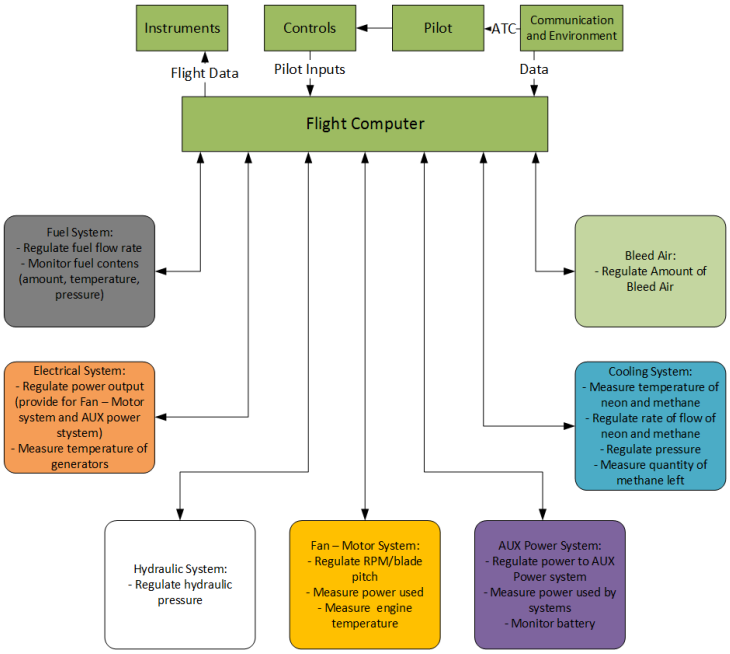

Figure 8.2: Software Block Diagram

8.1.1 Environmental Control

The Environmental Control System (ECS) of an aircraft refers to the system that is responsible for establishing and maintaining an acceptable environment for a given payload, be it goods or passengers. This is done by providing and regulating air supply, thermal control and cabin pressurization. Most ECS today use bleed air from the engines as the primary circulation fluid. In conventional aircraft, after thrust, "*the ECS is the main secondary power consumer from the engines (75% of non-propulsive power on cruise)*" [54].
ECS systems receive bleed air from the compressor stage of the engines, which is already at a high temperature and pressure. This is then conditioned in an Environmental Control Unit (ECU), which removes excess moisture and regulates the temperature required to maintain a comfortable environment in the aircraft. Figure 8.3 presents a schematic of a proposed ECS. Due to the relative lack of system complexity, the ECS is expected to be very similar to aircraft such as the A321. Minor changes, if any, will be visible mostly in the layout, not in the architecture or component sequence.
The reader can follow the fluid flow from the compressor stage "bleed air" outlet all the way to the cabin. Along the way, some of this air is supplied to the avionics which require an air supply. After further filtering and passing the air through a heat exchanger, it is supplied to the cabin. After flowing through the cabin section, the air may then be re-routed into the system to conserve the energy put into it, or may be ejected into the atmosphere, as a fresh flow of air is always guaranteed as long as the turbines are running.
The schematic in Figure 8.3 proposes two separate airflow paths, one which directly takes air in from ram air inlets, to use for avionics purposes, and another, from bleed air, which needs to be filtered and adapted further for use in the cockpit and cabin. The first pathway is simple and does not have any intermediate components as the air intake to the avionics does not need to be filtered to the same extent as that for human consumption.
Throughout the latter pathway, flow control valves are placed to regulate the flow of the outside air to the cabin. It is also passed through heat exchangers (HEX), in order to cool it to the temperature required for cabin air-conditioning units. This is done 2 times in the schematic, as a redundancy feature. The first HEX also includes a temperature sensor and rerouting valve (re-routed or overflow air pathways are shown in blue instead of red), in case the heat exchanger does not cool the air sufficiently in the first pass. Finally, the system includes an overflow control and particulate filter before the air is supplied to the cabin.

8.1.2 Hydraulic System

The principle of hydraulic systems is based on the fact that liquids are almost incompressible [55], using fluids under pressure to move mechanical components. Multiple components of an aircraft are hydraulically powered, which are the following but not limited to:

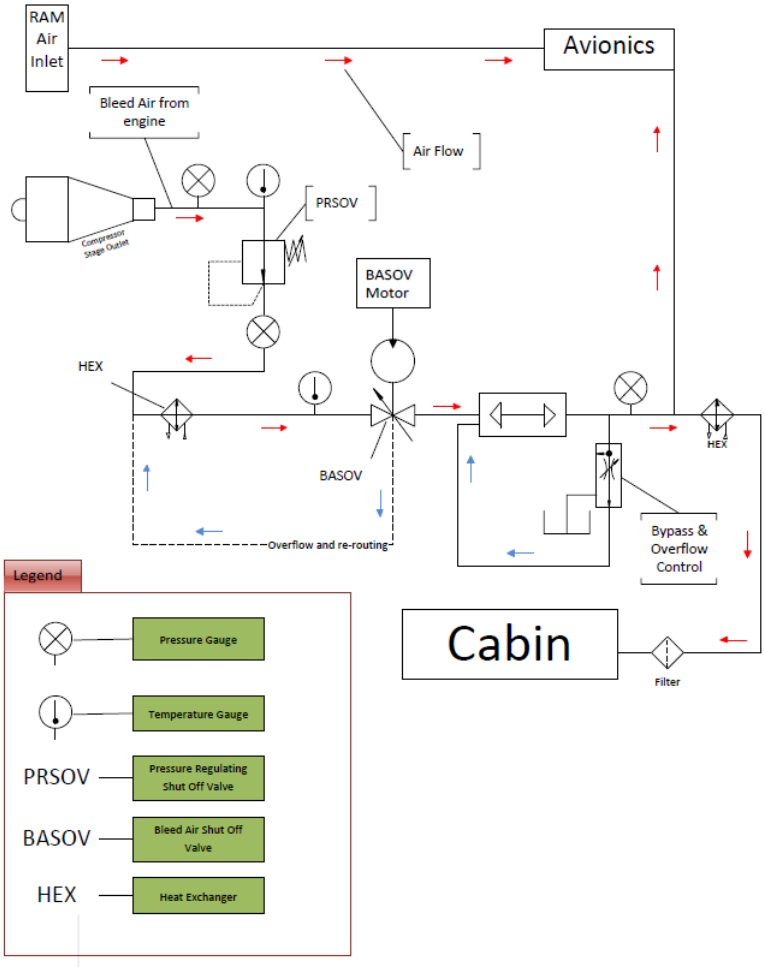

Figure 8.3: Schematic of the Environmental Control System

- Wheel brakes
- Spoilers
- Flight controls
- Nose steering
- Doors
- Shock absorbers
- Windshield wipers
- Fan pitch control

The hydraulic system is governed by Pascal's Law. The hydraulic fluid is in contact with both sides of the piston. By regulating the pressure, mechanical work is performed. While theoretically any fluid can be used, a special hydraulic fluid is optimal. This is because of its high operating pressure, which is between 207 and 345 bar, the environmental conditions and the safety criteria which it has to comply with.
The fluid should also have a high flash point. This is to prevent ignition in the case of a leakage. It is also important for the fluid to have an adequate viscosity since it operates in a wide range of temperatures inside the aircraft, and should maintain an adequate velocity over this range. The fluid should also act as a lubricant for hydraulic systems components, have anti-corrosion properties and be thermally stabl e. Finally, the fluid should also act as a system coolant, being able to absorb and release heat.
There are three types of hydraulic systems used[1]. These are mentioned and explained below and in Figure 8.4.

- System 1 (Red and diagonal lines filled). This hydraulic system powers the flight controls only. These are the most crucial aircraft components.

[1]URL "http://www.skybrary.aero/index.php/Hydraulic_Systems", [cited 21 May 2015]

- System 2 (Green and checkered). This is the emergency hydraulic system. This may be activated by the pilot in case the pressure in the red color hydraulic system is lost.
- Utility system (Vertical lines filled). This hydraulic system powers the landing gear, speedbrakes, nose steering and engine air bypass flaps.

In Figure 8.4 a schematic of the hydraulic system is given. The different colors indicate the type of hydraulic system, as described above. The hydraulic pump pumps the fluid from the reservoir to the various actuators. System 1 contains two hydraulic pumps for redundancy. Between the two, a main relief valve is located. This is a type of valve which controls and limits the pressure and ensures that the fluid cannot move in the opposite direction. Any excess fluid at this point is also re-routed back to the tank after passing through a filter to ensure that impurities are not present in the system. A pressure gauge is then located to ensure adequate pressure during operation. In case System 1 fails, System 2 can take over its tasks.
The priority valve is set to a certain pressure. If the pressure drops below this value, the utility system gets shut off. This is to ensure that the hydraulic system can still operate the crucial aircraft components.

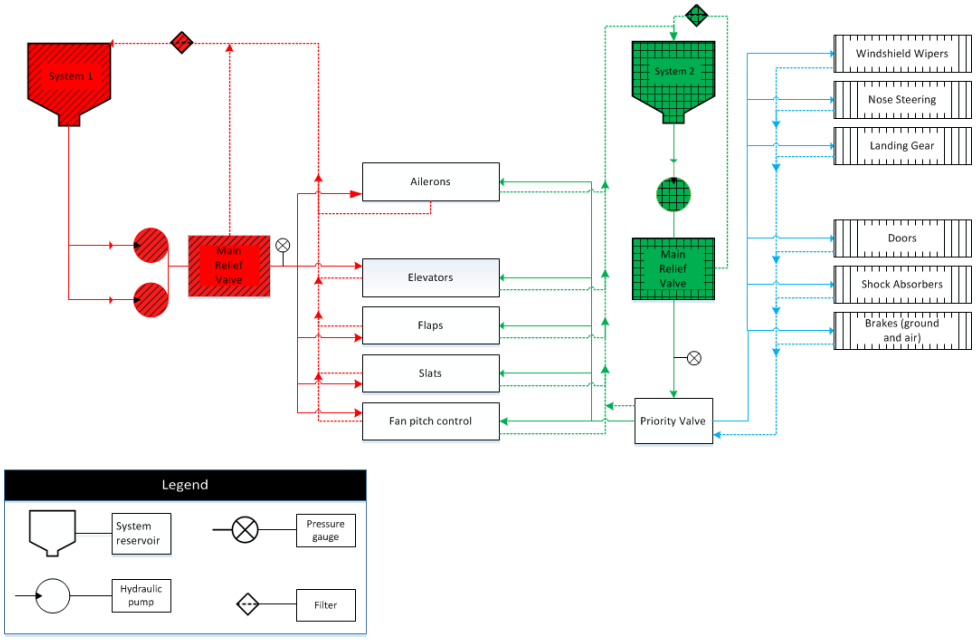

Figure 8.4: Schematic of the hydraulic system

In Figure 8.4 it can also be seen that every actuator has two pathways, a pressure line (solid in the figure) and a tank line (dotted line in the figure). The first is to ensure that the actuator is supplied with fluid at all times, while the latter completes the loop by bringing back the hydraulic fluid to the tanks.

8.1.3 Fuel System

The task of the aircraft fuel system is to store, manage and deliver the fuel to the propulsion system [55]. The aircraft has multiple fuel tanks stored inside the wing and fuselage. The aircraft also has methane tanks which are placed in the cargo hold of the aircraft. The tanks are interconnected by transfer valves. These valves serve two purposes.
The first function is to shut off the fuel flow, to prevent fuel reaching the engines in case of an engine fire. The second function is for the pilot to choose which tank to feed which engine and pump fuel between tanks to ensure symmetric weight. Each tank is vented for it to allow air to replace the burned fuel.
The fuel system also contains a cross-feed valve. This is to ensure that in case of an engine failure, all the fuel tanks are able to supply the other engine. Fuel dumpers are installed near the wing tips. This is to dump excessive fuel in the event of an unexpected early landing, to reduce the aircraft to its maximum landing weight. Kerosene is the only fuel that will be dumped as liquid methane will evaporate when dumped and is a greenhouse gas.
Vent tanks (or surge tanks) are located near the outboard of the main wing tanks. These are tanks that are normally empty, and are used for fuel overflow. They are also used for fuel system venting.

In Figure 8.5 a schematic of the fuel system is given. As can be seen in the schematic, each tank contains two fuel pumps for redundancy purposes. The methane tanks are connected to the main tanks, so that the jet and methane fuel can be mixed. There are spill pipes installed between the methane/jet fuel tanks. This allows fuel to flow to the center tank if the outer tanks are already full. It could also be used for refueling purposes. The methane tanks are connected to cryocoolers, to keep an adequate temperature. The cryocoolers are not incorporated in the fuel system schematic, as it is part of the propulsion system. The propulsion system schematic which includes the cryocoolers can be found in Section 6.9.

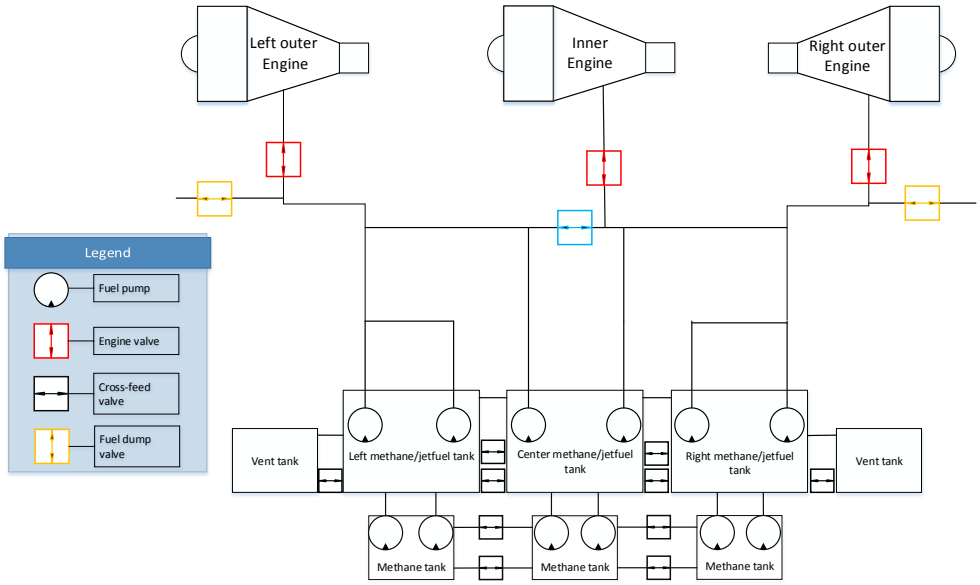

Figure 8.5: Schematic of the fuel system

8.1.4 Electrical System

The main task of aircraft electrical systems is to generate, transmit, distribute and utilize electrical energy. Due to the unique layout of the propulsion system architecture, the power transmission lines from the turbines to the fans are part of the electrical system. In addition to this, the electrical system has to power multiple other components. A non-exhaustive list of these components can be found below:

- Flight deck displays
- In-flight entertainment
- Flight controls

The aircraft uses multiple voltage systems, using a combination of alternating current (AC) and direct current (DC) busses to power the aircraft components. AC is obtained from the engine generator or can also be externally obtained from the ground support equipment (GSE). DC is obtained from accumulator/battery or transformer rectifier. Most aircraft use $115V$ AC power and $28V$ DC power [56]. The primary power generated by the aircraft is AC. Multiple Transformer Rectifier Units are used to convert AC to DC, in order to be transferred by the DC buses. In the event that all AC power generation fails, an inverter is used to convert DC to AC.

AC and DC motors serve different purposes [2]. DC are used for starter functions, fuel valve actuation, and linear and rotary actuators. AC motors are used for the continuous flight operations. Most hydraulically and pneumatically actuated systems can fall back on the electrical system if they fail.
The functions which fall under DC motors are the electronics, cargo and cabin doors. Under electronics is meant avionics, computer systems, sensors and cockpit indicators. Conversely, the functions which fall under

[2]URL "http://www.ece.tamu.edu/~huang/files/Materials615/ElectricPowerInAirplane.pdf", [cited 23 June 2015]

AC motors are the heating, lighting and mechanical power. 'Heating' would include equipment such as the coffee machine, oven, window heating and the pitot tube (as it would freeze and be rendered inoperative without dedicated heating).

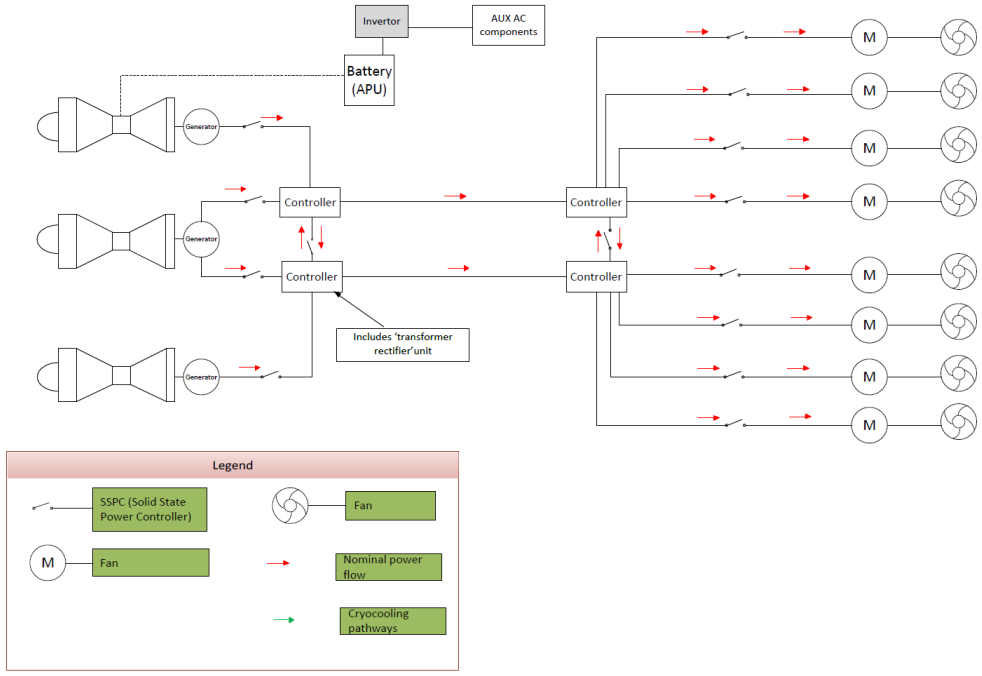

Figure 8.6: Schematic of the electrical power unit

A schematic for a general aircraft electrical system can be seen in Figure 8.6. Here, a battery unit is added with a link to the turbines, in case of excess power which may, if need be, used to recharge the batteries. The battery unit is, in regular flight, used as an APU as explained in Subsection 6.8.1.

For further details of the electrical system that directly link to the propulsion system architecture, the reader is referred to Chapter 6.

8.2 Communications and Data Handling

Communication flow architectures represent the flow of data to and from its environment. For Vimana's design this can be split up into two main components. The first one is the communication the pilots have with Air Traffic Controllers (ATC) to guide them and ensure safety. This is for Vimana not different than current conventional aircraft, therefore this aspect will not be addressed in detail.
The second one is the input Vimana gets from its environment via sensors to give the pilots the current state of the aircraft. Once all this information is gathered, it must be processed, thus imposing the need of a data handling system.
Communication flow architectures can be constructed on varying levels of complexity and depth. However, for the purposes of this report, phases from start up to begin of cruise are laid out in Figure 8.7. In addition, the key blocks 'throttle up' is detailed in Subsection 8.2.1.

Figure 8.7: Key Communication Flow Phases

8.2.1 'Throttle up' Phase

Figure 8.8 shows the steps that need to be taken in order to start up an aircraft. The flow of this process for Vimana is very similar to a current conventional aircraft. However, some differences can be noted and are indicated in yellow. Going from left to right, one notices that a battery provides part of the power needed to start the turboshaft engines instead of an APU (the rest of the load is carried by a huffer cart as explained in Subsection 6.8.1). Also, all different components related to the propulsion need to be checked. From motors and generators to methane tanks and cryocoolers. The communication with ATC is also clearly visible, once a component does not work properly this is communicated and take-off is aborted. Of course if an engine does not start from the first time, a second try can be performed. It is not just a one process loop, but if serious issues arise, this should be communicated.

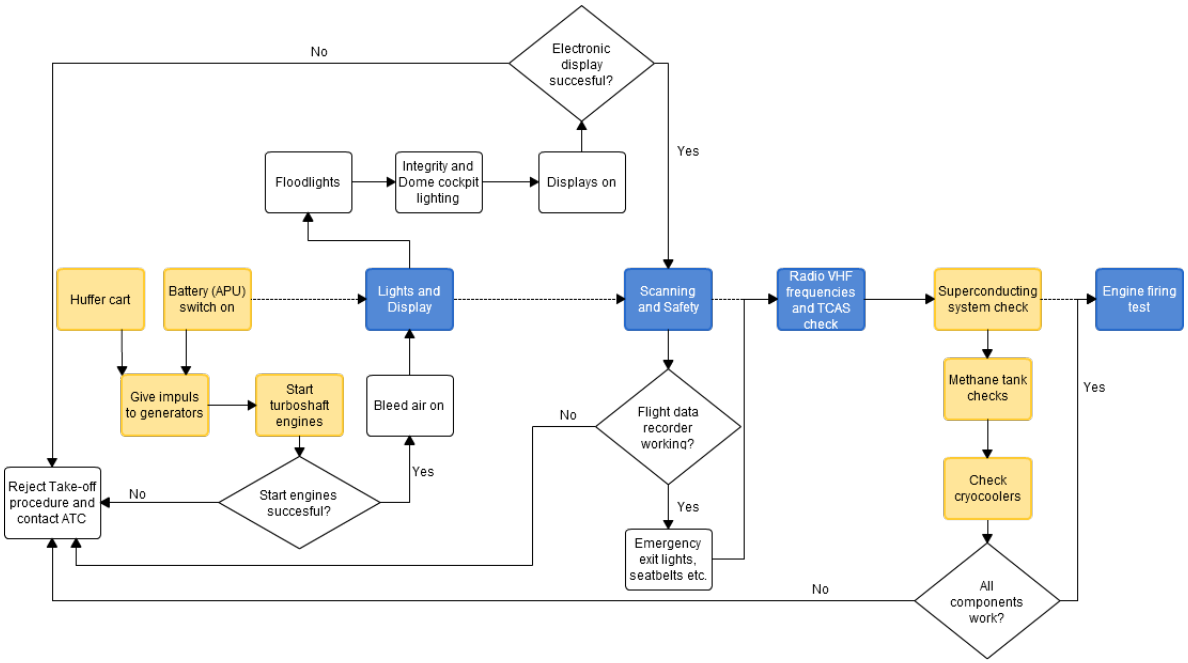

Figure 8.8: Detail of the "throttle up" phase

8.3 Configuration and Layout

In this section, the configuration and layout of the cabin and cockpit are explained. Drawings and explanations are presented of the cabin layout, for both the passenger cabin and the cargo area. A general explanation is given for the cockpit layout.

8.3.1 Cabin Layout

To comply with the requirement set of 180 passengers, the optimal configuration is a 3-3 single aisle cabin, because it optimizes the usage of space in the fuselage This means that the total row length is 30 seats. To optimize the spacing and the need for additional equipment such as lavatories, a seat pitch of 31 inch is used. The configuration is single-class, as shown in Figure 8.9, comparable to the economy class that many airliners use. Passengers sitting near the exits will benefit from a larger seat pitch, due to the clearance required for the exits. To increase the passenger comfort and accommodate for their needs, two lavatories are located in the front of the aircraft near the exits, as shown in Figure 8.9. Together with two additional lavatories, the galley is located in the back of the aircraft. The sizes of all components are given in Table 8.1.

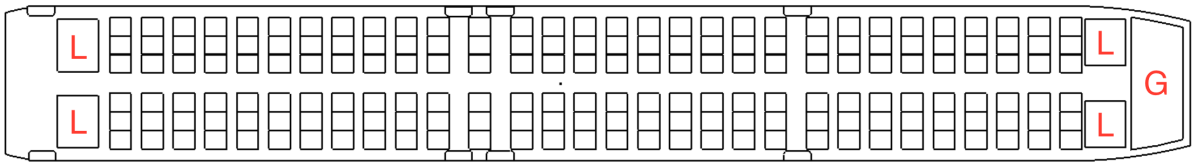

Figure 8.9: Cabin configuration of the aircraft, where L indicates the lavatories and G indicates the galley

Table 8.1: Aircraft cabin equipment, number and size.

Component	Number	Size [m x m]
Seats	180	0.54x0.46
Galleys	1	1.3x3.2
Lavatories	4	1.02x1.02
Doors type I	4	0.61x1.22
Doors type III	4	0.51x0.91

Furthermore, to account for the safety of all passengers on board of the aircraft, four exits are located on each side, of which the front and back doors are type I doors and the overwing exits are type III doors, which function as emergency exits and maximize the passenger evacuation efficiency in case of an emergency. It was noted that most aircraft have the rear doors all the way at the back, even further than the last window. However, the aircraft features a large duct near the rear of the aircraft, together with a turbine on each side, making passenger evacuation too risky in case the turbines are still operational. To account for this risk, the aft doors are located in front of the last ten seats, as can be seen in Figure 8.10.

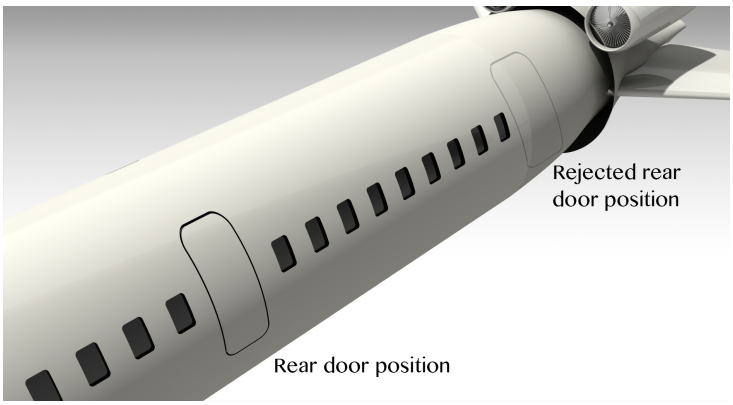

Figure 8.10: Rear door configuration, with the rejected configuration outlined in transparent

8.3.2 Cargo Cabin Layout

To optimize the freight capacity of the aircraft, the lower cabin was designed to hold eight LD3-45 containers, which are contoured on both sides. These containers are 2.44m x 1.53m in size and fit in the fuselage with a limited margin.

As the propulsion system features a methane cooling system, the gas is also stored in the cargo cabin. A visual representation of the gas tank storage, together with the standard LD3-45 containers, is shown in Figure 8.11, where C indicates the containers and M shows the location and size of the methane tanks. Here it can be noted that the tanks have the same size as the containers, due to the fact that the gas tanks are also stored in LD3-45 sized containers, to optimize the maintainability and increase the ease at which the tanks can be refuelled. Locating the tanks below the cabin poses no danger to the passengers because of the low pressurization in the tanks. Furthermore, the non-toxicity of methane ensures a safe working environment for the personnel.

The doors are located near the containers, to optimize the speed at which they can be taken out. There are two doors on the right side, one located in front of the wing and one behind the wing, as there are two different cargo bays, separated by the central wing box structure. The left side of the aircraft is the side where

passengers will board the aircraft, and therefore is not considered for cargo loading, also because two doors is sufficient to load or unload the cargo.

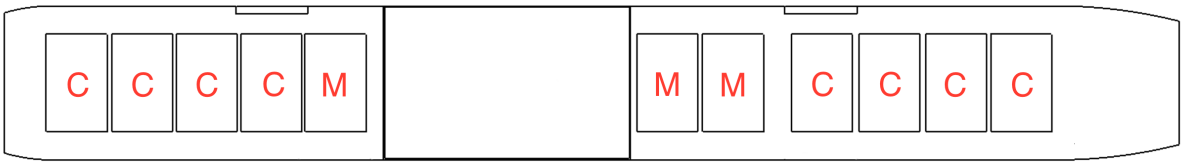

Figure 8.11: Cargo cabin configuration of the aircraft, where C indicates the LD3-45 containers and M indicates the methane tanks

8.3.3 Cockpit Layout

The aircraft cockpit, like almost all aircraft, is located in the front. The cockpit contains all the flight instruments and controls which enable the pilots to fly the aircraft. The most significant alternation difference of the cockpit with a reference aircraft is the throttle control.
As mentioned before, the aircraft has a relatively large number of propulsive units, compared to conventional transport aircraft. These all require adequate control.
A battery is also part of the propulsion system. This battery does not need a control system for particular power settings. Therefore, a master switch is sufficient to have in order to turn the battery on and off, as is the case in many modern aircraft.
The engines, fans/motors however, of course do require a power setting that is controllable. To control the eight fans, there will be four thrust levers present: one lever for two fans. Furthermore, one thrust lever will be present to control the power settings of the turboshafts, making it a total of five levers.
Engine shutdown buttons will be present located at the center overhead console, which allows the engines to be shutdown in case of an engine failure. Finally, motor/fan shutdown buttons will also allow for these particular components to be shutdown manually if required.
The cockpit has room for two pilots. According to FAA regulations, based on the maximum range, two pilots are required [3].
The cockpit is equipped with computer tablets, to store the necessary books. This is to save weight, and make it more convenient for the pilots.
The aircraft is equipped with what is called a glass cockpit [57]. This implies that the cockpit will feature electronic flight instruments, instead of the conventional analog dials and gauges. This technology has typically large LCD displays installed in the cockpit. The sensors that are used, are also made electronically. For example, the attitude control. Instead of a traditional mechanical gyroscopic flight instruments, attitude and heading reference systems are installed. The advantage is a more accurate system and a higher reliability.
The aircraft can be either flown with a stick, a side-stick or a yoke. A side-stick is chosen, based on its minor advantages, such as increased visibility and pilot comfort. Another minor advantage is that side-stick input is easier to convert to an electrical signal, than for a yoke. The reference aircraft, the A321, also makes use of a side-stick.

Flight Instruments

As in any aircraft, basic flight instruments will also be present such as the altimeter, airspeed indicator and the magnetic direction indicator. In addition to these instruments, there will also be additional instruments that are related to a specific control group of the aircraft.

Engine Instruments

Next to the basic flight instruments, engine instruments will also be present, being part of the glass cockpit. These will measure and indicate the quantity, temperature and pressure of the turboshafts, motors and generators. In addition, they also measure and indicate the power settings and speeds of the aforementioned components. Therefore, pressure, fuel and oil quantity gauges will be present. Furthermore, tachometers will

[3] URL "http://www.ecfr.gov/cgi-bin/text-idx?SID=3106877474ac09000d0514ac960925c7&node=14:3.0.1.1.7.18&rgn=div6", [cited 20 June 2015]

be present, that constantly keep track of the rotational speeds of the turboshafts, motors and generators. These instruments will be placed at the center of the cockpit, as this enables it to be easily visible to the pilots.

Navigation Instruments

As mentioned before, navigational instruments are required, which will contribute information used by the pilot to guide the aircraft along a definite course. These instruments include various compasses, some of which also utilize GPS to ensure a specific flight course.
In addition to these directional and positional navigation instruments, there are also navigational instruments designed to direct the pilot's approach to landing at an airport. A so called Instrument landing system will be used, which is a ground-based instrument approach system that provides precision lateral and vertical guidance to an aircraft approaching and landing on a runway, making use of GPS. A satellite based system will dramatically reduce delays, as take-off and landings are more streamlined [4]. A GPS navigation system will also result in more precise landings and take-offs. Danger for mid-air collisions is also reduces, as the location of nearby air traffic is more precise.

[4] URL "http://mashable.com/2012/02/07/faa-gps/", [cited 30 June 2015]

Chapter 9 | Sustainability

In order to ensure that the design meets the expected quality standards and environmental regulations, a special focus must be put upon sustainability, not only in the final product but also in the design process. In order to approach this issue in a systematic manner, the aspects of system sustainability have been subdivided as follows: production and assembly, operation, maintenance and disposal of systems. Identifying the key aspects in each of these domains will ensure that adverse impacts are minimised and system sustainability is maintained. It is important to point out the fact that the scope of this project allowed deviations from the conventional tube-and-wing design only if those design choices were absolutely necessary for the distributed propulsion system. Hence, no additional considerations were taken for sustainability outside the propulsion system environment.

9.1 Production and Assembly

The first step in delivering a sustainable aircraft is that the production must be carried out in a sustainable manner. In order to reduce the ecological footprint, the Vimana project aims to implement additive manufacturing concepts such as the direct metal laser sintering (DMLS) concept currently being developed by EOS Aerospace in conjunction with Airbus Group [1]. The use of direct metal laser sintering manufacturing technologies benefits the overall project sustainability in 3 main points:

- The high degree of freedom associated with additive manufacturing technologies entails that only the essential structural elements of each part will be present. As there are no limitations in terms of casting or machining allowances, all parts can be designed and optimized for an all-around low weight performance.
- Additive manufacturing techniques completely eliminate the scrap material emanating from machining and casting processes, allowing an efficient use of raw materials.
- Initial studies of aerospace parts fabricated under the DMLS procedure have shown that lower energy consumption levels during part manufacturing can be achieved, reducing even more the environmental footprint of the process[1].

It is of course pertinent to mention the fact that the advantages of additive manufacturing techniques, as well as other innovative production and assembly techniques, will only make themselves evident after the detailed definition of all the aircraft's components. Additionally, in order to increase the overall production and assembly sustainability, the Vimana project envisions to implement the Blue5 initiative of Airbus during the manufacturing process [2]. This production philosophy entails reduction in five specific areas: energy, water, waste, CO_2 and volatile organic compounds.
Finally, the introduction of a completely new propulsion system still entails the need to develop and build new facilities, tooling and machinery, which inevitably have a negative contribution to the overall sustainability of the project.

9.2 Operations

A sustainable aircraft also means that it should be environmentally friendly during actual operation. The European community has formulated goals that are directed to the realization of a sustainable and environmentally friendly means of air transport, by achieving major reductions in fuel consumption, noise and pollutant emissions. These targets can be achieved by breakthrough innovations and radical design changes to the design of transport aircraft. Distributed propulsion is one of these innovations, which could lead to achieving these goals.
The Vimana project, making use of engines with an overall lower specific fuel consumption greatly outperforms current state-of-the-art aircraft. According to the estimates presented in Subsection 7.6.4, a remarkable reduction in CO_2 and NO_x of over 20% can be achieved by using a distributed propulsion system. This reduction has by all means an extremely important contribution towards sustainability and defines a new benchmark for future aircraft developments. This reduction in fuel consumption can be traced to two important design choices: the removal of the vertical tail ensuring for an overall reduction in drag and the embedded

[1] URL "http://www.onlineamd.com/3d-printing-laser-sintering-lightweight-122314.aspx", [cited 19 June 2015]
[2] URL "http://www.airbus.com/company/eco-efficiency/eco-initiatives/", [cited 19 June 2015]

turboshaft on the back of the aircraft, which is responsible for boundary layer ingestion and wake filling, allowing further drag reductions.
The main ambition of the Vimana project in terms of sustainability in operation lies in the methane use and production. As described in Chapter 6, methane is used both as a coolant for the superconductive cabling and as the propellant for the turboshaft engines. Partially using natural gas instead of a fully conventional Jet-A1 fuel mixture opens the possibility to greatly improve emissions in terms of fuel production. The Vimana project aims to obtain all the methane required from renewable sources, particularly from maize crops which achieve the highest methane yield from all agrarian biomass fuel sources [58]. The envisioned timeframe between the end of this DSE project and the expected entry into service should allow a sufficient long enough period for a coherent sustainable methane production and distribution support system to develop.
Finally, a word should be said about noise emissions too. The Vimana aircraft features upper-wing located ducted fans. This design choice yielded three positive effects on noise emissions. The first one of them is the inherent noise shielding: locating the engines on top of the wing instead of below offers the advantage of reducing the perceived noise on the ground. Secondly is the reduction of the landing gear size: due to the fact that the fans are located on top, the engine clearance constraint disappears, allowing for a smaller, less noise producing landing gear to be installed. Finally, the increase in effective by-pass-ratio means that further reductions in jet noise will be perceived. For a more detailed noise emission analysis, the reader is referred to Section 7.6.

9.3 Maintainability

The maintenance of aircraft is an important factor for airlines when buying a new aircraft as it presents between 10 and 20% of direct operating cost [59]. Next to that, maintenance has to be taken into account for the sustainability of the new aircraft. The Vimana aircraft will use HTS cabling instead of normal cabling due to its 100% efficiency. Besides, HTS cabling has the advantage that it creates less wear, aging and heat than normal cabling. This will result in a less maintenance sensitive aircraft. On the other hand, Vimana will have a total of 8 motors and fans, plus 3 turboshafts in the back of the aircraft. The fact that more moving pars are present will increase the friction and wear. A more detailed investigation has to be performed to mitigate the increase in required maintenance. The fact that HTS cabling has to be integrated in combination with one engine embedded in the fuselage means that the team has to take care that it will make sure that all parts are easily accessible in case maintenance has to be performed. As stated in Chapter 6, multiple new technologies will be implemented in the Vimana aircraft. The included cryocoolers, battery and HTS cabling means that new equipment and tools have to be designed that make maintenance possible. For the detailed phase of the Vimana project, the team will spend a certain period of time to look for ways to increase the sustainability of the maintenance program. First of all, employees will try to increase the number of similar parts and items in the aircraft, such that the amount of different items will be decreased. This results in a maintenance inventory that can be decreased in size as well since a smaller number of parts has to be present. A different option is to implement a high number of sensors in the aircraft to monitor the state of certain items and parts. In that case, the required maintenance can be better anticipated and therefore the expected items and parts that are needed can be estimated in a better way. This could be an option to reduce the size and number of parts present in the inventory of the maintenance facilities.

9.4 Disposal

Disposal procedures should be kept in mind during every step of the design process and choices should be made accordingly. This is important to ensure that the product can be handled at EOL (End-of-Life) with minimum waste and minimum impact on the environment. At this stage of the project, some benchmarking was done from existing EOL procedures in industry, two of which are presented below[3]:

1. **Airbus PAMELA project**, which demonstrated that 85% of a representative aircraft (Airbus A320 in this case) can be recovered by recycling.
2. **Rolls Royce EOL procedures**, which report that 75% of an aero-engine's metal by weight can be recycled to aerospace smelters.

[3]URL "http://www.sustainableaviation.co.uk/wp-content/uploads/end-of-aircraft-life-initiatives-briefing-paper-11.pdf", [cited 19 June 2015]

It has to be kept in mind, however, that regulations such as REACH (Registration, Evaluation, Authorisation and Restriction of Chemical substances) and the aforementioned EOL procedures have been developed for present day aircraft. The distributed propulsion system that will be developed in this project has a forecast development period of 15 years as presented in Section 14.3. Therefore sufficient time is available to perform a similar EOL procedure, in which the team should try to do this in parallel with the detailed design phase. Part of the time span of this process should be used to look to what extent recyclable items can be implemented in the Vimana aircraft. This EOL procedure should also include a research to the possibilities of modular aircraft systems, as it increases the easiness of removing parts for disposal.
The Vimana aircraft is based on a hybrid propulsion concept Superconducting materials that are included for this concept consist of three elements (HTS cabling, cryocoolers and methane tank) that will require new procedures for maintenance and this also applies to their disposal. For example, disposal of the pressurized methane tanks will have to be done in a safe, controlled environment. Similar disposal procedures can be expected for the integrated battery. No detailed design has been done yet but it is expected that the aircraft and propulsion system, both, will have a high percentage of composites. This presents further issues with dismantling and recycling as the industry procedures for aluminium, which is more common at the time of writing, will not be applicable for the materials of the future.

9.5 Sustainability within the Group

A sustainable environment in the group must be created in order to minimize the waste produced by the group. Below are some steps to be taken to obtain a minimal waste production:

- Reduce the amount of paper, mainly used for printing reports and articles. This can be replaced by using a good administration to avoid double printing, or by using digital versions at all.
- Turn off the lights, laptops and other electric devices when possible, to reduce the electricity used. Also turn off the heating when the windows are opened or when heating is not needed.
- Reduce the direct waste, caused by food, drinks etc. This is also related to keeping the project table and thus Fellowship a clean and tidy place to work in.

It is the groups uttermost intention to create a sustainable working environment, based on the steps stated above.

Chapter 10 | Technical Risk Assessment

As in every design process, numerous of risks are involved. In this chapter these risks are identified, evaluated and mitigated if necessary. To conclude, a reflection is given on the risks encountered during the project.

10.1 General Risk Assessment

The general risk assessment is done using the following procedure:

1. Identification of (potential) risks
2. Assessment of probability of occurrence
3. Assessment of impact on the project and what parts of the project (e.g. cost, quality, safety)
4. Assessment and mitigation of risks in a risk register
5. Indicating risks prior and after mitigating measures in a risk assessment matrix

In Subsection 10.1.1, the risks assigned to each category will be identified. After that, those risks will be assessed and ranked. In order to reduce these risks, mitigation methods are suggested. This can be found in Subsection 10.1.2.

10.1.1 Identification

The following risks have been identified. These are associated with the design of Vimana. In further design phases they may need to be adapted.

Technology

TEC.1 The cryocoolers do not meet the goal of $3kW/kg$
TEC.2 HTS cabling is not yet available for use in aircraft
TEC.3 The superconducting motors do not meet the power density used in the design
TEC.4 The superconducting generators do not meet the power density used in the design
TEC.5 The technological advancement of the turboshaft engines is insufficient
TEC.6 The methane storage tanks have a larger mass than accounted for

Environmental Impact

ENV.1 The environmental unfriendly coolants used pose an environmental hazard
ENV.2 Fuel dumping of methane (greenhouse gas)
ENV.3 Sustainable requirements not met due to the use of non-environmental friendly components (e.g. battery)

Resource Availability

RES.1 Investors do not keep funding the development of the project
RES.2 The availability of kerosene decreases or becomes very expensive
RES.3 The availability of methane decreases or becomes very expensive
RES.4 The facilities to manufacture the aircraft need modification or have to be built
RES.5 Airport infrastructure needs large adaptations due to unconventional system

Safety

SAF.1 The electric engines are less reliable then anticipated
SAF.2 Yaw control is compromised with one engine inoperative
SAF.3 The electric system is susceptible to failure
SAF.4 The electric system creates hazardous scenarios during maintenance and ground handling
SAF.5 The battery is a fire hazard during operations
SAF.6 The neon used for cooling creates a safety hazard to passengers
SAF.7 The turbine placed in the fuselage creates a dangerous failure scenario for the airplane and passengers
SAF.8 The fans over the wing create a hazardous situation when a fan blade fails
SAF.9 During evacuation, the fans over the wing are dangerous for the passengers
SAF.10 In case of an emergency landing in water, the electrical system creates a dangerous scenario

SAF.11 In case of a belly landing, the methane tanks which are located in the cargo holds can create a dangerous scenario

Manufacturing Complexity

MAN.1 The HTS cabling is very complex to install impacting work load and production cost
MAN.2 The HTS cabling is susceptible to installation errors
MAN.3 The HTS cabling is easily damaged during manufacturing and installation
MAN.4 The cryocoolers need special built production facilities
MAN.5 The cryocoolers are very complex to install impacting work load and production cost
MAN.6 The propulsive system complexity increases production errors
MAN.7 To allow for the high level of engine integration, special production facilities are required
MAN.8 The quality and speed of parts produced by additive manufacturing is not sufficient

Quality

QUA.1 The aircraft is less fuel efficient and does not reduce CO_2 and NO_x emissions.
QUA.2 The aircraft produces more noise than a conventional aircraft
QUA.3 The aircraft can not fly the range required at the required payload
QUA.4 The aircraft has a short lifespan
QUA.5 The aircraft can not meet certification requirements
QUA.6 Takeoff requirements are not met

Schedule

SCH.1 First delivery of the aircraft is delayed
SCH.2 Certification takes longer than expected
SCH.3 Internal deadlines are not met during development
SCH.4 Low production rate of the aircraft
SCH.5 Subcontractors cannot deliver at the required intervals

Financial

FIN.1 Research and Development is more expensive than budgetted for
FIN.2 Operating cost of the aircraft is higher than expected
FIN.3 Production cost of the aircraft is higher than expected
FIN.4 Market demand decreases for single-aisle aircraft
FIN.5 Market demand decreases for aircraft in general

10.1.2 Assessment and Mitigation

The risks mentioned above are categorised in a risk register as can be seen in Tables 10.1 to 10.3. In these tables the risks with their corresponding consequence, promise, impact, likelihood and mitigation method are described. The promise is the projects component which is impacted. The impacts are divided into five categories. These categories are numbered from one to five with the severity as described below. Two numbers are presented in the likelihood column, the left one being the likelihood before risks mitigation and the right being the likelihood after risk mitigation.

1. Insignificant
2. Minor
3. Moderate
4. Major
5. Catastrophic

The probability of occurrence is also ranked from one to five, where one is rare/only occurs in exceptional circumstances and five is almost certain to occur. For the impact also two numbers are presented in the likelihood column, the left one being the impact before risks mitigation and the right being the impact after risk mitigation.

Table 10.1: Risk register (1)

Risk-ID	Consequence	Promise	Likelihood	Impact	Mitigation
TEC.1	Weight increase of the final design	Quality	3 → 2	3 → 3	Closely monitor development of cryocoolers
TEC.2	Normal cabling must be used, thus increasing mass of engines and generators due to efficiency losses	Quality	2 → 1	3 → 2	Closely monitor development of superconductive technologies and account for in contingencies
TEC.3	Weight increase of the final design	Quality	2 → 2	2 → 1	Account for in contingencies
TEC.4	Weight increase of the final design	Quality	2 → 2	2 → 1	Account for in contingencies
TEC.5	Specific fuel consumption increases	Quality	2 → 1	4 → 4	Closely monitor turbine developments
TEC.6	Weight increase of the final design	Quality	2 → 1	2 → 2	Account for in contingencies
ENV.1	Special containment required	Cost	1 → 1	3 → 2	Perform research into coolant systems
ENV.2	Emissions increase	Quality, Environmental	4 → 0	2 → 0	Only dump kerosene when fuel dumping is necessary
ENV.3	Recycling cost increase or product cannot be recycled at all	Cost, Environmental	2 → 1	2 → 2	Make use of sustainable approach throughout the project
RES.1	Other investors need to be found or the project will be terminated	Schedule	2 → 1	5 → 3	Closely manage stakeholders and get insurance
RES.2	The operating cost will increase	Quality	4 → 4	4 → 3	Design the aircraft to use alternative fuels
RES.3	The operating cost will increase	Quality	2 → 2	3 → 2	Design the aircraft to use more kerosene instead of methane
RES.4	Manufacturing cost will increase and the schedule might be compromised	Cost, Schedule	3 → 2	3 → 3	Account for the necessary investment and time
RES.5	Market decreases as airport are not keen on making large changes to infrastructures	Cost	2 → 1	3 → 3	Take into account during design so airports need minimal adaptations
SAF.1	Availability decreases which makes the aircraft less attractive to buy	Quality	2 → 1	3 → 3	Extensively test the electric engines
SAF.2	The aircraft does not meet one engine inoperative regulations	Schedule, Cost	2 → 1	4 → 4	Take into account during design phase
SAF.3	The aircraft does not have thrust and yaw control	Quality, Safety	2 → 1	5 → 5	Extensively test the electric system and design with redundancy

Table 10.2: Risk register (2)

Risk-ID	Consequence	Promise	Likelihood	Impact	Mitigation
SAF.4	Employees can get injured	Stakeholders, Safety	2 → 1	3 → 2	Design the system such that minimal interaction is required with personnel and get insurance
SAF.5	Fire inside the aircraft forces the aircraft to land, thus decreasing safety and availability	Safety	2 → 1	4 → 4	Extensively test the battery system and take into account during design
SAF.6	Neon can cause burn marks if the cooling system leaks	Safety	1 → 1	3 → 2	Isolate the system from the cabin
SAF.7	In case of a blade off scenario, the fuselage or passengers can get damaged/injured	Safety	2 → 2	4 → 3	Design the system such that a blade off scenario is contained
SAF.8	Other fans can get damaged, as well as the fuselage, empennage and turbines	Safety	2 → 2	4 → 3	Design the system such that a blade off scenario is contained
SAF.9	Passengers can get injured during evacuation	Safety	3 → 3	4 → 3	Design the system such that the blades are stopped when a emergency exit is opened
SAF.10	Short circuits can be created, thus given shocks to the environment	Safety	2 → 1	4 → 4	Make use of circuit breakers and isolation
SAF.11	If stored under pressure it can explode and harm passengers. Also leakage needs to be taken into account	Safety	3 → 2	4 → 3	Use different technique to keep the methane liquid and make rigid tanks
MAN.1	Production cost increases	Cost, Quality, Schedule	3 → 2	2 → 1	Take into account in schedule and properly train staff
MAN.2	Production time increases thus delaying delivery	Quality, Schedule	3 → 2	2 → 1	Properly train staff and perform regular quality control
MAN.3	Both production cost and time will increase	Cost, Schedule	1 → 1	2 → 2	Properly train staff
MAN.4	Transportation time increases which delays delivery	Cost	3 → 1	3 → 3	Outsource production to contractor and monitor closely to ensure everything is on time
MAN.5	Both production cost and time will increase	Cost, Schedule	4 → 3	2 → 1	Properly train staff and take into account in schedule
MAN.6	Both production cost and time will increase	Cost, Quality, Schedule	3 → 2	3 → 3	Perform regular quality control
MAN.7	Production cost will increase as facilities need to be adapted	Cost	2 → 1	5 → 5	Investigate what production facilities are required in a early project phase
MAN.8	Some parts might not be able to be manufactured and need redesign. Also, the environmental footprint of the process will increase	Cost, Schedule	2 → 1	3 → 2	Monitor additive manufacturing closely and adapt design of parts if the development is not sufficient

Table 10.3: Risk register (3)

Risk-ID	Consequence	Promise	Likelihood	Impact	Mitigation
QUA.1	Emission reduction requirements are not met	Quality, Environmental, Stakeholders	3 → 2	4 → 4	Research potential emission reducing technologies and extensively quantify potential benefits
QUA.2	Noise reduction goals are not met	Quality, Environmental, Stakeholders	1 → 1	3 → 3	Research potential noise reducing technologies and extensively quantify potential benefits
QUA.3	Demand will decrease as the aircraft cannot deliver what the market wants	Quality, Cost	1 → 1	5 → 5	During design, keep track of performance and requirements
QUA.4	Market share will decrease as other aircraft have a longer lifespan	Quality	2 → 1	4 → 4	Design the aircraft for a long lifespan
QUA.5	Redesign is necessary because certification standards are not met	Cost, Schedule	3 → 2	4 → 4	During design, keep track of the regulations
QUA.6	Redesign is necessary because certification standards are not met	Quality	2 → 1	4 → 4	During design, keep track of performance and requirements
SCH.1	Profit will decrease	Cost, Schedule	4 → 2	4 → 4	Monitor the progress closely and increase funding if necessary
SCH.2	First delivery will be delayed	Cost, Schedule	4 → 4	3 → 2	Take into account in schedule
SCH.3	The development of other systems will also not be finished on time, thus delaying first delivery	Cost, Schedule	3 → 2	3 → 2	Insert contingencies in schedule, monitor processes closely
SCH.4	Market share will decrease as other aircraft can be built faster	Quality	3 → 2	4 → 4	Standardize production methods were possible, use existing manufacturing techniques
SCH.5	Production rate will decrease	Quality, Schedule	2 → 1	3 → 3	Make proper and detailed agreements with contractors
FIN.1	Profit will decrease	Cost	2 → 1	3 → 3	Properly define research objectives and budgets
FIN.2	Airlines will be less likely to buy this aircraft	Quality	2 → 1	4 → 4	Design the aircraft keeping operating cost as a main focus
FIN.3	Airlines will be less likely to buy this aircraft	Cost	2 → 1	3 → 3	Make use of proven techniques
FIN.4	Profit will decrease	Cost	2 → 1	5 → 5	Perform a market analysis
FIN.5	Profit will decrease	Cost	2 → 1	5 → 5	Perform a market analysis

In Table 10.4 the risks are displayed in a risk assessment matrix. The risk are ordered horizontally in terms of likelihood of occurrence, where more to the left means a higher likelihood of occurrence. Vertically the risks are ordered in terms of impact on the project where more downwards means a higher impact. Looking at this chart, it is clear that risks in the bottom left corner need to be mitigated whilst risks in the top right corner are less critical. Also, a color scheme has been applied, where risks in red (bottom left) are not acceptable, risks in yellow (diagonally) should be closely monitored and risks in green (top right) should be taken into account. In Table 10.5 the risks are displayed after mitigating measures have been taken. As can be seen, the risks tend to be more to the top right corner. No risks are in the critical region any more.

Table 10.4: Risk map before mitigation

	Likelihood				
Consequence	5	4	3	2	1
1					
2		ENV.2 MAN.5	MAN.1 MAN.2	TEC.3, TEC.4 TEC.6, ENV.3	MAN.3
3		SCH.2	TEC.1,RES.4 MAN.4,MAN.6 SCH.3	TEC.2,RES.3 RES.5,SAF.1 SAF.4,MAN.8 SCH.5,FIN.1 FIN.3	ENV.1,SAF.6 QUA.2
4		RES.2 SAF.11 SCH.1	SAF.9 QUA.5 SCH.4	TEC.5,SAF.2 SAF.5,SAF.7 SAF.8,SAF.10 QUA.4,QUA.6 FIN.2	
5			QUA.1	RES.1,SAF.3 MAN.7,FIN.4 FIN.5	QUA.3

Table 10.5: Risk map after mitigation

	Likelihood				
Consequence	5	4	3	2	1
1			MAN.5	TEC.3,TEC.4 MAN.1,MAN.2	
2		SCH.2		RES.3 SCH.3	TEC.2,TEC.6 ENV.1,ENV.3 SAF.4,SAF.6 MAN.3,MAN.8
3		RES.2	SAF.9	TEC.1,RES.4 SAF.7,SAF.8 SAF.11,MAN.6	RES.1,RES.5 SAF.1,MAN.4 QUA.2,SCH.5 FIN.1,FIN.3
4				QUA.1,QUA.5 SCH.1,SCH.4	TEC.5,SAF.2 SAF.5,SAF.10 QUA.4,QUA.6 FIN.2
5					SAF.3,MAN.7 QUA.3,FIN.4 FIN.5

10.2 Reflection on Risks

At the end of a project it is useful to look back and reflect on how several identified risks were underestimated and changed the design significantly. One example comes directly to mind; the use of a battery assisted

take-off. The cause for this major design change was the low power density of the Lithium-air batteries. This could have been avoided by researching more thoroughly in the early conceptual design phase.
Another technical setback is not reaching the goal of 25% reduction in CO_2 and NO_x emissions. Although, a reduction of slightly more than 20% is already a great achievement. Therefore the impact will not be graded with a '5' as is done in Table 10.3, but with a '2' as it is a minor setback.
The operating costs estimated in Chapter 11 for Vimana are also higher than for the A321. For the used estimation method fuel is not a driving factor, as this is where Vimana excels in. Assuming this will become more important in the future with increasing oil prices and taxes on gas emissions. Therefore, the likelihood is not graded high.
The final risk which is reflected on is the absence of team members during critical phases of the project. It was known in advance team members had important appointments during the DSE, however no action was taken regarding this. Together with the fact that one team member became ill during the project, it would have been more optimal to take these potential risks into account in the planning of the project by for example having a day every once in a while to catch up with tasks. In the end, the impact was insignificant, but such risks with a high likelihood should be taken into account.

Chapter 11 | Economic Analysis

This chapter aims to serve as a summary of the preliminary economical and cost-based analysis that has been conducted on Vimana. It is imperative to observe and identify the target market for such a product and this has been covered in the first section on 'Market Analysis'. Subsequently, methods proposed by Roskam in Book 8 of his Airplane Design series [60] have been used to come up with a 'Cost Breakdown' for Vimana. In order to aid the reader in visualizing the various aspects of the costs associated with such an aircraft, a Cost Breakdown Structure is also presented. The next logical step after cost identification is to verify the numbers with reference aircraft, in this case the Airbus A320/321 and Boeing 737. Finally, any potential investors in this project will be interested to know the details of the return on their investment, a preliminary analysis of which is done in the final section, 'Return on Investment'.

11.1 Market Analysis

In order to establish an accurate target cost for Vimana and to survey the potential opportunities and threats, a market analysis has to be conducted, which this section covers. The objective is to analyze the current and projected demand for a medium range aircraft, such as Vimana and the services that it can provide. This will be derived from the current market volume of the reference aircraft, the Airbus A320/A321 and the comparable Boeing 737. Thereafter, an analysis is done on the potential market share and profits that are expected to be generated by a distributed propulsion aircraft such as Vimana.

Current Market Volume

According to surveys conducted by Airbus [61] on its in-service fleet, 78% are single-aisle aircraft, which is defined as aircraft having between 100 and 210 seats. This is the category that Vimana also falls under, having been designed for 180 passengers. Furthermore, this class of aircraft accounts for 60% of all distances flown in 2013 [61]. Aircraft which fall under this category are the Airbus A320, A321 and the Boeing 737, all of which can serve as suitable reference aircraft for Vimana. The focus in the single-aisle market now seems to be a push for efficiency, coupled with an increase in capacity, either by cabin densification, or by a complete product redesign. This is why new, more fuel efficient single-aisle aircraft like the A320neo or 737max, effectively family extensions of the base Airbus and Boeing product, are expected to replace the current aging fleet. Another main reason for this trend is the aviation network itself, that is constantly evolving, driven by factors such as competition, demographics and tourism trends. This drive for efficiency and increased capacity has picked up momentum since 1993, with more and more airlines demanding higher fuel efficiency, and it is expected that this trend will continue further in the coming years. Currently, this trend has lead to an average seat count on single-aisle aircraft, of around 155 seats, typically what is provided from the A320-family and Boeing-737 aircraft.

Potential Market Share

Airline networks keep evolving as they strive to compete effectively and grow efficiently in the dynamic air transport market. Strategies like increase of frequencies or hub development are implemented by airlines in order to capture greater market share. In the coming 20 years, 57% of the single-aisle aircraft within Europe and North America will be replaced, which accounts for 5500 aircraft [61]. Furthermore, the Asia-Pacific market is expected to grow significantly, where a growth of 58% is projected. A total of 31,358 new aircraft are expected to be delivered between 2014-2033, 70% of which are single-aisle, as can be seen in Figure 11.1. Boeing calculated that the current market share of the single aisle aircraft is 60%, and will grow to 70% in 2033. The number of total aircraft will grow from 20,910 to 42,180 [62].

It is expected that distributed propulsion aircraft such as Vimana will be part of this growth, and will have a large market share of these single-aisle aircraft, due to its emphasis on efficiency and reduced emissions. Further research is required, however, to accurately forecast the exact share that Vimana will have of the total fleet in service. The Airbus A320 family has more than 18000 aircraft on order or in operation [1]. Vimana has an improved fuel consumption, less harmful gas emissions and lower noise emissions than the A321. It is therefore expected to be a more attractive aircraft for airline operators.

[1] URL "http://www.airbus.com/company/market/orders-deliveries/", [cited 29 June 2015]

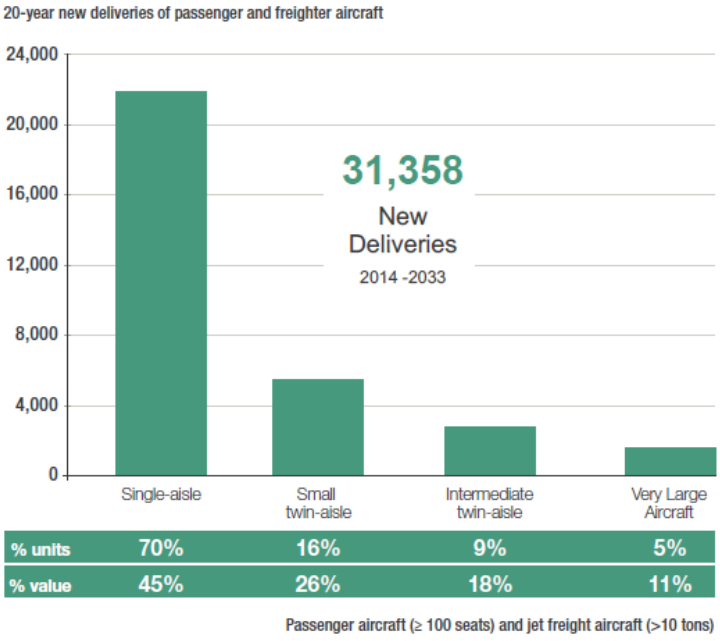

Figure 11.1: Demand passenger and freighter aircraft 2014-2033 [61]

Potential Profit

In Subsection 11.2.2 the profit of each aircraft is calculated and a cost breakdown is presented. This is done with estimation methods in Roskam [60]. The method does not take into account the volatile nature of the market. In a period of 20 years, till the actual production of the aircraft, parameters which affect the expected profit can vary significantly. These could range from political factors, all the way to unexpected advances in technology. For a more thorough analysis and to help identify these factors, a political, economical, social and technology (PEST) Analysis is performed in Subsection 11.2.9. This is also suggested as an analysis step for future research in the design of Vimana.
A factor that plays a large role in profits are oil prices. Oil prices are expected to rise in the upcoming years, but accurately forecasting these prices is extremely challenging. Nevertheless, the International Monetary Fund predicts the oil price to be around 270 euros per barrel (Figure 11.2) by 2030, corresponding to roughly 7.5 euros per US gallon for jet fuel. This is a drastic increase from the current 51 euros per barrel.[2] As can be seen in Figure 11.2, other institutions have also made oil price predictions which are lower than that of the International Monetary fund. The highest price point is chosen as the worst case scenario. This increase in oil prices will have a large impact on the profit generated from any aircraft operating on a pure jet-fuel propelled design. Vimana will be accordingly affected but due to its dual-fuel concept and the abundance and relatively low cost of Methane, it is expected to hold a competitive advantage over the A320 family variants that will be operational in a similar time period.
Another factor which could play a significant role in the potential profit is the volatility of the economy itself. As determined before, the market share is expected to grow, as well as the market volume. This has a positive correlation with the potential profit but one-off events, such as an economic or political crisis, will contribute to a weaker economical balance and negatively affect the market volume, and by relation, also the market share. Needless to say, the profit point may then also take a hit.

Potential profit could also be estimated by benchmarking from the current profit of a similar reference aircraft. The reference aircraft chosen is the A321. The listing price of the A321 as of 2015 is 113.7 million dollars[3]. The acquisition cost is normally 10% higher than the manufacturing cost [60]. This implies a profit of 10.3 million dollars. This number gives the reader a general direction of Vimana's expected potential cost.

[2] URL: "http://www.bloomberg.com/energy/", [cited 29 April 2015]
[3] URL "http://www.airbus.com/newsevents/news-events-single/detail/new-airbus-aircraft-list-prices-for-2015/#", [cited 16 June 2015]

Figure 11.2: Oil prices prediction [61]

11.2 Cost Breakdown

The costs associated with Vimana are calculated in this chapter. Using Book 8 of Roskam's 'Airplane Design' series [60], the various aspects of the expected cost values are identified, defined and finally, quantified.
The same procedure is followed for the reference aircraft for verification purposes. The costs are then compared to the A321. The cost calculations are divided into three separate parts. These are the 'Research, Development, Test and Evaluation' (RDTE) costs, 'Manufacturing and Acquisition' costs, and 'Operating' cost.

Two costbreakdown structures are presented. The first one, seen in Figure 11.3, is the cost breakdown structure as evaluated for the Vimana. This breakdown is done from the Vimana standpoint. For the cost estimations, the Roskam method has to be used, as it is the only adequate method in this design stage. The cost breakdown structure uses the devisions given in Figure 11.4. The Roskam cost breakdown structure is further explained and used for calculations in the rest of the chapter.

The economic process associated with the design, development, sale and use of Vimana requires a detailed cost and projected use treatment. This chapter attempts to outline the basics. On a simplified level, the profit expected on this aircraft is the price paid subtracted by the cost, that is, the total financial outlay in designing and manufacturing Vimana. That being said, it is imperative to note that profit, cost and price can be viewed from various economic standpoints, corresponding to the stakeholders associated with Vimana during its lifetime, such as the manufacturer, the aircraft operator, and finally, the consumer/taxpayer. In all cases, however, the stakeholders benefits from as low a cost as possible. The reader is now introduced to the various segments of a typical aircraft program, which is expected to be similar for the Vimana units to be manufactured.

- Phase 1: Planning and Conceptual Design
- Phase 2: Preliminary Design and System Integration
- Phase 3: Detail Design and Development
- Phase 4: Manufacturing and Acquisition
- Phase 5: Operation and Support
- Phase 6: Disposal

The total cost incurred during these phases is called the 'Life Cycle Cost' (LCC) and this can be divided as follows. Phases 1, 2 and 3 account for 'Research, Development, Test and Evaluation'(RDTE)costs. 'Acquisition' costs include the 'Manufacturing' and 'Production' costs and they refer to any financial outlay during Phase 4. 'Operating' costs include 'Direct' and 'Indirect' costs and these refer to Phase 5 of the life cycle. Finally, costs incurred in disposing of the aircraft pertain to Phase 6.

The following subsections present a consolidated summary of the key elements of the LCC, starting off with the RDTE costs, the 'Manufacturing and Acquisition' costs and finally the projected 'Operating' costs for Vimana. It is important to note at this stage that the cost estimation methods and formulae used here are based on an aircraft data that may very well be considered outdated and many technology based costs may, in fact, be vastly different to the ones approximated here. It is the author's intention to provide as close an estimate as possible at this time. However, further economical and technological developments may vastly

affect these numbers.

Vimana is targeted towards privately or government owned enterprises, and as such, it is noted that the objective of these enterprises is to make a profit. The numbers presented here may be looked at as an 'operating margin', since no taxation cut has been applied. This is because the tax situation of a company is expected to vary from quarter to quarter and from country to country. Another aspect to keep in mind while reviewing these numbers is the time it takes for an aircraft program to go through the life cycle phases presented above. The estimated program cost may be highly subjected to inflation and since the US Dollar is used as the currency in this analysis, any volatility in the value of the dollar will affect these numbers significantly. It is beyond the scope of this project to accurately account for this. However, since this is not an insignificant factor, it has been introduced in the calculations as a 'Cost Escalation Factor' (CEF). Calculations have been done for costs in the year 2030, and as such, the following scaling factor (Equation (11.1)) has been used.

$$CEF_{scaling} = \frac{CEF_{2030}}{CEF_{1989}} \tag{11.1}$$

Based on Figure C.1 in Appendix C, CEF_{1989} is 3.0 and extrapolating the same figure gives a CEF_{2030} of 4.0, assuming the plotted trend is followed. This leads to a CEF-ratio of 1.33, which is used to 'scale' various cost figures throughout the estimation process. The value for 1989 is used, as it is a known value from the Roskam method.

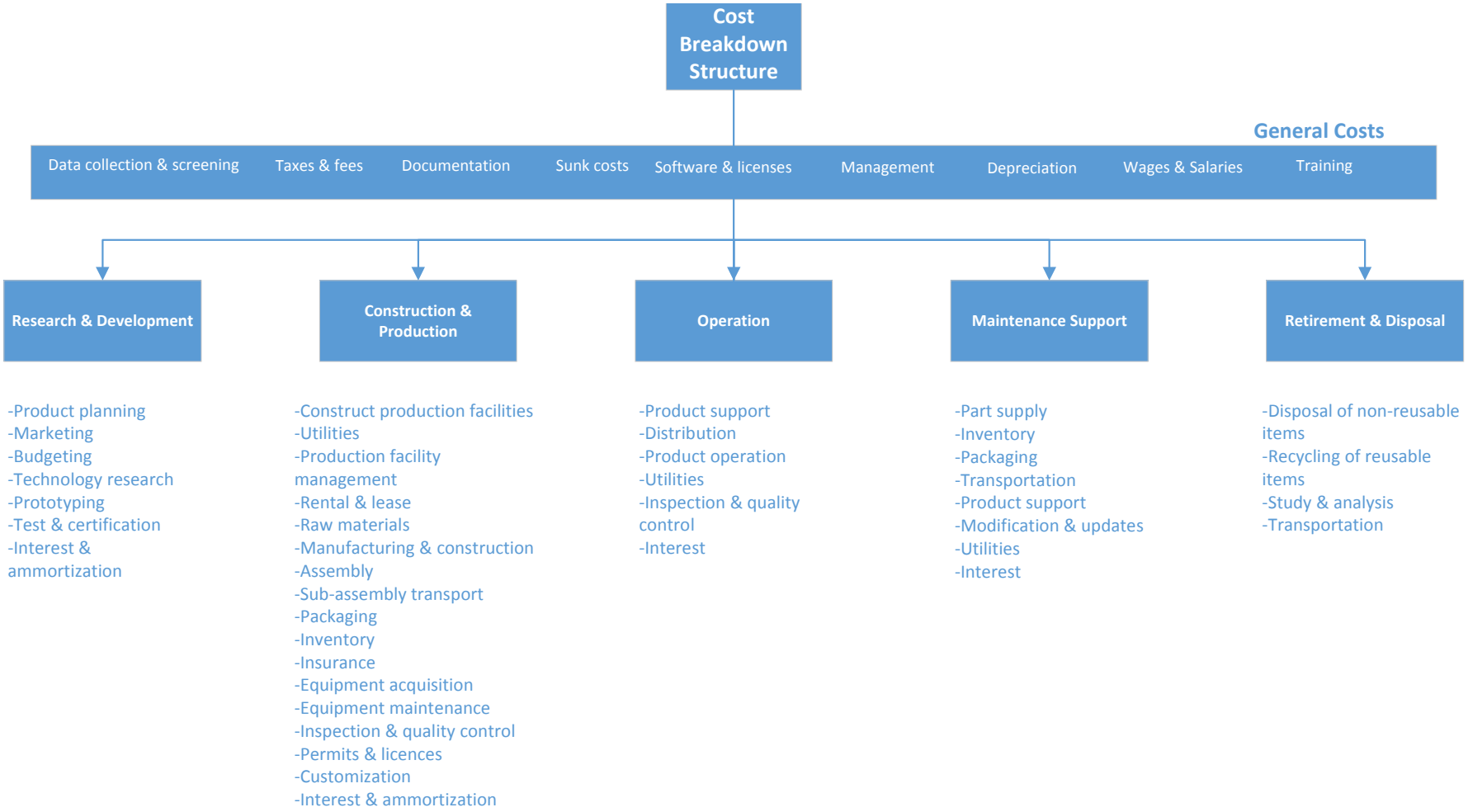

Figure 11.3: Cost Breakdown Structure of future activities

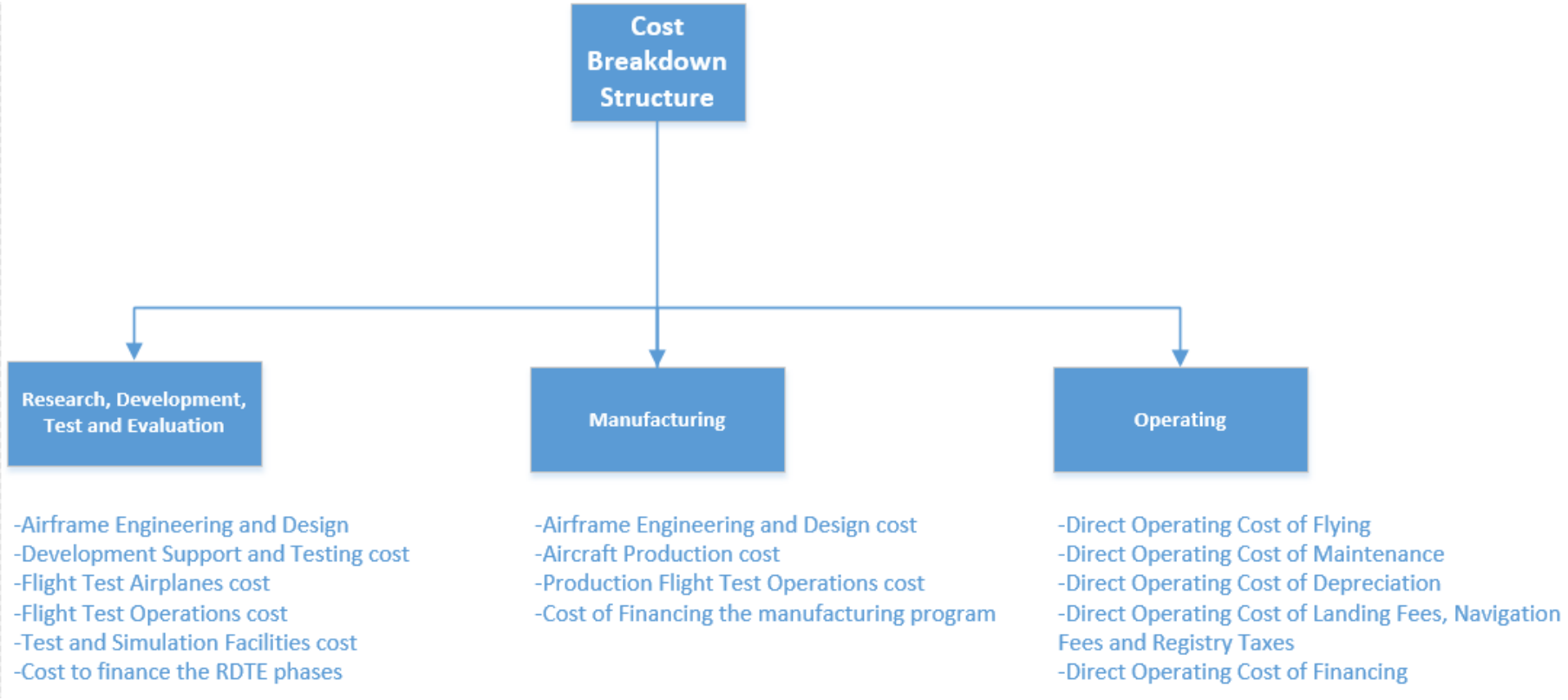

Figure 11.4: Cost Breakdown Structure of future activities, based on the Roskam method

11.2.1 Research, Development, Test and Evaluation Cost

The RDTE costs are accumulated during the design phases of the aircraft, effectively taking it from the planning and conceptual design stage, to certification. Roskam divides RDTE costs into 7 separate categories. These are the following:

- Airframe Engineering and Design cost
- Development Support and Testing cost
- Flight Test Airplanes cost
- Flight Test Operations cost
- Test and Simulation Facilities cost
- RDTE Profit
- Cost to finance the RDTE phases

Certain assumptions are made in order to calculate the RDTE costs. The number of aircraft produced during the RDTE stage normally ranges from 2 to 8 for commercial aircraft. For the Vimana program, a number of 8 is chosen. This is because of the new technologies implemented into the aircraft, which implies a more extensive RDTE phase. Furthermore, a judgment factor (F_{diff}) which takes into account complexity is used [60]. Due to the very aggressive use of new and advanced technologies, the highest possible F_{diff} factor of 2.0 is taken in the calculations. Also, it is naturally expected that the manufacturer will be experienced in the use of CAD software in the design and manufacturing process. A judgement factor of 0.8 is accordingly applied. Here, the reader can already see the drawbacks of using such an outdated cost estimation method, since, at the time of publishing, Roskam estimated that, by virtue of CAD being a relatively new development in engineering processes, such a factor would be imperative in cost estimation. However, with a timeline of around 2030, it is expected that CAD will be the norm rather than the odd technologically advanced exception. Similar to this, a correction factor depending on the material type used is applied. For this, the highest weight of 3.0 was chosen, which by definition, applies to a fully carbon composite airframe. Advanced materials such as 'GLARE' as expected to be used on Vimana.

In order to include labour payment rates, an 'Engineering Dollar Rate' of approximately 83 USD/manhour is used, including the CEF defined above. This is based on statistical data provided by Roskam. This value has not been verified with Labour Union data sheets and is to be done for a more detailed cost estimation. Although this is defined as the 'rate charged for the airframe engineering activity', similar 'labour rates', corresponding to various manufacturing activities, are present in the upcoming calculations. This rate is also expected to be highly variable as it is based on factors such as the local living cost, number of engineers in the job market at any given time (supply), the number of engineers required (demand) and union contracts.

In Table 11.1, the costs are given for the 7 separate categories as defined for RDTE cost breakdown, as well as the total RDTE cost.

Table 11.1: RDTE cost estimation

Category	**Cost in million [$]**
Airframe engineering and design cost	613
Development support and testing cost	261
Flight test airplanes cost	2,076
Flight test operations cost	100
Test and simulation facilities cost	469
RDTE profit	469
Cost to finance the RDTE phases	704
Total RDTE cost	4,694

11.2.2 Manufacturing and Acquisition Cost

In this section, the manufacturing and acquisition costs are shown. The results of the profit calculations are also presented, the profit being the difference between the manufacturing and acquisition cost. The definition of 'Manufacturing Costs' is self evident, but the 'Cost of Acquisition', which is the 'price paid by the user of an airplane' [60], depends on a few factors, such as the total number of aircraft built by the manufacturer, the number of aircraft actually acquired by the operator, the manufacturer's profit and finally, the cost of the

RDTE program, calculated previously.

The number of aircraft produced needs to be determined. This is done by looking at the demand of a reference aircraft. The total number of A320 family units on order or in operation is more than 18000[4]. Therefore a number of 18000 is taken for Vimana. This seems like an adequate benchmark to follow, but the reader must be aware that this value is highly variable and dependent on interpretation. The cost estimation may be done assuming that Vimana will take over all of the single-aisle market, which would result in a much higher value for the 'Number of Produced Aircraft'. However, it may also be that Vimana targets a niche, in which case, this number may be quite limited.
The total aircraft manufacturing cost is divided into four different categories. These are the following:

- Airframe Engineering and Design cost
- Aircraft Production cost
- Production Flight Test Operations cost
- Cost of Financing the manufacturing program

In these costs, an 'Engineering Man-hour Rate' is again to be estimated. This is subject to volatility as explained in the previous subsection. However, the same value of approximately 83 USD/manhour is used. Furthermore, as part of the 'Production Cost' estimate, it is required to estimate the cost of engines and propellers separately, if any of both are present in the design. Due to Vimana's novel design, taking a propeller cost for each motor would be a vast overestimation. It was therefore decided to estimate the price to be half that of a whole propeller assembly, in this case, $1,000,000\$$. The cost of the engine was kept to be the same as for a CFM-56 engine, used on an Airbus A321. For this, the list price was used[5], but then multiplied by the cost factor mentioned earlier, which led to a total cost per engine of $13,333,333\$$. The production flight test operations cost is neglected, as is normally done in preliminary cost estimating calculations [60]. The cost of financing refers to the costs associated with paying for the aircraft program, such as bank loan charges, or the interest based revenue lost since the money is now spent on financing the program. However, Roskam does not account for these costs in detail and mentions that 'methods for estimating these financing costs are judged to be beyond the scope' of his text. For preliminary purposes, this cost is judged to be a fraction of the manufacturing costs, the fraction depending on available interest rates. The final cost values, as computed based on these guidelines, can be seen in Table 11.2.

For the profit, a percentage of 10% of the manufacturing cost is suggested [60]. This is also the value taken for Vimana. The acquisition cost is then 1.1 times the manufacturing cost. In Table 11.2, the costs are given for the 3 different categories of the manufacturing cost, acquisition cost and the profit made on each aircraft.

Table 11.2: Manufacturing and acquisition cost

Category	**Cost in million [$]**
Airframe engineering and design cost	1,903
Aircraft production cost	1,903,120
Cost of financing the manufacturing program	258,536
Total manufacturing cost	1,292,678
Cost of acquisition	1,421,946
Profit	129,268

This leads to the total cost of one Vimana unit to be $79 million. The profit made on each Vimana is therefore $7.9 million. While reviewing these cost figures and the suggested aircraft price, it is important to mention the parameters that strongly affect them, which also happen to define Vimana's operating range. These are 'Aircraft Take-off weight', 'Design Cruise Speed', 'Total Number of Aircraft built' and 'Production Rate'. Take-off weight was taken to be 86302 kg, following on from the final design iteration that was performed in Section 7.1. Design cruise speed is defined in Roskam in Knots Equivalent Airspeed (KEAS), which, for 0.78 Mach (by design requirement), corresponds to 516kts. The number of aircraft built has been discussed previously, whereas 'Production Rate' is taken to be 40 units a month at peak expected production.
As a further analysis of the costs, it is interesting to observe the interdependency of the 'Number of Airplanes

[4]URL "http://www.airbus.com/company/market/orders-deliveries/", [cited 19 June 2015]
[5]URL "http://www.deagel.com/Turbofan-Engines/CFM56-5B_a001738004.aspx", [cited 19 June 2015]

Produced' and the estimated 'Cost per aircraft'. Based on the relations, it is expected to follow a trend as shown in Figure 11.5, which shows that the cost sharply drops till around 10,000 aircraft units, but after that, the effect is much less pronounced. Roskam suggests two reasons for this, the 'Learning Curve' effect and the hyperbolic decrease of RDTE cost per aircraft as the number of aircraft produced. The 'Learning Curve' effect is interesting as it states that the number of man-hours required per aircraft decreases with the number of aircraft produced. This could be due to various factors, such as already established tooling practices, economies of scale and production facility benefits as workers get used to the same work package by doing it multiple times, which reduced the throughput time per package.

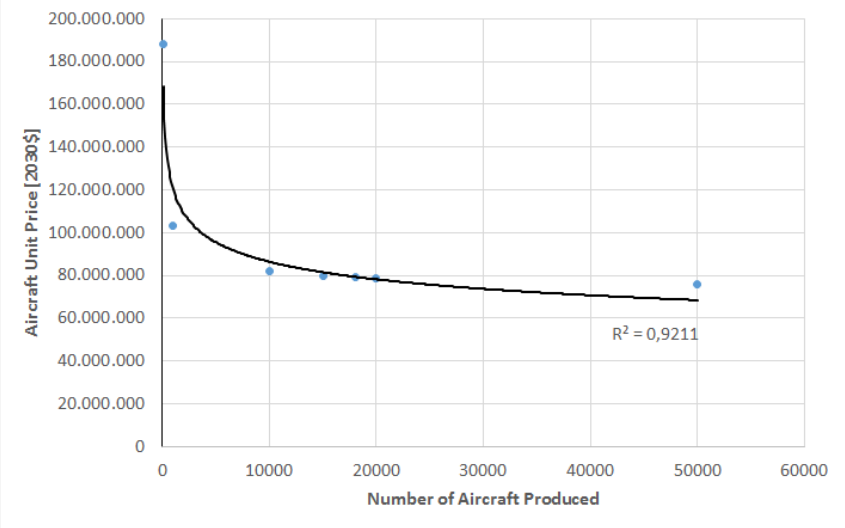

Figure 11.5: Effect of number of aircraft produced on cost per aircraft

11.2.3 Operating Cost

Total aircraft operating costs can be divided into 'direct' and 'indirect' cost sections, each pertaining to a different type of cost incurred in the process of running Vimana. Direct costs refer to expenses related to aspects such as landing fees, depreciation and maintenance; while indirect costs include elements such as meal costs, insurance expenses and administrative fees.
As is to be expected, indirect costs in aircraft operations vary significantly and depend on the operator. There is only so much that can be done in the design, so as to influence these costs. They are based on a host of non-influenceable external factors. Keeping this in mind, an estimation for indirect operating costs, as proposed by Roskam [60], is used. The reference expresses indirect costs as a fraction of direct costs. It is stated that this fraction is strongly dependent on block distance, R_{bl}, as well as on the type of aircraft. For Vimana, the factor was taken to be 0.5, based on a trend relating this factor to the block distance covered by Vimana [60]. The trend seems to have an asymptote at around 0.5 for aircraft with a R_{bl} of $3000NM$ or higher, which corresponds to Vimana, which is expected to have a R_{bl} of approximately $3290NM$. For further reference, this figure can be found in the Appendix as Figure C.2.

Furthermore, it is mentioned in the project guide that emissions (eg. cost of CO_2) should be taken into consideration for calculation of DOC. This was included in the part of the DOC that included 'landing fees, navigation fees and registry taxes'. CO_2 emission taxes are regularly imposed on airliners and this is based on the flight time and efficiency of the engines. It also varies per route but a simplified block range based assumption was taken in this case.
Direct Cost was defined as the sum of five different cost elements, as shown below:

- Direct Operating Cost of Flying
- Direct Operating Cost of Maintenance
- Direct Operating Cost of Depreciation
- Direct Operating Cost of Landing Fees, Navigation Fees and Registry Taxes
- Direct Operating Cost of Financing

In order to quantify a lot of these values, it is imperative to first establish the basic parameters of the flight profile of Vimana, such as Block Speed, Range and Time. Block distance depends on the flown routes and for

the purposes of this calculation, this was estimated by dividing the block range by the expected block time. The latter consists of various identified time segments, such as time spent in ground manoeuvres, time required to climb and accelerate to cruise speed etc. This resulted in an estimated block time of $7.8hr$ and, along with the previously mentioned range, a block speed of approximately $422NM/hr$. In order to visualize the concept of block range, a standard flight profile (as expected for a typical Vimana mission) is shown in Figure 11.6.

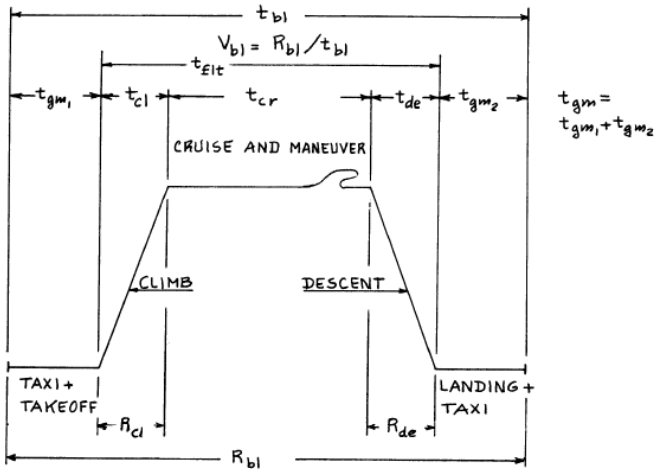

Figure 11.6: Standard flight profile for Vimana [60]

The DOC of flying included items such as Crew Cost, Fuel and Oil Costs and Cost of Airframe Insurance. Crew was identified to be one captain and one co-pilot, the salary value of each obtained from statistical methods proposed by Roskam. This is a highly variable value, of course. Cost of fuels and lubricating oils were taken from standard values of these products in 2015 USD prices. Furthermore, the DOC of maintenance includes estimations for labour costs, which were done based on empirical formulas, including elements such as expected number of maintenance man hours needed per block hour. These values were obtained from graphs presented in Roskam. The reader is made aware at this point that this data may be outdated but is expected to still hold true within a very small error margin, as manufacturing processes have not changed dramatically since the time of publication of Roskams method. The final three DOCs were obtained by direct application of provided formulas.

Table 11.3 summarizes the Direct and Indirect Operating Costs, as obtained by using the assumptions mentioned above, within the framework of Roskam.

Table 11.3: Summary of DOC and IOC for Vimana

Direct Operating Costs	28.5	**[**$/nm/aircraft$**]**
Indirect Operating Costs	14.2	**[**$/nm/aircraft$**]**
Annual Utilization	3248	**[**$Block\ Hours$**]**

11.2.4 Verification with the Reference Aircraft

The same procedure as described for the cost estimation for Vimana is done in this subsection for the Airbus A321 reference aircraft. This is done in order to compare and draw some relative conclusions on the feasibility of Vimana and how it is expected to perform economically. The procedure was to obtain key data about the A321 which are expected to greatly influence the cost outputs, such as Take-Off Weight, Cruise Speed and Block Range values. Table 11.4 summarizes these changes and the values are taken from Airbus [6]. These are then input into the tool, while keeping independent aspects such as number of crew and salaries the same.

[6] URL "http://www.airbus.com/aircraftfamilies/passengeraircraft/a320family/a321/specifications/", [cited: 22 June 2015]

The comparison is split up into RDTE cost, Manufacturing and Acquisition cost, and Operating cost. The discrepancies with the Vimana are also explained.

Table 11.4: Key A321 values input as verification changes to the tool

Take-Off Weight	93500kg
Cruise Speed	0.78 $Mach$ (same for Vimana)
Block Range	3000NM

Research, Development, Test and Evaluation Cost

The RDTE costs are presented in Table 11.5, where the costs are given for the 7 previously defined categories. In addition, the total RDTE cost is also included.

Table 11.5: RDTE cost estimation

Category	**Cost in million [$]**
Airframe engineering and design cost	285
Development support and testing cost	109
Flight test airplanes cost	818
Flight test operations cost	23
Test and simulation facilities cost	0
RDTE profit	186
Cost to finance the RDTE phases	280
Total RDTE cost	1,865

Manufacturing and Acquisition Cost

In Table 11.2, the costs are given for the 3 different categories of the Manufacturing cost, Acquisition cost and the Profit made on each aircraft, for the A321. The total cost of one aircraft is $48 million. Following the same 10% factor rule as was used in the case of Vimana, the profit made on each aircraft is $4.8 million.

Table 11.6: Manufacturing and acquisition cost

Category	**Cost in million [$]**
Airframe engineering and design cost	1,044
Aircraft production cost	627,930
Cost of financing the manufacturing program	157,243
Total manufacturing cost	786,216,434
Cost of acquisition	864,838
Profit	78,621

Operating Cost

The Operating Costs for the reference aircraft are outlined in Table 11.7.

11.2.5 Explanation of Discrepancies

Large discrepancies are observed on both the RDTE and Manufacturing cost. All the subcategories in the RDTE category have a significant decreasing cost for the A321. The parameter which contributes to the RDTE discrepancy the most, is the fact that the A321 has no propellers. The 8 propellers that the Vimana has contribute significantly to all the categories in the RDTE cost. Another parameter which contributes to a lower RDTE, is the use of less aggressive technology resulting in a lower number of built prototype aircraft. In the calculations, the test and simulation facilities cost are also non-existent. This is because the lowest judgment factor is used, because existing facilities already exist, as it is a conventional aircraft.

Table 11.7: Summary of DOC and IOC for the A321 reference aircraft

Direct Operating Costs	20.11	**[$/nm/aircraft]**
Indirect Operating Costs	10.05	**[$/nm/aircraft]**
Annual Utilisation	3264	**[Block Hours]**

The discrepancies for the manufacturing and acquisition cost are also significant. The A321 is significantly cheaper than the Vimana. Larger acquisition costs flow from the linear dependency of the manufacturing cost on the acquisition value. The manufacturing and acquisition cost depend on the same parameters as the RDTE cost calculations. Thus, the same discrepancy explanation is applicable as mentioned above for the RDTE cost.

The operating costs for the A321, as calculated with this cost model, are significantly smaller than for Vimana. This can be explained by the fact that the block range for the A321 was taken to be about 300 nautical miles (approximately 550 km) less than for Vimana. Furthermore, despite the MTOW being higher than for Vimana, the cost estimation included only two engines and no propellers, as per the design of the A321. Using Roskam, this puts Vimana at a big cost disadvantage because in its case, the costs of 8 propeller units, although scaled, were included, theerby significantly increasing all the costs.

It is also mentioned in the project guide that a reference of $0.024\$$ per available seat kilometre (based on a 150 pax seating configuration) should be used for comparison. It is not possible to completely perform a verification based on this number since it is not known what this reference number is based on. Despite this, as mentioned in Table 11.3, the estimated DOC of Vimana is $28.3\$$ per nautical mile, but, based on a 180 pax configuration. Therefore, the comparison, despite being done per passenger, is expected to be a bit skewed. This number then translates (for Vimama) to a value of $0.085\$$ per available seat kilometre, whereas it is $0.060\$$ for the reference aircraft.

The operating cost discrepancy is however expected to reduce, as the oil price increases. The DOC of Vimana are less dependable on the oil prices, as they have a lower SFC and make partially make use of methane. The Roskam method however has a dependency of 12% on the fuel price. Which, in every scenario, would still give a higher DOC for the Vimana. In table 11.8, the DOC are split into fuel dependent and fuel independent.

Table 11.8: Independent and dependent fuel DOC of the Vimana and A321

	Vimana	A321	Unit
Fuel dependent DOC	3.2	3.2	$/nm/aircraft
Fuel independent	25.3	16.9	$/nm/aircraft

11.2.6 List Price Comparison and Validation of Method

Now that the A321 manufacturing and acquisition costs have been calculated, they are compared to the actual, current list price of the aircraft as a validation step. This way, the accuracy of the Roskam method can be estimated. Airbus lists a price of $113.7 million for the A321[7]. The aircraft unit price calculated with the Roskam method is $48. The discrepancy is 237%, which is incredibly large.
There are numerous reasons why such a large discrepancy is observed. The first one of is the fact that the Roskam method stems from 1990. The inflation rate is thus not taken into account with the Roskam method, which is quite a significant parameter over a span of 25 years. The equations derived from aircraft in the era's before 1990. These equations might differ when current aircraft are used. Another reason for discrepancy is the accuracy of the method itself. The Roskam method is meant for preliminary cost estimations. The list price of the A321 is the eventual price, after the detailed design phase.
When taking into account the discrepancy of the Roskam method with the list price, and applying it to Vimana, we get the prices given in Table 11.9.

[7]URL "http://www.airbus.com/presscentre/pressreleases/press-release-detail/detail/new-airbus-aircraft-list-prices-for-2015/", [cited 19 June 2015]

Table 11.9: Vimana cost scaled with the list price of the A321

Category	Cost in million [$]
RDTE cost	11,119
Manufacturing per unit	188
Acquisition per unit	206
Profit per unit	19

11.2.7 Break-even Point

The values used to calculate the break-even point, are the costs with the A321 list price discrepancy adjustment. The break-even point is reached when the initial investment, the RDTE cost, are earned back. The investment into the aircraft project is the research, development, test and evaluation costs. The total cost of this stages of the project is $11,119 million. The total number of aircraft produced during the lifetime of the project is 18000. Airbus has plans to build 46 A320 family units per month in the second quarter of 2016 [8]. The same value can be taken for the Vimana, as it fits in the same category aircraft. The total production program of the Vimana is therefore estimated to be 33 years.

In Subsection 11.2.2, the profit per aircraft is calculated. Thus, to reach the break-even point, 586 aircraft have to be sold. The same procedure is done for the A321, to be able to compare the two aircraft. Following the same procedure, 151 aircraft have to be sold to get a return on the investment.
The A321 reaches its break-even point before the Vimana does, assuming the same production capacity. This is expected, as the RDTE cost are significantly lower than of the Vimana.

One could assume for the break-even point calculation, that the maximum production capacity is reached right from the start. This is of course a very aggressive assumption. Certain aircraft programs take years to break-even. For example the Boeing 787. The aircraft was introduced in 2011. It is expected to break-even later in 2015 [9]. This is a period of 4 years.
No adequate methods are available to accurately estimate the break-even point. It also heavily relies on the PEST factors, that will be discussed in Subsection 11.2.9. To make a more realistic break-even point time period, it is assumed that till break-even point, 50% of the maximum production capacity is reached. This results in a break-even point of 26 months.

Return on Investment

The return on investments flows from the cost estimations done in this section. As calculated before, the break-even point is reached after 26 months. After that, each aircraft will make a profit of $19 million.
The total program will have a profit of $330,885 million spread out over 44 years, which is equivalent to a total of 18000 aircraft.

11.2.8 Disposal Cost

During the end-of-life procedure, the aircraft is disposed. The total cost for the disposal process is estimated. During this process, hazardous materials will need to be removed and disposed. Residual which are recouped for sale, lessen the disposal cost.
As no adequate disposal cost estimations are available for Vimana sized aircraft, other methods have to be used. As there are available numbers for the F16 disposal cost, it is used for the estimation. The F16 acquisition cost is scaled linearly with that of the Vimana, to estimate the disposal cost.

The total disposal cost of one F16 is $6,868 [63]. This is including the sale of residual parts. The list price of the F16 is $ 14.6 million[10]. Thus when scaling it with the Vimana acquisition cost, the disposal cost is calculated to be $96,423 dollars.

[8] URL "http://www.airbus.com/presscentre/pressreleases/press-release-detail/detail/airbus-to-raise-a320-family-production-to-46-a-month-by-q2-2016/", [cited 19 June 2015]
[9] URL "http://www.fool.com/investing/general/2015/02/11/will-boeings-troubled-787-dreamliner-finally-pay-o.aspx", [cited 28 June 2015]
[10] URL "http://www.af.mil/AboutUs/FactSheets/Display/tabid/224/Article/104505/f-16-fighting-falcon.aspx", [cited 29 June 2015]

11.2.9 Discussion

The Roskam method is a good approximation to see the relative cost of all parameters. The tool itself is not accurate enough to draw conclusions from, as is explained in Subsection 11.2.6. The Roskam books are the only detailed cost estimation methods available to be applied to Vimana. Thus it had to be used.
With the discrepancy correction factor with respect to the A321, a better cost estimation can be given to Vimana. Namely, the manufacturing and profit cost, which are the two most important parameters. The break-even point doesn't change with the correction, as it scales linearly.
The aircraft will begin production in around 15 years. With such a large period, a lot of depended factors can be very volatile. A PEST analysis is therefore performed on the cost volatility over the next 15 years. Each factor is discussed below.

Politics

Politics can play a big roll in the cost factors for the aircraft production. The government can intervene in the economy which could lead to significant cost deviations. Examples are new environmental laws, tax raises, or new labor laws.

Economic

Economic factors could play a big roll in the decision making during the aircraft production, and alter the cost estimations. The economy itself is very volatile, which could lead to a positive or negative impact. Economic factors which play a roll are for example, interest rates, wages or inflation rates.

Social

The biggest social factors with respect to the cost of the aircraft production, are the age distribution and career choices. An aging population has a negative impact, as there will be less available man-force. Career choices are also critical. When the population will less often choose engineering as a discipline, it will have a negative impact on the development and manufacturing of the Vimana.

Technology

Technology is one of the most critical factors for the cost of the Vimana. Certain technologies and production procedures could have become significantly cheaper, which drastically changes the total cost. Certain processes could have become more efficient, which also has a positive impact on the cost. In Figure 11.7 a visual representation is given of the PEST analysis.

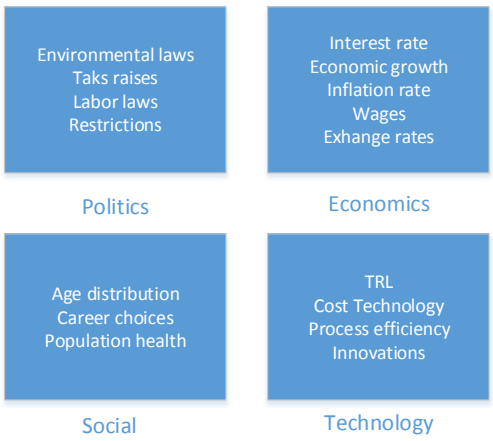

Figure 11.7: PEST analysis visual representation

Chapter 12 | Operational Analysis

This chapter covers the operations and logistics that are involved in the use of the to be designed aircraft. First a flow diagram is generated to give a clear visualization of the different operations and logistics. Further on, the maintenance of aircraft is discussed. Lastly, an analysis of the RAMS-characteristics is given.

12.1 Operations and Logistics

The ground handling forms a crucial part in an aircraft flying cycle. In Figure 12.1 the different operations of an aircraft are shown with a sequence of actions given for the ground handling. The boxes in light blue are optional; for some airports these operations are not necessary or possible. The use of this diagram is to determine system characteristics that must be part of the design. It can be used in further design stages in for example designing the connection between the huffer cart and the generators.
The phase starts directly after landing, after which the aircraft is marshalled to the ramp. There it will be connected to the ramp itself or to additional ground equipment to provide power. After the unloading takes place, directly followed by cleaning, servicing and loading of the payload. Once the payload is loaded completely, pushback is initiated and the flight can be started. In some cases it might be necessary to perform de-icing activities or external cleaning.

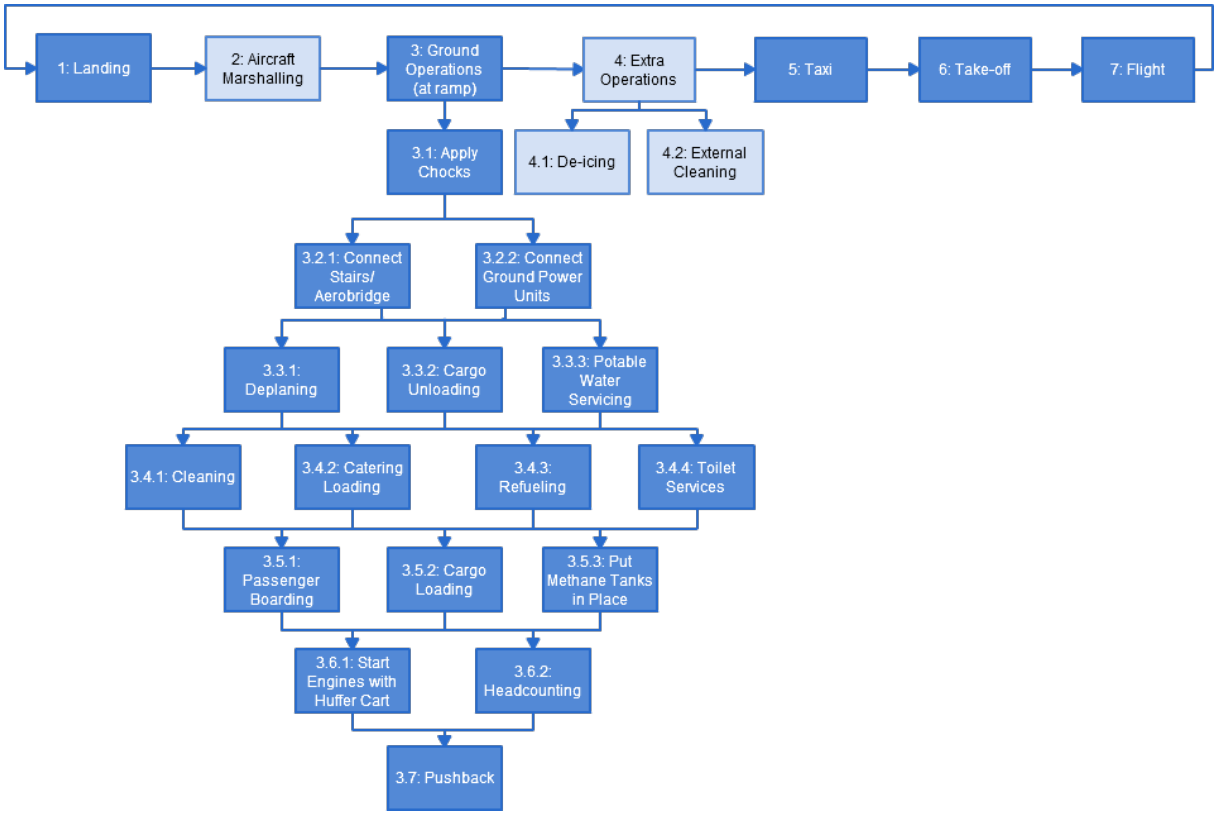

Figure 12.1: Flow Block Diagram of operations and logistics

The different operations are taken from the reference aircraft [64] with adaptions made for Vimana such as the methane tank placing (box 3.5.3) and the use of a huffer cart (box 3.6.1). In general, it is expected that the ground handling will be more complex compared to a conventional aircraft.
First of all, as discussed in Section 8.3, the rear doors are located further in front than normally. This means that certain gates that are built for aircraft of comparable roles might have trouble connecting these doors to the jet bridge. However, it is assumed that most aerobridges are flexible enough to make this problem negligible.
The aircraft also features a methane system. This might put constraints on the airports that can be used, or means that airports have to purchase methane refueling systems. Initially, smaller airfields might not have these systems available, because . Due to the high production count, as explained in Chapter 11, it is expected that this will only be present in the early life of the aircraft. ,

12.2 Maintenance

An important aspect to take into account in the lifetime of an aircraft is the frequency and thoroughness of maintenance checks. There are several checks, the one requires more man-hours than the other and the frequency depends from airline to airline. The numbers below are based on American Airlines [65].

PS-Check

This Periodic Service (PS) check is performed every two to three days overnight or during downtime. This type only contains a visual inspection and a check of the logbook for maintenance needs. This type of check only takes up 2 man-hours.

A-Check

This type of check is more elaborate than the previous one (10-20 man-hours) and is performed every 100 flight hours. This check can as well be executed overnight.

B-Check

During this maintenance check a detailed series of system and operational checks are executed. This is done every 500 to 600 flight hours and requires approximately 100 man-hours for a single aisle aircraft.

C-Check

When performing C-checks, the entire airframe has to be inspected. As this is extensive work, it can not be performed in any hanger as for the other checks. The airplane must be brought to engineering centers where the inspection can take up to three days. This type is performed every 15-18 months.

D-Check

What American Airlines calls a 'heavy' C-check, other airliners (like Lufthansa) call this a D-check. During this check the aircraft is taken out of service for several weeks (typically three to five). The aircraft is taken apart for inspection of every component. The damaged components are repaired or exchanged and afterwards the different components are assembled again. This check costs a lot of money due to the out of service time and the invested man-hours (20,000 - 30,000). Therefore this is only done after 30,000 flight hours[1].

12.2.1 Distributed Propulsion Maintenance

Adding engines increases the complexity of the system, although they will be smaller individually. It is expected that the maintenance checks, especially the more comprehensive B- and C-checks, will be more intensive than for conventional aircraft. As there are also turbines with generators on the back of the aircraft, it is expected that the overall maintenance time of the propulsion system increases.

Current jet engines are very reliable, as most aircraft only have two. However, increasing the number of motors to 8 thus lowering the overall criticality in case a fan fails. This also implies that the reliability, for safety reasons, does not have to be as high as with conventional aircraft. Airliners might decide to lower the overall maintenance intensity on the motors to decrease the working hours and lower the cost.
Lastly, compared to conventional aircraft, Vimana might require additional maintenance time for the HTS cooling system. The system also has not been proven in flight, meaning that personnel will require additional training and that maintenance might be done at a slower rate.
The use of methane as first a heat sink and secondly as fuel does bring along some additional maintenance. It needs to be ensured that the pressure regulating system does not fail for example. Maintenance time it however kept at a minimum by making the tanks interchangeable.

[1] URL "http://www.lufthansa-technik.com/aircraft-maintenance", [cited 6 May 2015]

12.3 RAMS Analysis

During the development of an aircraft, it is critical to take into account the Reliability, Availability, Maintainability and Safety (RAMS) characteristics of the aircraft. Each of these characteristics and their relation is described in the following sections below. Since this concept focuses mainly on the distributed propulsion system, this will also be the main focus of this chapter. Also, because the design of the aircraft is kept rather conventional, major changes in reliability, availability, maintainability and safety should only be caused by the propulsion system.

12.3.1 RAMS Relations

The RAMS characteristics of an aircraft are interconnected and reliant on each other. In Figure 12.2 these relations are visualized. As can be seen, these characteristics are heavily dependant on each other.

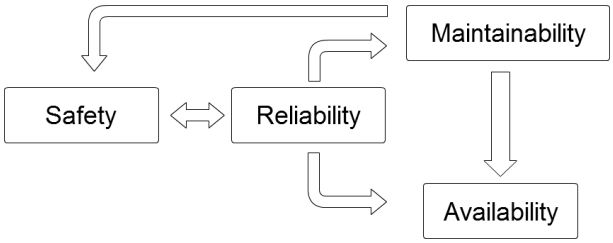

Figure 12.2: Diagram of the relations between Reliability, Availability, Maintainability, and Safety (RAMS) [11]

12.3.2 Propulsion System

In this section, the RAMS characteristics of the propulsion will be discussed. The designed propulsion system consists of multiple systems; the engines, the generators, the motors, the fans and the cooling system. Since this is a modularized system, the maintainability will generally speaking be better as in contrast to a turbofan, the entire system does not need to be taken apart. For a separate evaluation of the RAMS-criteria to the propulsion system, it is split up into four different subsystems. These are electrics, fans, cooling and methane storage, and turboshaft engines and fuel system.

Electrics

Reliability - Since the electric system has not yet been implemented in any current day aircraft, is should be carefully evaluated in terms of reliability. If the electric system fails at delivering power to the electric motors, the aircraft loses thrust and yaw control. Therefore, the electric system is designed with reliability as a main focus and with redundancy to cope with failures.
Availability - Because the electric system is highly integrated in the airframe, it should be designed in such a way that it has a high availability by having long maintenance intervals. If the electric system needs regular maintenance, the aircraft's availability would suffer substantially.
Maintainability - Because of the high integration of the electric system, it should be ensured that maintenance can be properly done when necessary. Special access hatches for the electric system should be present and it should be ensured components of the electric system are easily replaced and inspected.
Safety - To guarantee safety, the electric system will be redundant. Also, the hazards associated with a higher powered electric system should be accounted for. The system should be easy to inspect and should be designed with safety in mind.

Fans

Reliability - This criteria is important concerning the fans as they are not only used for propelling the aircraft but also to control it. Also, because eight of them are present, reliability needs to be high since all fans need to be running before the take-off procedure starts.
Availability - As mentioned in reliability the more fans there are, the worse will the availability be if the reliability is not high enough.
Maintainability - Since the fans are placed on top and can be taken off very easily, it has a relatively short maintenance time. However, because of the relative large number of fans compared to the reference aircraft, the maintenance time will be more or less equal.

Safety - One of the reasons the fans are ducted is to contain a possible blades that has been broken. This way it will not damage the other fans, the fuselage, the empennage or the intake of the turboshaft engines.

Cooling and Methane Storage

Reliability - Because the entire propulsion system depends on being supercooled, the cooling system is of utmost importance. If the cooling system does not work, the wires will not conduct any electricity, thus no power for the fans. Therefore, it should be designed with reliability as a primary concern and also with a certain degree of redundancy, just like the electric system.
Availability - Because the cooling system and methane storage make use of pressures regulators and operate at low temperatures, they need to be inspected and maintained regularly. Therefore, it is important to make these processes easy and fast to impact the availability the least.
Maintainability - As stated in availability, the cooling and methane storage system need frequent inspection. Therefore, these systems should be made easily accessible. Also, the systems should be easy to replace to ensure maintenance will have little impact on availability.
Safety - When designing the propulsion system, safety was one of the main priorities. Therefore, the methane is not stored at high pressure but at low temperatures. During an emergency (e.g. a belly landing) this will therefore not be more dangerous than the currently used kerosene. Also, the cryogen used is neon, which is harmless.

Turboshaft Engines and Fuel System

Reliability - Since turboshafts are already highly used in the present day, reliability will be high. However, since three turboshafts are used, a high reliability will be necessary to ensure availability.
Availability - As mentioned, more turboshafts are used which will compromise availability if no sufficient reliability is attained.
Maintainability - Since the turboshaft are placed in and on top of the fuselage, maintenance might be difficult due to reduced accessibility. Therefore, the engine placed in the fuselage should be made easily accessible and removable. The podded engines should also be easily removable.
Safety - Since one of the turboshaft is place inside the fuselage, special attention should be kept to safety. If this engine should fail, it should be contained and cause no damage to the structure of the tail or the horizontal tailplane.

Chapter 13 | Compliance with Requirements

This chapter is combining the design results as presented in Chapter 7 with the requirements and constraints set by the team as presented in Section 2.3. This comparison is summarised in Table 13.1, in which a check mark indicates that a certain requirements has been met. The last column of the table refers to the chapter or section that provides more information whether the team was compliant with that specific requirement.

Table 13.1: Compliance matrix

Identifier	Description	Met?	Section
	The aircraft shall have a distributed propulsion system	✓	6.1
	The aircraft shall only deviate from a conventional tube and wing concept if this is essential to obtain the maximum benefits of using distributed propulsion	✓	4
	The subsystems not related to the propulsion system shall have a technology readiness level of 9	✓	8
REQ-TL1	The aircraft shall accommodate 180 passengers in a single class configuration	✓	8.3
REQ-TL2	The aircraft shall be able to transport 18,500kg payload	✓	7.6.1
REQ-TL3	The aircraft shall have a maximum payload range of 6100km	✓	7.6.1
REQ-TL4	The aircraft shall have a cruise speed of M $=$ 0.78 at 11,000m	✓	6.1.3
REQ-TL5	The aircraft shall have a maximum speed of M $=$ 0.82 at 11,000m	✓	4.3
REQ-TL6	The aircraft shall require a take-off field length of no more than 2100m at ISA sea level and MTOW condition	✓	4.2.2
REQ-TL7	The aircraft shall require a landing field length of no more than 1600m at ISA sea level and MLW condition	✓	4.2.3
REQ-TL8	The aircraft shall have a service ceiling of 12,000m	✓	7.6.3
	Special attention shall have been paid to the OEI scenario and the minimum control speed of the aircraft	✓	7.5.4
	The energy storage and energy transfer system shall have equal safety compared to current propulsion solutions	✓	6.3.4
	The aircraft shall minimize CO_2 and NO_x emissions with a target: 25% reduction per passenger kilometre.	✗	7.6.4
	The aircraft shall reduce noise, compared to the Airbus A321, in take-off, climb, descent and landing phases	✓	7.6.5
	The aircraft shall have competitive Direct Operating Costs compared to current aircraft in this class, including cost of emissions.	✗	11.2.5
	The aircraft shall have minimal impact on the airport infrastructure and aircraft operations in case a hybrid-electric solution is proposed.	✓	12

Chapter 14 | Future Development Activities

The purpose of this Design Synthesis Exercise was to design an aircraft for around the N+3 timeframe, that is, for an expected entry into service from 2035 onwards. This chapter elaborates on the specific steps and processes this distributed propulsion aircraft needs to experience in order for it to be a successful, commercially and technologically viable model.
This chapter is divided as follows: Section 14.1 presents the design and development logic of the overall design and construction process while Section 14.2 focuses particularly on the specific projected activities for the distributed propulsion technologies. Section 14.3 provides an overview of the integral post-DSE activities in a Gantt chart format. Finally, Section 14.4 will state some recommendations for future activities

14.1 Project Design and Development Logic

Following standard ESA project management procedures [66] and the 787 development timeframe as baseline, a project design and development logic was established for the upcoming 20 years of aircraft development. Six main development phases were identified and for each phase a description of relevant activities was included. The integral project design and development logic diagram is presented in Figure 14.1. The rest of this section will elaborate on all identified phases with the exception of the distributed propulsion development phase, which will be treated in the next section.

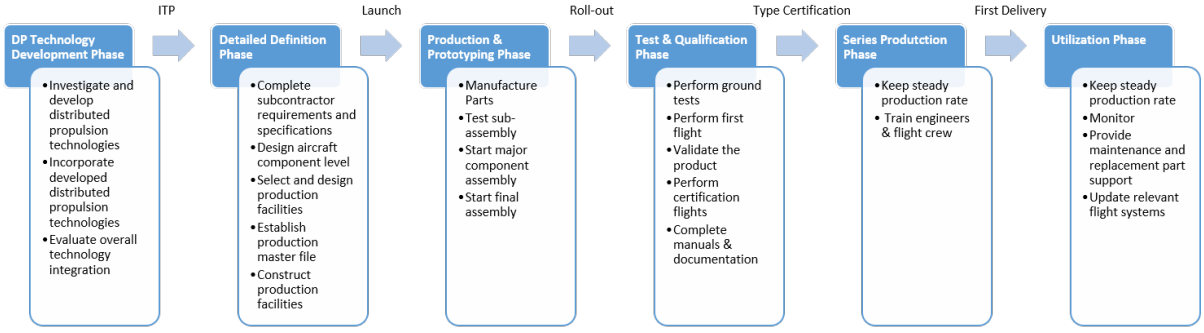

Figure 14.1: Project design and development logic diagram for the distributed propulsion aircraft

14.1.1 Detailed Definition Phase

Once the relevant distributed propulsion technologies have been brought to the appropriate Technology Readiness Level (TRL) and an instruction to proceed (ITP) has been granted by the manufacturer, the detailed definition phase can be commenced. This stage primarily concerns the component level design of the aircraft. Starting off from the iterated Class II estimation, the next step is to determine the sets of aerodynamic load cases for the entire flight envelope. With those sets, together with an initial estimate on the materials to be included and the preliminary CAD models of the outer surfaces, the thickness distribution and the weights of the main structural elements can be determined. Additionally, with help of computational fluid dynamics simulation software, all the flows should be evaluated on the individual airframe components as well as the overall integration in order to ensure the predicted aerodynamic performance. Finally, with finite element method-based approach and standard sizing catalogues, the overall detailed design of the aircraft can be concluded.
The detailed definition phase also focuses on the design and development of all the production facilities and the logistical operations between them. During this phase, the requirements and specifications for the individual subcontractors should be finished, as the outsourcing companies should be given the time to analyze, formulate and present their business proposal for the component at hand. Once all the proposals have been submitted, the selection and design of the production facilities and the supporting operations' strategy can be commenced. Meanwhile, just after the overall detailed design is concluded, the production master file should be redacted so that all the design specifications are contained into a unified, coherent document. With the production master file completed and the production facilities built, the official launch of the aircraft program can be performed. This milestone officially concludes the detailed definition phase.

14.1.2 Production and Prototyping Phase

This phase, as its name suggests, concerns the manufacturing and assembly of aircraft prototypes that will be used for verification, test and qualification purposes. During this phase, all the parts that comprise the complete aircraft system and its supporting units (maintenance equipment, ground support, etc.) should be manufactured and built. These parts will together form a set of sub-assemblies which should be already built, tested and qualified on a sub-system level. This will thus ensure that the major component assembly does not contain major technical or design omissions or mistakes. From the component assembly, the final assembly thus follows: in this stage all major component assemblies are brought into a single building at which they will be ultimately joined into a single aircraft. This stage is characterized by its heavy dependence on operations and logistics support as most of the wings, empennage and fuselage elements possess very large dimensions and are often brought from all around the globe. Regarding the newly introduced distributed propulsion system, the operations and logistics strategy envisioned for the Vimana project will classify all the constituent propulsive elements by their order of airframe integration. Devices such as the high temperature superconductive cabling which are highly integrated into the structure will be included early in the assembly process. However, the most expensive propulsive elements, the fans, motors and turbines, are designed to be mounted on the very last stages of assembly, just like regular turbofan engines, minimizing inventory costs and interest.
With the successful conclusion of the assembly of the first aircraft the production and prototyping phase is sealed close with the roll-out ceremony, in which a completed aircraft is presented to the media and the general public. Given the fact that the P&P Phase is located precisely in the middle of the post-DSE activities a buffer time of one year is scheduled in order to compensate for any delays caused by any of the previous project stages.

14.1.3 Test and Qualification Phase

This phase is the most crucial one of the entire aircraft program, as its airworthiness is at stake and any design change, re-evaluation or modification can results in serious additional costs and schedule delays. The test and qualification phase commences with a series of internal ground and flight tests before any qualification is attempted. This allows the manufacturer to validate all their design tools and methods and prepare the aircraft for external evaluation. Meanwhile the integral aircraft documentation (maintenance procedures, flight manuals, etc.) should be completed at this stage.
Vimana introduces substantial technology improvements in its propulsion subsystem. This means that a dialogue needs to be started together with the regulation authorities such as EASA and FAA in order to draft new performance requirements in order for the aircraft to be certified to fly. Two essential changes immediately stand out: the one engine inoperative scenario (OEI) and the controllability adaptation for tailless aircraft. Up until now, aircraft have been qualified on OEI performance for take-off and cruise. For Vimana, the OEI needs to be divided in two, namely one fan inoperative (OFI) and one turbine inoperative (OTI). One turbine operative should follow the same certification guidelines as for trijet aircraft such as the MD-11 or the DC-10. One fan inoperative scenarios should be drafted from scratch; they should be also coupled to the tailless characteristics of the aircraft, as the fans are used for yaw control. Furthermore, an agreement with the regulation authorities should be made regarding the extent to which combined fan/turbine failure scenarios will be considered. These decisions will of course alter the performance requirements of the aircraft; hence it is expected that the FAA and EASA will draft their respective stipulations in the 2015-2022 timeframe before the ITP point is reached. Furthermore, the cabling certification should roughly follow the same guidelines as for the hydraulics system: being a crucial component of the aircraft, similar redundancy levels should be achieved in order for the aircraft to continue its mission despite an electrical failure. Finally, the methane tanks should follow similar impact resistance and structural requirements as regular fuel tanks.
With all above tasks done, the aircraft is ready for series of scrutinizing certification flights performed by the pertinent aviation authorities. If successfully completed, the aircraft will receive its type certification, concluding herewith the test and qualification phase.

14.1.4 Series Production and Utilization Phases

Once the aircraft is airworthy, the nominal production and utilization activities can be initiated. These activities concern in general the operation and steady production of the particular aircraft model. It is of vital importance for the successful market implementation that a comprehensive and reliable (flight and ground) crew training, maintenance and spare parts support scheme is erected. It is also necessary to continuously monitor the aircraft's performance in a nominal environment in order to provide with pertinent updates and new technologies implementation if this particular model is intended to stay in the market for an extended

period of time (20 years or more). Three important milestones are identified for these last phases: the delivery of the first aircraft to the launch carrier, the entry into service and the break-even point.

14.2 Development of Distributed Propulsion Technologies

The propulsion system design as presented in Chapter 6 includes multiple novel technologies that do not satisfy the criteria of the ninth Technology Readiness Level. Therefore, the technologies of the distributed propulsion system have to be investigated over the upcoming 8 years in order to find out if the required level will be achieved before the detailed definition phase of the aircraft will be commenced. The team has set the target that the currently chosen technologies require at least a TRL of 6 by the end of this investigation, which has been set to the July 2022. The technologies that have to meet this deadline are explained in detail below:

Fan Design Literature published in 2007 states that the TRL of the ducted fan achieved a value of 6[1], which is the minimum level set by the team. However, more investigation is required to find out whether stated advantages can be used and if the ducted fan will fulfill the performance requirements at a high subsonic Mach number for a commercial aircraft of the size of an A321. For the fans the important further activities require foremost a combination of preliminary CFD analysis in conjunction with further wind tunnel testing throughout the entire flight envelope conditions. This includes testing for a potential blown flap concept, boundary layer ingestion and prevention of catastrophic vibrations. In a later stage, the construction has to be tested for a blade-out situation.

Cryocoolers Although cryocoolers are used in a wide array of applications including space [67], none of the currently available products has been optimized for aeronautical applications. As of 2008 proposals were being drafted for reaching an aeronautical-optimized cryocooler TRL of 4 [68]. Cryocoolers are thus one of the components that need to be developed more extensively. Research requirements involving these systems include foremost the validation of these technologies and the subsequent product development for the given design and performance requirements.

HTS Motors/Generators According to EADS (now Airbus Group), high temperature superconductive motors and generators for aircraft application possess a current TRL of 2 [69]. Research requirements desire investigations in aerospace-like environments in order to increase the TRL to the required level 6. This includes procedures that will validate the 100% efficiency of the HTS cabling. Besides, it has to be proven that the motors and generators can convert the required high powers from shaft power to electric power and vice versa. Also, the potential energy dump system as presented in Subsection 6.8.3 needs further investigation.

Engines A total of three turboshafts will be put at the back of the fuselage. Even though turboshaft engines have already been flying for multiple years, they have not been used in a hybrid configuration. Therefore, sufficient time is required for investigating the engine technology that will be used in order to increase the TRL of the core engine technology from 5 to at least 6 [70]. This research includes effects due to the fact that the engines will be a scaled down version of currently flying turboshaft engines. As the engines will be located in or close to the fuselage, part of the inlet flow is turbulent. CFD analysis and windtunnel tests are required to optimise the engines for this situation. In a later stage, the engines have to be optimised to use both kerosene and methane as a propellant.

Methane Tanks A methane tank is required to cool the superconductive motors and generators. This tank has to guarantee a constant pressure of 1 bar and a temperature of $111K$. Tests in simulated environments have to proof that these characteristics can be achieved. The most prominent factor is the tank insulation, which has a TRL of 2 as presented in literature [71]. Since the methane tank will be placed underneath the passenger cabin, the team has to be sure that the tank is impact resistant in order to maintain a sufficient level of safety for the passengers.

Overall System Integration Even though all systems achieved an individual TRL of 6 by 2022, the entire propulsive architecture needs to be validated constructed and optimised on a system level. Overall, the integral aircraft morphology described in this report possesses a TRL of 2. Following the approach from

[1]URL: "http://www.gpo.gov/fdsys/pkg/GAOREPORTS-GAO-07-376/html/GAOREPORTS-GAO-07-376.htm" [cited 15 June 2015]

the DisPURSAL project [70], the proposed further activities for the system integration entail three specific steps: the first one is a comprehensive CFD analysis of the entire architecture on the already developed airframe. Next proceeds a sub-scale test in windtunnel test. During this phase the benefits of fuselage boundary layer ingestion need to be quantified and validated with the initial predictions. Finally, the third step comprises the construction of a real size prototype which should be fitted to an existing flying test-bed. This last task should validate the operation of the entire propulsion system throughout the real expected flight envelope.

Technology Evaluation and Design Iteration Once all the individual systems are brought to a TRL of 6 and the entire propulsion system is validated across the entire flight envelope, a timeframe of 17 months will be allocated for the evaluation of the entire distributed propulsion technologies. In this phase, the overall feasibility for Vimana will be determined based on the differences between the expected technological developments described in the above paragraphs and the actual progress made. Concurrently, the same timeframe will also allow for further design iterations that can include the following elements: novel design analysis tools for propulsive systems, breakthrough innovations in aerospace technologies (for example, new lightweight materials) and change in customer needs and requirements, such as, for example, the explicit requirement to omit a propulsion system with a methane cooling device. Once these changes are taken into account and the overall design is deemed feasible, the instruction to proceed (ITP) will be granted.

14.3 Post-DSE Gantt Chart

In the previous section, the project design and development logic was presented and the individual components were elaborated on. In order to provide a chronological sense to this set of activities, this section will present them in the form of a Gantt chart. This diagram, portrayed in Figures 14.2 and 14.3, comprises a timeframe extending from the end of this DSE project in 2015 until its expected break-even point around 2037.

Figure 14.2: Gantt chart of the post-DSE activities part 1

Figure 14.3: Gantt chart of the post-DSE activities part 2

14.4 Recommendations

In this section, different recommendations will be given for future activities. This includes recommendations for the organisation part of a project as presented in Subsection 14.4.1. Items related to the lessons learned and recommendations regarding future research will be stated in Subsection 14.4.2 and 14.4.3 respectively.

14.4.1 Organisation

This subsection will cover the recommendations that are related to the group organisation.

1. In the Project Plan [72], the team has split the overall project in different disciplines. For each of these disciplines, multiple team members have been assigned based on the preference and expertise of each of them. However, the team has not followed this plan to the full extent as it turned out that some parts had to be written at a specific moment, even though the discipline expert was not available. For future activities, the discipline division shall be used to benefit from an expert's knowledge.
2. One of the goals of the Design Synthesis Exercise is related to group dynamics. This does include the fact of working with different students to gain experience with different personalities and point of views. Over the past few weeks, different sub-teams have been formed which have not changed their content many times. To achieve this goal to a larger degree, certain team member rotations should be done.
3. The team was mild, in case a certain deadline had not been met. An additional day was provided to make it possible to finish the task. For future work, the team may be more strict in order to be able to obtain more detailed results.

14.4.2 Lessons Learned

In this subsection a discussion will be given of the lessons that the team members have learned over the past few weeks.

1. By going from a design at concept level up to a more detailed level, the team had to make multiple complicated design choices ranging from the airfoil selection up till the removal of the vertical tail. Once a certain design choice had been made, it was not always verified that this design choice was the best option. Therefore, more iterations should be performed to check whether the design choice has resulted in the expected benefits and outcome.
2. Besides, the group should have focused on the most important and promising aspects of distributed propulsion, instead of spending little time on different points. For example, a more detailed insight can be given either about the removal of the vertical tail or the removal of the APU, instead of a little information about both of them.

14.4.3 Future Research

An explanation of future research related to the novel technologies used has been presented in Section 14.2. This subsection will give some additional items that should undergo additional investigation.

1. As stated in Subsection 7.5.4, a combination of differential thrust and split ailerons will be used for lateral control. More research will have to be done to create this system in more detail, such that in can be concluded with confidence that the tail can be removed.
2. As stated in Chapter 11, the operating cost of the Vimana aircraft is higher than the reference aircraft. The calculation is based on Roskam [60] written in 1990, and therefore multiple formulas are no longer valid for current days economy. Besides, the value is even significantly higher than the Airbus A321 aircraft, indicating a different approach method. Therefore, future research should look at the cost estimation method.
3. As can be seen in Chapter 13, the requirement regarding emissions has not been met. More research can be spend in other novel technologies and propellants in order to achieve the requirement to a larger extent.

Chapter 15 | Conclusion

Vimana was designed as a distributed propulsion aircraft, with a top level requirement to achieve significant environmental benefits in terms of emissions and noise, compared to a classical aircraft configuration. Foreseeing substantial growth for the next 20 years in the single aisle, medium range aircraft market segment, Vimana will transport 180 passengers and their luggage over a distance of $6100km$.

In order to systematically analyze the benefits caused by the distributed propulsion system, a comparison was made by designing a reference aircraft based on an A321. The design philosophy behind Vimana was to start off with a conventional design and to allow deviations only if they supported the distributed propulsion technology. This, along with the use of the same design tools for both aircraft, allowed for a fair comparison and resulted in valid conclusions on the benefits of distributed propulsion.

A hybrid solution containing three turboshaft engines, electrically powering eight fans distributed over the span of the wing, was chosen. Various novel design choices, enabled by the distributed propulsion concept, were implemented. These are summarized below:

- Superconducting generators and motors are used to minimize electrical losses. In order to ensure superconductivity, these rotating machines are cryocooled using liquid Neon as a coolant. The electric charge is circulated throughout the aircraft using high temperature superconducting cabling (HTS) which also minimizes losses.
- A large volume of air is being blown by the ducted fans, which results in a high propulsive efficiency.
- Boundary layer ingestion and wake filling are effects that the aircraft has been specifically designed for. This is observed at the aft of the fuselage with the body integrated turbine intake and the trailing edge of the wing, where fans ingest the wake.
- The vertical tail has been omitted and yaw control is done by differential thrust settings, combined with the use of split ailerons.
- Due to the placement of the fans on top of the wing, there is a less stringent requirement on ground clearance. Therefore, shorter landing gears are present.
- Methane is used as a heat sink for the generators and motors after they have been cryocooled. The heated methane is then mixed with jet fuel and used as a propellant.

Implementing the aforementioned design choices results in benefits in terms of noise, mass and emissions. Lower noise emissions are expected by virtue of the fan shielding, high air mass flow through the fans, resulting in a low outflow velocity, and engine placement within the fuselage. Despite the omission of the vertical tailplane and shortening of the landing gear, the empty weight of the aircraft is higher than that of the reference due to added components within the propulsion system. However, there is a marked reduction in the MTOW due to a lighter fuel load. Significant performance benefits are attained through the use of BLI and high electrical and propulsive efficiencies. This, in conjunction with the use of methane as an additional propellant, contributes to the aforementioned lighter fuel load. Most importantly, this also results in a more than 20% decrease in CO_2 and NO_x emissions.

A preliminary cost estimation results in an operating cost of $\$0.085$ per available seat kilometer for Vimana, as opposed to $\$0.060$ for the reference aircraft. Vimana is noticeably more expensive to operate, but it is certainly more eco-friendly.

Bibliography

[1] S. Ashcraft, A. Padron, K. Pascioni, and G. Stout, *Review of Propulsion Technologies for N+3 Subsonic Vehicle Concepts*. NASA Glenn Research Center, Cleveland Ohio USA, 2011.

[2] L. Hardin, G. Tillman, B. J. Sharma, O.P., and D. Arend, "Aircraft system study of boundary layer ingesting propulsion," tech. rep., NASA Glenn Research Center.

[3] A. Plas, M. Sargeant, V. Madani, D. Crichton, E. Greitzer, T. Hynes, and C. Hall, "Performance of a boundary layer ingesting (bli) propulsion system," pp. 8–11, 2007.

[4] H. D. Kim, "Distributed propulsion vehicles," in 27^{th} *International Congress of the Aeronautical Sciences*, (Nice, France), 2010.

[5] J. A. Schetz, S. Hosder, V. Dippold III, and J. Walker, "Propulsion and aerodynamic performance evaluation of jet-wing distributed propulsion," *Aerospace Science and Technology*, vol. 14, no. 1, pp. 1–10, 2010.

[6] H. D. Kim, J. L. Felder, M. T. Tong, and M. Armstrong, "Revolutionary aeropropulsion concept for sustainable aviation: turboelectric distributed propulsion," in *Challenges in Technology Innovation*, pp. 1859–1870, 2013.

[7] H. Steiner, P. C. Vratny, C. Gologan, K. Wieczorek, A. T. Isikveren, and M. Hornung, "Optimum number of engines for transport aircraft employing electrically powered distributed propulsion," *CEAS Aeronautical Journal*, vol. 5, pp. 157–170, 2014.

[8] M. Voskuijl, *Project Guide Design Synthesis Exercise, Distributed propulsion for commercial transport aircraft*. TU Delft, Delft, The Netherlands, 1 ed., 2015.

[9] D. group 17, "Mid-term report: Distributed propulsion for conventional transport aircraft," tech. rep., Delft Universtiy of Technology, 5 2015.

[10] J. Jackson, *Jane's All the World's Aircraft*. IHS, 2014.

[11] J. Melkert, "Aerospace Design and Systems Engineering Elements I ae1222-ii." Lecture slides from Aerospace Design and Systems Engineering Elements I AE2101 (TU Delft), 2012-2013.

[12] J. Roskam, "Airplane design: Part i, preliminary sizing of airplanes," *Preliminary Sizing of Airplanes*, vol. 1, 1985.

[13] D. Steenhuizen, "Aerospace Design and Systems Engineering Elements II ae2101." Lecture slides from Aerospace Design and Systems Engineering Elements II AE2101 (TU Delft), 2014-2015.

[14] J. Roskam, "Airplane design: Part ii - preliminary configuration design and integration of the propulsion system,"

[15] Joint Aviation Authorities, Saturnusstraat 10, PO Box 3000, 2130KA, Hoofddorp, The Netherlands, *Joint Aviation Requirements*, 14 ed., 5 1994.

[16] J. Roskam, *Airplane Design: Part iii, Layout design of cockpit, fuselage, wing and empennage*. Ottawa, Kansas: Roskam Aviation and Engineering Corporation, 1986.

[17] J. Roskam, *Airplane Design: Part v, Component Weight Estimation*. Ottawa, Kansas: Roskam Aviation and Engineering Corporation, 1986.

[18] G. La Rocca, "Systems Engineering and Aerospace Design ae3211-I." Lecture slides from Systems Engineering and Aerospace Design AE3211-I (TU Delft), 2014-2015.

[19] J. Roskam, *Airplane Design: Part vi, Preliminary calculation of aerodynamic, thrust and power characteristics*. Ottawa, Kansas: Roskam Aviation and Engineering Corporation, 1986.

[20] E. Torenbeek, *Synthesis of Subsonic Airplane Design*. Hingham, Maine: Kluwer Boston inc., 1982.

[21] R. Kawai, D. Friedman, and L. Serrano, "Blended wing body boundary layer ingestion inlet configuration and system studies," tech. rep., Boeing Phantom Works.

[22] G. Brown, *Weight and Efficiencies of Electric Components of a Turboelectric Aircraft Propulsion System*. NASA Glenn Research Center, Cleveland Ohio USA, 2011.

[23] B. Schiltgen, A. Gibson, M. Green, and J. Freeman, *More Electric Aircraft: Tube and Wing Hybrid Electric Distributed Propulsion with Superconducting and Conventional Electric Machines*, 9 2013.

[24] R. Beluga and A. Abrego, *Performance Study of a Ducted Fan System*. Moffett Field, California.

[25] W. Graf, *Effects of Duct Lip Shaping and Various Control Devices on the Hover and Forward Flight Performance of Ducted Fan UAVs*. Blacksburg, Virginia.

[26] A. Denaes, *Air Operations Part 2 (Take-off limitations)*. Toulouse: ENAC, 2014.

[27] J. Felder, H. Kim, and G. Brown, *Distributed Turboelectric Propulsion for Hybrid-Wing-Body Aircraft*. NASA Glenn Research Center, Cleveland Ohio USA, 7 2008.

[28] C. Pornet, s. Kaiser, A. Isikveren, and M. Hornung, *Integrated fuel-battery hybrid for a narrow-body sized transport aircraft*. Bauhaus Luftfahrt e.V., Munich Germany, 6 2014.

[29] J. Leishman, *Principles of Helicopter Aerodynamics*. Cambridge University Press, 2006.

[30] D. Unger and H. Herzog, "Comparative study on energy r&d performance: Gas turbine case study," tech. rep., Massachussets Institute of Technology, 8 1998.

[31] H. W. Neumuller, "Advances in and prospects for development of high-temperature superconductor rotating machines at siemens," 2 2006.

[32] J. Frauenhofer, "Basic concepts, status, opportunities, and challenges of electrical machines utilizing high-temperature superconducting (hts) windings," 3 2008.

[33] S. Baik, K. Y., and H. Kim, "Loss analysis of a 1 mw class hts synchronous motor," *Journal of Physics: Conference Series 153*, pp. 3–6, 2008.

[34] S. Wipf, "Ac losses in superconductors," tech. rep., Atomics International, a division of North American Rockwell Corporation.

[35] S. Baik, M. Sohn, and E. Lee, "Design considerations for 1 mw class hts synchronous motor," pp. 1–4, 6 2005.

[36] S. Kalsi, "Applications of high temperature superconductors to electric power equipment," tech. rep., Institute of Electrical and Electronics Engineers.

[37] H. ter Brake and G. Wiegerinck, ""low-power cryocooler survey," *Cryogenics,*, no. 11, 2002.

[38] P. Masson, D. Soban, and E. Upton, "Towards electric aircraft: Progress under the nasa ureti for aeropropulsion power technology," 11 2006.

[39] J. Zou, T. Flack, and H. Feng, "Desing and performance analysis of a 2.5 mw-class hts synchronous motor," tech. rep., Institute of Electrical and Electronics Engineers.

[40] G. Brown, "Weights and efficiencies of electric components of a turboelectric aircraft propulsion system," *The American Institute of Aeronautics and Astronautics*, p. 5, 1 2011.

[41] S. S. Kalsi, *Applications of High Temperature Superconductors to Electric Power Equipment*. Institute of Electrical and Electronics Engineers, 2011.

[42] Nexans Deutschland GmbH, "Superconducting cable systems," 2013.

[43] P. Ford and G. Saunders, "The rise of the superconductors," 10 2004.

[44] R. Radebaugh, *Cryocoolers for Aircraft Superconducting Generators and Motots*. National Institure of Standards and Technology, Boulder Colorado USA, 2012.

[45] J. Felder, H. Kim, and G. Brown, *Turboelectric Distributed Propulsion Engine Cycle Analysis for Hybrid-Wing-Body Aircraft*. NASA Glenn Research Center, Cleveland Ohio USA, 7 2009.

[46] University of Houston Law Center, *LNG Frequently Asked Questions*. Institute for Energy, Law and Enterprise.

[47] M. Drewes, *Tank to Thrust Analysis*. AIRLNG, 2010. Powerpoint slides.

[48] A. Geschiere, D. Willen, E. Piga, P. Barendregt, and I. Melnik, "Optimizing cable layout for long length high temperaute superconducting cable systems," 2008.

[49] Federal Aviation Administration (U.S. Dept of Transportation), "New etops regulations." Flight Standards Service, 1 2007.

[50] P. Raymer, *Aircraft Design: A Conceptual Approach*. American Institute of Aeronautics and Astronautics, 2 ed.

[51] A. Hughes and B. Drury, *Electric Motors and Drives: Fundamental, Types and Applications*. Elsevier, 2013.

[52] L. Cöllen, "Standardized geometry formats for aircraft conceptual design and physics-based aerodynamics and structural analyses," tech. rep., Royal Institute of Technology (KTH).

[53] Y. Guo and K. Yamamoto, "Experimental study on aircraft landing gear noise," *Journal of Aircraft*, vol. 43, pp. 306–317, 3 2006.

[54] I. Martinez, *Aircraft Environmental Control*. Universidad Politecnica Madrid, 1995.

[55] U. D. of Transportation, *Aviation Maintenance Technician Handbook - Airframe*. FAA.

[56] A. Ahmed, "Origin of 400hz in aircraft," *Academia.edu*, 2015.

[57] N. T. S. Board, "Introduction of glass cockpit avionics into light aircraft," 3 2010.

[58] T. Amon, "Methane production through anaerobic digestion of various energy crops grown in sustainable crop rotations," *Bioresource Technology*, vol. 3, no. 3, pp. 177–182, 2013.

[59] U. PeriyarSelvam, A. Tamilselvan, S. Thilakan, and M. Shanmugaraja, "Analysis on costs for aircraft maintenance," *Advances in Aerospace Science and Applications*, vol. 3, no. 3, pp. 177–182, 2013.

[60] J. Roskam, *Airplane cost estimation: design, development, manufacturing and operating*. Ottawa, Kansas: Roskam Aviation and Engineering Corporation, 1990.

[61] Airbus Group N.V., "Flying on demand," tech. rep., 2014.

[62] The Boeing Company, "Current market outlook 2014-2033," tech. rep., The Boeing Company, 2014.

[63] U. S. G. A. Office, "Dod's liability for aircraft disposal can be estimated," 11 1997.

[64] Airbus Group N.V., *A320/A230NEO Aircraft Characteristics - Airport and Maintenance Planning*, 3 ed., May 2014.

[65] American Airlines, *Aircraft Maintenance Procedures Fact Sheet*, 12 2011.

[66] European Cooperation for Space Standardization, Noordwijk, the Netherlands, *Space Project Management - Project Phasing and Planning*, 1996.

[67] R. Ross, R.G. & Boyle, "An overview of nasa space cryocooler programs—2006," *International Cryocooler Conference*, 2006.

[68] Creare Incorporated, "Thermal management system for superconducting aircraft." Proposal Summary.

[69] Airbus Group N.V., "A short overview of superconductivity." Conference Presentation.

[70] A. Isikveren, "Dispursal: D1.2 – report on the technology roadmap for 2035," tech. rep., Bauhaus Luftfahrt e.V.

[71] M. Sippel, A. Kopp, K. Sinkó, and D. Mattsson, "Advanced hypersonic cryo-tanks research in chatt," tech. rep., AIAA International Space Planes and Hypersonic Systems and Technologies Conference.

[72] DSE 2015 Group 17, "Project plan," tech. rep., TU Delft, April 2015.

[73] D. group 17, "Baseline report: Distributed propulsion for conventional transport aircraft," tech. rep., Delft Universtiy of Technology, 5 2015.

Chapter A | Propulsion System Background

In this appendix, the more detailed tables on the sensitivity analyses performed on the number of engines and placement can be found in Sections A.1 and A.2 respectively. Section A.3 shows a technical drawing of a coldhead.

A.1 Detailed Results of Sensitivity Analysis on Number of Engines

Table A.1: Weight and SFC criteria sensitivity with a 2 engined configuration

		Weight				
SFC	**3.1**	0.2	0.25	0.3	0.35	0.4
	0.2	2.6	2.65	2.7	2.75	**2.8**
	0.25	2.8	2.85	2.9	**2.95**	3.0
	0.3	3.0	3.05	**3.1**	3.15	3.2
	0.35	3.2	**3.25**	3.3	3.35	3.4
	0.4	**3.4**	3.45	3.5	3.55	3.6

Table A.2: Weight and SFC criteria sensitivity with a 3 engined configuration

		Weight				
SFC	**3.45**	0.2	0.25	0.3	0.35	0.4
	0.2	2.75	2.9	3.05	3.2	**3.35**
	0.25	2.95	3.1	3.25	**3.4**	3.55
	0.3	3.15	3.3	**3.45**	3.6	3.75
	0.35	3.35	**3.5**	3.65	3.8	3.95
	0.4	**3.55**	3.7	3.85	4.0	4.15

Table A.3: Weight and SFC criteria sensitivity with a 4 engined configuration

		Weight				
SFC	**3.2**	0.2	0.25	0.3	0.35	0.4
	0.2	2.2	2.3	2.4	2.5	**2.6**
	0.25	2.35	2.45	2.55	**2.65**	2.75
	0.3	2.5	2.6	**2.7**	2.8	2.9
	0.35	2.65	**2.75**	2.85	2.95	3.05
	0.4	**2.8**	2.9	3.0	3.1	3.2

Table A.4: Weight and SFC criteria sensitivity with a 12 engined configuration

		Weight				
SFC	**1.9**	0.2	0.25	0.3	0.35	0.4
	0.2	1.4	1.6	1.8	2.0	**2.2**
	0.25	1.45	1.65	1.85	**2.05**	2.25
	0.3	1.5	1.7	**1.9**	2.1	2.3
	0.35	1.55	**1.75**	1.95	2.15	2.35
	0.4	**1.6**	1.8	2.0	2.2	2.4

A.2 Detailed Results of Sensitivity Analysis on Placement of Engines

Table A.5: Safety and aerodynamics criteria sensitivity with configuration 1 (all engines inside)

Configuration 1		Safety				
Aerodynamics	**2.35**	0.2	0.25	0.3	0.35	0.4
	0.15	1.85	1.9	1.95	2.0	**2.05**
	0.2	2.05	2.1	2.15	**2.2**	2.25
	0.25	2.25	2.3	**2.35**	2.4	2.45
	0.3	2.45	**2.5**	2.55	2.6	2.65
	0.35	**2.65**	2.7	2.75	2.8	2.85

Table A.6: Safety and aerodynamics criteria sensitivity with configuration 2 (one engine inside, two outside)

Configuration 2		Safety				
Aerodynamics	**2.55**	0.2	0.25	0.3	0.35	0.4
	0.15	2.05	2.2	2.35	2.5	**2.65**
	0.2	2.15	2.3	2.45	**2.6**	2.75
	0.25	2.25	2.4	**2.55**	2.7	2.85
	0.3	2.35	**2.5**	2.65	2.8	2.95
	0.35	**2.45**	2.6	2.75	2.9	3.05

Table A.7: Safety and aerodynamics criteria sensitivity with configuration 3 (two engines inside, one outside)

Configuration 3	Safety					
Aerodynamics	**2.45**	0.2	0.25	0.3	0.35	0.4
	0.15	1.95	2.05	2.15	2.25	**2.35**
	0.2	2.1	2.2	2.3	**2.4**	2.5
	0.25	2.25	2.35	**2.45**	2.55	2.65
	0.3	2.4	**2.5**	2.6	2.7	2.8
	0.35	**2.55**	2.65	2.75	2.85	2.95

Table A.8: Safety and aerodynamics criteria sensitivity with configuration 4 (all engines outside)

Configuration 4	Safety					
Aerodynamics	**2.35**	0.2	0.25	0.3	0.35	0.4
	0.15	1.95	2.1	2.25	2.4	**2.55**
	0.2	2.0	2.15	2.3	**2.45**	2.6
	0.25	2.05	2.2	**2.35**	2.5	2.65
	0.3	2.1	**2.25**	2.4	2.55	2.7
	0.35	**2.15**	2.3	2.45	2.6	2.75

A.3 Coldhead Drawing

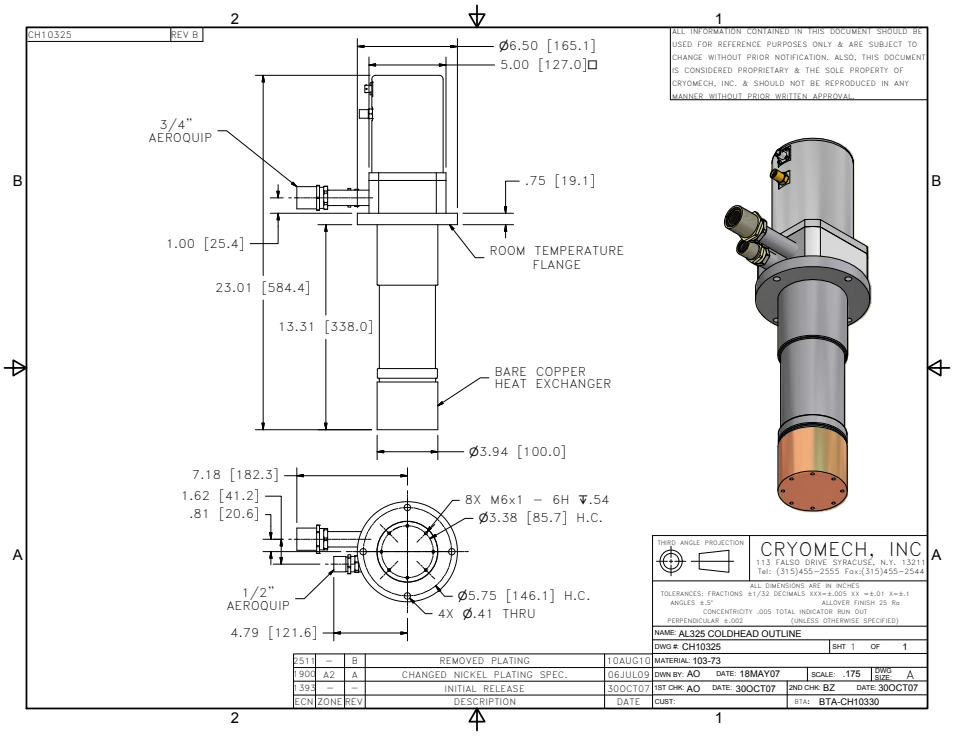

Figure A.1: AL325 coldhead engineering drawing [1]

[1] URL "http://www.cryomech.com/coldhead/AL325_ch.pdf", [cited 19 june 2015]

Chapter B | Functional Analysis

This appendix presents the Functional Analysis that has been performed. This includes a Functional Breakdown Structure in Section B.1 and Functional Flow Block Diagram in Section B.2.

B.1 Functional Breakdown Structure

In this section the Functional Breakdown Structure (FBS) is presented. It displays all the activities that should be performed to come up with the design, in a non sequential organisation. In the FBS, the blocks are ordered hierarchically, meaning that each block is a part of the block above it and each block is the sum of all blocks below it.
Two FBS diagrams can be found in this chapter. The first one provides a broad overview, involving the entire life-span of the aircraft. Figure B.1 depicts the first diagram. In this structure, the project has been divided into four main steps, which are the design, production, operation and disposal steps respectively. Of these four, the design, production and operation are subdivided into a lower level to show a higher level of detail. During the project, more details will become apparent. However, it is not possible to subdivide the FBS more whilst attaining a certain level of accuracy.
The second diagram focuses on the "Use Aircraft" block of Figure B.1. This particular block is identified as the most extensive one and thus a separate diagram was deemed appropriate. This additional diagram is depicted in Figure B.2. The "Use Aircraft" block was separated using a Sub-systems approach. Nine essential functions were identified in such a way that they can be easily pin-pointed to specific subsystems within the aircraft. Although some essential functions are straight-forward and only include one or two sub-functions, other functions are decomposed more detailed, such as "Passenger and Cargo" and "Provide Power".
The main focus of this project is the inclusion of a distributed propulsion system on the airplane and compare its performance to a typical engine distribution. In order to keep the same functionalities on the distributed propulsion aircraft, special attention should be paid to the functions dependent on the propulsion unit. In Figure B.2, these functions are highlighted in green.

B.2 Functional Flow Block Diagram

In order to visualise how the different functions relate to each other in a sequential manner, a Functional Flow Block Diagram (FFBD) is a very suitable tool. This diagram displays a multi-step, multi-level, time sequenced functional flow of the aircraft's life cycle and ranges from its design until its end-of-life disposal. This diagram is largely based on the Functional Breakdown Structure that has been explained in the previous chapter. The large difference between these two is that the FFBD is showing a time sequence of the different functional steps that have to be performed.
Figure B.3 commences with the top level of the aircraft's cycle and comprises four main functions: Design, Produce, Operate and Dispose. The first three main functions are further elaborated below. It is important to point out the numerous feedback loops present in level 2, particularly in the Design phase. This is due to the fact that aircraft design is a very iterative process and if a dead end is reached at any design stage, the designer needs to go up a level and reconsider the previous design choices.
An overview of a level 3 FFBD is given in Figure B.4 and concerns 3 key functions: Perform Detailed Definition (1.5), Produce Aircraft (2.3) and Use Aircraft (3.2). It is worth noticing the iterative nature of the design process present in the detailed definition part. The level 4 analysis which looks at 8 sub-functions of the Use Aircraft (3.2) block can be found in the Baseline Report [73]. Following the same procedure as in the Functional Breakdown Structure, the functions dependent on the propulsion systems are highlighted in green. It is important to point out that many of the functions identified in the FBS are not included in the FFBD, as these functions are not time-bound like "sustain loads", "manage power" and "provide comfortable environment"; they have to be present at all times.

Figure B.1: Functional Breakdown Structure

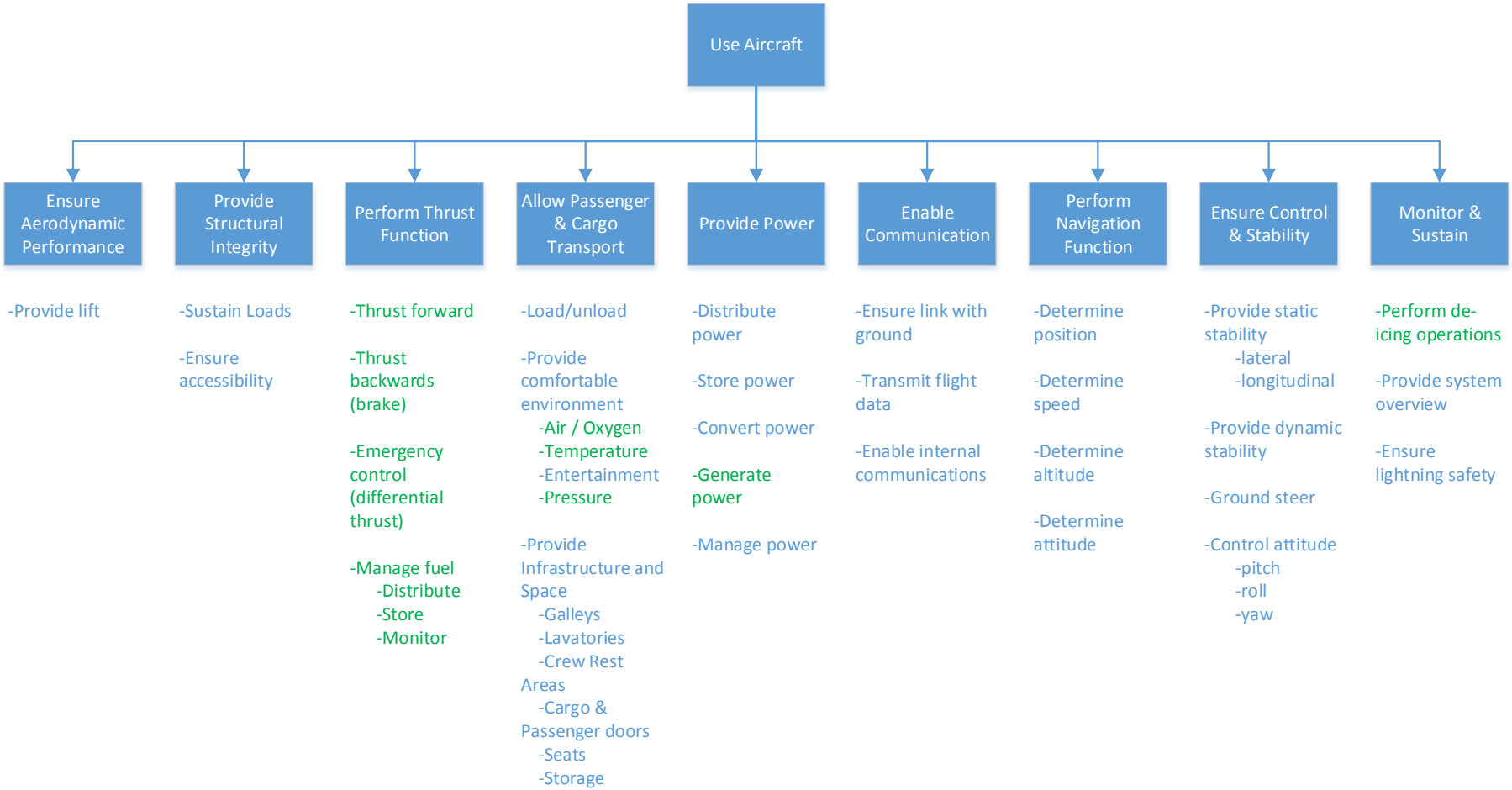

Figure B.2: Functional Breakdown Structure of aircraft operation

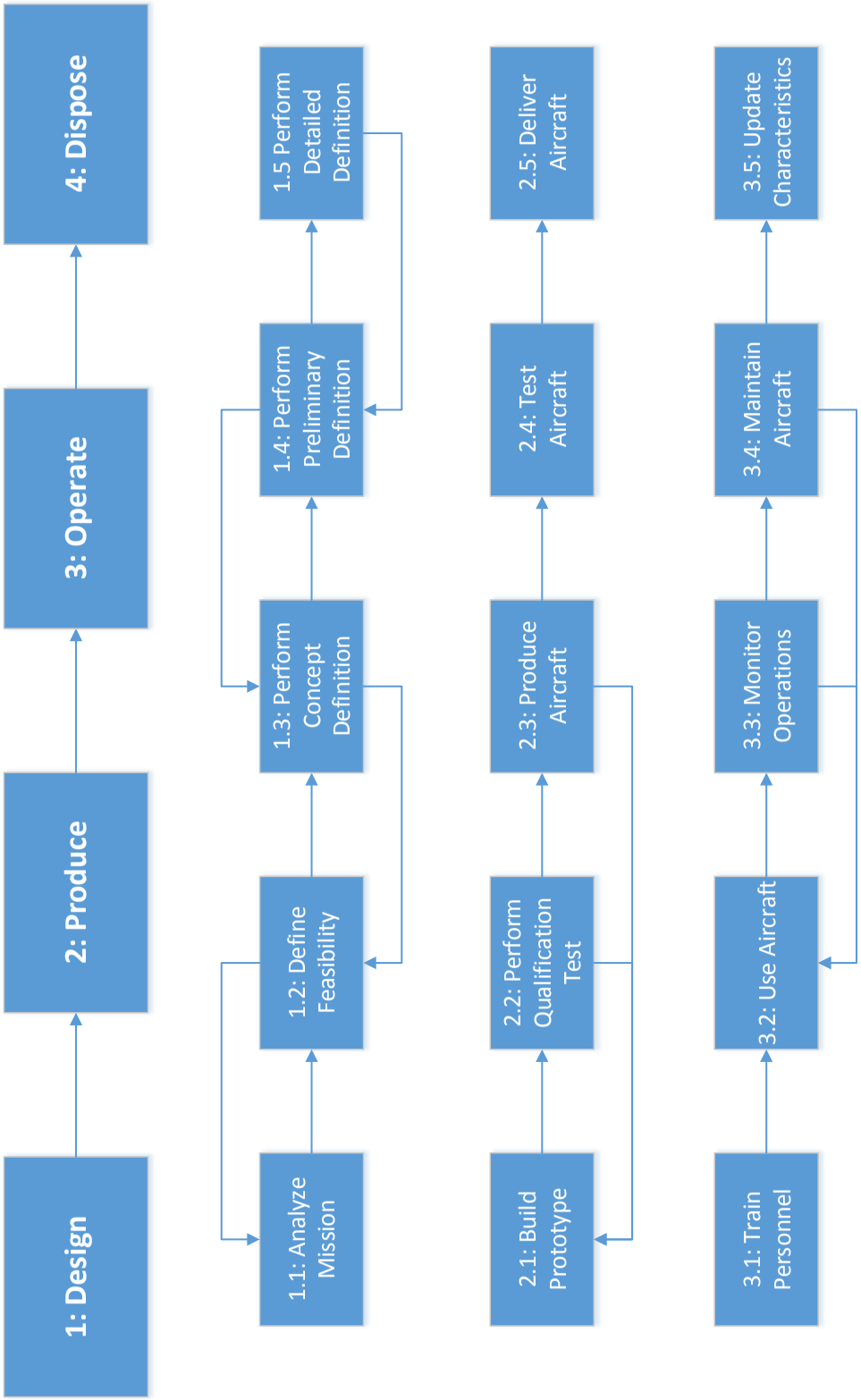

Figure B.3: First and second level of Functional Flow Block Diagram

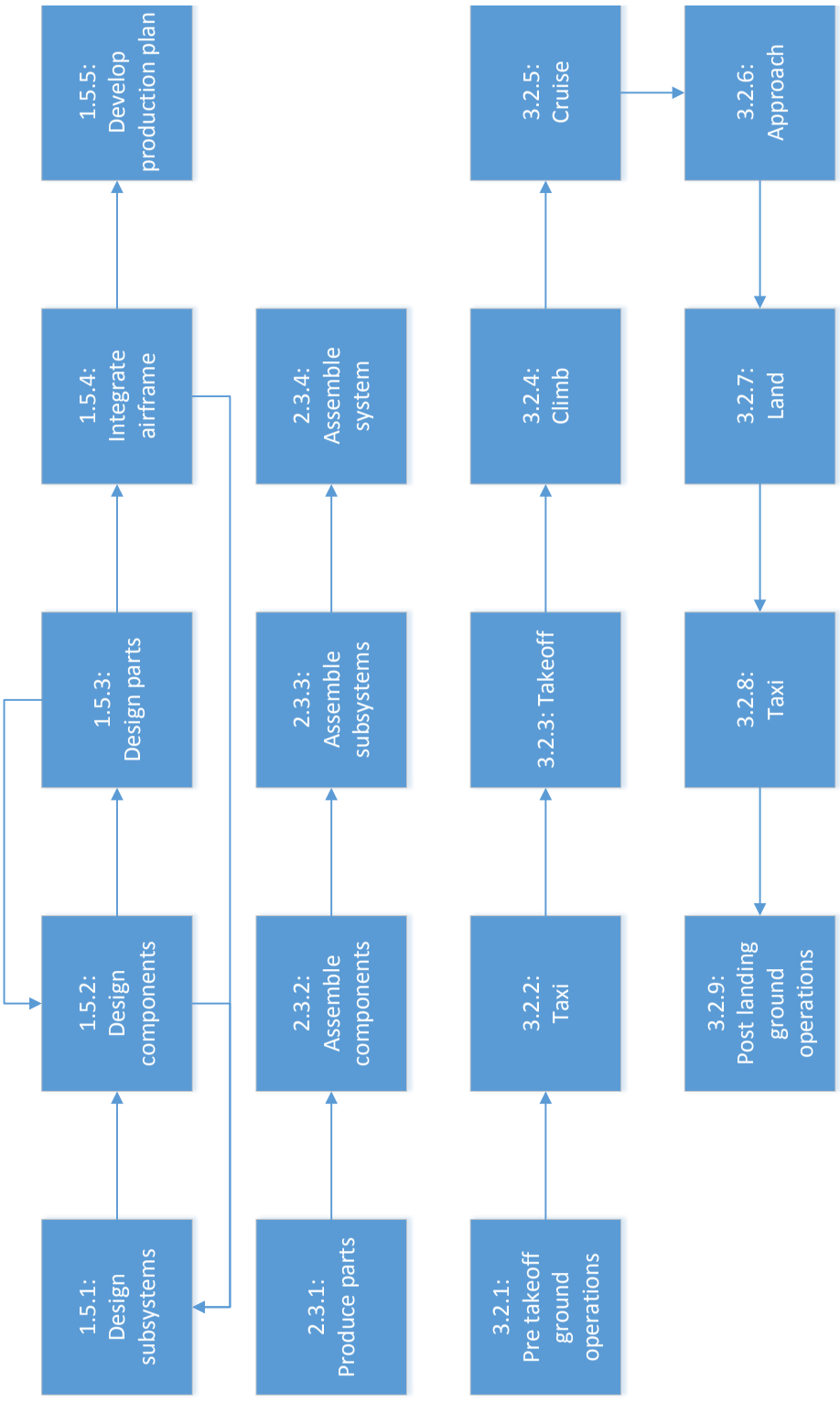

Figure B.4: Third level of Functional Flow Block Diagram

Chapter C | Cost Estimation Factor

This appendix displays the figures used from Roskam to perform the cost breakdown in Chapter 11.

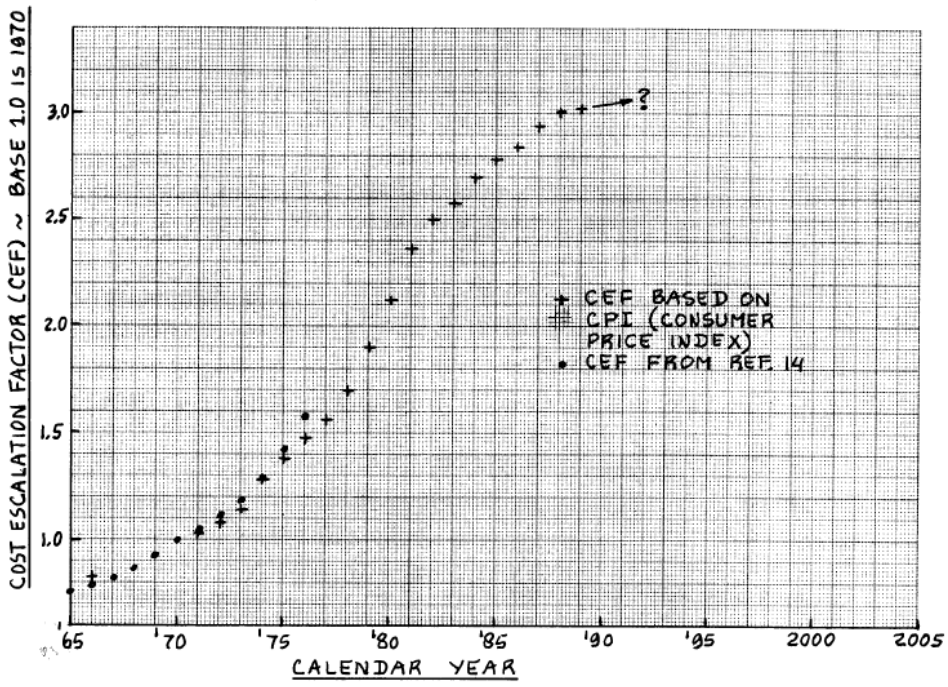

Figure C.1: Variation of Cost Escalation Factor (CEF) with time [60]

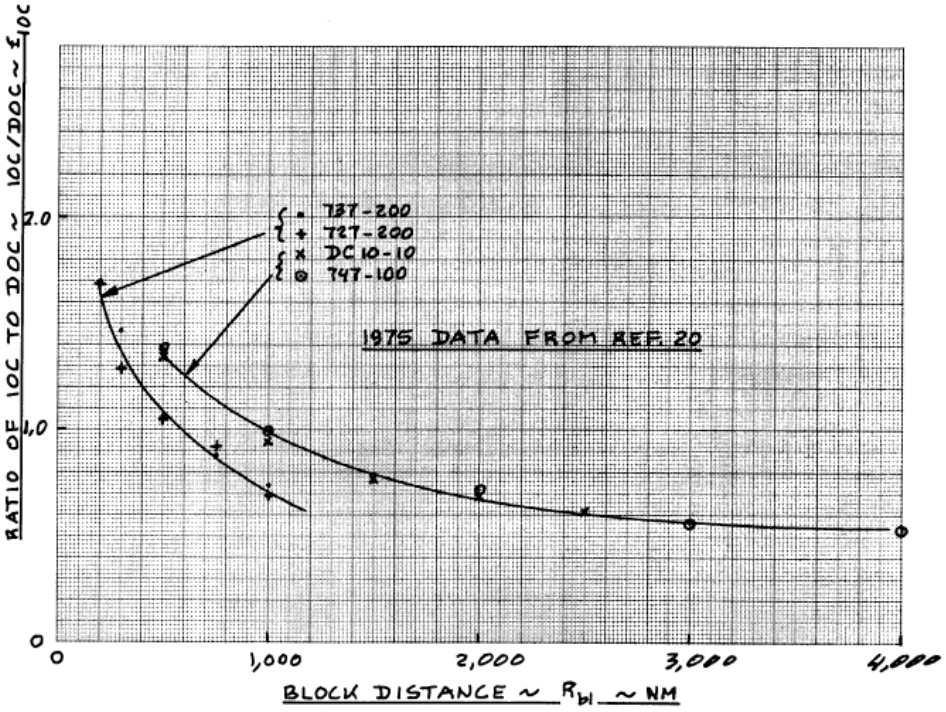

Figure C.2: Effect of Block distance on the ratio of IOC to DOC [60]

Chapter D | Work Distribution

This chapter shows the work distribution table as presented in Table D.1.

Table D.1: Work distribution per section

Chapter	Section	Name	Worked on it
1		Introduction	Maurice
2	1	Background	Vartan, Martijn
	2	Project Objective	Rutger
	3	Requirement Analysis	Maurice
3	1	Design Concepts	Jan
	2	Concept Trade-off Criteria and Weights	Jan
	3	Sensitivity Analysis	Martijn, Vartan
4	1	Class I Weight Estimation	Martijn, Maurice, Jordy
	2	Wing and Thrust Sizing	Martijn, Maurice
	3	Airfoil Selection and Wing Planform Design	Martijn, Jordy
	4	Control Surfaces	Maurice, Jordy
	5	Fuselage Design	Martijn
	6	Propulsion System	Maurice
	7	Class II Weight Estimation	Martijn, Jordy
	8	Empennage Design	Martijn, Jordy
	9	Drag Estimation	Martijn, Jordy
	10	Iteration Process	Martijn
5	1	Geometry and Weights	Martijn
	2	Final Results	Martijn
6	1	Fan Design	Luc, Jan, Timo
	2	Required Power	Luc
	3	Engines	Abhranil, Felix, Vartan, Rutger
	4	Motors and Generators	Felix, Abhranil
	5	Cabling	Rutger
	6	Controllers	Vartan
	7	Cooling	Vartan, Rutger
	8	Auxiliary Power Unit	Abhranil
	9	Final Architecture	Abhranil, Felix, Vartan, Rutger
7	1	Iteration Results	Martijn
	2	Mass Budget Breakdown	Martijn
	3	Aerodynamic Analysis	Timo
	4	Structural Analysis	Luc, Jan, Timo
	5	Control and Stability Analysis	Felix, Luc
	6	Performance Analysis	Martijn, Luc
	7	Verification and Validation	Rutger, Jordy
8	1	Hardware and Software Interaction	Abhranil, Martijn, Vartan
	2	Communication and Data Handling	Rutger
	3	Configuration and Layout	Maurice
9	1	Production and Assembly	Jan, Timo
	2	Operations	Jan, Timo
	3	Maintainability	Jan, Timo
	4	Disposal	Jan, Timo
	5	Sustainability within the Group	Maurice
10	1	General Risk Assessment	Rutger, Martijn
	2	Reflection on Risks	Rutger, Martijn
11	1	Market Analysis	Abhranil, Vartan, Luc
	2	Cost Breakdown	Jan, Timo, Abhranil, Vartan
12	1	Operations Analysis and Logistics	Maurice, Rutger
	2	Maintenance	Maurice, Rutger
	3	RAMS analysis	Martijn

13		Compliance with Requirements	Luc
14	1	Project Design and Development Logic	Jan, Timo
	2	Development of Distributed Propulsion Technologies	Jan, Timo
	3	Post-DSE Gantt Chart	Jan, Timo
	4	Recommendations	Timo
15		Conclusion	Luc, Abhranil
Appendix		Functional Analysis	Jan, Timo
		Task Division	Timo
Summary			Jan
Jury Summary			Jan
Poster			Martijn
CATIA			Jordy, Maurice
Layout/editing			Timo, Maurice